JAN MAYEN GLACIER CHANGES BETWEEN 2000-2020 IN HISTORIC, CLIMATIC, OCEANIC, AND GEOGRAPHIC CONTEXT

JADE COOLEY
Master of Science, Central Washington University, 2017

A thesis submitted
in partial fulfilment of the requirements for the degree of

MASTER OF SCIENCE

in

GEOGRAPHY

Department of Geography and Environment
University of Lethbridge
LETHBRIDGE, ALBERTA, CANADA

JAN MAYEN GLACIER CHANGES BETWEEN 2000-2020 IN CLIMATIC, OCEANIC, AND GEOGRAPHIC CONTEXT

JADE COOLEY

Date of Defense: 29 November 2021

Dr. H. Jiskoot Supervisor	Professor	Ph.D.
Dr. P. Bonnaventure Thesis Examination Committee Member	Associate Professor	Ph.D.
Dr. T. Bartholomaus Thesis Examination Committee Member University of Idaho Moscow, ID, USA	Assistant Professor	Ph.D.
Dr. C. Coburn Chair, Thesis Examination Committee Member	Professor	Ph.D.

ABSTRACT

Jan Mayen is a small, remote, glacierized volcanic island in the North Atlantic between Greenland, Svalbard, Iceland, and Scandinavia. Its most recent glacier map (RGI) is based on airphotos from 1949-1975, and only the glacier Sørbreen has previously been studied in detail. This thesis presents the first study of glacier fluctuations for the entire island, including the retreat of marine-terminating glaciers from historic maps since 1861 and the annual to decadal frontal variations of 16 of the island's 20 glaciers from satellite imagery. Between 2000 and 2020, Jan Mayen lost 2.2 km^2 or 2% of its ice area and had a frontal ablation of 0.20 km^3. Glaciers retreated 20-460 m with an average annual retreat rate (-9±7 m/yr) slower than in the surrounding regions, while Jan Mayen's temperature increased more. Correlation analysis with 18 climatic and oceanic parameters suggests that the main driver of Jan Mayen's glacier fluctuations is PDD.

ACKNOWLEDGEMENTS

I would like to thank my supervisor Dr. Hester Jiskoot and committee members Dr. Philip Bonnaventure and Dr. Timothy Bartholomaus for sticking with me through a fluctuating graduate experience. You have all been very helpful and taught me more than this thesis could show.

I would also like to thank the University of Lethbridge for my graduate school experience, and the School of Graduate Studies for the opportunity to be a graduate teaching assistant. While the extra funding was deeply appreciated, the chance to teach and be a part of university classes from a logistical and teaching viewpoint was invaluable. This research would not have bene possible without the funding of NSERC, which I received through Dr. Hester Jiskoot.

One of the best parts of being a graduate student is the amazing places you get to visit and the amazing programs you get to be a part of. I would like to express my appreciation for RemoteEx, through which I was able to participate in the McCarthy International Glaciology Summer School, which was an incredible adventure in learning about glacier mass balance and walking on glaciers; AG825 Glaciology at the University Centre in Svalbard, wherein I deepened my understanding of glacial hydrology and got to visit glacier caves; and the RemoteEx UAV workshop at Castle Mountain, which I was able to be involved with logistically and also fly a drone.

TABLE OF CONTENTS

Abstract iii
Acknowledgements iv
List of Tables viii
List of Figures x
List of Abbreviations xiv

1. Chapter 1: Introduction 1

1.1. Glaciers and Glacier Studies 1
1.2. Research Objectives 4
1.3. Thesis Structure 6

2. Chapter 2: Literature Review 7

2.1. Why and How Study Glaciers? 7
2.2. First Order Factors Influencing Glacier Accumulation and Ablation 14
2.2.1. Surficial Processes 14
2.2.2. Frontal Processes 16
2.2.3. Basal Processes 19
2.3. The Importance of the Arctic, and Jan Mayen's Place Within It 22
2.3.1. Greenland 26
2.3.2. Svalbard 27
2.3.3. Iceland 28
2.3.4. Scandinavia 29
2.4. Study Area 30
2.4.1. Introduction to Jan Mayen 30
2.4.2. Weather and Climate 33

2.4.3. Glaciers and Previous Glaciological Studies 36
2.4.4. Volcanic Activity and Seismic Studies 43
2.4.5. Why Study Jan Mayen? 47
2.5. Filling the Gaps in Knowledge 47
3. Chapter 3: Methods 49
3.1. Data 49
3.1.1. Randolph Glacier Inventory 49
3.1.2. Historical Maps of Jan Mayen 50
3.1.3. Weather Station Data 51
3.1.4. Climate Reanalysis Data 53
3.1.5. Positive Degree Days 54
3.1.6. Sea Ice Extent 55
3.1.7. Seismic Station Data 56
3.1.8. Remote Sensing Data 57
3.2. Analysis 61
3.2.1. Georectifying Images and Drawing the Coastline 61
3.2.2. Glacier Margin Delineation 62
3.2.3. The Box Method 65
3.2.4. Ice Thickness, Velocity, and Frontal Ablation 68
3.2.5. Annual Retreat Rates 70
3.2.6. Geographic Context 71
3.2.7. Glacier Response Time 72
3.2.8. Climatic and Oceanic Context 72
4. Chapter 4: Results 76
4.1. Comparison of Jan Mayen to Glaciers in other Regions Using RGI Attributes 76

4.2. Marine-terminating Glaciers from Historical Maps and Satellite data 78
4.3. Glacier Extent and Changes 2000-2020 88
4.4. Glacier Area Loss and Frontal Ablation 99
4.5. Glacier Response Time 102
4.6. Olonkinbyen Weather Station and Climate Reanalysis Results and Trends 102
4.7. Correlations Between Glacier Fluctuations and Climatic and Oceanic Drivers 111
5. Chapter 5: Discussion 121
5.1. Limitations of the Data Used in this Thesis 121
5.2. Jan Mayen Glacier Trends in Oceanic and Climatic Context 124
5.2.1. Glacier Trends 124
5.2.2. Climatic and Oceanic Parameter Trends 127
5.2.3. Correlation Between Glacier Trends and Oceanic and Climatic Parameters 130
5.3. Jan Mayen Glacier Changes in Geographic Context 139
5.3.1. Frontal Ablation in Context 144
5.4. Results in a Broader Geographical Context 145
6. Chapter 6: Summary and Conclusions 149
6.1. Future Studies 151
7. References 156
Appendix A: Creating Consistent Glacier Outlines 174
Appendix B: Full Glacier Fluctuations as Will Appear in WGMS FoG Database 176
Appendix C: SST Data 184

LIST OF TABLES

Table 2.1: Relevant summarized information for the four Arctic regions surrounding Jan Mayen. No. of Glaciers column includes the number of marine-terminating glaciers in parentheses. Values for Greenland refer only to the glaciers not considered attached to the ice sheet, except perhaps for the FoG retreat rates. References in text except sea level equivalence, which is from AMAP (2017). Values for Frontal Ablation based on Kochtitzky et al. (in prep) as of 1 Dec 2021. 27
Table 2.2: Attributes of the glaciers on Jan Mayen from RGI version 6.0 (RGI Consortium, 2017) 39
Table 3.1: All satellite scenes used in this study, and the glaciers which had frontal lines drawn using that scene. 59
Table 3.2: Jan Mayen glaciers separated into east and west sides and categorized according to terminus status in the year 2000. 71
Table 3.3: Climatic and oceanic primary and derived parameters used in this study 73
Table 4.1: Marine-terminating glaciers as indicated by the historical maps (from 1861, 1877, 1882, 1938, 1961 and 1975; Figs 4.3-4.8) and observed in this study (2000 and 2020). Glacier number from Hagen et al. (1993); see Fig 4.8. 85
Table 4.2: Observation period, number of measurements, and average, maximum, and minimum number of days between measurements. 89
Table 4.3: Maximum advance (a.), maximum retreat (r.), and average retreat/advance rates for each glacier considered in this study and the time period over which the rate was observed, year of most advanced and most retreated position, the total retreat, and years over which the glacier was observed. Each rate is in units of m/yr, even when the time period the rate spans is more than one year. 91
Table 4.4: Average, maximum, and minimum retreat/advance rates for different bins of the glaciers on Jan Mayen. Glaciers which experienced the maximum or minimum retreat/advance pattern are named to the right of their respective value. Only values between matching terminus states (i.e., marine- or land-) are considered for their respective bins. 98
Table 4.5: Frontal ablation low and high estimates and ice area lost for each glacier considered in this study for the entire time period (2000–2020). Included for context is glacier area (from RGI; Pfeffer et al., 2014) and the percentage of that area that was lost. 99
Table 4.6: Values used to calculate the frontal ablation (FA) for 2000-2020. Low estimate assumes a maximum glacier thickness of 80 m, high estimate assumes 100 m. 101
Table 4.7: Maximum and minimum values and associated years for all climatic and oceanic parameters. 104
Table 4.8: Trends, R^2, and mean average of all parameters between most current climate (1991–2020) and previous 30–year period (1961–1990). Trend change refers to the change in slope between 1961-90 and 1991-2020, with any changes < 0.01 assigned “0”, similarly for mean average value change. Values that increase are in red, values that decrease are in blue. *SST measurements start in 1975. 109
Table 4.9: Pearson’s r correlation coefficient for pairwise correlations between all parameters. Bold numbers have a p-value < 0.05, and bold, italicized, blue numbers have a p-value < 0.01. Significant and highly significant correlations are highlighted according to

strength: Black cells indicate very strong correlations, dark grey strong, and light grey moderate. 112
Table 4.10: Summary of relationship direction, significance, and strength for all parameters that correlated with at least one of the glacier trends. All strong and very strong relationships are in bold. 116
Table 5.1: Each significantly correlated parameter for which R^2 increased when shifting the trendline from linear to exponential or logarithmic, and the corresponding R^2. 123
Table 5.2: The correlation direction, trend, and mean average parameter value for the 15-year period (glacier response time) before glacier front line measurements and for the most recent time period, and change direction between the two time periods for the driving parameters. 139
Table 5.3: Repeated here is Table 2.1, with *Jan Mayen results from this thesis added. 141
Table 5.4: Mean annual average temperature and yearly precipitation sum for Greenland, Svalbard, Iceland, Scandinavia (Norway and Sweden), and Jan Mayen for 1961-1990 and 1991-2020, and how they have changed. Data except for Jan Mayen from https://climateknowledgeportal.worldbank.org/download-data. 142

LIST OF FIGURES

Figure 1.1: Colored lines represent cumulative mass change from glaciers in labeled regions. Glaciers that generally gain mass would have a line tending upwards, glaciers in balance with the current climate would have a horizontal trend. From WGMS (2020). 2
Figure 2.1: Components of surface energy balance and accompanying fluxes. Blue box represents a glacier. From Oerlemans (2010). 9
Figure 2.2: Diagram indicating the three glacier boundaries and one internal area included in mass balance studies. The equilibrium line altitude (ELA) is indicated as the average lowest elevation where snow from the previous winter still exists by the end of the melt season. 12
Figure 2.3: Observed relationship between ice front position and sea ice conditions for Umiámáko, central West Greenland. Dotted vertical lines indicate first ice-free day of year. From Howat et al. (2010). 18
Figure 2.4: Locations of measured GHF and geothermal vent temperatures, including some implied contours in the Northeast. Note the large changes along the east coast, from 20 mW/m^2 at Dye3 to as high as 260 mW/m^2 at GHF. From Rysgaard et al. (2018). 21
Figure 2.5: Arctic region political map from 2002, with three lines corresponding to different definitions of the "Arctic". Blue dashed line indicates 66°34'N, green line indicates the point at which the landscape is frozen and there are no trees, red line indicates where the average daily summer temperature is below 10° C. Jan Mayen circled in black. From https://nsidc.org/cryosphere/arctic-meteorology/arctic.html. 23
Figure 2.6: Greenland, Svalbard, Scandinavia, and Iceland in context of ocean currents which deliver heat to the glaciers. Jan Mayen Island circled in purple. Modified from AMAP (2017). 25
Figure 2.7: Bathymetry of Jan Mayen and surrounding areas at increasing scales; a) Jan Mayen indicated by white arrow; modified from Olesen et al. (2010). b) contours in meters, modified from https://www.ncei.noaa.gov/maps/bathymetry/ 32
Figure 2.8: Jan Mayen's location within a) annual average SST (image from https://svs.gsfc.nasa.gov/3652; data from Locarnini et al., 2006) and b) main circulation of warm North Atlantic (red arrows) and cold East Greenland surface currents (blue arrows). Bathymetry in 1000 m contour interval, KR = Kolbeins Ridge; MR = Mohns Ridge; JMFZ = Jan Mayen Fracture Zone. From Lysa et al. (2021). 35
Figure 2.9: Map of Jan Mayen, with glacier outlines and names corresponding to GLIMS ID numbers. Modified from Hagen et al. (1993). Inset shows location of 1970 eruption. 1 - lava streams; 2 - main eruption fissures; 3 - active craters; 4 - extinct craters; 5 - probable course of deep-seated dextral strike-slip fault; 6 - glacier margin. Modified from Skreslet et al. (2004).....37
Figure 2.10: Length and elevation of the Jan Mayen glaciers on Beerenberg. Data from RGI 6.0 (RGI Consortium, 2017) 38
Figure 2.11: Glacier margin delineation map for Sørbreen, showing retreat between 1882 and 1949 and slight readvance up to 1978. From Anda et al. (1985). 42
Figure 2.12: Mass balance curves reconstructed from field measurements on Sørbreen. Curves for 1972/73 and 1973/74 are from Orheim (1976). Curve from 2008 is from Hulth et al. (2010) and includes the mass balance curves from 1973/74 for context. 43

Figure 2.13: GHF around Jan Mayen. Visualization from Lucazeau (2019), data points from https://ihfc-iugg.org/products/global-heat-flow-database/data 45
Figure 2.14: New land created by the September 1970 lava flows shown by lined area. Solid black dots indicate craters, stippled area is tephra deposits, and the parabola is the tephra fallout pattern from the 1985 eruption. From Orheim (1993). 46
Figure 3.1: Scientific stations on Jan Mayen relevant to this thesis. Background image is Landsat 8 satellite image from 28 Aug 2020. 52
Figure 3.2: Example of how manually-mapped glacier outlines can differ between individuals. This is glacier Vadret d'Urezzas in Austria. Each colored outline is a different scientist's outline of the glacier. All scientists received the same satellite scene and the same instructions. From Paul et al. (2013). 63
Figure 3.3: Box Method. a) Shows an example glacier inside a box drawn such that the side of the glacier pass through opposite sites, with arbitrary ends perpendicular to glacier flow. b) Shows how retreat rates are calculated, with the ice area inside the box (pale orange area) from an earlier year subtracted from ice area of a later year, such that retreat is negative and advance is positive. 66
Figure 3.4: Comparing areas across time periods over which the glacier retreats onto land. a) shows in orange the ice area that would be used for marine-terminating calculations for the last year the glacier was marine-terminating (here 2003). b) shows the line from the last year the glacier was marine-terminating extended so that it can cut the land-terminating box (purple), creating an ice area (orange) to be subtracted form the first land-terminating area. c) indicates the areas that would be used to calculate the area change between the last year the glacier was marine-terminating and the first year it was land-terminating. 67
Figure 4.1: Length comparison of glaciers on Jan Mayen and surrounding regions, with number of glaciers listed above whisker. Data from RGI (RGI Consortium, 2017), with a minimal area cutoff of 0.225 $km^2$and using only Greenland peripheral glaciers. Outliers in length range as high as 50 000–70 000 m for Greenland, Iceland, and Svalbard; for clarity these are not shown. 77
Figure 4.2: Log-log plot of average slope (degrees) relative to average length (km) of glaciers on Jan Mayen and surrounding regions. Data from RGI (RGI Consortium, 2017). Iceland (blue) and Scandinavia (yellow) have nearly complete overlap. Greenland includes glaciers peripheral to the ice sheet with CL0 only (Rastner et al., 2012). 77
Figure 4.3: Map of Jan Mayen and the sailing route undertaken by Vogt, Berna, and others on the ship the Joachim Hinrich in the summer of 1861. Image by F.C. Klimsch, based on map in Vogt (1863). Numbers mark the location of the ship on the indicated days of August, 1861. Red lines mark routes between dates. For larger map: https://upload.wikimedia.org/wikipedia/commons/1/17/Jan_Mayen_map_by_Carl_Vogt_1863.jpg 79
Figure 4.4: Map constructed from earlier maps and survey data from 1877 by Mohn and Wille (1882). For larger map: https://upload.wikimedia.org/wikipedia/commons/5/50/Jan_Mayen_Mohn.png 80
Figure 4.5: Map from an Austrian expedition to Jan Mayen in 1882 for the First International Polar Year (Boldva et al., 1886). For larger map: https://upload.wikimedia.org/wikipedia/commons/0/05/Jan_Mayen_map_1884_Schritt2_sw.png 81

Figure 4.6: Map from The Imperial College of Science expedition to Jan Mayen in 1938 (Jennings, 1948). 82
Figure 4.7: Map based on the University of London Jan Mayen Expedition in 1959 and the University of London Beerenberg Expedition in 1961(Kinsman and Sheard, 1963). 83
Figure 4.8: Map based on glacier extent data from aerial photos from 1959-1975 (Hagen et al., 1993) 84
Figure 4.9: Relative length of all glaciers on Jan Mayen with measurements taken in this study. Glaciers that were marine-terminating in 2000 are solid lines, glaciers that were land-terminating 2000–2020 are dashed lines. 90
Figure 4.10: East side relative length glacier fluctuations separated into a) marine- and b) land-terminating. Lines are same colors as in Figure 4.9. For periods when glaciers are marine-terminating, lines are solid, while land-terminating glacier lines are dashed. Lines connecting the last marine-terminating measurement to the first land-terminating measurement are dashed. Prins Haralds Bre is included with the marine-terminating glaciers and not the land, as it has only 2 land-terminating measurements. 94
Figure 4.11: West side relative length glacier fluctuations separated into a) marine- and b) land-terminating. Lines are same colors as in Figure 4.9. For periods when glaciers are marine-terminating, lines are solid, while land-terminating glacier lines are dashed. Lines connecting the last marine-terminating measurement to the first land-terminating measurement are dashed. Gjuvbreen is included with the land-terminating glaciers and not the marine, as it has only 2 marine-terminating measurements. 95
Figure 4.12: All digitized lines for all glaciers considered in this study, with the four representative glaciers named. Background image is Landsat 8 Band 8 of 19 August 2016. 97
Figure 4.13: Velocity map of Jan Mayen from ITS_LIVE methods (Gardner et al., 2019) with Sentinel-2 images provided by Dr. Mark Fahnestock (pers. comm, Feb 2019). 101
Figure 4.14: Air temperature, precipitation, and SST from the weather station on Olonkinbyen and air temperature from climate reanalysis. Grey shaded area indicates time when weather station was not at its current location. Air temperature can be considered continuous, but precipitation cannot. 103
Figure 4.15: Annual average, summer average, or sum of all parameters barring precipitation (next page) with trendline for 1991–2020 (black dotted line). Gray bars indicate years that Jan Mayen was within the Fram Strait sea ice, pink lines indicate Beerenberg volcanic eruption years. a) Annual average and summer (JJA) temperature average for air temperature and SST as taken at the weather station on Olonkinbyen; b) PDD for weather station and both climate reanalysis levels; c) PDDN for weather station and both climate reanalysis levels; d) relative humidity and fractional cloud cover annual average for both climate reanalysis levels. 106
Figure 4.16: Precipitation sums as observed at the weather station on Olonkinbyen. Only data taken from the weather station at its current position (1962+) are included. The trendline for years 1991–2020 (black dotted line) is shown. Gray bars indicate years Jan Mayen was within the Fram Strait sea ice, pink lines indicate eruption years. 107
Figure 4.17: Relationship between T_{1000} (ground level climate reanalysis annual average temperature) and T_a (Olonkinbyen weather station observations of annual average temperature) between 1950 and 2020. Note the difference in range of measurements. Solid purple line is a 1:1 line. 114

Figure 4.18: Scatterplots for all relationships between Prins Haralds Bre glacier fluctuations and parameters with a p value < 0.05. 117
Figure 4.19: Scatterplots for all relationships between Sørbreen glacier fluctuations and parameters with a p-value < 0.05. 117
Figure 4.20: Scatterplots for all relationships between Kerckhoffbreen glacier fluctuations and parameters with a p-value < 0.05. 118
Figure 4.21: Scatterplots for all relationships between the all-glacier trend and parameters with a p-value < 0.01. The all-glacier trend additionally was significantly (but not highly significantly) correlated with T_{1000}, T_{850}, and PDD_{1000}, which are not shown. 119
Figure 5.1: a) Svend Foynbreen and Kjerulfbreen, and b) Kjerulfbreen and Weyprechtbreen as seen from the ocean in June 2016 (http://www.mrietze.com/web16/JanMayen16.htm). At this time, Weyprechtbreen and Kjerulfbreen are still considered "marine-terminating" but Svend Foynbreen is not. 126
Figure 5.2: Monthly NAO index during the time of relevance for this study (1960-2020). Data from https://www.ncdc.noaa.gov/teleconnections/. 129
Figure 5.3: Temperature anomaly of the top 5 m of the North Atlantic Ocean for 2000-2010 compared to 1995-99. Jan Mayen is circled in yellow. Modified from Carr et al. (2017). 136
Figure 6.1: Examples of different sea ice conditions around the island of Jan Mayen. In March 1988, Jan Mayen was considered within the sea ice exported through the Fram Strait (March through August Ice Edge Positions in the Nordic Seas, 1750-2002 version; https://nsidc.org/data/G02169/versions/1). Both images are from Landsat 5. 153
Figure 7.1: Petersenbreen, on the East side of the island. The rippling pattern downstream of the glacier could be debris on top of glacier ice, or an area of glacial runoff, therefore it is not included in the glacier outline. Medium grey cells are assumed glacier ice, white is assumed snow. Background is Landsat 8 image Band 8 from 19 Aug 2016. 175
Figure 7.2: Number of daily average SST measurements for each year there were SST measurements taken at Olonkinbyen. Teal bars indicate years with measurements every day, purple bars indicate years with fewer measurements than days. Data from web portal https://seklima.met.no/ 184
Figure 7.3: Number of daily average SST measurements for each month, in the years there were not SST measurements taken every day. Any value not showing on the bar chart was 0. Teal bars indicate months with measurements every day, purple bars indicate months with fewer measurements than days. Data from web portal https://seklima.met.no/ 185

LIST OF ABBREVIATIONS

C_{1000}	Fraction of cloud cover annual average from climate reanalysis at level 1000 hPa
C_{850}	Fraction of cloud cover annual average from climate reanalysis at level 850 hPa
DEM	Digital Elevation Model
ELA	Equilibrium Line Altitude
FA	Frontal Ablation
FoG	Fluctuations of Glaciers
GHF	Geothermal Heat Flux in mW/m^2
IGRA	Integrated Global Radiosonde Archive
IRIS	Incorporated Research Institutions for Seismology
NAO	North Atlantic Oscillation
P_a	Precipitation annual sum at the Olonkinbyen weather station (mm)
PDD_{1000}	Positive Degree Days from climate reanalysis at level 1000 hPa (°C)
PDD_{850}	Positive Degree Days from climate reanalysis at level 850 hPa (°C)
$PDDN_{1000}$	PDD annual sum from climate reanalysis at level 1000 hPa
$PDDN_{850}$	PDD annual sum from climate reanalysis at level 850 hPa
$PDDN_O$	PDD annual sum at the Olonkinbyen weather station
PDD_O	Positive Degree Days at the Olonkinbyen weather station (°C)
P_w	Precipitation winter sum at the Olonkinbyen weather station (mm)
RGI	Randolph Glacier Inventory
RH_{1000}	Relative humidity from climate reanalysis at level 1000 hPa (%)
RH_{850}	Relative humidity annual average from climate reanalysis at level 850 hPa (%)
SPSS	Statistical Package for the Social Sciences
SST_a	Sea surface temperature annual average at the Olonkinbyen weather station (°C)
SST_s	Sea surface temperature summer average at the Olonkinbyen weather station (°C)
T_{1000}	Temperature annual average from climate reanalysis at level 1000 hPa (°C)
T_{850}	Temperature annual average from climate reanalysis at level 850 hPa (°C)
T_a	Temperature summer average at the Olonkinbyen weather station(°C)
T_s	Temperature annual average at the Olonkinbyen weather station (°C)
WMGS	World Glacier Monitoring Service
WMO	World Meteorological Organization

1. CHAPTER 1: INTRODUCTION

1.1. Glaciers and Glacier Studies

Frozen water on land covers ~10% of the Earth's surface and comprises ~70% of the world's fresh water (NSIDC, 2020a). Glaciers are perennial bodies of frozen water which lie completely or partly on land. They are found in mountainous and polar regions and are distinct from other bodies of ice in that they flow under their own weight and can have seasonal to multi-annual patterns of retreat and advance (Benn and Evans, 2010; Cuffey and Paterson, 2010). Observations of these glacier fluctuations reach as far back as the 1600s via historical maps, and hundreds to millions of years further with dating of deglaciated landforms and sediments (Oerlemans, 1994; Benn and Evans, 2010; Hannesdóttir et al., 2015b). Directly mapping changes in glacier size and shape is the first step in understanding why and how they change.

Glaciers, in addition to ice sheets and permafrost, add to sea level rise, and freshwater ecosystems downstream depend upon the seasonal variation in timing and amount of glacial runoff (AMAP, 2017). Increased melt rates tend to increase ice flow and iceberg discharge, which impacts shipping and other human activities (Joughin et al., 2012). The most influential factors on glacier fluctuations are air temperature, solid precipitation, and solar radiation (Hock, 2005; Oerlemans, 2010; Vaughan et al., 2013). Under current changing climate conditions, these first-order factors have caused changes in glacier area and volume that are increasingly negative (Fig. 1.1).

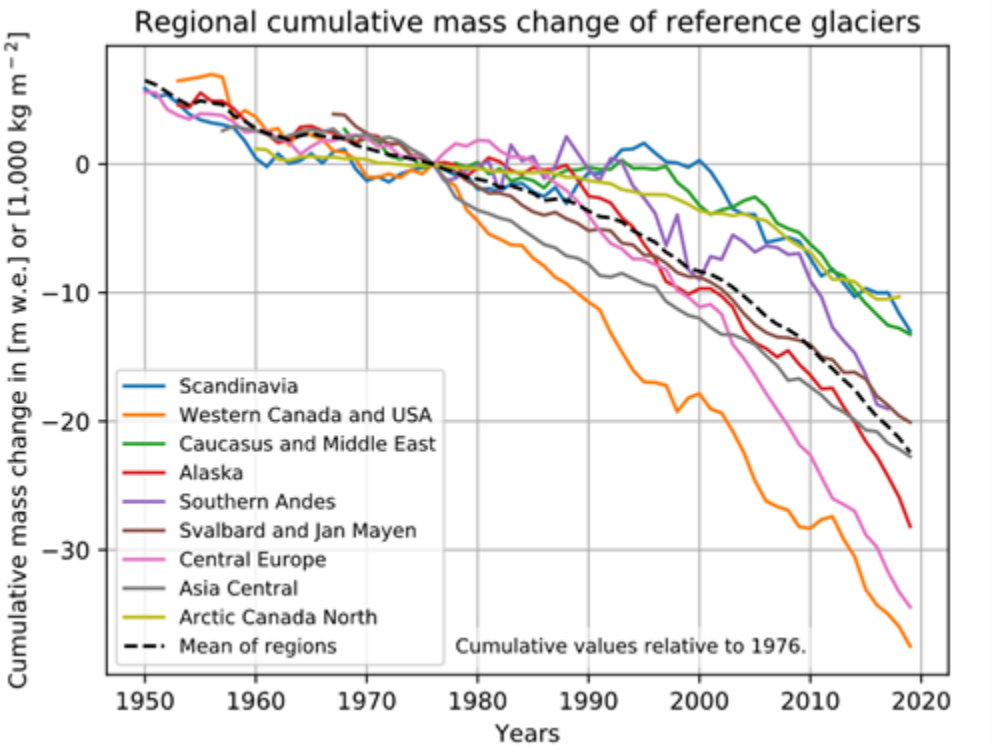

Figure 1.1: Colored lines represent cumulative mass change from glaciers in labeled regions. Glaciers that generally gain mass would have a line tending upwards, glaciers in balance with the current climate would have a horizontal trend. From WGMS (2020).

With 10% of the world's population living in low-lying coastal zones, rising global sea level is a major concern (IPCC, 2019b). Estimates of sea level rise range widely (30-60 cm by 2100 is a conservative estimate) and are dependent on both the rate of industrialization and carbon use as well as on the poorly quantified ranges and types of contributors (AMAP, 2017; IPCC, 2019b). The main cause of sea level rise is thermal expansion of the ocean water body, accounting for 75% of the total measured global sea level rise from 1900-current, but the melting of Arctic glaciers accounts for 2/3 of the remaining sea level rise budget (Vaughan et al., 2013; Edwards et al., 2021). This percentage has been increasing in recent time frames as thermal expansion slows and land ice melts faster. At current rates, land-based ice in the Arctic alone would add 25 cm to sea level by 2100, and many glaciers would disappear entirely by 2050 (AMAP, 2017).

Ice sheets contain a much larger volume of ice than glaciers, and thus would have a larger effect on sea level. Although ice sheet response time has been grossly underestimated until recently, when the susceptibility of ice shelves and tidewater outlets to changing atmospheric and oceanic drivers was better understood, ice sheets' immense mass means they have higher thermal inertia, and thus have been disappearing slower than glaciers. Many glaciers are projected to disappear completely within this century (AMAP, 2017; IPCC, 2019a; Smith et al., 2020). Therefore, it is of much more impending importance to study glaciers now. Many factors affect how glaciers melt throughout an annual and seasonal time scale. As these factors can be highly variable and the speed with which glaciers respond to them is in the range of 10s-100s of years, the best way to determine how a glacier has changed is to measure the physical changes directly (Klok and Oerlemans, 2004; Cuffey and Paterson, 2010). Glaciers are often difficult or dangerous to physically visit, however, and so glacier changes are frequently measured using satellite data or aerial imagery.

Glacier fluctuation histories have led to many insights on glacier behavior. It is not uncommon for glaciers side by side to change in drastically different ways (Moon and Joughin, 2008). Sometimes it is easy to determine the cause for this: land-terminating glaciers are subject to different forcings than marine-terminating glaciers, and, similarly, glaciers with different aspects or slopes can have different responses (Benn and Evans, 2010; AMAP, 2017). Other changes require further studies to explain, such as a glacier downwind of another receiving snow that is scoured off the upwind glacier, or a glacier that directly overlies a volcanic fissure and thus over an area of higher geothermal heat flux (GHF), resulting in faster sliding or losing mass at a heightened rate when compared to others nearby (Jóhannesson et al., 2020). Measuring individual glacier changes directly expands detailed process understanding to larger glacier

populations and helps dictate the direction of further scientific study. In addition, determining past glacier front positions works as a paleoclimate proxy, when tree rings and ice cores are not available (Davis et al., 2009).

The North Atlantic region of the Arctic contains four important glacierized areas: Greenland, where numerous local glaciers surround the only northern hemisphere ice sheet, which is important due to its effect on and response to ocean temperature and circulation; Svalbard, with its low-elevation marine-terminating and surging glaciers; Norway, where glaciers are maritime and close to a significant population; and Iceland, where many glaciers and ice caps overlie active volcanoes. In the middle of these is an often-overlooked volcanic island, Jan Mayen. The ability to compare the midpoint of these regions will be helpful for understanding glacier changes in the Arctic in general, and for glaciers on volcanoes in the Arctic in particular.

1.2. Research Objectives

The goal of this thesis is to quantify how the shape of the glaciers on the island of Jan Mayen change, how these changes fit into the broader region, and to discover the first-order factors affecting these changes. To this end, the objectives of this thesis are as follows:

1. Objective 1: Jan Mayen glacier frontal variations from the earliest available date (~1850) to the present.

   What is the frontal variation of the glaciers on Beerenberg, Jan Mayen?

   Have the glaciers experienced a steady or oscillating retreat pattern? How far back can we determine this pattern?

2. Objective 2: Glacier volume change from earliest available date (~1950) to the present.

   What changes have occurred in the volume of Jan Mayen glaciers during this period?

   How does this compare to the frontal variations?

3. Objective 3: Estimate of 2000-2020 frontal ablation

Since Jan Mayen is often overlooked as a potential contributor to frontal ablation, a quantification of this will be the first of its kind. This work will also contribute to a contemporaneous Pan-Arctic tidewater ice flux project, coordinated by Dr. Luke Copeland and Will Kochtitzky (University of Ottawa).

4. Objective 4: Correlation of the glacier fluctuations (Obj. 1) to oceanic and atmospheric drivers.

   Do first order factors of ocean and air temperature and precipitation correlate with observed glacier changes, or is investigating second order factors such as volcanic activity necessary?

5. Objective 5: Discussion of glacier fluctuations in geographic context: marine- vs land-terminating, aspect, and in relation to glacier fluctuation patterns in the North Atlantic regions (Iceland, Greenland, Svalbard, Norway).

   Which other regions in the world can Jan Mayen glaciers be compared to in terms of glacier type, dynamics, and general climate?

   What does placing Jan Mayen in geographic context of glaciated areas nearby tell us about glacier behavior in general?

1.3. Thesis Structure

This Thesis consists of six chapters and appendices. The first chapter introduces the general importance of the work. The second chapter reviews the background on subjects relating to the results and discussion, including an introduction to the study of glaciers, important areas on glaciers where mass change and transfer occur, the importance of glacier fluctuations, the Arctic, and Jan Mayen. The third chapter methodically describes all data and methods used in this thesis to come to a conclusion. This includes satellite imagery, weather data, sea surface temperature, sea ice extent, climate reanalysis, and digital elevation models (DEMs). Chapter four results in an overview of the glacier fluctuation history, the climate and ocean data, and the correlations between the two. Chapter five discusses the limitations of this thesis, the glacier fluctuations and correlations, and compares Jan Mayen glacier changes to the four nearby areas: Greenland, Svalbard, Norway, and Iceland. In conclusion, chapter six summarizes the findings and scientific importance of this thesis and suggests further studies which could build on this work.

2. CHAPTER 2: LITERATURE REVIEW

2.1. Why and How Study Glaciers?

Glaciology is the study of ice in the environment and improves predictions of river flows and sea level rise, advances understanding of the effects of glaciers on landscapes and the climate system, and informs those studying Arctic and alpine ecosystems. A glacier is defined as a body of ice that flows under its own weight and is constrained by the topography it overlays (Cuffey and Paterson, 2010). This is in contrast to ice sheets and ice caps, which drown out topography, and niche glaciers, which do not flow under the weight of gravity (Cuffey and Paterson, 2010; Singh et al., 2011). After snow is deposited, it is compacted either by the weight of the snow above it or by refreezing of water between snow grains which metamorphoses snow into firn, dense grains of frozen water that are compacted into densities ~400-830 kg/m^3. When density exceeds 840 kg/m^3, pores of air or water become closed off from each other within the material, and it is then considered glacial ice (Cuffey and Paterson, 2010). Glaciers flow at a rate that can be observed over short time scales, with a general range in speed from 10s to 1000s of meters in a year, and glacier ice deforms both in a plastic (such as crevasses) and ductile manner (by flowing; Benn and Evans, 2010; Cuffey and Paterson, 2010). Glaciers are present on other planetary bodies, and the study of their dynamics on Earth can be generalized to other planetary bodies such as Europa and Mars (Smellie and Edwards, 2016). However, the most socially relevant reasons to study glaciers currently is to understand their response to climate change and their capacity to affect downstream hydrology and raise sea level.

The most important factor for a glacier's contribution to sea level rise is the rate at which they lose mass or melt (Vaughan et al., 2013; AMAP, 2017; IPCC, 2019a). One way to determine

how a glacier melts is by quantifying their annual mass balance, which in simple terms is the net gain or loss of glacier ice over a hydrologic year (Benn and Evans, 2010; Singh et al., 2011). It is measured in units of water equivalent (w.e.), or the equivalent volume of water that would result from the snow, ice and firn that melted during that time (Hock, 2005). The mass balance of a glacier is the sum of the accumulation and ablation of mass, where ablation is melt, sublimation, and calving. There are several different ways to write a mass balance equation, one example is:

$$\dot{M} = \dot{B} + \dot{D}/_{S} \qquad \textit{(Eq 2.1)}$$

Where $\dot{B}$ is the glacier-wide mass-balance rate from both surface and basal processes, $\dot{D}$ is the frontal ablation along the perimeter of the calving margin, and S is the area of the glacier (Cogley et al., 2011).

The surface term of the mass balance equation is the sum of the amount of different types of energy a surface receives and emits, representing the total energy available for raising snow and ice temperature or phase changes within it (Hock, 2005; Hulth et al., 2010). This involves measuring shortwave radiation from the sun and longwave radiation from atmospheric sources and the turbulent sensible and latent heat fluxes (Fig 2.1).

$$Q_M = Q_N + Q_H + Q_E + Q_G + Q_R \textit{ (Eq 2.2)}$$

Where Q_M is the energy available for melt, Q_N is net radiation, Q_H is sensible heat flux (energy associated with temperature), Q_E is latent heat flux (energy associated with changing phase), Q_G is the ground or ice heat flux, and Q_R is the sensible heat flux from rain. To calculate Q_N, a glaciologist must measure and sum incoming (↓) and outgoing (↑) short- (S) and longwave (L) radiation (Hock, 2005):

$$Q_N = S\downarrow + S\uparrow + L\downarrow + L\uparrow \quad \textit{(Eq 2.3)}$$

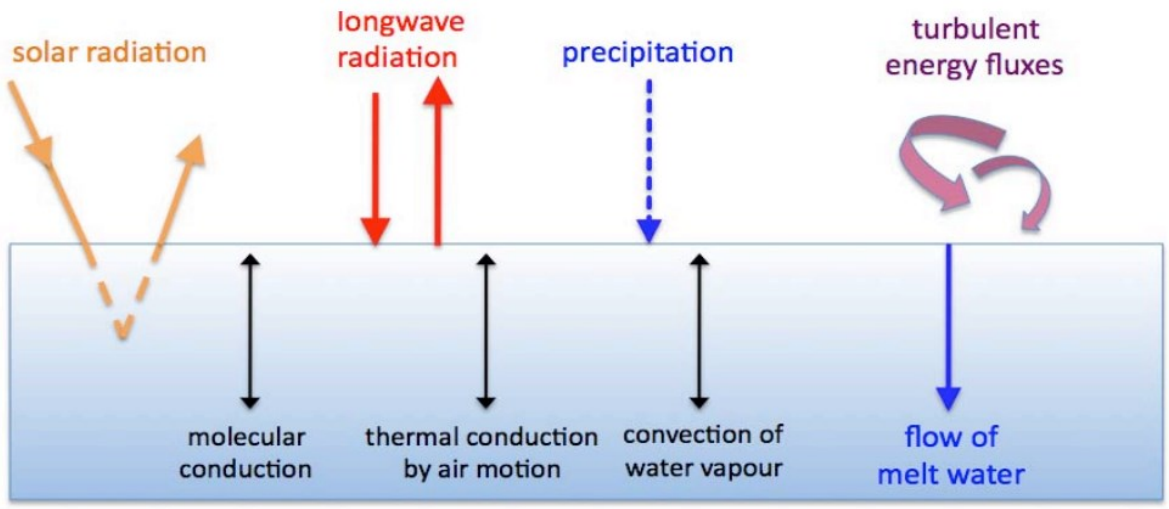

Figure 2.1: Components of surface energy balance and accompanying fluxes. Blue box represents a glacier. From Oerlemans (2010).

Albedo is an important consideration in net radiation, and net shortwave radiation can also be expressed as $S(1-\alpha)$, where α is albedo. Surface energy balance equations sometimes contain expressions for direct and diffuse radiation, terrain irradiance, and other factors (Hock and Holmgren, 2005).

Another way to measure glacier change is by quantifying glacier length and area (i.e. Anda et al., 1985; Stearns, 2011; Paul et al., 2013; Leclercq et al., 2014). Glacier length and area changes can be measured with relatively high frequency (from monthly/seasonally to sub-decadal) and up to hundreds of years in the past, whereas glacier volume (mass) changes can only be done for years with available DEMs, which is usually at the multi-year to decadal scale (Pellicciotti et al., 2005; Hulth et al., 2013; Paul et al., 2013). Written glacier length changes go as far back as the 1600s, and glacier length and area can also be recreated using scientific techniques such as dating moraines and tills or through geographic feature mapping (Anda et al., 1985; Oerlemans, 1994; Hannesdóttir et al., 2015a). More recent glacier shape changes can be mapped from satellite or aerial imagery and terrestrial photogrammetry (Bjørk et al., 2012; Hill et al., 2018). As glaciers are sensitive to climate and have a relatively quick response compared to

other climate proxies, mapping glacier extent and recording fluctuations are crucial for climate system monitoring (Vaughan et al., 2013; AMAP, 2017). Mapping changes can also be useful for hydrological modelling and determining how seasonal runoff will change in the years to come.

Mapping glacier extent is useful for measuring seasonal fluctuations in glacier positions. Glaciers speed up in the spring/summer and slow down in winter, and the difference is much more pronounced for glaciers with floating tongues (Cuffey and Paterson, 2010; Howat et al., 2010; Kneib-Walter et al., 2021). Glacier tongues are extensions of the glacier that are within or on water; most marine-terminating glaciers have grounded or floating tongues. The seasonal changes in discharge of these glacier tongues are relevant for marine travel and trade in polar regions. Marine-terminating glaciers have noticeable seasonal changes, whereas land-terminating glaciers simply slow their retreat in winter as opposed to advancing (Cuffey and Paterson, 2010).

When glaciers change rapidly in ways different from their usual oscillatory seasonal pattern, this indicates that the glacier is not in equilibrium with the climate (Benn and Evans, 2010). There is currently a worldwide pattern of mass loss for glaciers with retreat rates of ~1 km over the 20th century, or close to10 m/yr (Leclercq et al., 2014). Occasionally, glaciologists observe a glacier changing at a noticeably different rate than glaciers that are in the same climate and region. This can sometimes be easily accounted for by obviously different dynamics, such as where the glacier terminus rests or the relative amount of solar radiation one glacier might receive over another. When the changes are not completely accounted for by these factors, this phenomenon requires further investigation**,** inspiring new studies and leading to new insights.

Mass changes occur within a glacier and at three glacier boundaries. These are surficial (at the glacier surface-atmosphere boundary), basal (along the base of the glacier), and frontal (at the vertical cliff of a glacier terminus) processes, with internal processes referring to those that

occur within the glacier (Fig 2.2; Cuffey and Paterson, 2010). These processes can be measured in a variety of ways such as through field work (e.g. measurement of ablation stakes and snow pits), remote sensing (e.g. geodetic changes in surface elevation and volume), or modelling (distributed degree-day mass balance or energy balance models; Hock, 2005; Benn and Evans, 2010; AMAP, 2017). A glacier can be separated into an accumulation and ablation zone, with the line delineating the boundary between them called the snowline (Fig 2.2). The accumulation zone experiences a net mass increase throughout a hydrologic year, where the ablation zone experiences a net mass decrease. The snowline is where accumulation and ablation are equal over a year, and its position changes from year to year. The 30-year average elevation of this line is called the equilibrium line altitude (ELA). There are several mechanisms that can lead to mass loss and mass gain of a glacier. Mass is mostly lost through melt or calving, but wind can also scour a glacier and avalanches can move mass from a different location to the glacier (Benn and Evans, 2010). Mass is gained mainly through solid precipitation or wind transfer during the winter season and retained throughout the summer (melt) season (Benn and Evans, 2010; Cuffey and Paterson, 2010).

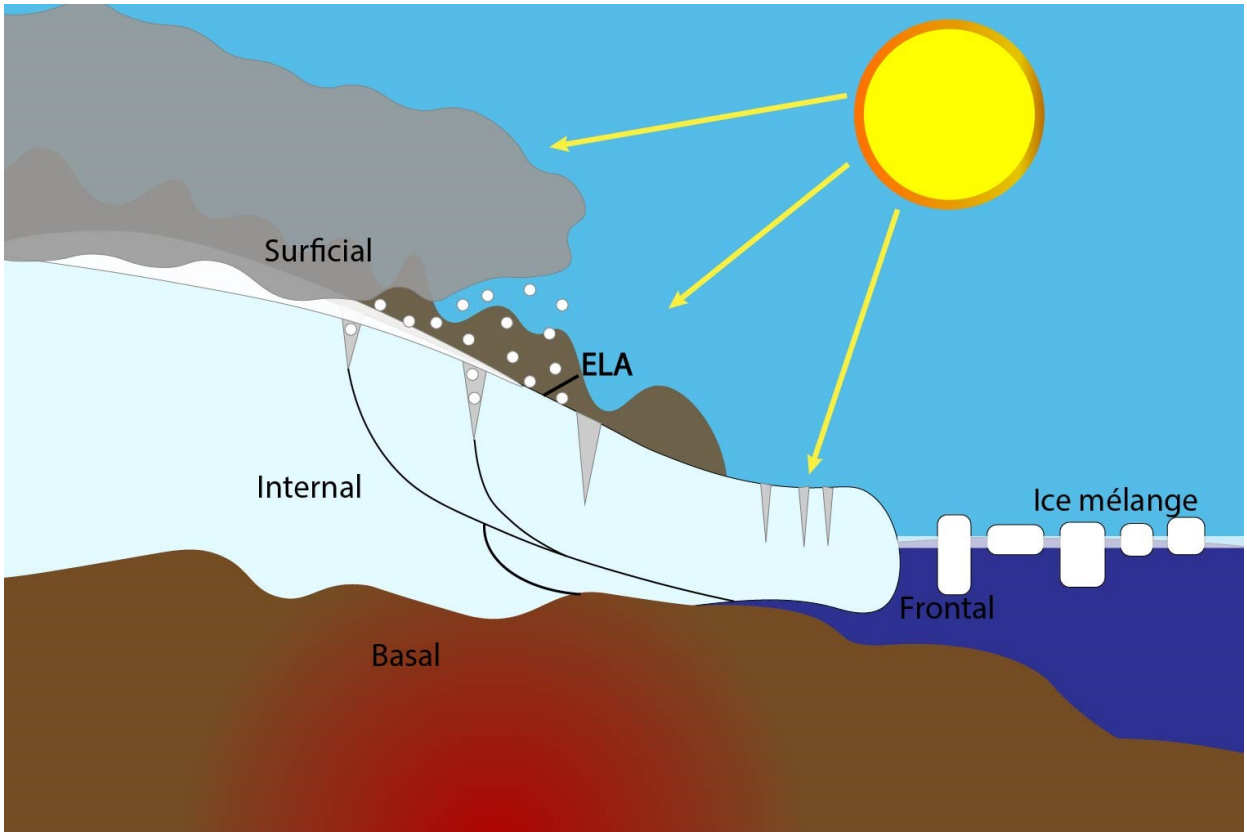

Figure 2.2: Diagram indicating the three glacier boundaries and one internal area included in mass balance studies. The equilibrium line altitude (ELA) is indicated as the average lowest elevation where snow from the previous winter still exists by the end of the melt season.

Surface processes tend to have the greatest control on the timing and intensity of mass loss, but factors that work on the glacier from below or at the glacier terminus (lowest end of the glacier) can have noticeable effects as well (van der Veen et al., 2007; Bartholomaus et al., 2013; Vaughan et al., 2013). These first order factors that control glacier melt are described in detail in Section 2.2.

Internal processes do not contribute to the loss of mass, but rather redistribute mass and heat energy (Cuffey and Paterson, 2010). Internal factors include the flow of meltwater through a glacier, channels that appear during the melt season, microfractures, and heat conduction through the firn (Benn and Evans, 2010; Cuffey and Paterson, 2010). The control on these are any source of energy within a glacier such as penetrating solar radiation near the surface, latent heat release

by refreezing, shear strain heating due to density or velocity differences within the glacier, and metamorphism from snow to firn to ice (Cuffey and Paterson, 2010). Internal processes tend to be erratic, and difficult to predict. Buried tephra (volcanic ash) and sediment can also affect internal processes by influencing ice crystal growth, and creating ice lens layers which affect the permeability of the ice (Dadic et al., 2013).

Changes in glacier mass can be based on physical measurements, geodetic measurements, or modelling. Snow accumulation (glacier mass gain) is generally measured using snow pits: a pit is dug in the accumulation zone of a glacier, and mass is calculated from the height and density of the snow layers deposited over the period of interest (usually over the last hydrological year; Hooke, 2005; Hulth et al., 2010). Ablation (glacier mass loss) is frequently measured using ablation stakes: stakes are drilled into the ice, and measurements taken at the beginning and end of the year are differed to ascertain mass loss (Hooke, 2005; Nield et al., 2013). Geodetic mass changes can be quantified by differencing elevation at different points on the glacier using topographic data from stereophotography, global positioning systems (GPS), or digital elevation models (DEMS), which are now often constructed from satellite data. Common models for mass balance include: temperature index, which determines melt energy from air temperatures only and are also called degree-day models (i.e. Huintjes et al., 2010; Wake and Marshall, 2015); radiation-enhanced temperature index which determines melt energy from temperature and radiation (Pellicciotti et al., 2005; Litt et al., 2019); and full energy balance models, which use all elements of energy balance (Eq 2.2), and require a full energy balance station (i.e. Hock and Holmgren, 1996; Hulth et al., 2010).

2.2. First Order Factors Influencing Glacier Accumulation and Ablation

2.2.1. Surficial Processes

Surficial processes include all processes that take place at the atmosphere-ice boundary, and are most often the dominant factor in mass balance for land-terminating glaciers (Hock, 2005; Benn and Evans, 2010; Cuffey and Paterson, 2010). The major surficial processes that affect mass balance are solid precipitation (snow), avalanche and wind deposition, melt, sublimation and refreezing of water. In some cases, these processes are solely accumulation or ablation processes, such as solid precipitation falling on a glacier or high atmospheric temperatures melting ice from above. Some are more complex, however, such as wind moving snow from glaciers, or liquid precipitation that can refreeze or contribute to melt. The processes of snowfall, melt, refreezing of water, and sublimation are largely dependent on humidity and temperature, and are thus well-understood. Avalanche and wind deposition are less predictable, but only significantly affect certain glaciers and thus can be studied on an individual basis (Benn and Evans, 2010).

The energy available for melt, sublimation and refreezing are given in the surface balance energy equation (Eq 2.2), of which the radiative and turbulent fluxes are the dominant components. Incoming solar radiation is important for melting of glaciers both by the transfer from radiant energy to thermal energy, increasing the temperature at the surface boundary, and by radiation penetrating deeper in the snow surface. Incoming solar radiation can penetrate snow to as deep as 1 m, and ice to 10 m (Hock, 2005). Cloud cover directly affects how radiation reaches a glacier's surface (direct or diffuse) and what kind of radiation is dominant (shortwave or longwave), and can influence air temperature and humidity as well (Hock and Holmgren, 1996; Hulth et al., 2013; Van Tricht et al., 2016). The effect of clouds and fog is the least understood

factor in the context of changing climatic conditions (Vavrus et al., 2011; Stocker et al., 2015). Clouds and fog can reduce glacier melt by shading a glacier from solar radiation, increase melt through enhanced longwave radiation and by affecting latent heat, and shroud satellite information (Hock and Holmgren, 1996; Mernild and Liston, 2010). Fog is directly in touch with the glacier surface, and so it can also alter the albedo (reflectivity) of the glacier by inducing growth of rime ice and affect the temperature and humidity directly at the surface of the glacier (Mortimer and Sharp, 2017).

The term "turbulent flux" refers to transport of a quantity by eddies (AMS, 2012). Sensible heat refers to energy stored in temperature alone, and latent heat is energy associated with phase changes. Sensible and latent heat will move along and in scale to gradients in their respective quantities, i.e., heat will move from a higher temperature area to a lower temperature area until the two areas are in thermal equilibrium, and the same for humidity, creating a turbulent exchange of heat and moisture (Oerlemans, 2010). These fluxes are important over all surfaces including oceans and land, and are important considerations in glacier mass balance, second only to radiation (Oerlemans and Klok, 2002; Acharya and Kayastha, 2018; Steiner et al., 2018). An example of a common turbulent flux over glaciers are katabatic winds, which are the result of the contrast between temperatures on ice-covered and ice-free areas, and the higher density of colder air (Benn and Evans, 2010). To estimate these turbulent fluxes, near-surface temperature and humidity gradients, along with wind speed, must be measured (Benn and Evans, 2010). These atmospheric effects are measured either through automatic weather stations placed directly on glacier surfaces, extrapolating from weather stations nearby, or from climate reanalysis.

Another process that can affect the surface melt regime of a glacier is the deposition of sediment, soot, or tephra (volcanic ash) on the ice or snow surface. This can occur through a variety of mechanisms, such as wind, rockslides, or gravity-induced deposition if the glacier is very near a volcano (Dragosics et al., 2016; Möller et al., 2016). Initially, this deposition of soot and sediment affects the amount of energy available for melt at the surface, of which the main control is the thickness of the deposit. The sediment thickness at which the energy effect switches from absorbing extra radiation and thus warming the glacier to insulating it from further air temperature-induced melt ranges from a few millimetres to a few centimetres depending on the size of the ash or sediment grains (Benn and Evans, 2010; Dragosics et al., 2016). Once these surface deposits are buried by an ensuing snowfall, they can continue to affect the glacier mass balance via englacial processes, as mentioned earlier.

2.2.2. Frontal Processes

Frontal processes occur at the terminus of a glacier, and include iceberg calving and submarine melt (Cuffey and Paterson, 2010). Calving is defined as the separation of ice blocks from a glacier's margin and can take place either on land (called "dry calving", takes place in situations such as when the glacier terminus is on a cliff) or, more commonly, in lake or marine waters (Benn and Evans, 2010; Cuffey and Paterson, 2010). It is an important ablation process that often accounts for most of the mass loss from a marine-terminating glacier (Benn and Åström, 2018). The greatest control on marine calving is ocean temperature and bathymetry (Bartholomaus et al., 2013; Benn and Åström, 2018). Ocean temperatures are currently rising (+0.78°C between 2003-2012; Stocker et al., 2015) and warm currents are moving onto continental margins where glaciers meet the ocean (Murray et al., 2010). Due to these increases in temperature, especially in the ocean where glacier tongues terminate or float, calving rates are

expected to rise throughout this century (Østerhus and Gammelsrød, 1999; Lloyd et al., 2011; Luckman et al., 2015).

For the floating part of marine-terminating glaciers, icebergs do not directly contribute to sea level rise but rather the loss of ice mass at the terminus reduces the glacier's restraining force on the ice upstream, which in turn will flow faster towards the sea (Joughin et al., 2012). In fjords in front of a calving margin ice-mélange may form, which is a combination of sea ice, icebergs, and snow that freezes together during the winter and provides a small but influential backwards force, pushing on the calving face of the glacier and thus reducing the number of calving events. This restraining force is called the "buttressing effect", and is also important for the stability of ice shelves (Fürst et al., 2016). According to studies in fjords in Alaska, Greenland, and Svalbard, spring breakup of sea ice and ice mélange is often correlated to the start of a year's calving events, causing a seasonal pattern in calving (Fig 2.3; Reeh et al., 2001; Benn et al., 2007; Amundson et al., 2010; Howat et al., 2010; Robel, 2017). The relationship between calving and ice mélange breakup is only understood in a broad sense, and the effect of sea ice buttressing on glaciers that calve into the open ocean (as opposed to fjords) is even less well-studied. An additional water-ice interaction that can affect this buttressing is the ability of freshwater runoff to increase the likelihood of sea ice forming (Bintanja et al., 2013). Freshwater has a higher freezing point than highly saline water, but the extent to which this self-stabilizing process prevails is not well-understood (Robel, 2017).

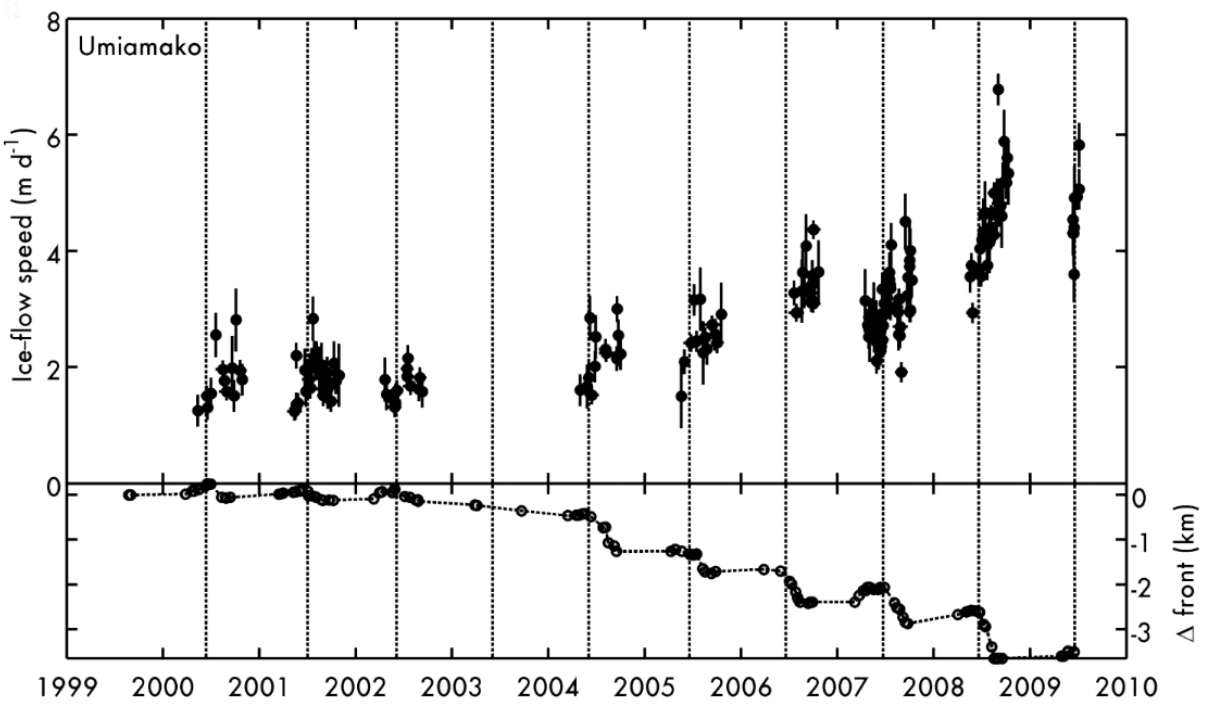

Figure 2.3: Observed relationship between ice front position and sea ice conditions for Umiámáko, central West Greenland. Dotted vertical lines indicate first ice-free day of year. From Howat et al. (2010).

Controls on the size of the icebergs that calve include the size of the glacier from which they calve and depth of the water at the front (Benn et al., 2007). Most calving consists of smaller pieces breaking off, but large calving events have the largest net effect (Benn and Åström, 2018). A single block breaking off is often taller than it is wide, and buoyant forces cause it to rotate to achieve equilibrium. Both the initial calving and the rotation can create large waves that endanger any ships nearby.

Calving is difficult to study, as it involves unstable blocks of ice disintegrating in an unpredictable manner. It is therefore most often studied using satellite imagery, timelapse photography, and seismic records, or a combination thereof. Satellite imagery and photography can give an indication of the size, exact location, and to some extent the physical mechanisms of a calving event over different temporal scales (Vieli and Nick, 2011; Walter et al., 2012). Passive seismic studies use the same seismic instrumentation that are used for detecting earthquake

tremors. These instruments are generally broadband, which means they record over a large range of frequencies, and can be situated on rock or ice for glacial studies (Podolskiy and Walter, 2016; Aster and Winberry, 2017). Seismic signals can determine the general direction of the epicenter of an event, or if there is enough instrumentation and the event is large enough, an approximate location.

2.2.3. Basal Processes

Basal processes occur at the bedrock-ice interface and can include accumulation and ablation mechanisms. The processes that govern basal mass balance are more complicated than surface or frontal processes, and involve prevailing ground or ocean temperature and availability of liquid water (Cuffey and Paterson, 2010). The thermal state at the base of a glacier (i.e. frozen or lubricated by liquid water) greatly affects its flow, and the three main sources for basal heat are basal friction through ice motion (sliding over the bed), strain heating, and geothermal heat (van der Veen et al., 2007). Ablation occurs through melting at the base of the glacier by warm ocean currents if the ice rests on water, or through warming at the rock-ice interface by geothermal heat. During the ablation season, channels of relatively warm water can flow at the base of a glacier, which will also contribute to mass loss. Accumulation can occur when water freezes onto the base of the glacier as basal channels develop, and can be significant in special cases and in ice shelves (Cuffey and Paterson, 2010).

The cases in which geothermal heat is considered in glacier mass balance are rare, as most often basal melt rates are negligible in comparison to surficial processes except in volcanic regions such as Iceland or South America (Magnússon et al., 2005; Rivera et al., 2012; Jóhannesson et al., 2020). However, recent ice mass loss estimates in Greenland have proven inconsistent with observations, and the inconsistencies are likely related to how GHF is

approached (Greve, 2005; van der Veen et al., 2007; Rysgaard et al., 2018). In models, GHF is generally assumed to be a constant value based on the type of bedrock and thickness of earth crust beneath the glacier, and thus a single value is applied to the entire area covered by the model. This has become problematic for the larger ice sheets, which cover an area that could have a widely variable GHF regime. For example, in northern Greenland the basal melt rate was found to be ~0.2 m/yr; a value much too high for the assumed GHF of 57 mW/m^2 (corresponding to basal melt of ~0.005 m/yr; Dahl-Jensen et al., 2003; van der Veen et al., 2007). This prompted further study, and very recently it has been shown that GHF ranges from ~20 mW/m^2 in the south to ~140 mW/m^2 in central Greenland (Fig 2.4; Rysgaard et al., 2018). Although GHF is most often highest in deep valleys where the earth crust is thinner, one cause of large changes in GHF over relatively small distances is local volcanic activity and mantle plumes. This could be the source for the areas of high geothermal heat in Greenland and Iceland (Fahnestock et al., 2001; Rysgaard et al., 2018).

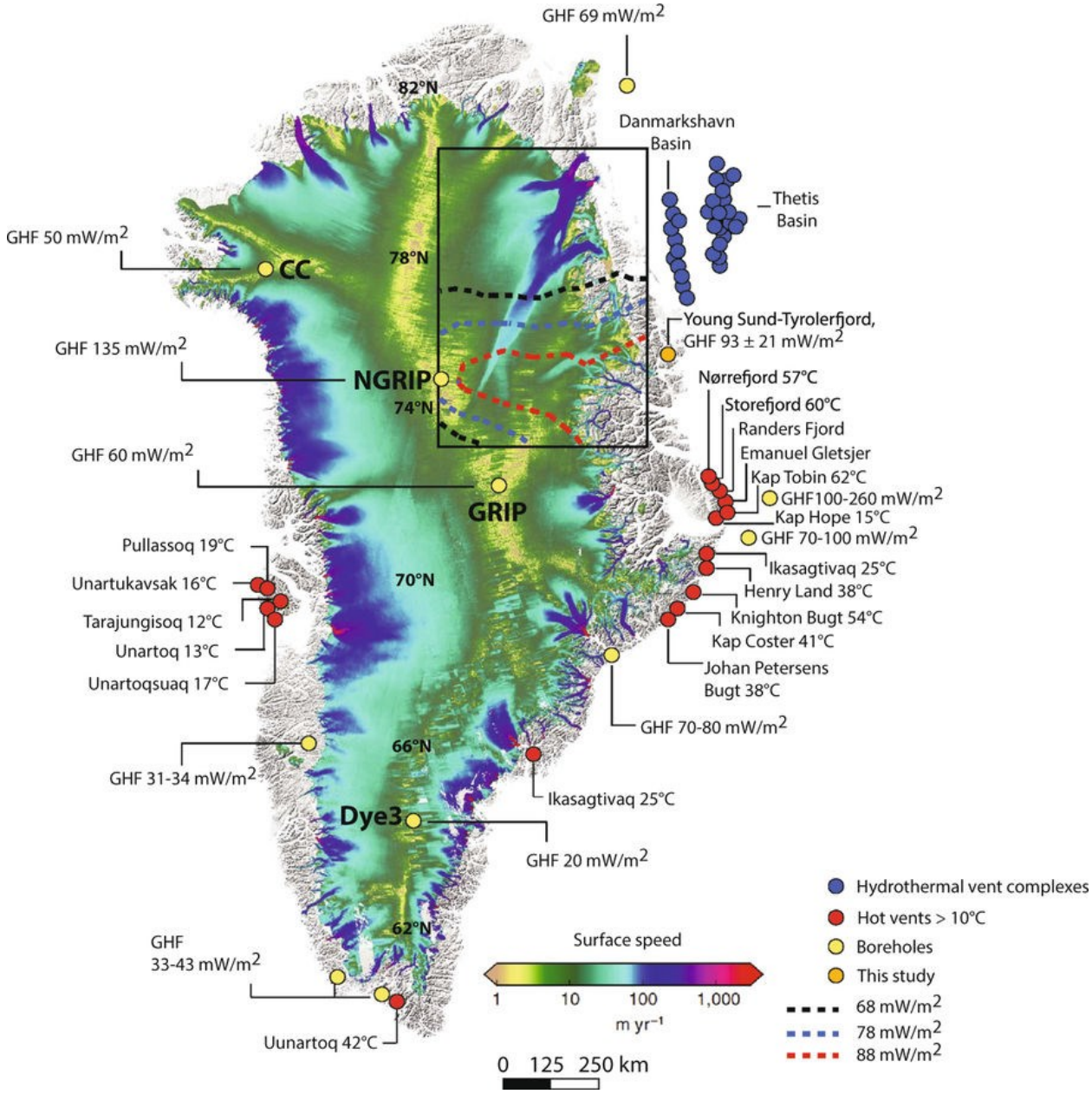

Figure 2.4: Locations of measured GHF and geothermal vent temperatures, including some implied contours in the Northeast. Note the large changes along the east coast, from 20 mW/m^2 at Dye3 to as high as 260 mW/m^2 at GHF. From Rysgaard et al. (2018).

The magnitude of the GHF beneath a glacier resting on or near a volcano is much higher than glaciers overlying thick continental crust, and GHF can increase very quickly during and just before volcanic eruptions (Smellie and Edwards, 2016). This becomes relevant to glacier-clad volcanoes, which can respond to these changes in geothermal heat by increasing flow, creating basal lakes, or by outburst floods (van der Veen et al., 2007; Rivera et al., 2012). Recent studies

indicate that volcanic activity can influence glaciers more substantially than other first-order factors in some cases (Reinthaler et al., 2019; Jóhannesson et al., 2020). This directly affects populated centers in areas such as Iceland, where there are many active volcanoes underneath the ice, and outburst floods are common (Björnsson, 2011). Studying volcanoes and the GHF underneath an ice sheet is inherently difficult, however, and it would be easier to understand volcanic activity underneath an ice cap or glaciers and search for proxies of similar behavior.

2.3. The Importance of the Arctic, and Jan Mayen's Place Within It

All glaciers on Earth could together add 0.41 m to sea level, and Arctic land ice accounted for 35% of sea level rise between 2004-2010 (IPCC, 2019b). One way the Arctic Circle is defined is as the region north of the 66°34'N latitude (Fig 2.5; NSIDC, 2020). This latitude marks the furthest south point at which the sun does not set on summer solstice and does not rise on winter solstice. However, there are different ways of defining the Arctic such as the tree line or temperature (Fig 2.5). Arctic land consists of parts of the USA (Alaska), Canada, Finland, Greenland, Iceland, Norway, Russia, and Sweden. This study focuses on the four glacierized regions of the North Atlantic sector of the Arctic, directly surrounding the island of interest Jan Mayen. These are Greenland, Iceland, Svalbard, and Scandinavia.

Figure 2.5: Arctic region political map from 2002, with three lines corresponding to different definitions of the "Arctic". Blue dashed line indicates 66°34'N, green line indicates the point at which the landscape is frozen and there are no trees, red line indicates where the average daily summer temperature is below 10° C. Jan Mayen circled in black. From https://nsidc.org/cryosphere/arctic-meteorology/arctic.html.

Ocean circulation patterns drive broad weather patterns and are an important control on regional climate and sea ice extent (Fig 2.6; Hidore et al., 2010). Along the west coast of Norway flows the warm and highly salinated North Atlantic Current, which returns as the cold East Greenland Current flowing southward to merge with warmer currents near the coast of Iceland (Hurrell et al., 2003). Ocean and climate circulations have natural oscillations at a variety of time scales. Additionally, the regions around Jan Mayen are subject the Northern Atlantic Oscillation (NAO), an important atmospheric oscillation. NAO is measured by the difference between the Subtropical High (near the Azores Islands) and the Subpolar Low pressure (southwest of Iceland) systems at sea level. A "positive" phase of the NAO results in higher temperatures in the eastern United States and northern Europe, cooler temperatures in Greenland, increased precipitation in northern Europe, and decreased precipitation in southern Europe, while a negative phase will show opposite temperature and precipitation trends (NOAA, 2020). The NAO can also cause changes in the North Atlantic jet stream and storm track. Positive and negative phases of the NAO change quickly, normally lasting only one to a few months.

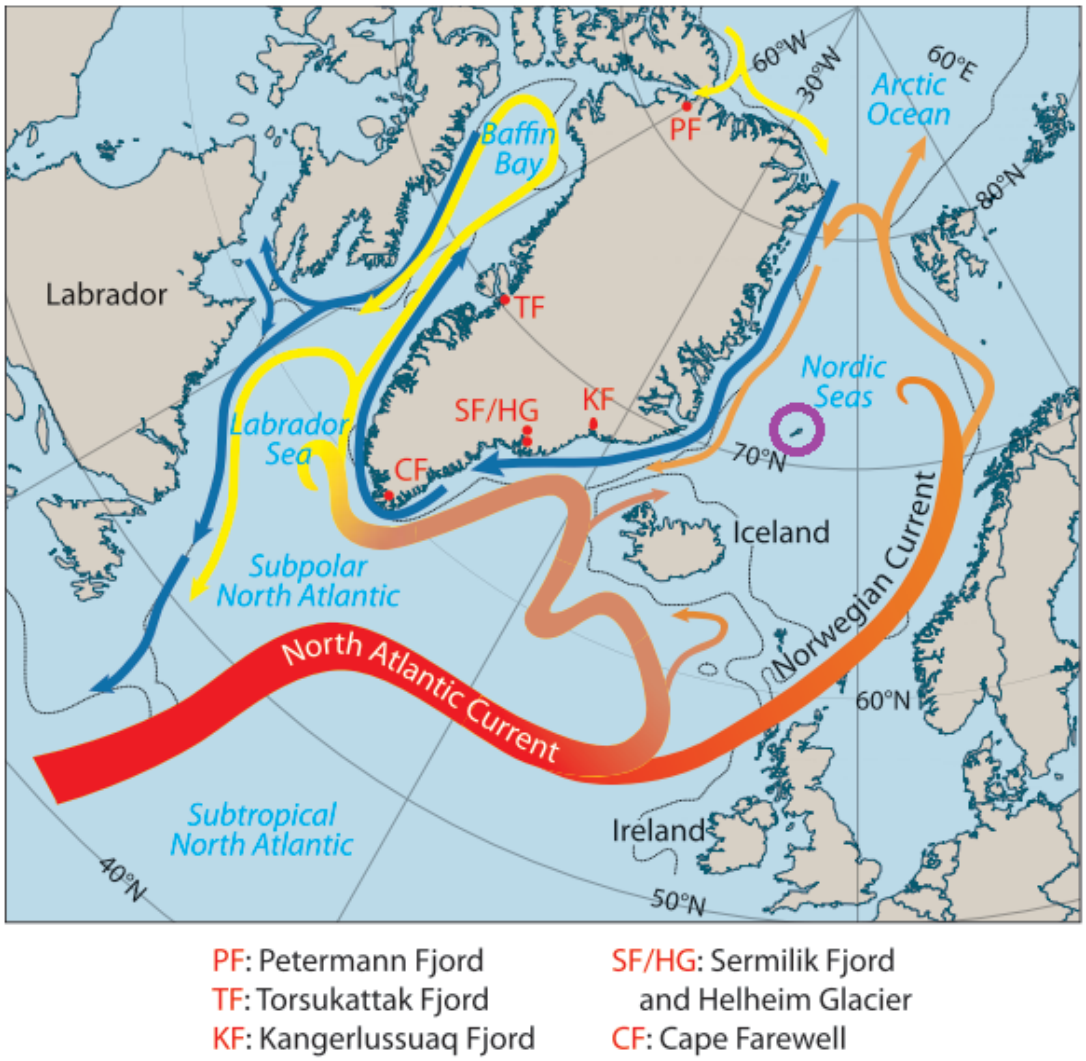

Figure 2.6: Greenland, Svalbard, Scandinavia, and Iceland in context of ocean currents which deliver heat to the glaciers. Jan Mayen Island circled in purple. Modified from AMAP (2017).

Below is presented information on population, exports, and glaciers statistics for Greenland, Svalbard, Iceland, and Scandinavia. For three of these four regions, a literature review yielded average retreat rates for years 2000 and later. However, such a value for Iceland could not be found. Therefore, a second technique was applied to all four regions: the world glacier monitoring system (WGMS) has a Fluctuations of Glacier (FoG) database (WGMS, 2021), aimed to provide global glacier changes at two-year intervals (WGMS, 2021; https://wgms.ch/data_databaseversions/). Using data from the WGMS FoG database,

observations from 2000 and later were converted into a yearly rate for each glacier, then the average of these was calculated.

2.3.1. Greenland

Greenland has an estimated population of 56 081 in 2020, located mostly on the southwest coast (Statistics Greenland, 2020). Most (90%) of Greenland's exports are fishing, and so changes in amount and timing of glacier runoff are important as these dictate the life cycle of the fish (Walsh, 2017). The Greenland Ice Sheet is the smaller of the two ice sheets currently on Earth, with 1 808 568 km^2 total ice area, about 4% of which is held by glaciers not attached to the ice sheet (Pfeffer et al., 2014; RGI Consortium, 2017). It also contains the world's fastest glacier, Jakobshavn Isbrae (or Sermeq Kujalleq), which can move in excess of 30 m/day (Joughin et al., 2020). It is difficult to understate the influence of mass loss from Greenland, as in addition to changes to sea level, this cold freshwater influx affects thermohaline circulation. Cooling of the Gulf Stream affects weather in Europe, and could result in increased storm severity (AMAP, 2017). The glaciers in Greenland that are not considered attached the ice sheet lost 4.0 ± 1.5 km^3/yr through solid discharge in 2010-2020 (Table 2.1; Kochtitzky et al., in prep), and the average retreat rate for these same glaciers from literature review increased from -8 m/yr for 1980-2000 to -19 m/yr for 2000-2010 (Bjørk et al., 2012). According to manipulation of data from the WGMS FoG database (WGMS, 2021), average retreat rate for Greenland glaciers after 2000 was -18 m/yr, although this might include some glaciers that are attached to the ice sheet.

Table 2.1: Relevant summarized information for the four Arctic regions surrounding Jan Mayen. No. of Glaciers column includes the number of marine-terminating glaciers in parentheses. Values for Greenland refer only to the glaciers not considered attached to the ice sheet, except perhaps for the FoG retreat rates. References in text except sea level equivalence, which is from AMAP (2017). Values for Frontal Ablation based on Kochtitzky et al. (in prep) as of 1 Dec 2021.

Region	No. of glaciers (marine-term.)	Glacierized area (km^2)	% Ice cover	Sea level equivalence (mm)	Frontal Ablation 2010-2020 (km^3/yr)	Lit. ret. rate 2000+ (m/yr)	FoG ret rate 2000+ (m/yr) (No. of glaciers)
Greenland	17500 (534)	130071	0.6	53	4.0 ± 1.5	-19	-18 (86)
Svalbard	1567 (157)	33959	55	24	12.4 ± 13.5	-40	-64 (8)
Iceland	568 (1)	11060	11	11	0.08 ± 0.12		-37 (24)
Scandinavia	3417 (0)	2949	0.4	0.6	0	-20	-20 (66)

2.3.2. Svalbard

Svalbard is a Norwegian archipelago comprised of nine islands. It is a common jest that there are more polar bears on Svalbard than people; however, the human population is estimated at 2 939 in 2020 while the polar bear population is estimated closer to 270 (Aars et al., 2017; Statistics Norway, 2020). Svalbard is mostly used for used for coal mining, research, and tourism. While most of the research and tourism is focused around wildlife and the Aurora Borealis, glaciers are another important attraction. Jan Mayen glaciers are often grouped with Svalbard (e.g. Hagen et al., 1993), as they are both a part of the Kingdom of Norway, but Svalbard without considering Jan Mayen glaciers contains 1567 glaciers covering 33 959 km^2, or ~55% of the archipelago (Pfeffer et al., 2014; RGI Consortium, 2017). The highest elevation on the archipelago is only 1717 m a.s.l., thus, most glaciers on Svalbard have a gradual slope. Additionally, a large proportion of the glaciers in Svalbard are of surge-type (Lefauconnier and Hagen, 1991; Jiskoot et al., 1998; Sevestre et al., 2015). A surging glacier oscillates between long "quiescent phases" and short "surging phases" (Jiskoot, 2011). During a surging phase, the ice flow abruptly increases to 10-1000 times faster than normal flow, and this behavior can obscure the climate signal (Yde and Paasche, 2010). Svalbard's glaciers have not seen as dramatic an

increase in mass loss as many other Arctic regions for the past 50 years, with the exception of 2013 (AMAP, 2017). In this year, the melt in Svalbard was unusually high and corresponded with atmospheric circulation in a south-south westerly flow over Svalbard (different from the usual west-southwesterly flow). If this relationship holds true, the relatively small glacier mass loss could be due to the recent shift of atmospheric circulation to a northwesterly flow. Even with small increases in rate, in 2002-2010 Svalbard glaciers' mass loss rates were among the highest in the world and had the most negative mass balance years for Svalbard in the past 50 years (AMAP, 2017). Marine-terminating glaciers in Svalbard had an ice flux of 12.4 ± 13.5 for 2010-2020 (Kochtitzky et al., in prep; Table 2.1). Average retreat rates for Svalbard glaciers according to literature were -40 m/yr for 1990-2007 (Nuth et al., 2013). This observation does include some extreme surging behavior (±150–350 m/yr), which can skew the number in either direction but in this case likely toward a more negative value. Average retreat rates from manipulation of data from the WGMS FoG database yields a much higher rate of -64 m/yr.

2.3.3. Iceland

The island of Iceland has an estimated population of 364 134 (Statistics Iceland, 2020), with 60% of the population located near Reykjavik. Iceland's main exports are aluminum smelting, fishing, and tourism, the latter likely due to the 48 volcanoes located on the island, 31 of which are considered active (International Trade Administration, 2019). Iceland is the southernmost of the four Arctic regions considered in this thesis and has the warmest climate. The highest mountain in Iceland reaches an elevation of 2110 m a.s.l. Therefore, the glaciers on Iceland are likely steeper than those in Svalbard**,** and as they are in a marine climate they experience high ablation as well as high accumulation (AMAP, 2017). This high turnover rate means these glaciers are more sensitive to atmospheric warming. As these glaciers are almost all

on active volcanoes, basal processes can be dominant mass loss mechanisms (Jóhannesson et al., 2020). Iceland has an ice area of 11 060 km^2, covering ~11% of the island. The most important long-term glacier fluctuation study on Iceland is on the Vatnajökull ice cap, which has observations going back to 1650 (Hannesdóttir et al., 2015a, 2015b). Iceland had only one marine-terminating glacier for the period of this study, and its ice discharge was 0.08 ± 0.12 km^3/yr for 2010-2020 (Kochtitzky et al., in prep; Table 2.1). While a number for average retreat rate for Iceland glaciers after 2000 could not be found through literature review, manipulation of data from the WGMS FoG database yielded -37 m/yr.

2.3.4. Scandinavia

For the purposes of this study "Scandinavia" refers to Norway and Sweden, as their glaciers are grouped together in the RGI and Denmark does not currently have glaciers. Scandinavia is the most populated of the four Arctic regions considered in this thesis, with 5 432 580 people in Norway in 2020 (Statistics Norway, 2020), and 10 379 295 in Sweden in 2020 (Statistics Sweden, 2020). Scandinavia is famous for its fjords and other glacially sculpted landscapes, and polar conditions are central to Scandinavian culture. Due to increased temperatures and ablation, Sweden's highest point lowered in 2019 from 2095.6 m a.s.l. to 2096.8 m a.s.l., as the glacier on the southern peak of Kebnekaise melted to below the height of the non-glaciated norther peak (Rosqvist, 2019). Norway's highest point is 2469 m a.s.l. The total ice area of Scandinavia is 2949 km^2, or 0.4% of the land area of Norway and Sweden combined. Norway has many of the largest glaciers of mainland Europe, even though ice covers only ~1% of the mainland. Scandinavian glaciers are maritime, thus, similarly to Iceland, experience large amounts of both ablation and accumulation. If summer temperatures increase by 2 ºC, ~98% of Norway's glaciers will be gone by 2100 (Nesje et al., 2008). There were no marine-terminating

glaciers in Scandinavia during the period of the study (Pfeffer et al., 2014; RGI Consortium, 2017). Average glacier retreat rates in Norway according to a literature review were -5.5 m/yr for 1990-2000, and increased to -20 m/yr for 2000-2018 (Table 2.1; Winsvold et al., 2014; Andreassen et al., 2020). Average retreat rates after 1999 from manipulation of data from the WGMS FoG data for Norway and Sweden yielded -20 m/yr.

Glaciers play an important role in the economics and geology of all four of these regions, and these glaciers are changing rapidly. Many subtle factors could affect these changes, and it would be useful to have observations at a point in the middle of these important atmospheric and oceanic circulations. This brings us to the island of Jan Mayen.

2.4. Study Area

2.4.1. Introduction to Jan Mayen

The island of Jan Mayen (71.0° N, 8.3° W) lies upon the Mid-Atlantic Ridge at the northern tip of the Jan Mayen Ridge and south of the seismically active Jan Mayen Fracture Zone. The island is 53.6 km long and 15.8 km wide at its widest point, covering a total area of 381 km^2 (Skreslet et al., 2004). It is remote, being 550 km east of the nearest landmass of Greenland, and 650 km north of Iceland. Jan Mayen has the northernmost subaerial volcano, Beerenberg, which is still active with 6 eruptions since 1732 (Anda et al., 1985; Hagen et al., 1993). It reaches a height of 2277 m a.s.l. – higher than any mountain in Iceland or Svalbard, and most in Norway and the Greenland periphery. The most recent bedrock addition on Jan Mayen is from the 1970 eruption of Beerenberg (Orheim, 1993).

Jan Mayen island is the northern end of the Jan Mayen microcontinent, which extends 500 km southwards and contains the ridge that separates the Norwegian Sea from the Greenland

Sea (Kodaira et al., 2000). The microcontinent lies between the active Kolbeinsey Ridge to the west, the inactive Aegir Ridge to the east, and the Jan Mayen Fracture Zone which runs roughly northwest-southeast to the north (Fig 2.7). South of Jan Mayen is a continental platform that is relatively shallow (no deeper than 200 m below sea level for ~50 km south), while to the north the bathymetry drops off steeply to depths of 1000 m below sea level within 5 km offshore (Fig 2.7; NOAA, 2021). Jan Mayen and much of the continental platform south of it was covered by a large ice cap until 17–16 cal. ka BP, when the ice cap retreated into the glaciers that are now present on the flanks of Beerenberg only (Lysså et al., 2021).

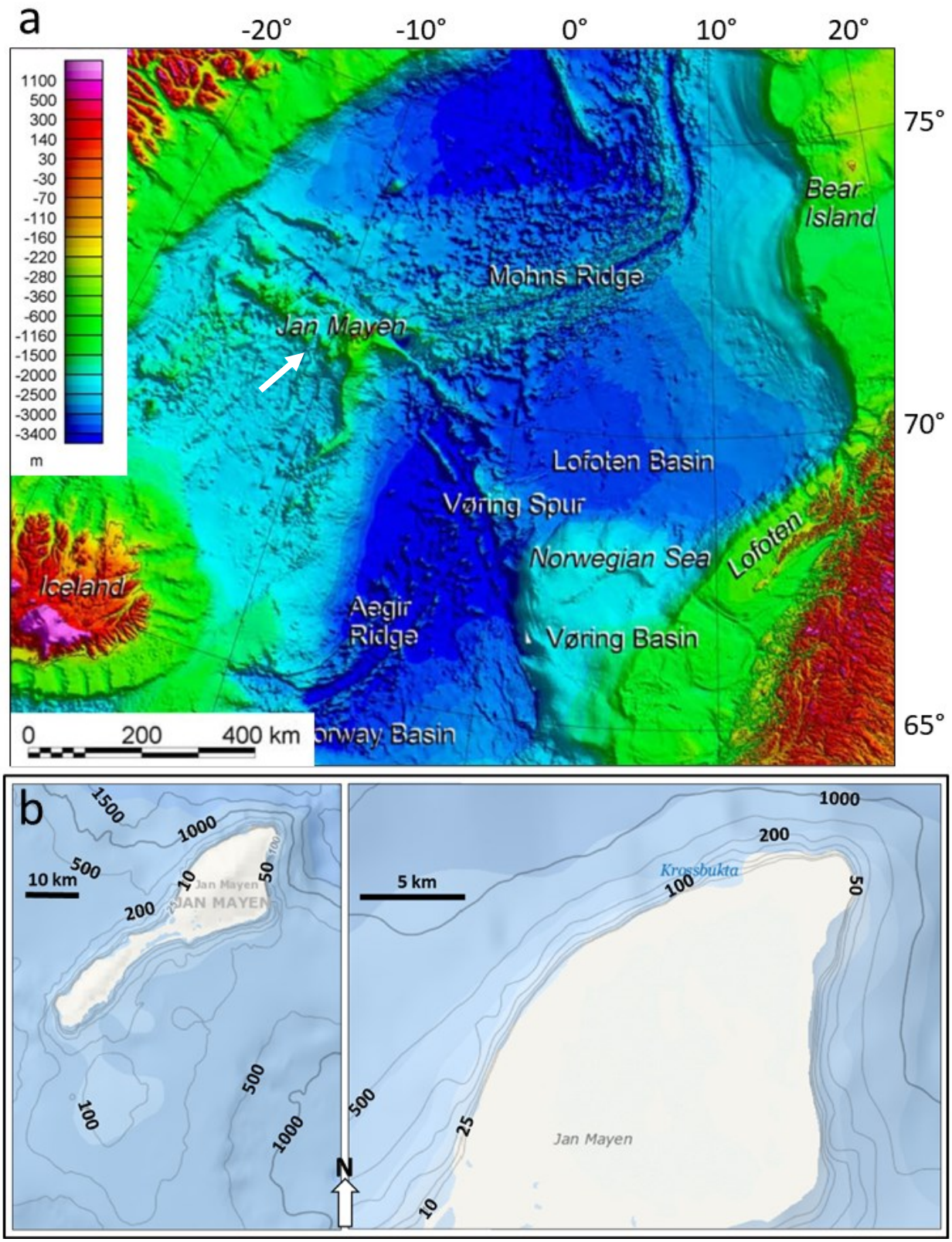

Figure 2.7: Bathymetry of Jan Mayen and surrounding areas at increasing scales; a) Jan Mayen indicated by white arrow; modified from Olesen et al. (2010). b) contours in meters, modified from https://www.ncei.noaa.gov/maps/bathymetry/

Discovered by Dutch whalers in the summer of 1614, Jan Mayen has a long history of scientific observations (Skreslet et al., 2004). Glacier observations go as far back as 1861, and weather observations on the island are unbroken since 1921 (Anda et al., 1985; Hagen et al., 1993). Whalers have visited Jan Mayen for over four centuries (Vogt, 1863; Skreslet et al., 2004), and there have been frequent visitors to the island. A permanent human presence was not established until 1921, but the population is only enough to upkeep the meteorological station and navigational facility run by the Norwegian government, and the occasional scientific study (Skreslet et al., 2004). The population is neither perennial (shifts tend to be 3-6 months) nor large (12-20).

2.4.2. Weather and Climate

Jan Mayen has a polar maritime climate, with only small fluctuations in temperature throughout the year. Mean annual average temperature was -1.4°C for 1961-90, and the mean annual precipitation sum was 682 mm (Hulth et al., 2010). The warmest months are July and August, the rainiest months September and October, and wind is consistently between 4 and 8 m/s year-round. Wind and precipitation generally come from the north or northwest, implying that the north- and west-facing glaciers of the island receive the greatest accumulation (Anda et al., 1985; Orheim, 1993). This could also imply that ice is scoured from the glaciers on this side and deposited by wind on the east- and south-facing glaciers (Hulth et al., 2010). However, each glacier creates its own microclimate, and studies on Jan Mayen indicate that winds on a glacier are dominantly from upstream of the glaciers irrelevant of its aspect (i.e., katabatic winds).

Those who have visited Jan Mayen are familiar with the persistent fog; maps of Jan Mayen dating back to 1860 portray this (Vogt, 1863). As it is a small island surrounded by hundreds of miles of ocean, there is a constant source of moisture and thus there is frequent cloud

cover (Orheim, 1993; Skreslet et al., 2004). On average, less than 5 days a year are completely clear, and only 0.2 days are clear for June through September (Steffenson, 1982). This has been noted as a great difficulty when it comes to applying remote sensing to this location, as finding cloud-free satellite data is difficult, especially during the ablation season (Orheim, 1993). Temperature inversions are common in coastal areas and usually accompany fog (Gultepe et al., 2007; Gilson et al., 2018), and, indeed, Jan Mayen has a persistent elevated temperature inversion (Hulth et al., 2010). The tops of the low clouds are generally around 1000 m a.s.l., which is an approximate indication of the top of the inversion as well (Anda et al., 1985; Orheim, 1993; Skreslet et al., 2004; Hulth et al., 2010). A single observation on 4 Sep 2008 measured an inversion base at 900 m a.s.l. and inversion top at 1200 m a.s.l., indicating the temperature inversion is not always at the toe of the glaciers (Hulth et al., 2010). Jan Mayen is located between two major surface ocean currents: the warm North Atlantic and cold East Greenland Currents (Fig 2.6). These greatly affect patterns of air temperature, precipitation, and cloudiness or fogginess on the island. Fig 2.8 shows the average annual ocean temperature and surface current pattern around Jan Mayen.

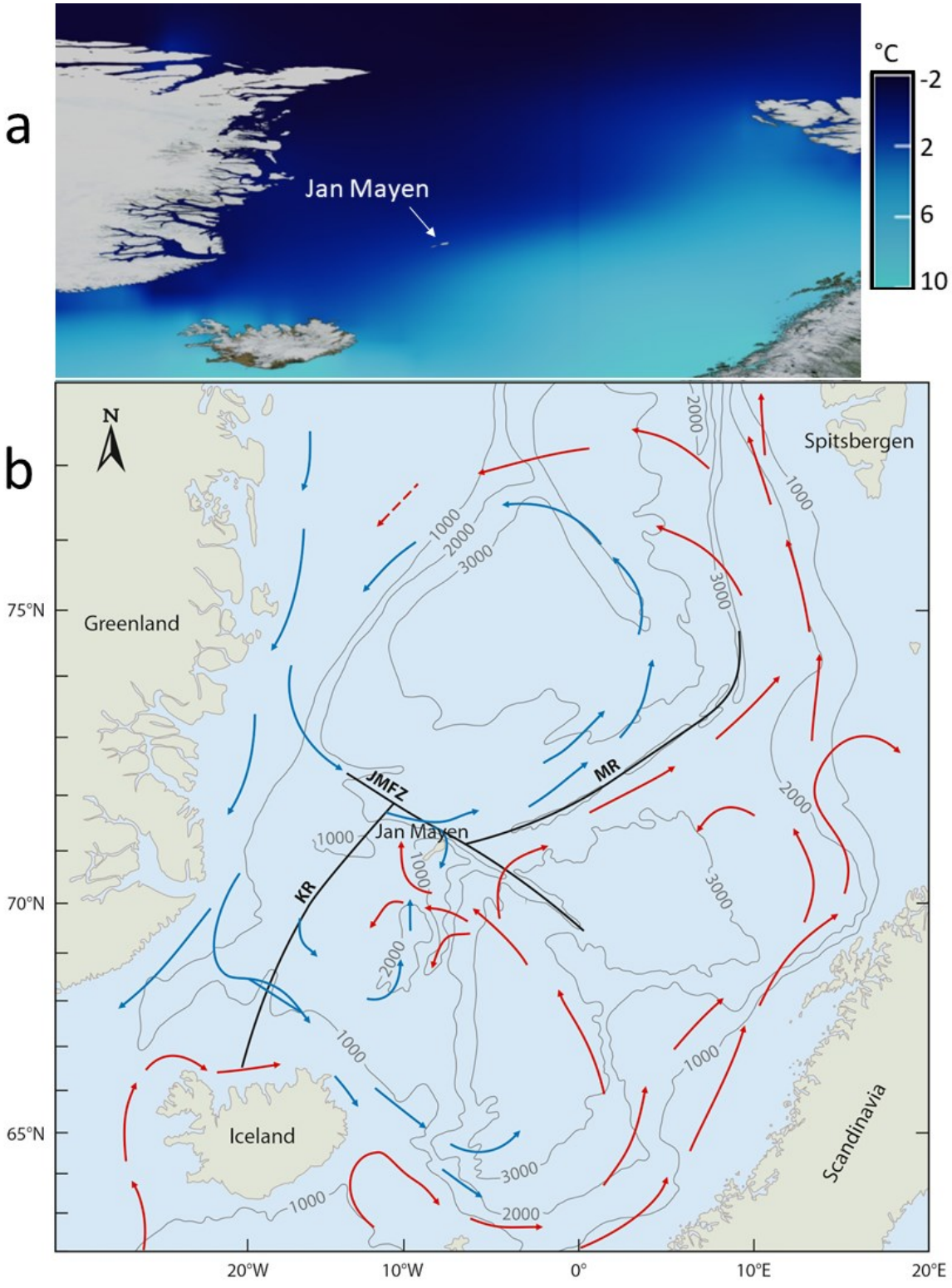

Figure 2.8: Jan Mayen's location within a) annual average SST (image from https://svs.gsfc.nasa.gov/3652; data from Locarnini et al., 2006) and b) main circulation of warm North Atlantic (red arrows) and cold East Greenland surface currents (blue arrows). Bathymetry in 1000 m contour interval, KR = Kolbeins Ridge; MR = Mohns Ridge; JMFZ = Jan Mayen Fracture Zone. From Lysa et al. (2021).

2.4.3. Glaciers and Previous Glaciological Studies

Jan Mayen is a somewhat simple location: it has only one mountain instead of being situated in a highly complex mountainous region, and the glaciers are of the single-basin type, have no tributaries, and are relatively easy to separate into individual ice flow units of comparable sizes with distinct basins. However, each glacier is in itself a case study: some are marine-terminating, some overlie volcanic fissures, and some are more often enshrouded in fog than others. Factors that make glacier changes on Jan Mayen unique are the glaciers' positions on a steep active volcano, and the maritime locale with frequent temperature inversions and fog.

The volcano Beerenberg has 20 named glaciers that drain radially from its steep flanks (Fig 2.9). These covered 118 km^2, 31% of the island, in 1975, and this number has yet to be updated (Hagen et al., 1993; Pfeffer et al., 2014; RGI Consortium, 2017). In fact, there have not been systematic measurements of glacier fluctuations for the entire island since 1975. Even the glacier outlines in the Randolph Glacier Inventory (Pfeffer et al., 2014; RGI Consortium, 2017) are based on glacier extent data from aerial photos from 1949-1975 and before (and were hand-traced from the maps in Hagen et al., 1993), and these do not accurately reflect the shape of the glaciers, as well as including several snow patches misclassified as individual "glaciers" (Hagen et al., 1993). These glaciers are numbered counterclockwise, with Sørbreen as #1.

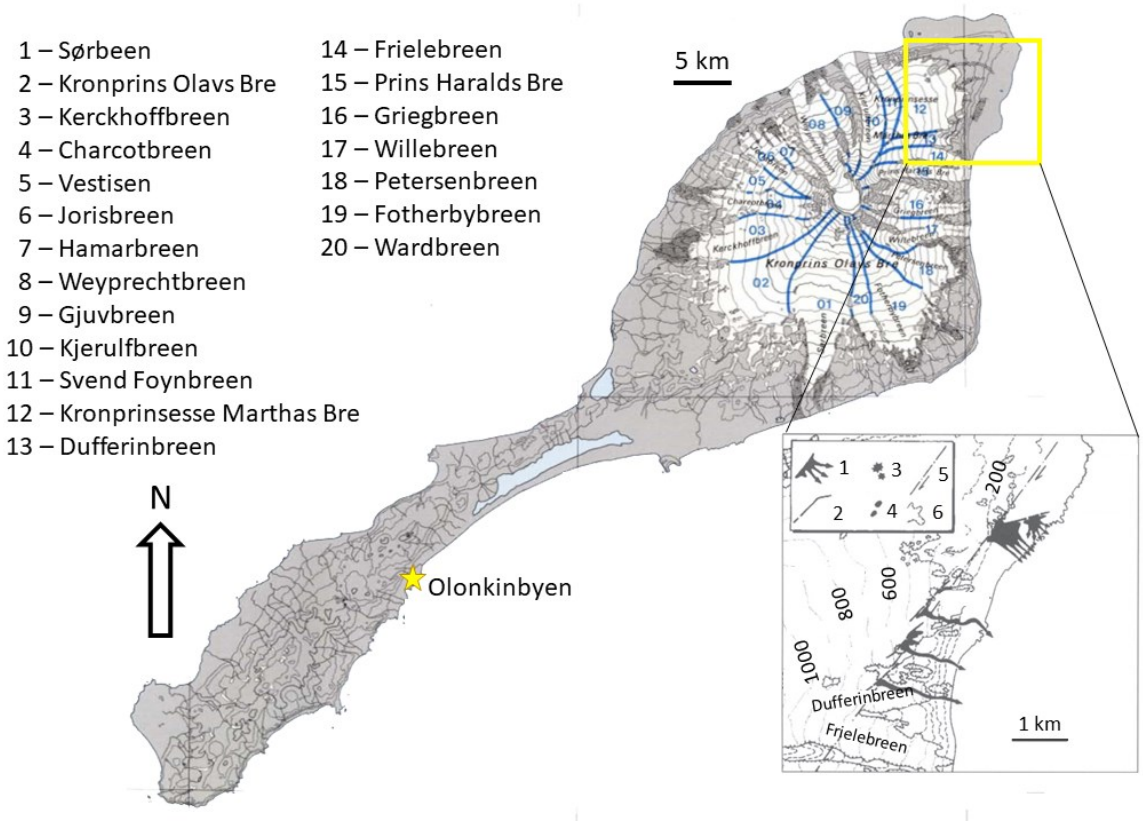

Figure 2.9: Map of Jan Mayen, with glacier outlines and names corresponding to GLIMS ID numbers. Modified from Hagen et al. (1993). Inset shows location of 1970 eruption. 1 -lava streams; 2 - main eruption fissures; 3 - active craters; 4 - extinct craters; 5 - probable course of deep-seated dextral strike-slip fault; 6 - glacier margin. Modified from Skreslet et al. (2004).

Jan Mayen glaciers are steep, descending ~2000 m over 4-9 km (Fig 2.10, Table 2.2). The highest elevation a glacier on this island reaches is 2260 m a.s.l, which corresponds to the glacier Jorisbreen, originating on the west side of Beerenberg's central crater (#6 in Fig 2.9; Pfeffer et al., 2014; RGI Consortium, 2017). Jorisbreen is land-terminating, but its terminus is only ~2 km from a marine-terminating glacier: this phenomenon of marine- and land-terminating glaciers side by side is one reason to conduct glaciological research on Jan Mayen, as the climate and forcings each glacier is subject to will be relatively similar except for conditions at the terminus and individual glacier characteristics. All glaciers on the island are highly crevassed, which may be due to a combination of the steep slope, uneven basalt layers, differential geothermal heat, or differential erosion of rock underneath the glaciers (Fig 2.9; Hulth et al., 2010). Additionally,

glaciers on composite volcanoes are rare in the Arctic, and most glacier-volcano interactions are studied in the mid-latitudes and tropics or the ice caps of Iceland (Rivera et al., 2012; Reinthaler et al., 2019; Edwards et al., 2020).

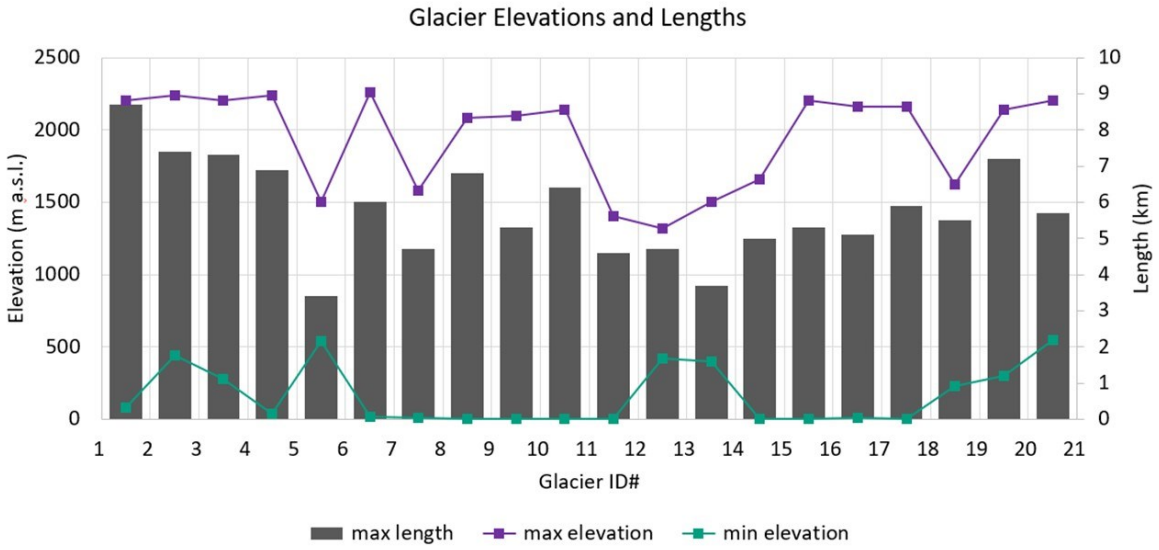

Figure 2.10: Length and elevation of the Jan Mayen glaciers on Beerenberg. Data from RGI 6.0 (RGI Consortium, 2017)

Table 2.2: Attributes of the glaciers on Jan Mayen from RGI version 6.0 (RGI Consortium, 2017). Glacier No. refers to the numbers on the map in Fig 2.9.

Glacier No	Name	RGI ID	GLIMS ID	Area (km^2)	Min. elev. (m)	Max. elev. (m)	Slope (deg)	Aspect (deg)	Length (m)
1	Sørbreen	RGI60-07.01568	G351816E71042N	15.4	151	2175	14.4	188	4678
2	Kpr Olavs Bre	RGI60-07.01569	G351730E71043N	16.9	290	2208	12.9	237	4479
3	Kerckhoffbreen	RGI60-07.01570	G351719E71067N	9.1	216	2135	13.8	270	6897
4	Charcotbreen	RGI60-07.01571	G351736E71081N	5.4	292	2251	16.8	284	6419
5	Vestisen	RGI60-07.01572	G351726E71092N	3.1	173	1397	16.3	303	2652
6	Jorisbreen	RGI60-07.01573	G351754E71099N	4.0	140	2005	18.2	315	4388
7	Hamarbreen	RGI60-07.01574	G351773E71106N	2.3	184	1429	17.6	328	3286
8	Weyprechtbreen	RGI60-07.01575	G351816E71107N	8.2	0	2188	19.8	328	7042
9	Gjuvbreen	RGI60-07.01576	G351838E71118N	2.7	0	1876	24.1	314	5311
10	Kjerulfbreen	RGI60-07.01577	G351869E71120N	5.3	0	1902	20.4	340	4782
11	Svend Foynbreen	RGI60-07.01578	G351896E71127N	2.5	0	1268	18.3	331	4386
12	Kprs Marthas Bre	RGI60-07.01579	G351944E71127N	9.0	5	1217	14.3	42	3947
13	Dufferinbreen	RGI60-07.01580	G351934E71108N	1.6	476	1387	17.8	77	3083
14	Frielebreen	RGI60-07.01581	G351942E71102N	2.6	34	1550	19.2	100	4737
15	Pr Haralds Bre	RGI60-07.01582	G351928E71095N	3.4	36	2046	24.2	92	5304
16	Griegbreen	RGI60-07.01583	G351932E71082N	4.5	0	2160	23.8	107	5162
17	Willebreen	RGI60-07.01584	G351925E71070N	4.9	0	2118	22.4	95	4070
18	Petersenbreen	RGI60-07.01585	G351938E71056N	5.5	255	1614	15.9	82	4462
19	Fotherbybreen	RGI60-07.01586	G351906E71041N	9.0	332	2126	11.9	148	4076
20	Wardbreen	RGI60-07.01587	G351866E71043N	3.6	480	2175	14.5	170	6778

In 2000, six glaciers had calving faces, and Weyprechtbreen, which drains from the central basin of the volcano, had the longest calving face (Pfeffer et al., 2014; RGI Consortium, 2017). These marine-terminating glaciers end along an open coast, rather than terminating within a fjord. Therefore, sea ice cannot adhere to the sides of a fjord, and would thus have less buttressing force, limiting how laterally confined the glacier fronts in the ocean are. Additionally, the area immediately around Jan Mayen (~1-2 km) slopes very gradually, so the marine-terminating glacier fronts rest in relatively shallow water (Fig 2.7b; Kodaira et al., 2000). Non-fjord marine-terminating glaciers are greatly understudied, as they are generally rare in

contemporary times (Pfirman and Solheim, 1989). The lack of an extensive floating tongue is an important distinction: the thinning of this terminus is generally considered the catalyst for increased glacier retreat, as it reduces stress at the bed of a marine-terminating glacier (Pritchard and Vaughan, 2007). This increased rate is then controlled by the geometry of the fjord. Because neither of these are present for the Jan Mayen glaciers, the glaciers will be affected only by shallow ocean temperatures in addition to the atmospheric and subglacial heat forcings which affect the land-terminating glaciers. These shallow ocean waters erode the glacier from below, undercutting it and making the terminus unstable, thus creating calving events (Luckman et al., 2015; Vallot et al., 2018; Ma and Bassis, 2019).

The average ELA for all glaciers on Jan Mayen is ~850 m a.s.l. Sørbreen's ELA was measured during Orheim's 1976 study to be at 950 m a.s.l. (Orheim, 1976), while the ELA of glaciers on the northwest side of the island were observed to be between 600-700 m a.s.l. (Anda et al., 1985). ELA of the northwest glaciers was determined to be lower only because during the two years the weather station on the island was moved further north, higher precipitation was observed (Anda et al., 1985). This, therefore, may not be correct to assume.

The entire glaciated area of Jan Mayen has been mapped with modern techniques only once, and DEM differencing was last done in 2011 (Hagen et al., 1993; Rolstad Denby and Hulth, 2011). Beyond these, field-based glaciological research on the island has focused on the glacier Sørbreen (frequently referred to as "South Glacier"), as it is the easiest to access. The major studies are: mass balance studies in 1972–74 (Orheim, 1976) and 2007–2011 (Hulth et al., 2010), University of London glacier front fluctuation studies (Fitch et al., 1962), University of London measurements of ablation, accumulation, and frontal speed in 1961 (Kinsman and Sheard, 1963), and a glacier fluctuation history from 1850-1978 (Anda et al., 1985). According to

these studies, Sørbreen's furthest retreated extent was in 1949, after which it advanced ~100 m between 1949 and 1959, and ~100 m further during the following two years (Fitch et al., 1962; Orheim, 1993). Aerial photographs from the Norsk Polarinstitutt showed further advances which likely culminated in 1965, followed a mostly stagnant frontal position until 1978 (Fig 2.11; Orheim, 1993). This advance was likely due to reduced summer temperatures during the 1940s-1960s (Anda et al., 1985).

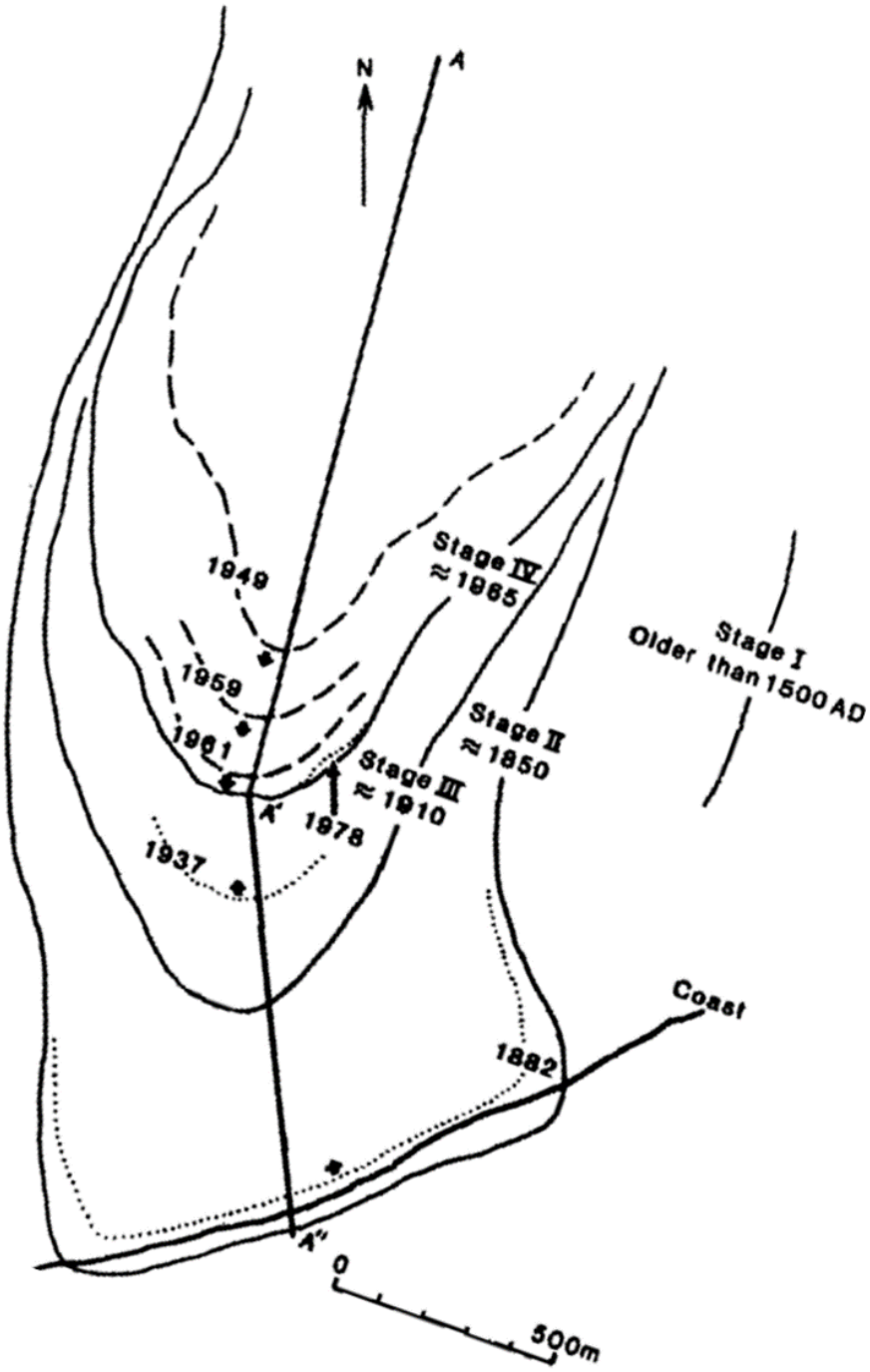

Figure 2.11: Glacier margin delineation map for Sørbreen, showing retreat between 1882 and 1949 and slight readvance up to 1978. From Anda et al. (1985).

Mass balance studies on Sørbreen determined that there is an area of melt that is constant with elevation (or possibly that increases with elevation) at lower elevations on Sørbreen (Fig 2.12). The reason for this is theorized to be reduction of shortwave radiation and air temperature due to the fog and temperature inversions, which might be less important for northwest glaciers (Anda et al., 1985; Orheim, 1993). The temperature inversion on Jan Mayen is thought to be caused by advection of cold air from the ocean replacing warm air near the ground, and so may reduce melting rates.

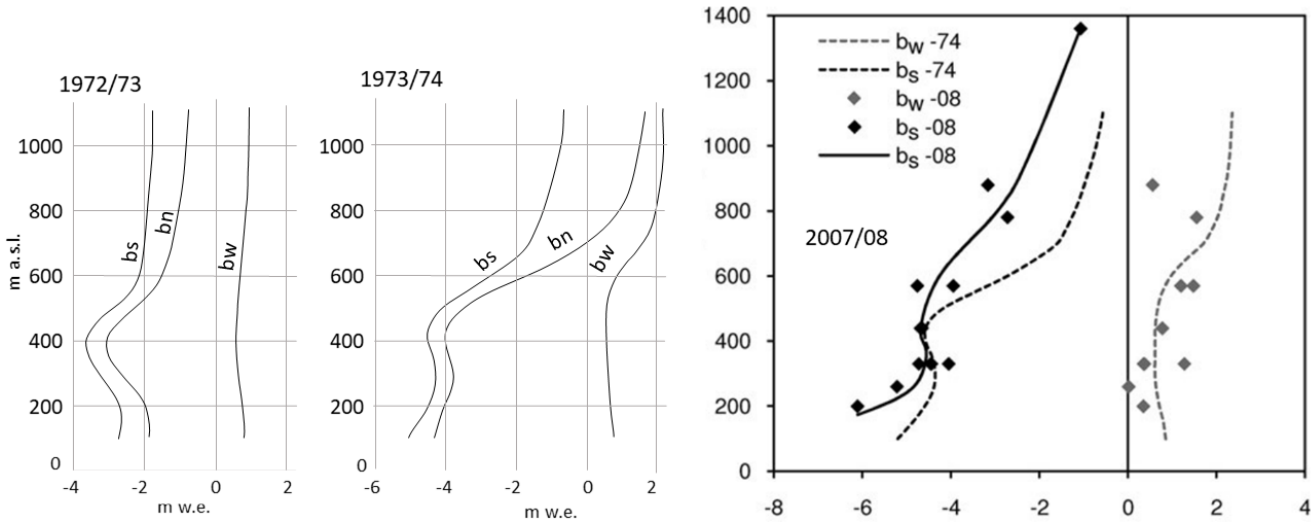

Figure 2.12: Mass balance curves reconstructed from field measurements on Sørbreen. Curves for 1972/73 and 1973/74 are from Orheim (1976). Curve from 2008 is from Hulth et al. (2010) and includes the mass balance curves from 1973/74 for context.

2.4.4. Volcanic Activity and Seismic Studies

Jan Mayen is dominated by its stratovolcano Beerenberg, and the entire island is riddled with signs of other volcanic activity such as cinder cones to the south (Hagen et al., 1993; Skreslet et al., 2004). The oldest rocks on the surface of the island are 2 Mya, but this volcano is still active and has erupted 6 times since 1732 (Skreslet et al., 2004). The most recent eruption was in 1985, although in 1997 some weak fumarole activity was observed as steam rising from

the central crater (Global Volcanism Program, 2013b). All Holocene eruptions have been from fissures opening on the east side of the mountain, rather than from the central crater, very near the glaciers Dufferinbreen and Frielebreen and (Fig 2.9) so these glaciers might show a larger than average ablation (Hagen et al., 1993; Skreslet et al., 2004). However, steam is occasionally seen rising from the central crater, which could affect flow and melt patterns of Weyprechtbreen (Orheim, 1993; Global Volcanism Program, 2013b).

As an active volcano on a tectonically active ridge and fracture zone, the GHF at this location is ~100 mW/m^2, which is higher than the standard continental background of ~60 mW/m^2 (Fig 2.13; Pollack et al., 1993; Lucazeau, 2019). This increases during volcanic activity, and is likely even higher at the site of the fissures on Jan Mayen (Smellie and Edwards, 2016). The most recent bedrock addition is from the 1970 eruption, which resulted in ~4 km^2 of new land off the northeastern tip of Nord-Jan (Fig 2.14; Orheim 1993). This activity is important for two considerations: firstly, the ground near the fissures will have a higher GHF, which could affect flow dynamics and melting rates of Dufferinbreen, Frielebreen, and possibly other glaciers nearby (increased melting at Dufferinbreen was observed after the 1970 eruption; (Anda et al., 1985); secondly, the creation of new land in 1970 formed a buffer of land between Dufferinbreen and the ocean which changed the forcings that the glacier is subjected to (Vogt, 1863; Anda et al., 1985; Hagen et al., 1993; Orheim, 1993).

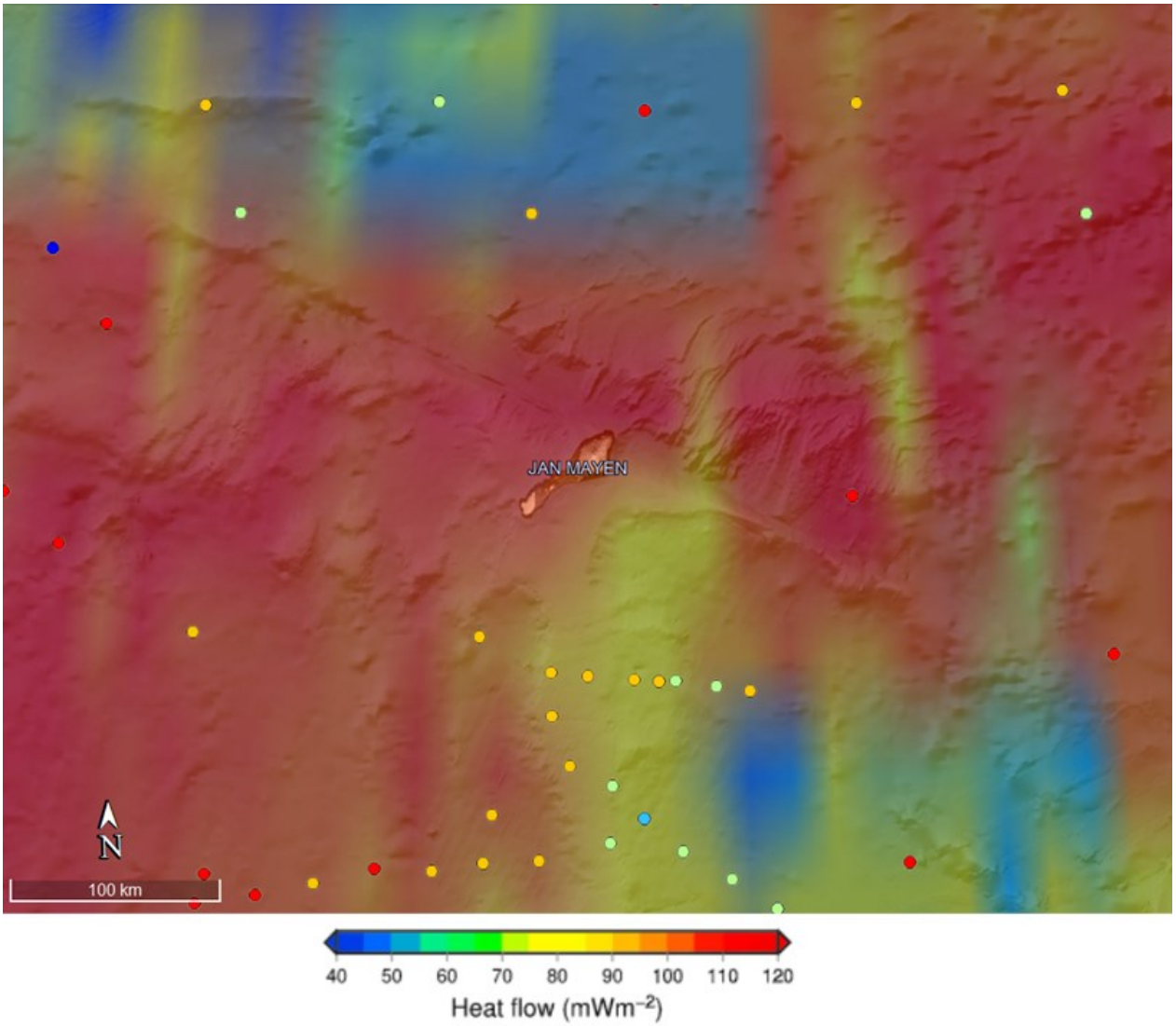

Figure 2.13: GHF around Jan Mayen. Visualization from Lucazeau (2019), data points from https://ihfc-iugg.org/products/global-heat-flow-database/data

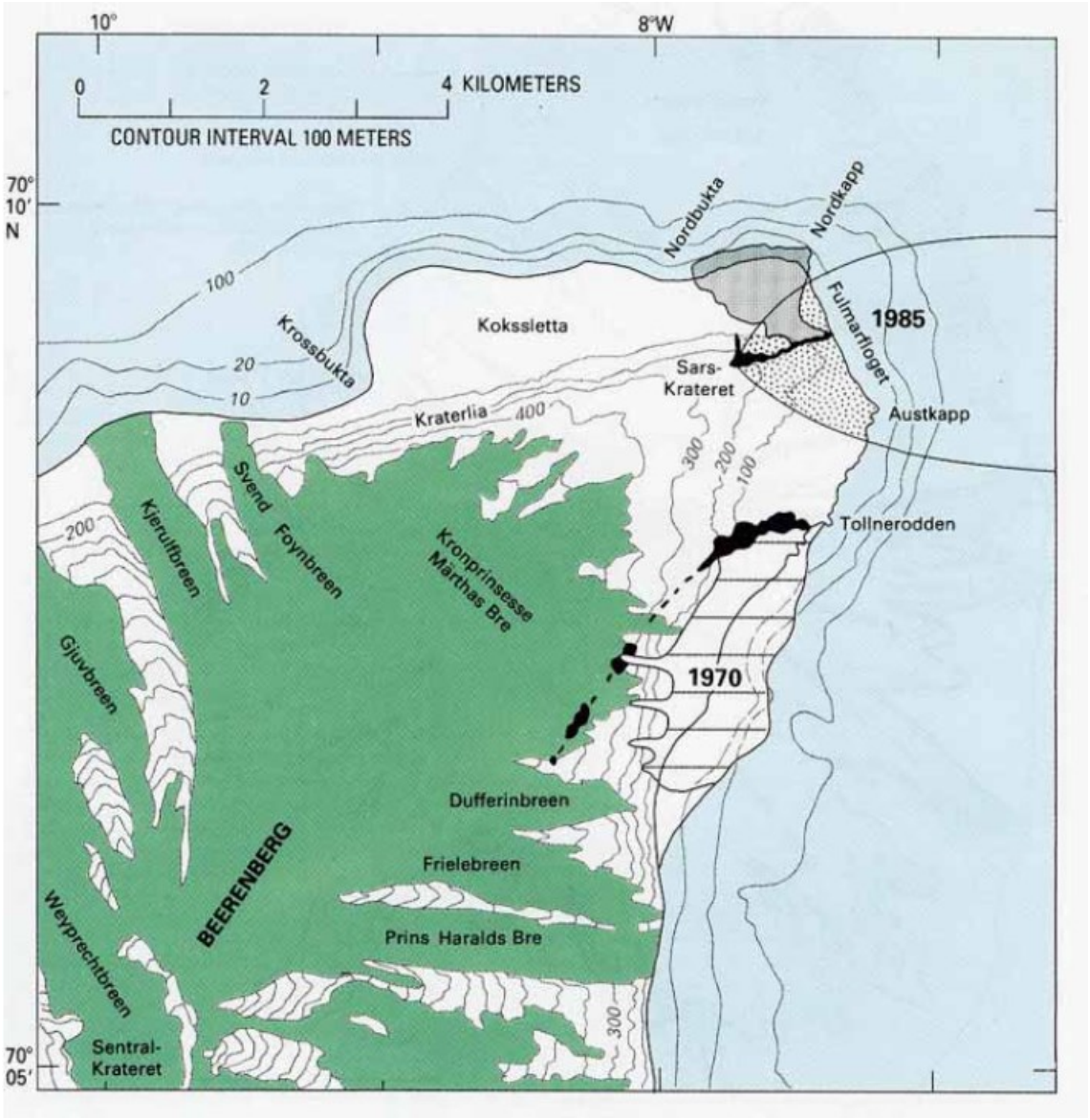

Figure 2.14: New land created by the September 1970 lava flows shown by lined area. Solid black dots indicate craters, stippled area is tephra deposits, and the parabola is the tephra fallout pattern from the 1985 eruption. From Orheim (1993).

Three seismic stations run by the University of Bergen (UiB) and the Norwegian National Seismic Network (Norsar) have been active on Jan Mayen starting at different times no later than 2004, monitoring activity from the active fault off the northeastern edge of the island. Passive broadband stations can pick up glacier activity such as calving, as demonstrated for Svalbard and Antarctica (Bartholomaus et al., 2012; Podolskiy and Walter, 2016; Aster and Winberry, 2017; Gajek et al., 2017).

2.4.5. Why Study Jan Mayen?

Past glacier studies on Sørbreen reveal that the frontal position and retreat/advance rate can vary wildly between years, with retreat rates ranging from 10-60 m/yr over a 10-year period (Fitch et al., 1962; Kinsman and Sheard, 1963; Anda et al., 1985). This indicates that the glaciers on Jan Mayen are particularly sensitive to climate change and could be signifiers of what is to come in the regions nearby, as much as they are correlated to those regions. Therefore, it would be valuable to quantify the glaciers' frontal positions in recent years, and with a higher temporal frequency than has previously been applied. These observations could lend insight beyond glacier changes in the regions surrounding Jan Mayen, as well. Beerenberg is an isolated mountain with no other topography nearby to complicate weather patterns or shade glaciers, and marine- and land-terminating glaciers with relatively simple basins lay side by side at all aspects. Whether these glaciers change in parallel or not and to which climatic and oceanic factors they respond will further understanding of glacier dynamics in general.

2.5. Filling the Gaps in Knowledge

This thesis provides a history of the Jan Mayen glacier changes, including all previously determined frontal positions, their terminal type (marine- or land-terminating) and digitized annual margins between 2000-2020 to bring this history up to the present, as well as the frontal ablation from the remaining marine-terminating glaciers between 2000-2020 and the overall ice area change for this same period. These glacier length changes are further correlated to first order factors, both climatic (temperature and precipitation trends), and oceanic. The glacier length changes on Jan Mayen are additionally compared to glacier length changes in the four regions nearby (Svalbard, Greenland, Iceland, and Scandinavia), to ascertain spatial coherence of glacier fluctuation patterns and determine whether the study of Jan Mayen glaciers can elucidate which

second-order or regional factors could be important (inversions, fog, volcano). (Kochtitzky et al., in prep). In addition, an attempt was made to detect calving events from seismic records on Jan Mayen, but due their small scale and large distance to seismic stations this was not pursued further (for more detail see Section 3.1.7). The results of this thesis will add to two international databases. The last front variation data entered into the WGMS FoG database for Jan Mayen glaciers is from 1975 (Leclercq, 2012; WGMS, 2021). Results from this thesis will update the FoG database, and ice flux from this thesis has already been incorporated into a pan-Arctic project, run by Dr. Luke Copland and students from the University of Ottawa, with the goal of having a comprehensive view of all marine-terminating glacier fluxes in the period 2000-2010 and 2010-2020. This study is unique in the sense of scale, as it rests between that of a single glacier study (i.e. Ødegârd et al., 1992; Hulth et al., 2010), and regional studies (i.e. Bjørk et al., 2012; Zemp et al., 2015).

3. CHAPTER 3: METHODS

3.1. Data

For this project glacier inventory, historic maps, mass balance, remote sensing, velocity, elevation, climate, sea surface temperature and sea ice data are all used. All field data used in this project were collected in previous years by various researchers, over various time scales. This section outlines all data sources, what parts of the data were used and how, and the specific statistical analyses used.

3.1.1. Randolph Glacier Inventory

The Randolph Glacier Inventory (RGI) is a collection of shapefiles of global glacier extents (excluding the ice sheets) with various attributes (Pfeffer et al., 2014; RGI Consortium, 2017). The original RGI release contained shapefiles that were mostly mapped from satellite imagery around the year 2000, but in some cases glaciers were redrawn from existing maps as early as the 1970s. The current release (RGI6.0), contains various regional updates as well as additional datasets such as debris cover (RGI Consortium, 2017; https://www.glims.org/RGI/). RGI is accessed via the GLIMS portal (https://www.glims.org/RGI/rgi60_dl.html), and data can be downloaded for use in GIS or in spreadsheet form. For the purpose of this study the attributes of slope, length, area, and glacier outline shapefiles were used. Slope and length were used for comparison to glaciers in the nearby regions of Iceland, Svalbard, Scandinavia, and Greenland; glacier area was used to give context to glacier ice area loss. Jan Mayen glacier outline shapefiles in the RGI are out of date (Hagen et al., 1993; Skreslet et al., 2004; Pfeffer et al., 2014; RGI Consortium, 2017), but updating these shapefiles and constraining the entire glacier shape is

outside the scope of this study. Hence these RGI data are used sparingly: as a visual aid for outlining glacier fronts and as the outlines for determining ice loss from DEMs.

Glacier outlines in the RGI are often semi-automatically generated, and frequently include "glaciers" that are in fact snow patches or light-colored rock (Paul et al., 2013; Pfeffer et al., 2014). The RGI outlines for Jan Mayen were created by J.G. Cogley (RGI Consortium, 2017), who traced the historic glacier inventory from Hagen et al. (1993), which contains a large number of small snow patches. The maximum area for any of these patches on the island of Jan Mayen is 0.223 km^2. Therefore, removed from further consideration in this thesis are any glaciers with an area below 0.225 km^2, for all regions, even though this is larger than what is generally used for such cut-offs (0.1 km^2; Leigh et al., 2019). Additionally, the frequency of these small "glaciers" is generally high in any region of the RGI (Pfeffer et al., 2014) and thus may skew interpretation of aggregate glacier metrics.

Analysis of Greenland glaciers in this thesis includes only glaciers categorized as having no connection (CL0) to the ice sheet in RGI 6.0 (Rastner et al., 2012). RGI composite thickness data were not used as they yielded thicknesses of 0.5-2.3 m (Farinotti et al., 2019). This is possibly because thickness estimates depend upon higher quality DEMS than are available at Jan Mayen.

3.1.2. Historical Maps of Jan Mayen

Whalers and arctic explorers have visited Jan Mayen for over four centuries (Vogt, 1863; Skreslet et al., 2004). Several of these sailors drew maps that show different impressions of the island. While historical accuracy cannot be guaranteed, these maps can still reveal information of relative positions of glaciers, and whether and when certain glaciers had calving fronts. Historical

maps that either name the glaciers and/or which are clear enough to derive glacier margin conditions were selected for use in this thesis. These maps were created from observations from several expeditions: Carl Vogt and Georg Berna on a privately financed expedition in 1861 (Vogt, 1863), an exploratory Norwegian Expedition through the North Atlantic featuring three scientists in 1877 (Mohn and Wille, 1882), an Austrian expedition to Jan Mayen organized for the First International Polar Year, 1882 (1882-83; Bóbrik von Boldva, 1886; Barr, 2008), a survey in 1938 by the Imperial College of Science (Jennings, 1948), two University of London expeditions in 1959 and 1961 specifically studying the geology and climatology of Jan Mayen and Beerenberg (Kinsman and Sheard, 1963), and data from aerial photos from 1949-1975 which resulted in the map used to create RGI outlines, shown in Figure 2.9 (Hagen et al., 1993). The 1861 map is based on the direct mapping by William Scoresby in 1820 of the southeast side of the island (https://commons.wikimedia.org/wiki/File:Jan_Mayen_map_1820_by_William_Scoresby.jpg), and mapping by the Dutch sailor Cornelius Zorgdrager in 1720 on the northwest side, but was updated with observations made during the 1861 excursion (Vogt, 1863). The 1720 and 1820 maps do not include sufficient details of the glacier for use in this thesis. These historical maps are used in this thesis for a qualitative examination of glacier length and retreat, and approximate time periods in which glacier fronts met the ocean.

3.1.3. Weather Station Data

Synoptic weather observation data including temperature, precipitation, atmospheric pressure, relative humidity, wind direction and wind speed have been recorded from the Norwegian Meteorological Institute station near Olonkinbyen on Jan Mayen since the early 20th century. The observing station is operated according to WMO observing standards (WMO,

2006). There is an unbroken chain of daily measurements, barring the end of 1940 and beginning of 1941 due to complications from World War II (Orheim, 1993; Skreslet et al., 2004). The station has been moved multiple times, and while parallel measurements indicate that temperature can be used continuously without alterations, this is not true for precipitation (Steffenson, 1982). Fig 3.1 shows the current location and approximate previous locations of the weather station. As the last time the station was moved was 1962 (Anda et al., 1985; Skreslet et al., 2004), this is unlikely to affect analyses for this thesis. Slightly higher precipitation was measured in the years the station was the furthest north and west (position 3 in Fig 3.1), which led to the hypothesis that the west side of the island received more precipitation, which was later supported by observed broad weather patterns (Anda et al., 1985; Orheim, 1993).

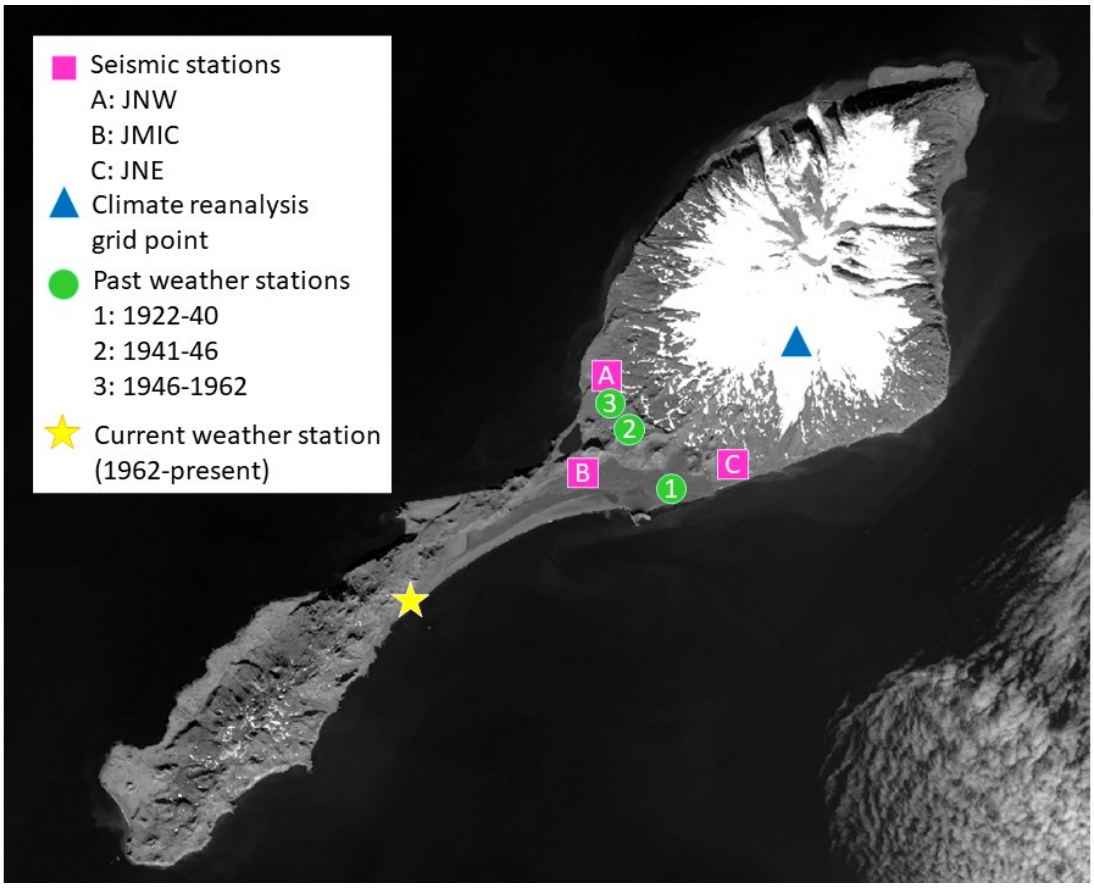

Figure 3.1: Scientific stations on Jan Mayen relevant to this thesis. Background image is Landsat 8 satellite image from 28 Aug 2020.

In addition to weather data, sea surface temperature (SST) is measured near Olonkinbyen. Previous studies indicate that temperatures on Jan Mayen have been slowly increasing, from -1.01 ºC for 1983/84 (Sep-July) to -0.94 ºC 1992/3 (Nov-July; Østerhus and Gammelsrød, 1999). SST and weather data from the Jan Mayen stations are available on request from the Norwegian Meteorological Institute through the web portal https://seklima.met.no/. SST, precipitation sum, and temperature average measurements will be used in a statistical analysis for determining possible drivers of glacier retreat on Jan Mayen.

3.1.4. Climate Reanalysis Data

For measurements of temperature, relative humidity, and cloud cover at elevations higher than ground level, climate reanalysis data is used. Climate reanalysis combines physical observations and modeling to create a numerical description of the recent climate. For this thesis the European Centre for Medium-Range Weather Forecasts (ECMWF) Reanalysis data, version 5 (ERA5) is used as it has a high temporal and spatial resolution (hourly data, 0.75 DEGREE grids), and has been used successfully in previous similar studies at nearby locations (Rye et al., 2010; Carr et al., 2014). ERA5 is separated into monthly or hourly averages for multiple pressure levels for various time periods: 1979-present (Hersbach et al., 2019; https://cds.climate.copernicus.eu/cdsapp#!/dataset/reanalysis-era5-pressure-levels?tab=form) and 1950-1978 (Bell et al., 2020; https://cds.climate.copernicus.eu/cdsapp#!/dataset/reanalysis-era5-pressure-levels-preliminary-back-extension?tab=form). Surface level data (1000 hPa) are used for comparison to synoptic weather station measurements to determine how the climate reanalysis matches the measured data and thus determine the validity of higher elevation data. The ERA5 850 hPa level is used to represent climate at an elevation that is less influenced by the ocean, sea ice, and temperature inversions. This level corresponds to an altitude of ~1500 m a.s.l.,

half the general glacier elevation range on Jan Mayen and just above its temperature inversion and the theorized ELA. This level has been determined by previous studies to be the most relevant for Arctic glaciers at lower elevations, while for higher mountainous regions the 700 hPa or 500 hPa can be used (Carr et al., 2014). Relative humidity and cloud cover data were downloaded as monthly averages for time stamps every three hours starting at UTC 00, while temperatures were in daily averages at the same times. The cloud cover parameter is specific to the level at which it is downloaded, and does not include clouds in the entire atmospheric column above or below it era (Hersbach et al., 2019; Bell et al., 2020). Fig 3.1 shows the location of the gridpoint center from which these data were extracted.

3.1.5. Positive Degree Days

Air temperature is most frequently the dominant factor controlling glacier surface ablation, but there are a variety of ways air temperature can be utilized for such studies (Ohmura, 2001). More important than yearly or seasonally average temperatures are positive degree days (PDD; Braithwaite, 1995; Cogley et al., 2011; Kochtitzky et al., 2020). PDD is the yearly sum of the daily average of positive temperatures and is a first order approximation for melting energy available over the year. Positive degree day values are calculated from sub-daily measurements by:

$$Y = \frac{1}{M}\sum_{m=1}^{m=M}\sum_{n=1}^{n=N}\alpha_{nm}T_{nm}$$

$$where\ \ \alpha_{nm} = \begin{cases} 1\ if\ T_{nm} > 0 \\ 0\ if\ T_{nm} \leq 0 \end{cases} \quad (Eq\ 3.1)$$

Where M is the total number of measurements in the *n*th day, α_{nm} is either 1 or 0 depending on if the temperature is above 0, and T_{nm} is the temperature in ºC for the m^{th}

measurement of the n^{th} day. Braithwaite (1984) states that for glaciological purposes PDD is ideally calculated from several measurements in a day, with a maximum of 6-hours between them. Therefore, the climate reanalysis data were downloaded for 3-hour intervals. The synoptic station measurements, however, were only available as daily averages, so PDD for climate reanalysis at the ground level might be higher than it is for physical measurements, as the physical measurements daily averages include negative numbers that thus decrease the daily average.

In addition to PDD, the number of days in a year that had an average temperature above 0 was calculated as the number of positive degree days (PDDN):

$$Y = \sum_{d=1}^{d=365\ or\ 366} \alpha_d$$

$$\alpha_d = \begin{cases} 1\ if\ T_d > 0 \\ 0\ if\ T_d \leq 0 \end{cases} \quad \textit{(Eq 3.2)}$$

3.1.6. Sea Ice Extent

The extent and concentration of sea ice can restrict calving rates in marine-terminating glaciers by providing buttressing and, at the same time, affect the atmospheric moisture contribution (and hence accumulation rate), as open water will allow turbulent exchange between the ocean and atmosphere while sea ice cover prevents this (Raper et al., 2005; Tsai et al., 2008; Amundson et al., 2010; Robel, 2017). Sea ice also dampens the magnitude of ocean waves and may therefore also diminish calving frequency or magnitude (Squire, 2020).

Sea ice extent and sea ice concentration data are publicly available freely online, via the National Snow and Ice Data Center (NSIDC) website (https://nsidc.org/data). The NSIDC extent of sea ice is determined from 25x25 km grid cells and measured from passive microwave satellite

data: when 15% or more of the cell contains sea ice, it is counted as sea ice, otherwise as open ocean. Sea ice and water are differentiated by their brightness from passive microwave satellites. Using these data to a quantitative degree requires extensive processing of the raw data, and additionally a 25x25 km grid cell is large in comparison to the island (55 km long). Therefore, for the purpose of this study the preprocessed shapefiles from the dataset *March through August Ice Edge Positions in the Nordic Seas, 1750-2002 version 1* (https://nsidc.org/data/G02169/versions/1) were used. The ice edge in this product is defined as the outer boundary of ice having at least 30 % ice concentration. By visually examining these shapefiles, the specific years that Jan Mayen was within the Greenland Sea sea ice extent was determined. While it is possible Jan Mayen had its own limited extent of landfast sea ice around it in any given winter, Jan Mayen's glaciers are not in fjords, so this sea ice cannot form mélange that holds onto the shore walls and create a strong buttressing effect (Carr et al., 2014; Fürst et al., 2016).

3.1.7. Seismic Station Data

Preliminary examination of seismic data was from station JMIC (Fig 3.1), available using the BREQ_FAST request system of Incorporated Research Institutions for Seismology (IRIS; https://ds.iris.edu/ds/nodes/dmc/forms/breqfast-request/). First a catalog of events was created, determined by their signal-to-noise ratio, then events were manually inspected. There are three characteristics that distinguish calving events from tectonic or other events: calving events do not have clear P- and S-wave arrivals where tectonic events do, calving events are emergent where tectonic events have abrupt onsets, and calving events have spectra peaks generally between 1-5 Hz where tectonic events are in higher frequencies (Qamar, 1988; O'Neel et al., 2010; Bartholomaus et al., 2012; Walter et al., 2012). Preliminary examination evaluating these three

characteristics of the JMIC seismic data concluded that the distance between the seismic stations on Jan Mayen and glacier calving fronts (~15-20 km) was too large to measure significant glacial signals.

3.1.8. Remote Sensing Data

Optical satellite imagery from Landsat**,** MODIS, ASTER and Sentinel are publicly available free online, while digital elevation models (DEMs) from some datasets such as SPOT, WorldView and Ikonos were supplied by Dr. Robert McNabb (pers comm, Jan 25, 2019). Landsat is a series of Earth-observing satellite missions managed by NASA and the U.S. Geological Survey (USGS; https://www.usgs.gov/core-science-systems/nli/landsat/landsat-satellite-missions?qt-science_support_page_related_con=0#qt-science_support_page_related_con). This mission began in July 1972, with the launch of Landsat 1. Since then, there have been 8 missions, launched in 1975, 1978, 1982, 1984, 1993, 1999, and 2013. For this study only Landsat 5 and up are used, barring Landsat 6 which never achieved orbit. Landsat 5, launched in 1984, has been updated throughout the years with currently operational Landsat 7 (launched in 1999) and Landsat 8 (launched in 2013). Landsat 7 and 8 currently image the entire Earth every 16 days offset from each other by eight days (USGS, 2017). This means that a single location may have an image available every eight days, but cloud cover may obscure the earth surface at that location. The resolution of these satellite data has increased from Landsat 5 with a resolution of 60 m, to Landsat 8 with a resolution of 15-30 m (dependent on the spectral band). The different bands on Landsat missions correspond to different wavelengths, which have different uses. For example, band 2 of Landsat 8 is used to differentiate different types of vegetation from each other, and from bare soil.

Most images in this study are from Landsat 7 and 8 while only one image is used from the Landsat 5 mission. For the delineation of glacier margins from Landsat 7 and 8, band 8 was used, which is panchromatic and has a resolution of 15 m. For the distinction of glaciers and moraines in the debris covered areas occasionally thermal infrared bands 10 and 11 of Landsat 8 (resolution 100 m), and band 6 of Landsat 7 (resolution 30-60 m) were used. For Landsat 5, visible and NIR bands from Landsat 5 Thematic Mapper (TM), which were a combination of Bands 5-7, were used (https://www.usgs.gov/core-science-systems/nli/landsat/landsat-5?qt-science_support_page_related_con=0#qt-science_support_page_related_con). All images were selected to cover the ablation season, which is from June to September. This is a wide range of dates as cloud cover is frequent and many images throughout the ablation season were unusable. Some images showed only cloud cover over one side of the island, while the other side was completely clear. This division was most frequently delineated by a northwest/southeast aspect, which corroborates observations that wind and precipitation generally come from the northwest (Orheim, 1993; Hulth et al., 2010). All images used in this study are listed in Table 3.1.

Table 3.1: All satellite scenes used in this study, and the glaciers which had frontal lines drawn using that scene.

Satellite	Scene Name	Glaciers
Landsat 7	LE07_L1GT_217010_20000721_20170210_01_T2_B8	Weyprechtbreen, Kjerulfbreen, Frielebreen, Svend Foynbreen, Gjuvbreen, Hamarbreen
Landsat 7	LE07_L1GT_218010_20000930_20170209_01_T2_B8	Prins Haralds Bre, Petersenbreen, Dufferinbreen
Landsat 7	LE07_L1GT_217010_20010622_20170204_01_T2_B8	Svend Foynbreen, Sørbreen
ASTER	AST_L1A_00306242001123858_V123	Weyprechtbreen, Kjerulfbreen, Prins Haralds Bre
Landsat 7	LE07_L1GT_216010_20010717_20170204_01_T2_B8	Frielebreen
Landsat 7	LE07_L1GT_216010_20010802_20170204_01_T2_B8	Kerckhoffbreen
Landsat 7	LE07_L1GT_218010_20020904_20170128_01_T2_B8	Kjerulfbreen, Svend Foynbreen, Jorisbreen, Charcotbreen
Landsat 7	LE07_L1GT_216010_20020906_20170128_01_T2_B8	Fotherbybreen
Landsat 7	LE07_L1GT_217010_20020913_20170129_01_T2_B8	Weyprechtbreen, Prins Haralds Bre, Frielebreen, Gjuvbreen, Sørbreen
ASTER	AST_L1A_00306282003123257_V123	Kerckhoffbreen, Charcotbreen, Willebreen
ASTER	AST_L1A_00307162003123008_V123	Prins Haralds Bre, Weyprechtbreen, Kjerulfbreen, Svend Foynbreen, Gjuvbreen, Jorisbreen, Petersenbreen
Landsat 7	LE07_L1GT_216010_20030925_20170124_01_T2_B8	Frielebreen
Landsat 7	LE07_L1GT_216010_20040810_20170120_01_T2_B8	Weyprechtbreen, Kjerulfbreen, Prins Haralds Bre, Frielebreen, Svend Foynbreen, Griegbreen, Sørbreen, Kerckhoffbreen, Willebreen, Dufferinbreen
Landsat 5	LT05_L1GS_218010_20060721_20161120_01_T2_B8	Weyprechtbreen, Kjerulfbreen, Svend Foynbreen
Landsat 7	LE07_L1GT_216010_20060816_20170107_01_T2_B8	Prins Haralds Bre, Frielebreen
Landsat 7	LE07_L1GT_217010_20080913_20161225_01_T2_B8	Weyprechtbreen, Kjerulfbreen, Prins Haralds Bre, Frielebreen
Landsat 7	LE07_L1GT_217010_20100903_20161212_01_T2_B8	Weyprechtbreen, Kjerulfbreen, Prins Haralds Bre, Frielebreen, Svend Foynbreen
ASTER	AST_L1A_00306202011123022_V123	Prins Haralds Bre, Frielebreen, Sørbreen, Griegbreen
Landsat 7	LE07_L1GT_216010_20120715_20161130_01_T2_B8	Prins Haralds Bre, Frielebreen
Landsat 8	LC08_L1GT_218010_20130606_20170504_01_T2_B8	Weyprechtbreen
Landsat 8	LC08_L1GT_216010_20130726_20170503_01_T2_B8	Prins Haralds Bre, Jorisbreen, Frielebreen
Landsat 8	LC08_L1GT_217010_20130802_20170503_01_T2_B8	Kjerulfbreen
Landsat 8	LC08_L1GT_218010_20140625_20170421_01_T2_B8	Weyprechtbreen, Kjerulfbreen, Prins Haralds Bre, Gjuvbreen
Landsat 8	LC08_L1GT_217010_20150605_20170408_01_T2_B8	Prins Haralds Bre
Landsat 8	LC08_L1GT_218010_20150831_20170404_01_T2_B8	Weyprechtbreen, Kjerulfbreen, Hamarbreen

Landsat 8	LC08_L1GT_216010_20160819_20170322_01_T2_B8	Sørbreen, Svend Foynbreen, Frielebreen, Dufferinbreen, Fotherbybreen, Charcotbreen, Weyprechtbreen, Kjerulfbreen, Prins Haralds Bre, Kerckhoffbreen, Willebreen, Petersenbreen
Landsat 8	LC08_L1GT_218010_20180604_20180615_01_T2_B8	Frielebreen, Svend Foynbreen, Griegbreen, Prins Haralds Bre, Kjerulfbreen
Landsat 8	LC08_L1GT_217010_20180629_20180716_01_T2_B8	Sørbreen
Landsat 8	LC08_L1GT_216010_20180708_20180717_01_T2_B8	Weyprechtbreen, Gjuvbreen
Landsat 8	LC08_L1GT_216010_20180910_20180927_01_T2_B8	Kerckhoffbreen, Fotherbybreen, Petersenbreen
Landsat 8	LC08_L1TP_218010_20200828_20200906_02_T1_B8	Weyprechtbreen, Gjuvbreen, Kjerulfbreen, Dufferinbreen, Prins Haralds Bre, Willebreen, Jorisbreen, Hamarbreen, Charcotbreen, Frielebreen, Kerckhoffbreen

An issue unrelated to the geography of Jan Mayen but to the satellite sensors themselves is the Landsat 7 ETM+ SLC-off data. This refers to any image recorded by Landsat 7 after 31 May 2003, when the Scan Line Corrector (SLC) failed. The result of this is images with diagonal lines of no data ~80-150 m wide. This complicated drawing glacier frontal lines, as Landsat 8 was not launched until a full decade later, and therefore some images with these lines running through glacier fronts still had to be used for drawing glacier lines.

For DEM coregistration in this thesis, a tool by Dr. Robert McNabb (https://github.com/iamdonovan/dem-coregistration) was used for georeferencing and resampling DEMs. The two DEMs which were differenced are the DEM built from aerial photography and topography map from 1949-1975 (Norsk Polarinstitutt), as it is the most complete and earliest date DEM available, and one created from an ASTER image on 20 June 2011, as it is the most complete later DEM available. These DEMs should not be considered as representative of a single year, but rather a range of years each. All DEMS for this thesis were provided by Dr. McNabb. However, there were complications in the processing of the DEMs, and due to time constraints the volume change of Jan Mayen glaciers was not calculated.

Velocity data was generated using auto-RIFT (Gardner et al., 2018) and provided by the NASA MEaSUREs ITS_LIVE project (Gardner et al., 2019). The default for this process is to use Landsat, which results in image chips of 300 m x 300 m, and so does not have adequate data points on glaciers as small as those on Jan Mayen. A specific inquiry to Dr. Mark Fahnestock, one of the creators of ITS_LIVE, for data for the Jan Mayen glaciers, resulted in useable data. For these data, center flowlines for each of the 20 Jan Mayen glaciers were drawn and sent to Dr. Fahnestock, who then extracted velocity data from Sentinel-2 images, which have higher resolution and more frequent coverage than Landsat images. The result was 200 m x 200 m pixel image chips, with ~1800 image pairs with time separations from 20 to 90 days (personal communication Mark Fahnestock, 6 Feb 2019). The final result used in this study was the median speed from each pair at each point. These data do not account for seasonal fluctuations of velocity.

3.2. Analysis

3.2.1. Georectifying Images and Drawing the Coastline

Satellite images were georeferenced in ArcMap. As Landsat 8 images are orthorectified already, the clearest Landsat 8 image was chosen to rectify all other images to: 19 Aug 2016. There were several points recognizable on the island which could be used as georeferencing points, although all of these are geological and not human-made, so there are no hard corners and there is possible change or movement associated with them. All images contain at least three of these 20 common georeferencing points, but all images also contain additional points unique to that image due to cloud cover, snow cover, or quality of image. Each georeferencing process utilized at least 10 points and resulted in an RMS error <10 m. Each image was afterwards carefully manually examined to ensure landmarks and coastlines matched (taking into account

tide level) between the newly rectified image and the 19 Aug 2016 image, as well as to other images within that year.

To determine the part of a glacier front that is marine-terminating, there must be a coastline that is constant throughout the entire time period. This will help determine if all or part of the glacier front is marine-terminating, and also when a glacier retreats onto land completely. A coastline shapefile was available from two sources: https://geodata.npolar.no/ (Norwegian Polar Institute, 2014) and https://www.ngdc.noaa.gov/mgg/shorelines/ (Wessel and Smith, 1996), however, these coastlines sometimes count the glacier front as the coastline, and thus would affect ice flux measurements. Jan Mayen beaches are generally rocky with cliffs, and tidal range is ~1 m (Skreslet et al., 2004; www.kartverket.no). To draw a coastline for this study, the 19 Aug 2016 Landsat image was used, as it was at the time the clearest image and was the image used to georectify other images. On 19 Aug 2016, the tide was lowest near 1 pm (www.kartverket.no), thus, when the image was taken at 2:19 pm (Jan Mayen time), the tide was still relatively low, better exposing the lowest coastline. Reliability of the coastline throughout the time period for this study was ensured through manual inspection of the coastline against every image for years previous. As some glacier fronts never recede far enough back to reveal the coast underneath the ice (at the time the coastline was drawn images up to only 2016 were available), it was most imperative to determine where the coastline was at either end of the calving front, and the line continuing through the glacier front is more for completeness than for accuracy.

3.2.2. Glacier Margin Delineation

Glacier extent is generally mapped through manual or automated detection of glacier termini or by delineating entire glacier boundaries (Fig 3.2). Quantifying changes in glacier extent can be limited to measurements of changes along a single line across the furthest extent of

the glacier terminus, or by measuring area loss or gain along the outline of the entire glacier (Paul et al., 2013). Many factors can make determining glacier outlines difficult, including shade on images, debris covered glacier fronts, and personal interpretation. Because of this, exact glacier outlines often differ across studies, to as much as 30% differences in total glacier area (Fig 3.2; Paul et al., 2013).

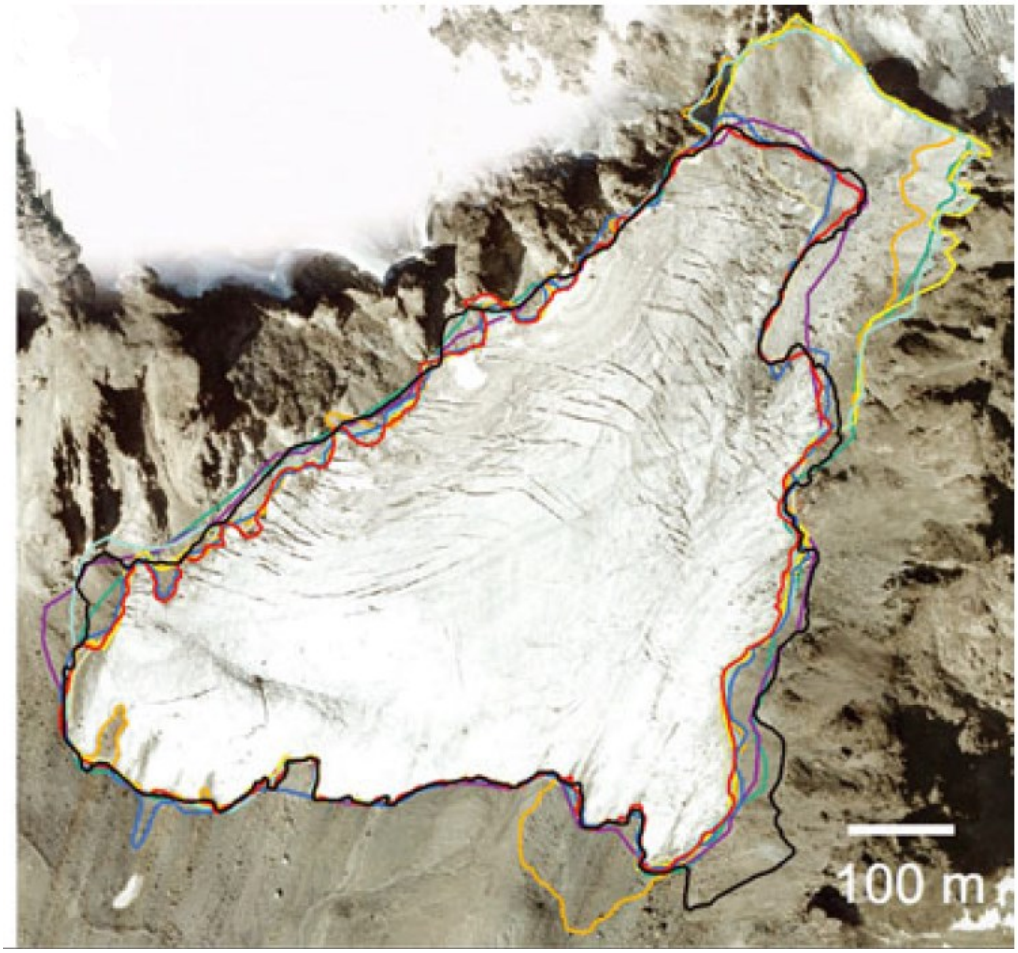

Figure 3.2: Example of how manually-mapped glacier outlines can differ between individuals. This is glacier Vadret d'Urezzas in Austria. Each colored outline is a different scientist's outline of the glacier. All scientists received the same satellite scene and the same instructions. From Paul et al. (2013).

While aerial photographs have high resolution and can obtain multiple angles, making it easier to determine glacier shape, it is limited in areal extent and hampered by logistics. Therefore, satellite imagery is widely used in glaciological disciplines, from glacier fluctuation

histories to ice flow velocity records and iceberg volume estimation (i.e. Moon and Joughin, 2008; Nuth et al., 2013; Reinthaler et al., 2019). Optical satellite imagery from Landsat (since 1972), ASTER (since 1999), Sentinel (since 2014), and Worldview (since 2009) are publicly available online. Landsat 7 and 8 currently image the entire Earth every 16 days and offset from each other by eight days. This means that a single location may have an image available every eight days, but heavy cloud cover may completely obscure the earth surface at that location.

For this thesis, glacier frontal margins for the years 2000-2020 were manually digitized as polyline shapefiles at a 1:12 000 zoom scale in ArcGIS (except Fotherbybreen, which has a frontal margin too wide for this scale thus its lines were drawn at a scale of 1:15 000). This resolution allowed for a view of the full front width of most glaciers as well as some of the surrounding terrain to determine glacier from snow or land. The outlines of the calving glacier fronts always terminated within 10 m of the coastline. This resulted in a shapefile of polylines associated with a specific glacier and specific year, so the change in overall length and shape of the glaciers are easily quantified using the box method (Moon and Joughin, 2008; McNabb and Hock, 2014).

Manually drawing glacier margins for land-terminating glaciers is inherently subjective (Paul et al., 2013), and Jan Mayen glaciers are especially difficult as they frequently have debris-covered fronts and fluctuations are small in comparison to the satellite resolution. Several of Jan Mayen's land-terminating glaciers are debris covered for the entire time period, and the fronts were too indeterminate to discern well enough to draw. This was the case for Kronprins Olavs Bre, Vestisen, Kronprinsesse Marthas Bre, and Wardbreen, which were also difficult to discern from the terrain in DEMs. Therefore, there are no measurements for these four glaciers in this study.

Consistency is important for determining rates of change. Towards this end, glacier fronts for each glacier were drawn individually over the entire time period 2000-2016 before another glacier outline was begun. Returning to the data in 2021 to add lines from 2018 and 2020 resulted in new insight, and some corrections to earlier years. Along with consistency of measurements for a single glacier, consistency across the entire island was achieved by using as few as possible images for each year. The maximum number of images used within a year was four, which occurred in both 2001 and 2018 and was due to partial cloud cover. The longest time span covered by the images within one year used to draw glaciers lines was 98 days and occurred in the year 2018. For details on the methodology of glacier margin line delineation see Appendix A.

3.2.3. The Box Method

To calculate changes in margin area over time, the box method was utilized. This method has been widely used to determine the area change of marine-terminating glacier fronts, as it accounts for the irregular shapes of the fronts as the glaciers retreat (Moon and Joughin, 2008; McNabb and Hock, 2014; White and Copland, 2019). A rectangular box is drawn around the glacier front, which contains all the margin lines drawn for every year such that these lines cut across opposite lateral sides of the box and the box contains only ice for all years of the time period. Margin lines from each year are then used as one side of the box while the straight lateral and upglacier sides of the box are used to enclose that area (Fig 3.3a). Yearly changes were calculated by subtracting the ice area value of the earlier year from the ice area value of the later year, so retreat is negative and advance is positive (Fig 3.3b). Note that marine-terminating margins and land-terminating margins may have a different box size and shape for the same glacier.

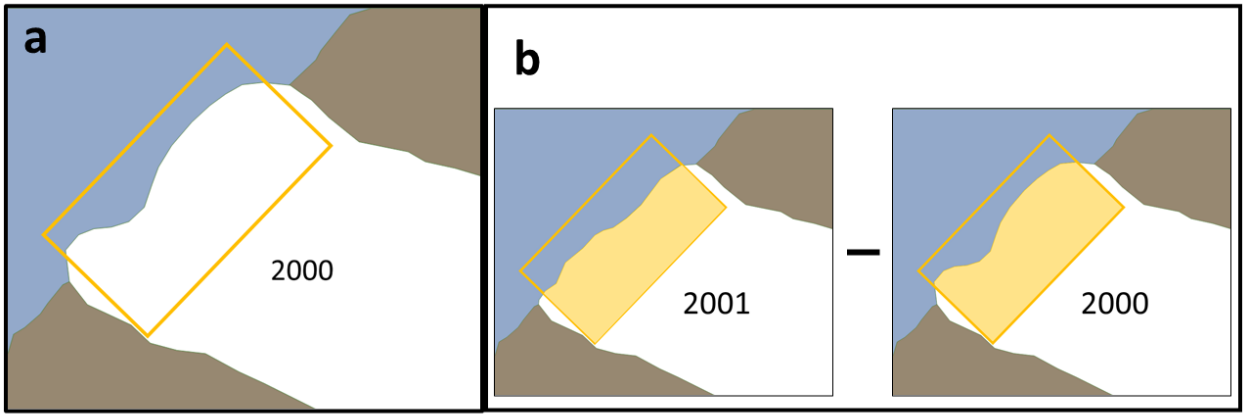

Figure 3.3: Box Method. a) Shows an example glacier inside a box drawn such that the side of the glacier pass through opposite sites, with arbitrary ends perpendicular to glacier flow. b) Shows how retreat rates are calculated, with the ice area inside the box (pale orange area) from an earlier year subtracted from ice area of a later year, such that retreat is negative and advance is positive.

The box method also presents a way to compare glacier length changes (Moon and Joughin, 2008; McNabb and Hock, 2014; White and Copland, 2019). The width of the box for each glacier is known, so each yearly area divided by this width results in the average length of the glacier front for the ice area within the box. To calculate yearly length changes (i.e. glacier retreat and advance), the same technique as for area changes was used: subtracting the earlier year value from the later year value, divided by the number of years which separated them. This number indicates the average advance or retreat (in m/yr) of the front of the glacier. These length changes are compared to past known changes of the glaciers (Kinsman and Sheard, 1963; Anda et al., 1985; Orheim, 1993).

Marine-terminating glacier fronts were drawn with a higher frequency than land-terminating glacier fronts, both because calving fronts can be more dynamic and because it is easier to see them (as there is no sea ice around Jan Mayen). To compare area changes between years that a glacier was marine-terminating and land-terminating, the outline from the last year it was marine terminating was extended, tracing the edge of the glacier such that it can be used as the downglacier end for the land-terminating box (Figure 3.4). This creates an area for the last

year the glacier was marine-terminating that can be subtracted from subsequent land-terminating ice areas. So that relative length can be consistent and comparable across the entire time period for glaciers that retreated onto land, similarly the glacier outline along the sides of the glacier for the first year there was a measurement drawn was extended so that it can be used as the downglacier end for the land-terminating box. The length which results from this is used as the first length measurement, to be subtracted from subsequent land-terminating lengths.

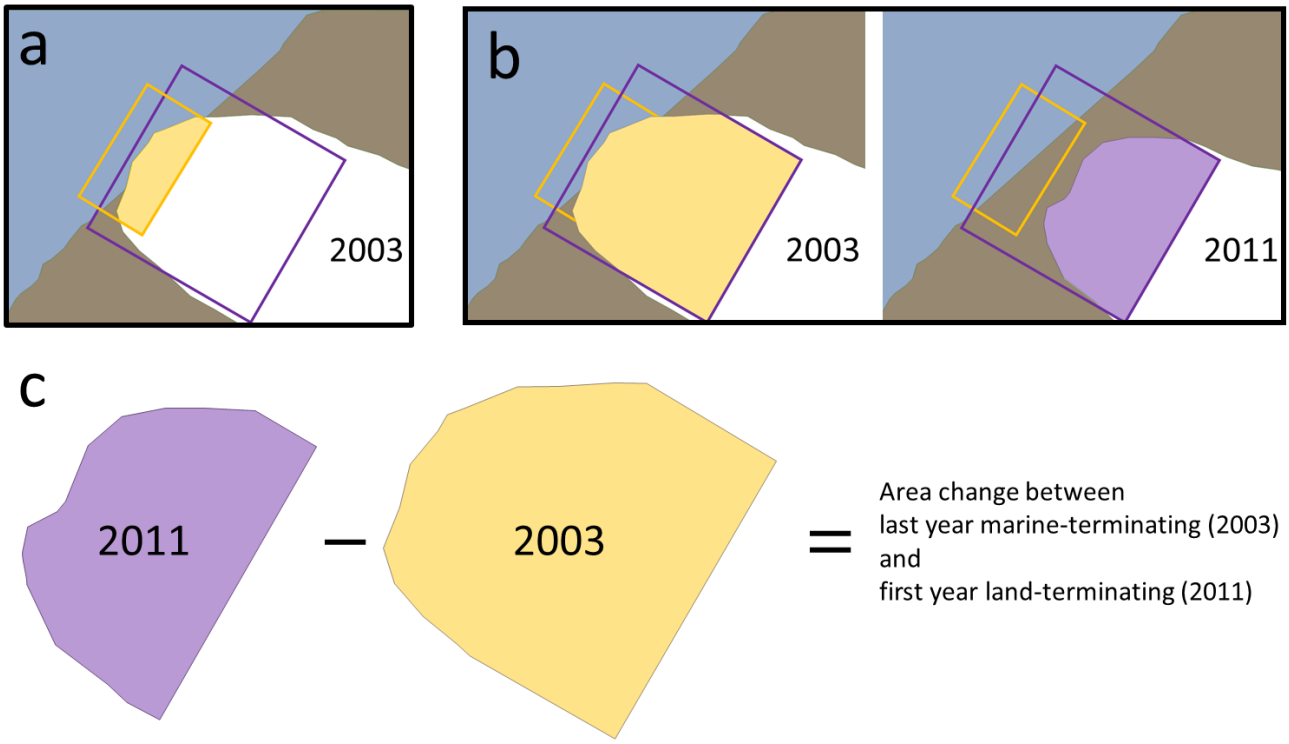

Figure 3.4: Comparing areas across time periods over which the glacier retreats onto land. a) shows in orange the ice area that would be used for marine-terminating calculations for the last year the glacier was marine-terminating (here 2003). b) shows the line from the last year the glacier was marine-terminating extended so that it can cut the land-terminating box (purple), creating an ice area (orange) to be subtracted form the first land-terminating area. c) indicates the areas that would be used to calculate the area change between the last year the glacier was marine-terminating and the first year it was land-terminating.

To get total ice area lost 2000-2020 for marine-terminating glaciers, the frontal line for 2000 and the frontal line for 2020 were connected by delineating the side of the glacier for 2000 down to the 2020 front, which is a standard way to calculate glacier area changes (i.e. Paul et al., 2004; Andreassen et al., 2008; Khromova et al., 2014; Shahgedanova et al., 2017). This

technique could not be applied to land-terminating glaciers however, as their fronts change erratically and the glacier front lines crossed several times (marine-terminating glaciers that retreated onto land naturally could not have crossing front lines). Therefore, to get total ice area lost for 2000-2020 for land-terminating glaciers, the 2000 ice area was subtracted from the 2020 ice area using the box method.

The spatial error associated with length and area changes is calculated using common error addition, thus by taking the square-root of the sum of the squared input data and digitization errors. For the input data, the cartographic accuracy of Landsat 8 is 12 m or better, while the pixel resolution of Landsat 7 and 8 are 15 m, for georectifying precision the root mean square was always below 10 m, and for human error again one pixel width is used, or 15 m. The error in area changes is then spatial error added in quadrature.

3.2.4. Ice Thickness, Velocity, and Frontal Ablation

Frontal ablation for Jan Mayen was calculated from ice discharge minus any mass change from terminus position change (which can be positive or negative). The following standard equation was used (Kochtitzky et al., in prep):

$$FA = \rho \sum_{n=1}^{w/d} (v_n T_n d) - \rho \Delta A_{net} T_{mean} \text{ (Eq 3.3)}$$

Where ρ is the vertically averaged density of the ice column (917 kg/m^3), w is the glacier width, d is the bin size over which ice discharge is summed (in this case, 100 m), v_n is the vertically averaged ice velocity (assumed to be 95% the surface velocity), T_n is the thickness at the n^{th} flux gate point, ΔA_{net} is the net area change for the glacier terminus, and T_{mean} is the average thickness of the terminus at that point.

Ice flux for a point on a glacier was calculated as the depth integrated velocity multiplied by ice thickness multiplied by column width. This calculation was performed for points spaced 100 m along a transect for each glacier, then summed. Velocity estimates were extracted from ITS_LIVE, using lines across the ice such that each point is on a cell that completely covers ice (instead of dirt or ocean). For most glaciers, this means velocity extraction lines are within ~20 m of the calving front. However, these ITS_LIVE data are from Sentinel 2 and thus start in 2015. Therefore, some glaciers had retreated far enough onto land (Svend Foynbreen, Frielebreen, and Gjuvbreen) that they did not have a wide enough transect of ice near the coastline for velocities to be considered ice velocities. For these glaciers, the velocity extraction lines are drawn as close to the glacier front as possible, while still measuring ice for the full time period.

There have not been any direct measurements of the thickness of Jan Mayen glaciers. Therefore, thicknesses were estimated from Fig 6 in Anda, et al. (1985). In this figure, the thickest ice at the most recent position was ~50 m in 1975. In Mohn's account of the 1876-78 expedition to Jan Mayen, he mentions the calving front of Kjerulfbreen reaching 150 feet (~45 m) above the ocean. These observations suggest glacier thickness should be no lower than 50 m. Ice thickness for the width of the marine-terminating glaciers is then estimated assuming a parabolic shape with maximum depth at 80 m for the low estimate and 100 m for the high estimate of frontal ablation.

Frontal ablation results from this thesis have been incorporated into a pan-Arctic study of marine-terminating glacier changes and ice flux over the period 2000-2020 (Kochtitzky et al., in prep).

3.2.5. Annual Retreat Rates

Due to frequent cloud cover, each glacier had lines drawn over a different sequence of years, and there is no single year for which all glaciers in this study had a frontal line measurement. To account for poor or missing data leading to several years between frontal line measurements, area and length changes are calculated as annual rates. Retreat rates for each year between 2000 and 2020 were calculated for each glacier by dividing the area change by the number of years between the measurements. For the analysis of possible correlations between retreat rates and climatic and oceanic drivers, however, relative glacier front is used, similar to past studies (Carr et al., 2014; McNabb and Hock, 2014). Relative length is the average length of the ice area within the box method box, relative to the first year for which that specific glacier has a measurement. For nine glaciers in this study, this is the year 2000, for two it is 2001, for three it is 2002, for one it is 2003, and for one it is 2004.

A best-fit x^2 trendline was fit to glacier relative length changes for all 16 glaciers, and correlations between this line and climatic and oceanic forcings were tested statistically. Both previous research and manual examination of satellite images indicate that weather generally comes from the north or northwest, and the topography of the island naturally separates it into a "west side" and "east side" (Table 3.2). Therefore, to identify trends of driving forces on each side of the island and between land- and marine-terminating glaciers, four representative glaciers were used to test correlations. Sørbreen was chosen as the land-terminating glacier on the east side, as it has the longest history of observation. There was no obvious choice for a representative west side land-terminating glacier, but Kerckhoffbreen had the most distinct glacier front and thus most reliable frontal line measurements for west-side land-terminating glaciers, and so is used as representative of these. Both Sørbreen and Kerckhoffbreen are on the south flank of

Beerenberg. Weyprechtbreen is the last glacier to remain marine-terminating, and Prins Haralds Bre was marine-terminating for nearly the entire observation period (until 2018), thus these were chosen as the marine-terminating glaciers for the west and east side, respectively. All other marine-terminating glaciers had become land-terminating earlier during the 2000-2020 study period.

Table 3.2: Jan Mayen glaciers separated into east and west sides and categorized according to terminus status in the year 2000. Glacier No. refers to the numbers on the map in Fig 2.9.

East side glaciers			*West side glaciers*		
Glacier No.	Glacier name	marine- or land-terminating	Glacier No.	Glacier name	marine- or land-terminating
15	Prins Haralds Bre	marine	8	Weyprechtbreen	marine
14	Frielebreen	marine	10	Kjerulfbreen	marine
13	Dufferinbreen	land	11	Svend Foynbreen	marine
19	Fotherbybreen	land	9	Gjuvbreen	marine
16	Griegbreen	land	4	Charcotbreen	land
18	Petersenbreen	land	7	Hamarbreen	land
1	Sørbreen	land	6	Jorisbreen	land
17	Willebreen	land	3	Kerckhoffbreen	land

3.2.6. Geographic Context

Retreat rates of the glaciers on Jan Mayen were compared to retreat rates in nearby regions – Iceland, Svalbard, Scandinavia, and Greenland's peripheral zone. Utilizing glacier attributes from the RGI, the length and average slope of Jan Mayen glaciers and these regions were compared. Further, ocean currents and different climates were considered, specifically trends in SST and air temperatures in these nearby regions, and trends previous literature has considered most relevant in affecting the glacier retreat rates. Fitting Jan Mayen into this geographic context completes the picture of glacier retreat in the North Atlantic, by adding a data point between these regions.

3.2.7. Glacier Response Time

To determine the time frame to compare the glacier changes to, the glacier response time must be estimated. Glacier response time is the length of time for a glacier to come into equilibrium with a new state after a change in its physical conditions, such as climate change (Benn and Evans, 2010; Cuffey and Paterson, 2010). This indicates that the years which are most likely to be showing their effect on the glaciers during the time period for which frontal lines were drawn for the glaciers. There are multiple ways to calculate glacier response time, however, the more widely used calculation and one this thesis uses is:

$$\tau_M \sim \frac{h}{-b(l)} \quad \textit{(Eq 3.4)}$$

Where *h* is the ice thickness near the ELA (usually maximum ice thickness) and *b(l)* is the balance rate (usually negative) at the terminus (Johannesson et al., 1989; Hoelzle et al., 2003; Cuffey and Paterson, 2010). For these values the thickness estimated from Anda et al. (1985) was again used, and mass balance curves reconstructed from field measurements by Orheim (1972/73 and 73/74) and Hulth (2008).

3.2.8. Climatic and Oceanic Context

For this thesis 18 weather and ocean parameters (Table 3.3) were compared to relative length changes of the glaciers with the most complete records that were deemed representative for each of the types and sides of Beerenberg: Weyprechtbreen (west side marine-terminating), Prins Haralds Bre (east side marine-terminating), Kerckhoffbreen (west side land-terminating), and Sørbreen (east side land-terminating), and the best-fit x^2 line for all glacier relative length changes.

Table 3.3: Climatic and oceanic primary and derived parameters used in this study

Parameter Symbol	Parameter Description
P_a	Precipitation annual sum at the Olonkinbyen weather station (mm)
P_w	Precipitation winter sum at the Olonkinbyen weather station (mm)
SST_a	Sea surface temperature annual average at the Olonkinbyen weather station (°C)
SST_s	Sea surface temperature summer average at the Olonkinbyen weather station (°C)
T_a	Temperature summer average at the Olonkinbyen weather station(°C)
T_s	Temperature annual average at the Olonkinbyen weather station (°C)
T_{1000}	Temperature annual average from climate reanalysis at level 1000 hPa (°C)
T_{850}	Temperature annual average from climate reanalysis at level 850 hPa (°C)
PDD_O	Positive Degree Days at the Olonkinbyen weather station (°C)
PDD_{1000}	Positive Degree Days from climate reanalysis at level 1000 hPa (°C)
PDD_{850}	Positive Degree Days from climate reanalysis at level 850 hPa (°C)
$PDDN_O$	PDD annual sum at the Olonkinbyen weather station
$PDDN_{1000}$	PDD annual sum from climate reanalysis at level 1000 hPa
$PDDN_{850}$	PDD annual sum from climate reanalysis at level 850 hPa
RH_{1000}	Relative humidity from climate reanalysis at level 1000 hPa (%)
RH_{850}	Relative humidity annual average from climate reanalysis at level 850 hPa (%)
C_{1000}	Fraction of cloud cover annual average from climate reanalysis at level 1000 hPa
C_{850}	Fraction of cloud cover annual average from climate reanalysis at level 850 hPa

These parameters were selected as they generally have the strongest correlation with glacier mass balance, and are therefore commonly used in related studies (Cuffey and Paterson, 2010; Bjørk et al., 2012; Carr et al., 2014). Annual and winter precipitation are used as proxies for glacier accumulation. Yearly temperature, PDD, and NPDD from both weather station observations and the climate reanalysis at both levels (near the ground and ~1500 m a.s.l., above the fog and temperature inversion) are common ways to estimate the first-order melt factor of air temperature, and summer temperatures should be related to glacier ablation. Additionally, the correlation between each parameter was analyzed to test how well the ground level climate reanalysis parameters match their corresponding physical measurements, as a way to indicate the confidence level of other climate reanalysis parameters, and to search for interesting relationships such as if temperature, PDD, and NPDD are significantly correlated.

A linear correlation analysis was conducted between each of the potential climatic and oceanic drivers and the glacier response by calculating the Pearson correlation coefficient (r) and the significance (p-value) for each of these parameters with each other, the four representative glaciers' relative length changes, and the all-glacier trend using the software Statistical Package for the Social Sciences (SPSS), accounting for glacier response time. The Pearson product-moment correlation coefficient is the most widely-used method to test for the level of correlation between two variables (Davis, 2002), and is common in glaciological studies correlating glacier frontal changes to climatic and oceanic factors (i.e. O'Neel et al., 2007; Hulth et al., 2013; Carr et al., 2014; Zemp et al., 2015). Pearson's r (r) is calculated by:

$$r = \frac{[\sum(X-\bar{X})(Y-\bar{Y})]/N}{S_X S_y} \quad \textit{(Eq 3.5)}$$

Where $(X-\bar{X})$ is the deviation of a single term in the first parameter from its mean, $(Y-\bar{Y})$ is the deviation of a single term the second parameter from its mean, N is the number of paired data values, and S_X and S_Y are the standard deviation of X and Y, respectively. Pearson's r varies between -1 (inverse correlation) to + 1 (direct correlation) and for the purpose of this thesis, the strength of the relationship is defined by the absolute value of the Pearson r in the following way: 0-0.19 is very weak, 0.20-0.39 is weak, 0.40-0.59 is moderate, 0.60-0.79 is strong, and 0.80-1.0 is very strong.

The p-value indicates the significance of the correlation – the likelihood the correlation is not due to chance. A p-value < 0.05 signifies that the correlation is significant at the 95%, while a p-value < 0.01 signifies that the correlation is significant at the 99% confidence level. These values are the generally accepted practice rather than a mathematical rule, and there is debate on their arbitrariness (Wasserstein and Lazar, 2016). Therefore, this thesis uses p-values < 0.05 and

< 0.01 as indications of what relationships to focus on and presents results from all correlations. The p-value is calculated by:

$$p = r\sqrt{\frac{N-2}{1-r^2}} \quad \textit{(Eq 3.6)}$$

Where *r* is the Pearson correlation coefficient and *N* is again the number of paired values (Davis, 2002).

Climate is the 30-year average of weather (Hidore et al., 2010) and, therefore, to investigate whether Jan Mayen's climate has changed over time, trendlines and their regression coefficient (R^2) for both the period 1961-1990 and 1991-2020 were drawn for each parameter. This was done in python, with a random set checked in Excel.

4. CHAPTER 4: RESULTS

4.1. Comparison of Jan Mayen to Glaciers in other Regions Using RGI Attributes

The 20 outlines in the RGI which reflect true glaciers on Jan Mayen were introduced in Section 2.4.3. Compared to the nearby regions of Greenland, Iceland, Scandinavia, and Svalbard, Jan Mayen glaciers are generally long (Fig 4.1) and steep (Fig 4.2). The steepness is not surprising, as Beerenberg is one of the highest mountains in the five regions and all Jan Mayen glaciers reach almost down to sea level. While, statistically, Jan Mayen glaciers are generally longer, with the median being over 1800 m longer than the second-ranked region (Svalbard: Fig 4.1), Jan Mayen has only 20 glaciers. Each of the surrounding regions has far more glaciers within the Jan Mayen length range (2652–7042 m) with 2832, 84, 446, and 208 glaciers for Greenland, Iceland, Svalbard, and Scandinavia, respectively. Even when not considering glaciers with an area below 0.225 km^2, the dominance of shorter glaciers is noticeable in all of these regions (Fig 4.1).

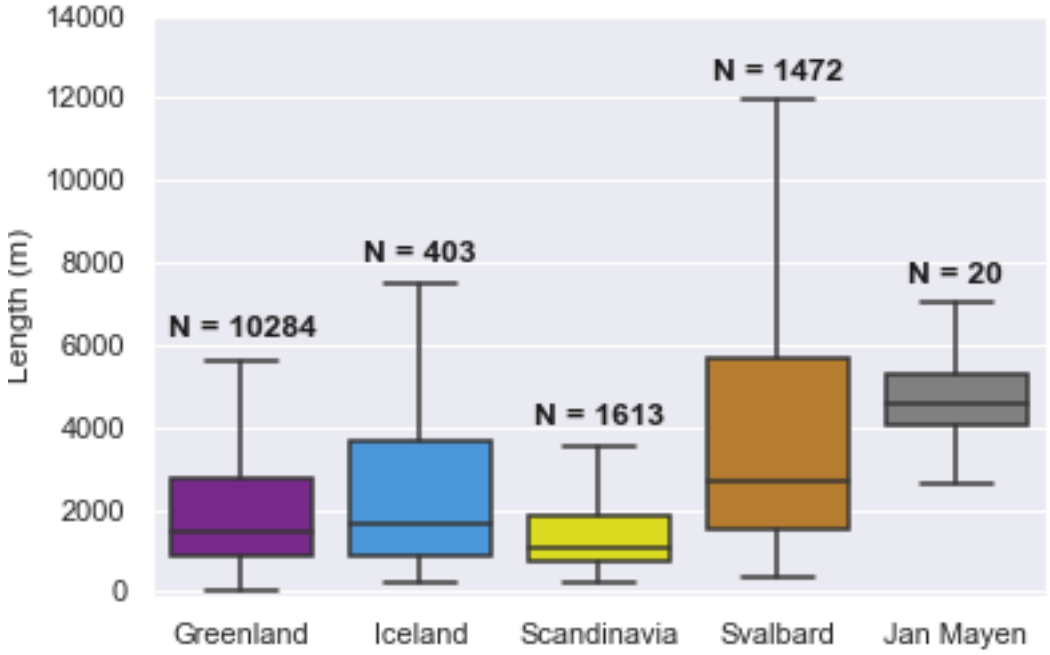

Figure 4.1: Length comparison of glaciers on Jan Mayen and surrounding regions, with number of glaciers listed above whisker. Data from RGI (RGI Consortium, 2017), with a minimal area cutoff of 0.225 km^{2}and using only Greenland peripheral glaciers. Outliers in length range as high as 50 000–70 000 m for Greenland, Iceland, and Svalbard; for clarity these are not shown.

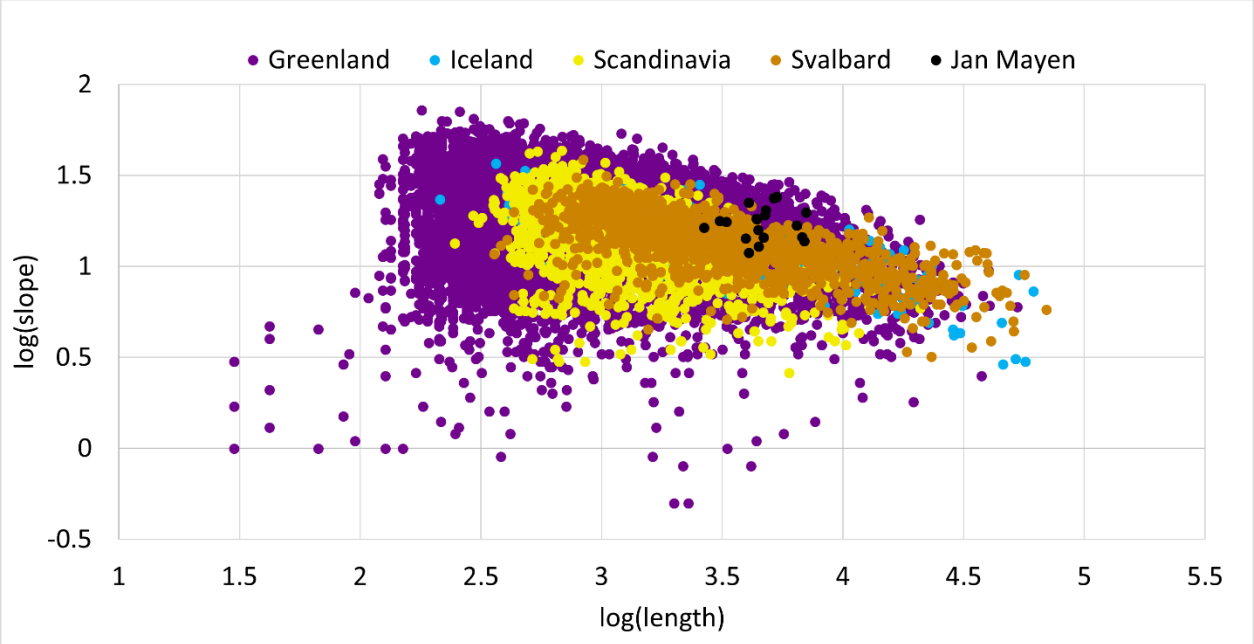

Figure 4.2: Log-log plot of average slope (degrees) relative to average length (km) of glaciers on Jan Mayen and surrounding regions. Data from RGI (RGI Consortium, 2017). Iceland (blue) and Scandinavia (yellow) have nearly complete overlap. Greenland includes glaciers peripheral to the ice sheet with CL0 only (Rastner et al., 2012).

4.2. Marine-terminating Glaciers from Historical Maps and Satellite data

Past scientific studies revealed that Sørbreen was last marine-terminating around 1882 (Anda et al., 1985), but little is known about the terminus condition of other glaciers on Jan Mayen. Detailed frontal variations for 16 of the 20 glaciers on Jan Mayen were drawn for 2000-2020, while qualitative conclusions were drawn for years before this. According to historical maps from observations in 1861 (Fig 4.3; Vogt, 1863), 1877 (Fig 4.4; Mohn and Wille, 1882), 1882 (Fig 4.5; Bóbrik von Boldva, 1886), 1938 (Fig 4.6; Jennings, 1948), 1959 and 1961 (Fig 4.7; Kinsman and Sheard, 1963), and 1975 (Fig 4.8; Hagen et al., 1993), and observations from this thesis from satellite scenes for the period 2000-2020, there were 11-13 marine-terminating glaciers at the end of the 19th century (~1882; Vogt, 1863; Mohn and Wille, 1882; Bóbrik von Boldva, 1886), seven in 1938 (Jennings, 1948), six in 2000, and only one in 2020 (Table 4.1). Glacier frontal change observations for the current time period (2000-2020) are limited by the cloudiness of satellite images, which results in observations being made at inconsistent times within the ablation season.

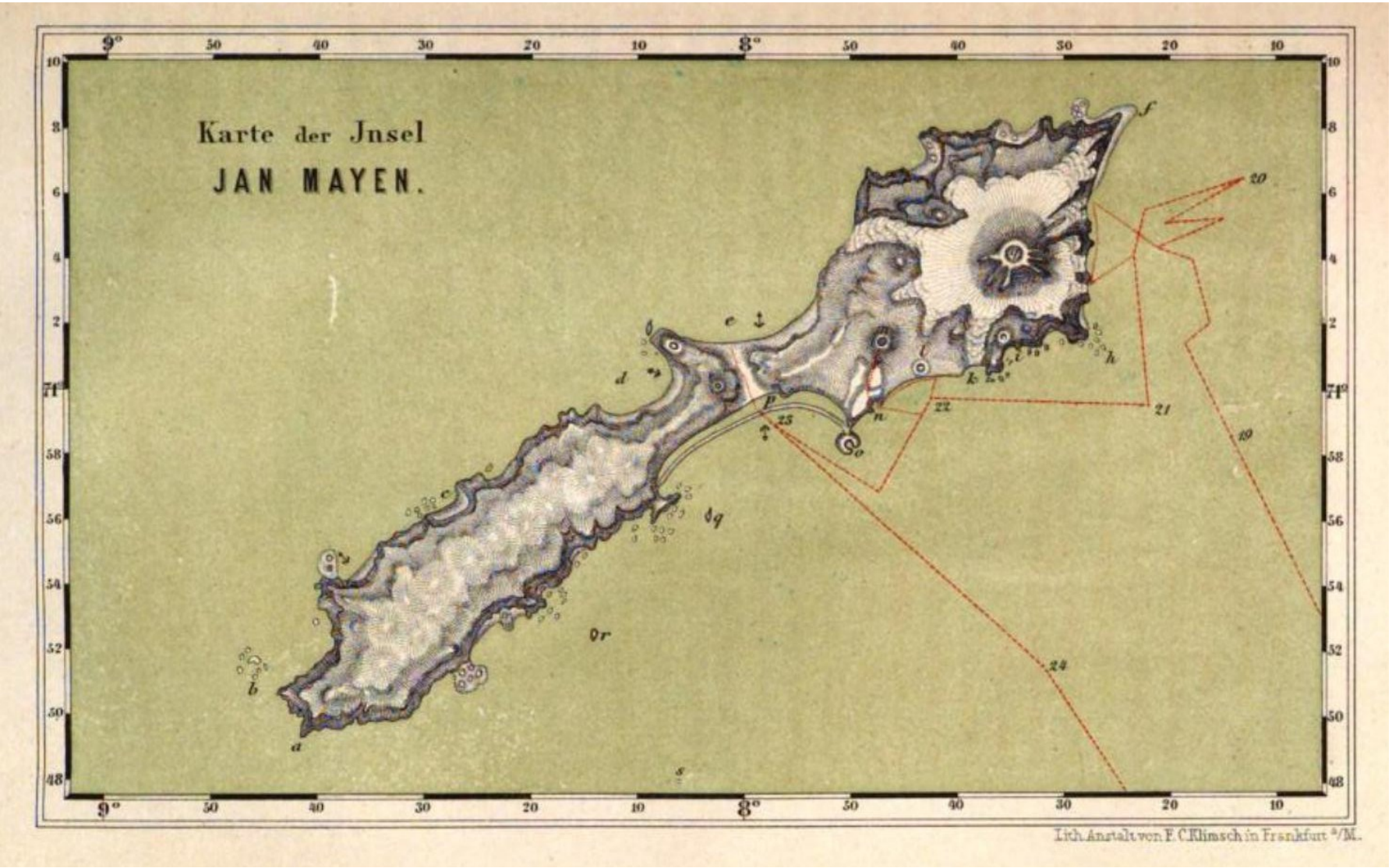

Figure 4.3: Map of Jan Mayen and the sailing route undertaken by Vogt, Berna, and others on the ship the Joachim Hinrich in the summer of 1861. Image by F.C. Klimsch, based on map in Vogt (1863). Numbers mark the location of the ship on the indicated days of August, 1861. Red lines mark routes between dates. For larger map: https://upload.wikimedia.org/wikipedia/commons/1/17/Jan_Mayen_map_by_Carl_Vogt_1863.jpg.

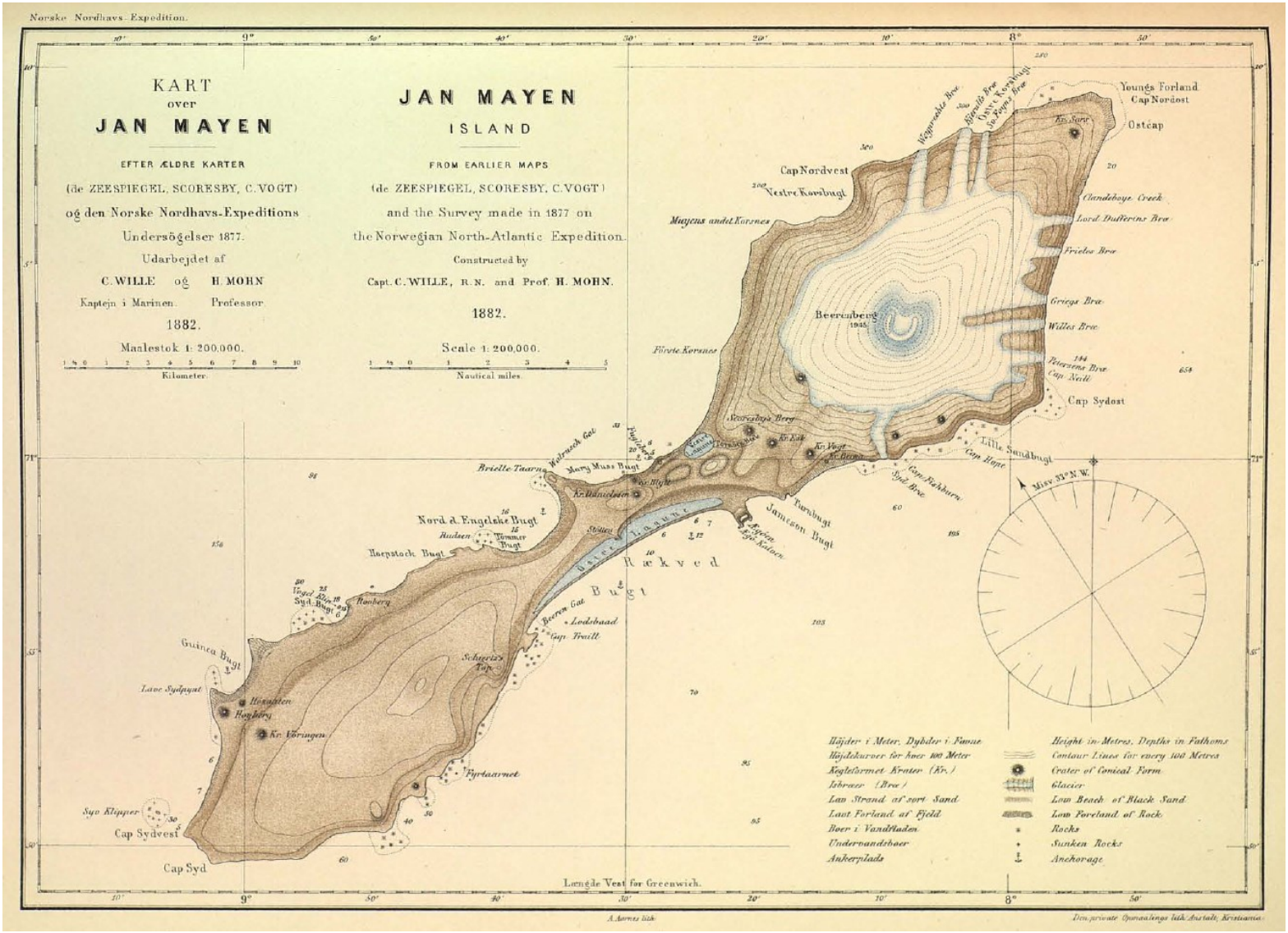

Figure 4.4: Map constructed from earlier maps and survey data from 1877 by Mohn and Wille (1882). For larger map: https://upload.wikimedia.org/wikipedia/commons/5/50/Jan_Mayen_Mohn.png

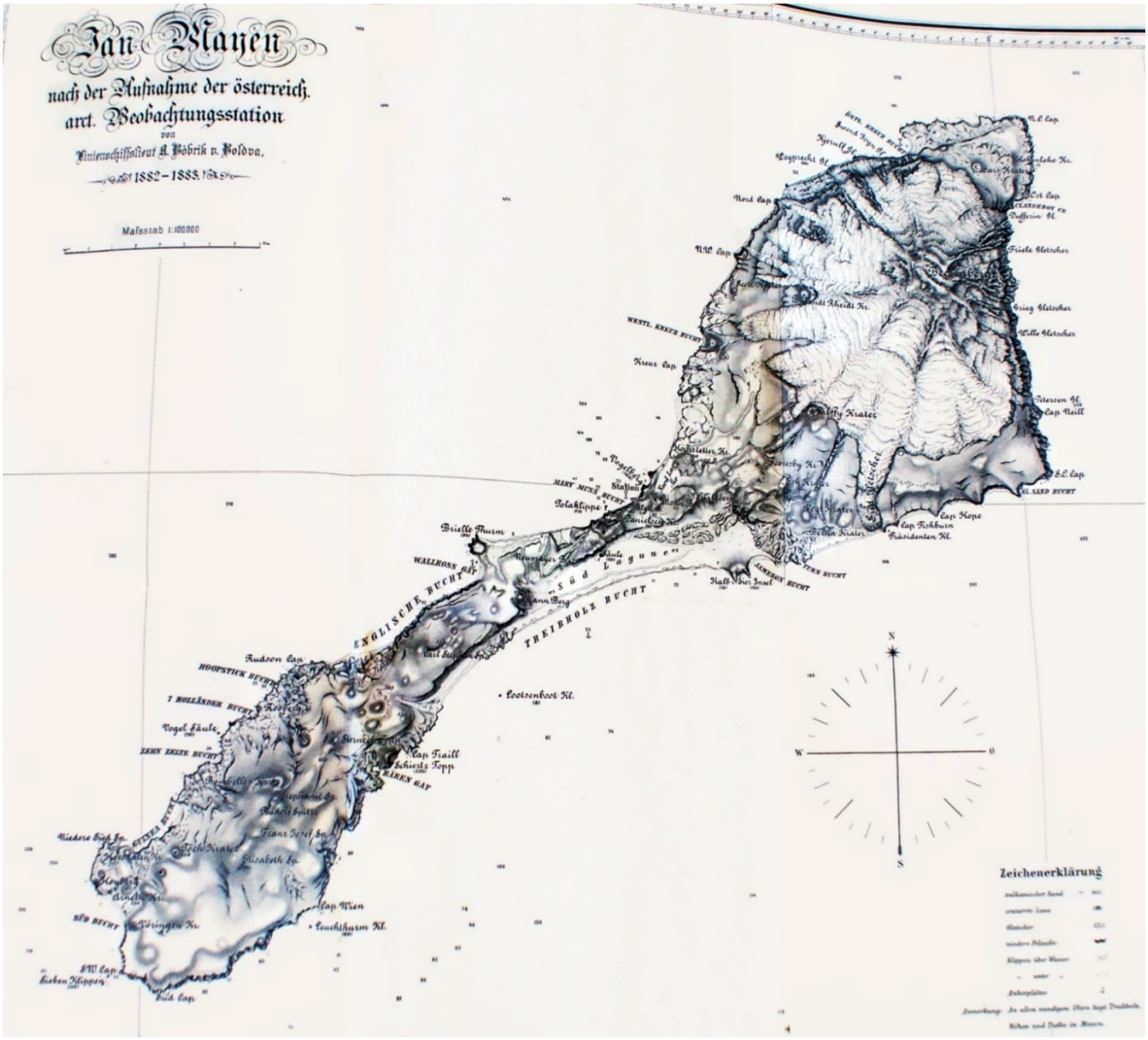

Figure 4.5: Map from an Austrian expedition to Jan Mayen in 1882 for the First International Polar Year (Boldva et al., 1886). For larger map: https://upload.wikimedia.org/wikipedia/commons/0/05/Jan_Mayen_map_1884_Schritt2_sw.png

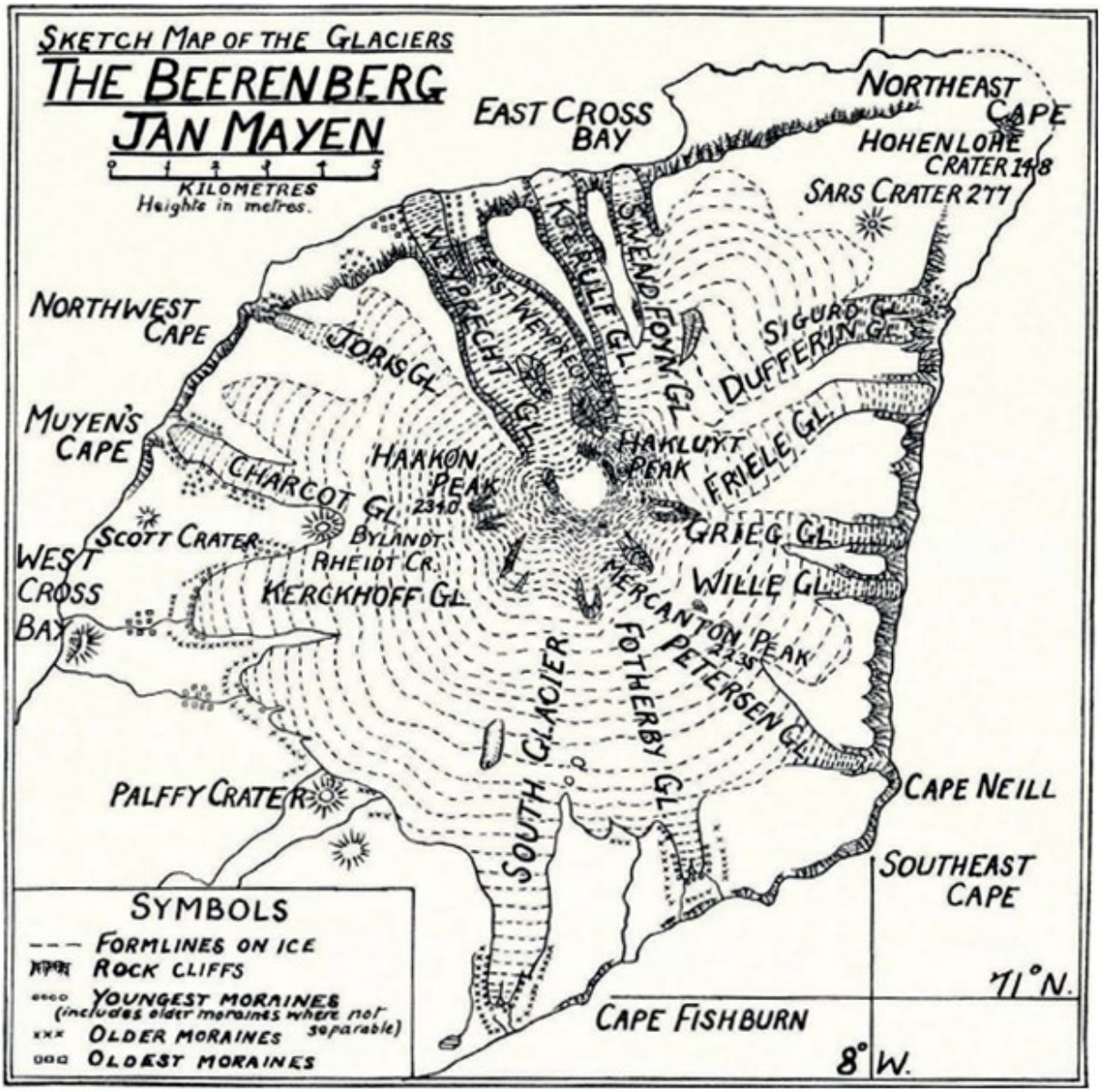

Figure 4.6: Map from The Imperial College of Science expedition to Jan Mayen in 1938 (Jennings, 1948).

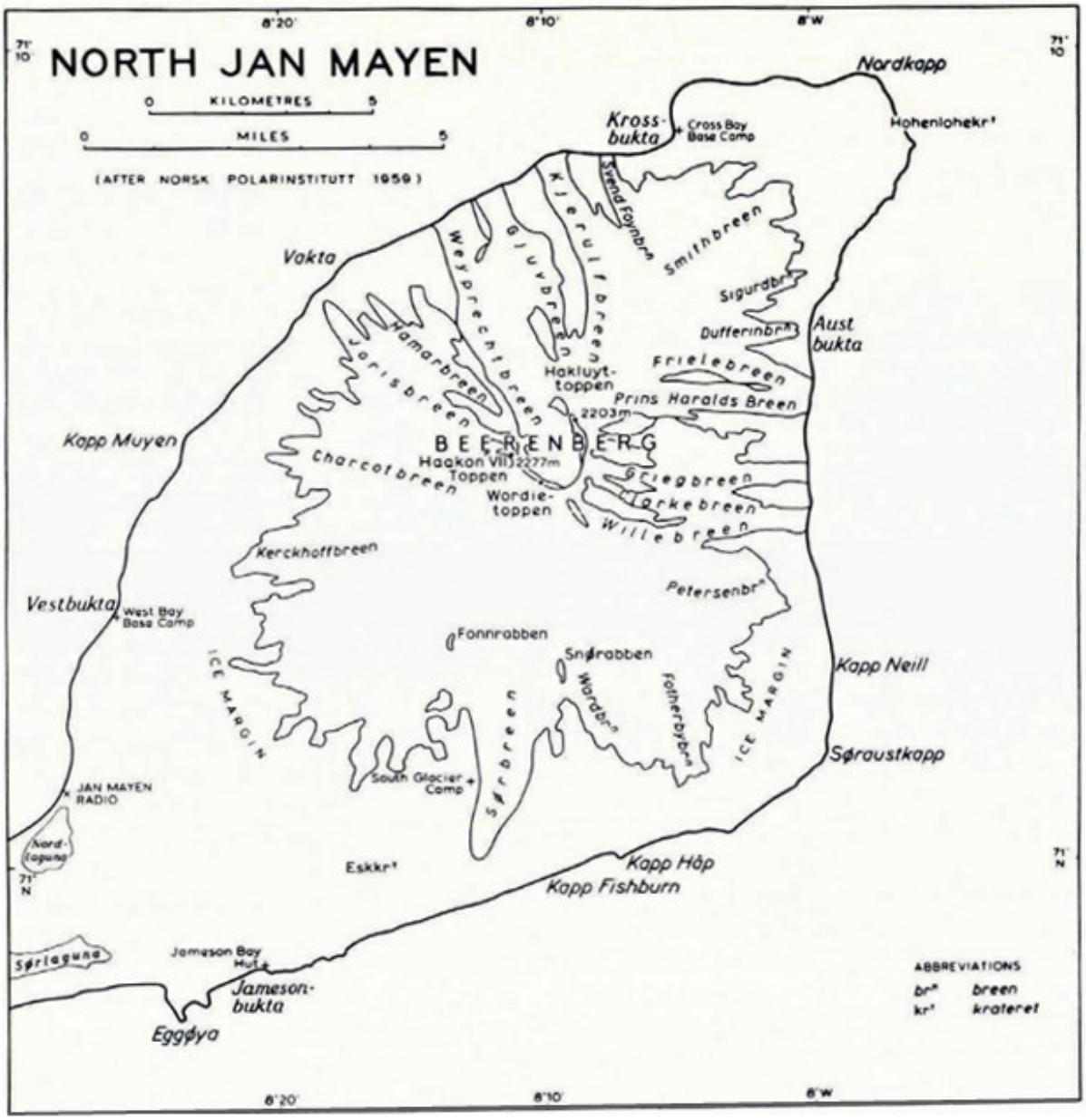

Figure 4.7: Map based on the University of London Jan Mayen Expedition in 1959 and the University of London Beerenberg Expedition in 1961(Kinsman and Sheard, 1963).

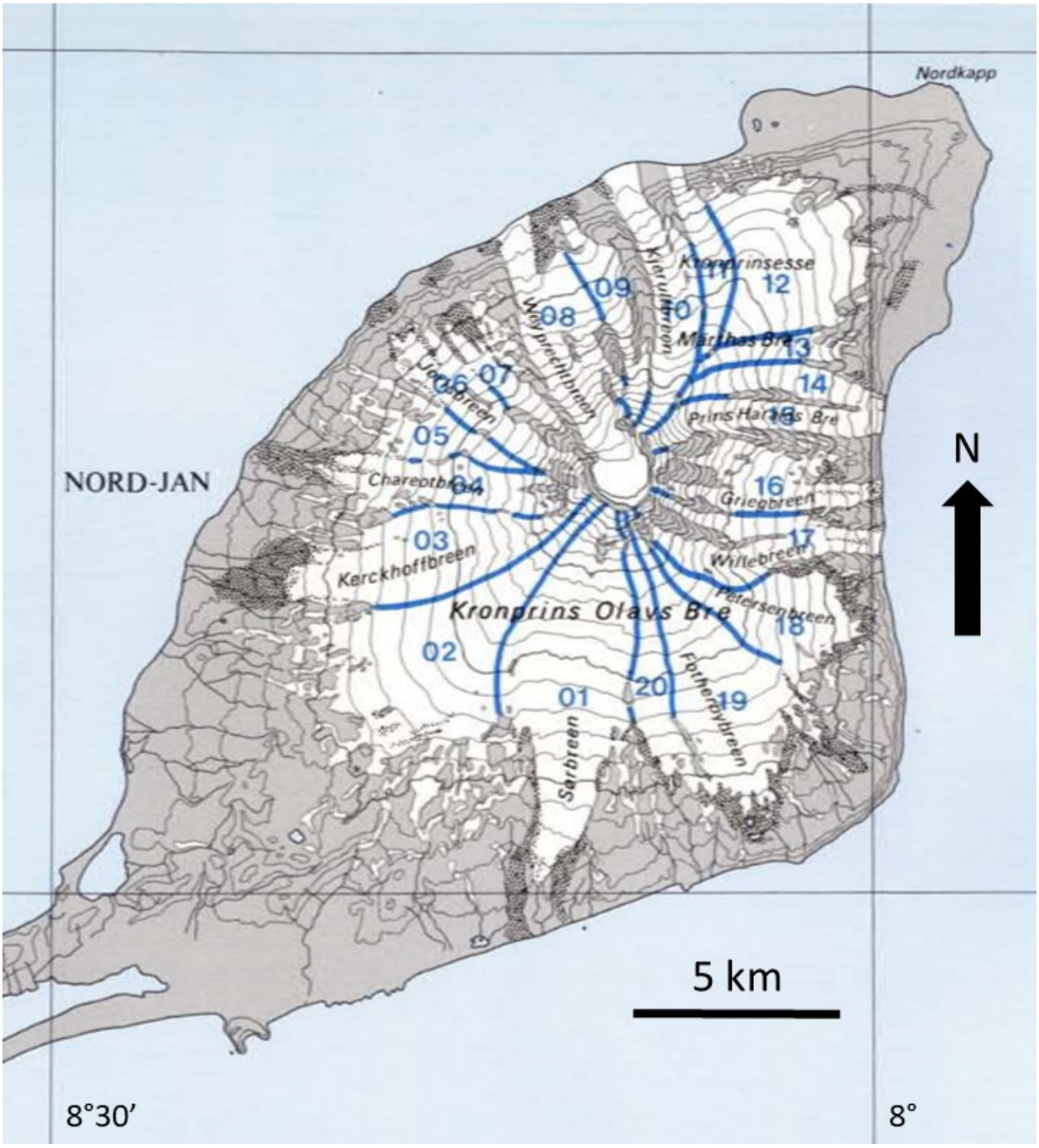

Figure 4.8: Map based on glacier extent data from aerial photos from 1959-1975 (Hagen et al., 1993)

Table 4.1: Marine-terminating glaciers as indicated by the historical maps (from 1861, 1877, 1882, 1938, 1961 and 1975; Figs 4.3-4.8) and observed in this study (2000 and 2020). Glacier number from Hagen et al. (1993); see Fig 4.8.

Glacier No	W or E side	Glacier name	1861	1877	1882	1938	1961	1975	2000	2020
1	E	Sørbreen	x	x	x					
2		Kpr Olavs Bre								
3	W	Kerckhoffbreen								
4	W	Charcotbreen			x					
5	W	Vestisen								
6	W	Jorisbreen			x					
7	W	Hamarbreen								
8	W	Weyprechtbreen	x	x	x	x	x	x	x	x
9	W	Gjuvbreen	x	x	x		x		x	
10	W	Kjerulfbreen		x	x	x	x	x	x	
11	W	Svend Foynbreen		x	x	x	x	x	x	
12		Kprs Marthas Bre								
13	E	Dufferinbreen	x	x	x					
14	E	Frielebreen	x	x	x	x	x	x	x	
15	E	Prins Haralds Bre	x	x	x	x	x	x	x	
16	E	Griegbreen		x	x	x	x	x		
17	E	Willebreen	x	x	x	x	x	x		
18	E	Petersenbreen		x	x					
19	E	Fotherbybreen								
20	E	Wardbreen								

Most historic maps indicate that Sørbreen, Gjuvbreen, Weyprechtbreen, Dufferinbreen, Frielebreen, Prins Haralds Bre, and Willebreen were marine-terminating. On the four earliest historic maps, both Prins Haralds Bre and Frielebreen were marked as marine-terminating in Table 4.1 whenever Frielebreen was indicated as being so, as these two glaciers were considered to be one and the same by these observers. It is easy to understand when one thinks of observing the island from the sea only. The Prins Haralds Bre - Frielebreen calving front was likely confluent and thus continuous in the past, and it would be difficult for observers from a ship to note the different drainage basins or to recognize medial moraines. Similarly, Gjuvbreen and

Weyprechtbreen likely had a continuous calving front in the past, thus whenever Weyprechtbreen was marked as marine-terminating Gjuvbreen was also marked as such for the earlier three maps. Neither Prins Haralds Bre nor Gjuvbreen were specifically named or drawn as distinct from their neighboring glaciers when they would clearly be marine-terminating at the same time for these three earlier maps.

Frielebreen and Prins Haralds Bre were labeled as distinct starting in the maps from the 1959/1961 expeditions, and Gjuvbreen (labelled "East Weyprecht") and Weyprechtbreen were distinct starting in the 1938 map. The 1938 Imperial College of Science expedition map shows Gjuvbreen's front as far inland from the coastline, as does the 1975 Hagen map. Jennings et al. (1948) describes this part of the glacier as "dead". However, the 1959/1961 map shows Gjuvbreen as marine-terminating, and makes a specific mention of this being distinct from the 1938 survey. Kinsman and Sheard (1963) observed that Gjuvbreen's front was 1000 m from the coast in 1938, and 1949 aerial imagery showed it as having advanced to 450 m from the coast. This advance continued, and in 1961 Gjuvbreen was observed as calving into the ocean. Gjuvbreen's accumulation area is at a lower elevation than other Jan Mayen glaciers (Kinsman and Sheard, 1963), thus shifts in the ELA might have a relatively greater effect on its glacier dynamics. Kinsman and Sheard (1963) also observed that Gjuvbreen's front was far less debris covered in 1961 than in 1959; indicating it is possible that Gjuvbreen was further advanced than previous studies showed, since it may have been difficult to distinguish the glacier surface from the surrounding topography. Jennings (1948) reports that the 1938 map from the expedition is "of a low order", as many observations were created using only a compass and photographs. Whether it is the changing debris cover or sensitivity to shifts in ELA (Cuffey and Paterson, 2010), there is precedent for the Gjuvbreen glacier front to quickly shift between marine- and land-terminating

states. Therefore, it is not unreasonable for the 1975 map to show Gjuvbreen as retreated far inland, and observations from this thesis to show it as marine-terminating in 2000.

Svend Foynbreen and Kjerulfbreen were marine-terminating in the two more detailed 19th century maps (1877 and 1882), yet in the 1861 map the west side of Jan Mayen has only one large marine-terminating glacier. It is possible that all four glaciers were marine-terminating and combined into a single floating glacier tongue, however, the outline of the island and place names on the 1861 map imply something else. North of the west-side marine-terminating glacier on the 1861 map (Fig 4.3) is a large bay. The 1877 map (Fig 4.4) had a bay in that approximate position labeled "Vestre Korsbugt", which translates to "West Cross Bay". The 1882 map (Fig 4.5) has a bay labeled "Westl. Kreuz Bucht", which also translates to "West Cross Bay", but which is smaller and in a more southerly position than in the two older maps. On contemporary Norwegian maps, this bay is called "Vestbukta" (translated "West Bay"; https://stadnamn.npolar.no/Vestbukta/Jan_Mayen), and as the island is now Norwegian, this bay will be referred to by its Norwegian name in this thesis (https://topojanmayen.npolar.no/). Vestbukta is located just south of Kerckhoffbreen, placing Weyprechtbreen, Gjuvbreen, Kjerulfbreen, and Svend Foynbreen all north of it. As Vestbukta is north of the glacier in the 1861 map, this implies that the marine-terminating glacier had a southerly aspect, while all marine-terminating glaciers on the west side in all other historical maps, and observed in this thesis, flow north. The 1877 expedition report (Mohn and Wille, 1882) mentions looking for a glacier between the two "Korsnes" (approximately the location of this south-facing glacier on the west side in the 1861 map), as a glacier had been drawn and indicated in multiple previous maps at this location. However, in 1877 the expedition only found "a few patches of snow scattered here and there" (Mohn and Wille, 1882), and no glacier that reached the sea. Mohn and Wille

(1882) state in this recount that many recent studies had only approached the east side of the island and depended on earlier Dutch maps to draw the west side. From the sailing and land routes outlined in red lines on the 1861 map, it seems likely that the earlier expedition did not see much of the northern side of Jan Mayen. It is unlikely that Weyprechtbreen and Kjerulfbreen were not marine-terminating at this time.

In the 19th century maps of Jan Mayen, nearly all glaciers on the east side of the island were marine-terminating regardless of north/south position on the coast, but on the west side the glaciers which faced south were not marine-terminating (except as suggested by the 1861 map). By the middle of the 20th century, many marine-terminating glaciers had retreated onto land. The 1961 expedition reported general advance of glaciers when compared to measurements form the 1938 expedition, yet only one glacier had possibly readvanced to a marine-terminating status (Jennings, 1948; Kinsman and Sheard, 1963).

4.3. Glacier Extent and Changes 2000-2020

The extents of marine-terminating glaciers were measured from satellite scenes with an average measurement frequency of 1.4 years, with a maximum of 1064 days (2.9 years) and a minimum of 267 days (0.7 years) between measurements (Table 4.2). Glaciers that were land-terminating over the full time period had a measurement frequency on average every 5.1 years, with a maximum of 5519 days (15.1 years) and a minimum of 297 days (0.8 years) between measurements. Glaciers had between 3-16 measurements in total over the time period, with a total length of observation period between 14-20 years (Table 4.2).

Table 4.2: Observation period, number of measurements, and average, maximum, and minimum number of days between measurements. Glacier No. refers to the numbers on the map in Fig 2.9.

Glacier No.	Glacier name	Observation period (years)	Last marine meas. (year)	meas. (count)	Avg. time between meas. (days)	Max. time between meas. (days)	Min. time between meas. (days)
West side glaciers							
8	Weyprechtbreen	2000-2020	2020	14	564.8	1007	306
10	Kjerulfbreen	2000-2020	2016	14	564.8	1064	315
11	Svend Foynbreen	2000-2018	2010	9	815.9	2177	315
9	Gjuvbreen	2000-2020	2002	6	1468.6	3997	306
4	Charcotbreen	2002-2020		4	2189.3	4801	297
7	Hamarbreen	2000-2020		3	3671.5	5519	1824
6	Jorisbreen	2002-2020		4	2189.3	3663	315
3	Kerckhoffbreen	2001-2020		6	1393.2	4392	409
East side glaciers							
15	Prins Haralds Bre	2000-2020	2018	15	484.8	816	267
14	Frielebreen	2000-2020	2013	14	564.8	1120	290
13	Dufferinbreen	2000-2020		4	2424.0	4392	1410
19	Fotherbybreen	2002-2018		3	2924.0	5096	752
16	Griegbreen	2004-2018		3	2523.0	2541	2505
18	Petersenbreen	2000-2018		4	2184.7	4783	752
1	Sørbreen	2001-2018		6	1243.2	2505	448
17	Willebreen	2003-2020		4	2090.3	4392	409

While the overall trend of the glaciers is retreat, the characteristic oscillating retreat/advance pattern noted in past studies of the island's glaciers (Anda et al., 1985; Orheim, 1993) is evident, which is indicative of a short response time to climate variability (Figure 4.9; Anda et al., 1985; Hoelzle et al., 2003). While several Jan Mayen glaciers experienced some period of advance in the time period 2000-2020, not all of them did. Therefore, "Maximum advance rate" as labeled in Table 4.3 is negative for the glaciers which did not have any observed advance. Maximum advance rates generally occur in the earlier part of the time period (~2000–2004), while maximum retreat rates generally occur in the later part (~2012–2019). The most advanced position is generally 2000–2004, and most retreated position is generally 2016–2020.

All glaciers had a negative average retreat/advance rate and thus have generally retreated between 2000–2020, although some to a very small degree. Gjuvbreen, Charcotbreen, Kerckhoffbreen, Frielebreen, Petersenbreen, and Sørbreen were the only glaciers to retreat >10 m/yr by average. All of these, except for Kerckhoffbreen, were marine-terminating in at least one of the historical maps, and all but Gjuvbreen and Frielebreen are located on the southern half of the mountain. Most glaciers had some time period over which they advanced, except for Gjuvbreen, Fotherbybreen, Hamarbreen, Jorisbreen, and Petersenbreen. The general trend of the glaciers of Jan Mayen for 2000-2020 was retreat (Fig 4.9), and the average retreat/advance rate for all glaciers with measurements on the island over the 2000–2020 was -9 m/yr, with a standard deviation of 7 m/yr (Table 4.3).

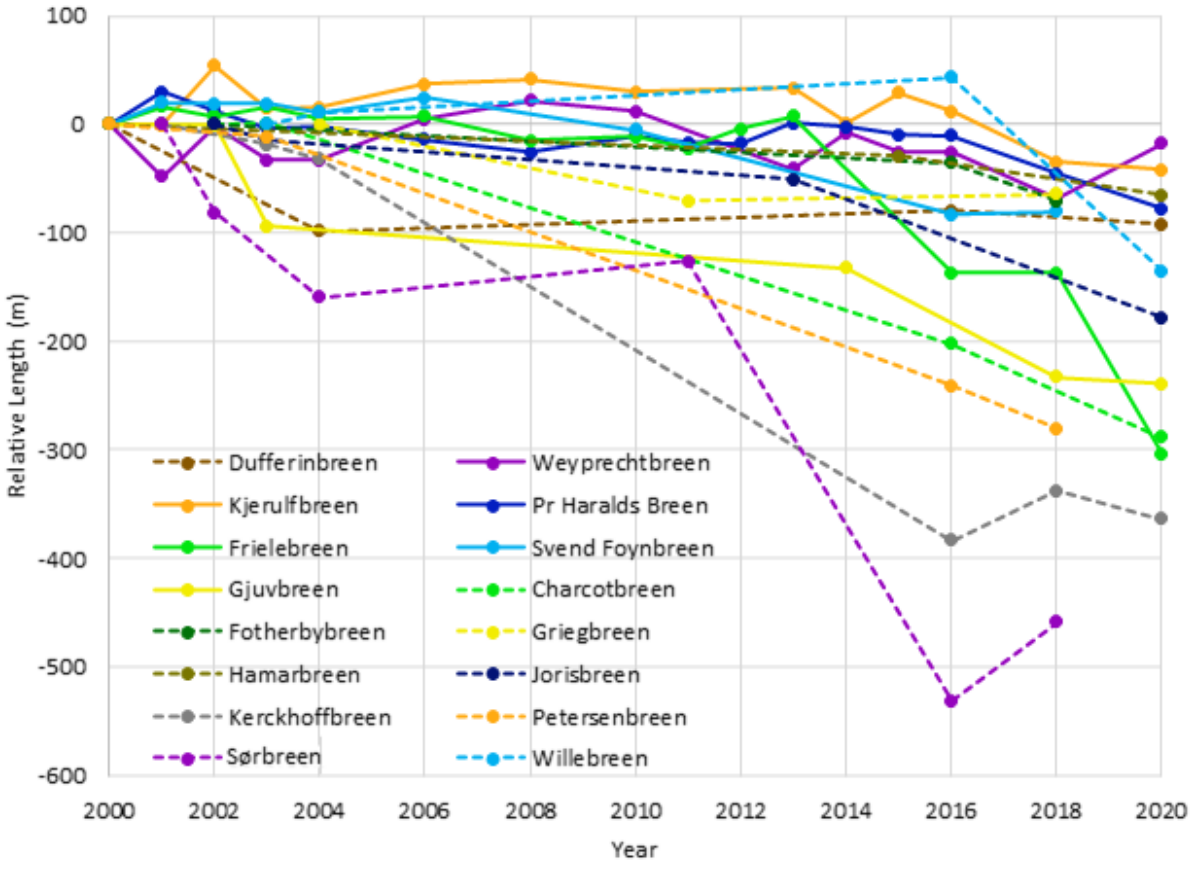

Figure 4.9: Relative length of all glaciers on Jan Mayen with measurements taken in this study. Glaciers that were marine-terminating in 2000 are solid lines, glaciers that were land-terminating 2000–2020 are dashed lines.

Table 4.3: Maximum advance (a.), maximum retreat (r.), and average retreat/advance rates for each glacier considered in this study and the time period over which the rate was observed, year of most advanced and most retreated position, the total retreat, and years over which the glacier was observed. Each rate is in units of m/yr, even when the time period the rate spans is more than one year.

Glacier name	Max. a. rate (m/yr)	Years	Max. r. rate (m/yr)	Years	Avg. rate (m/yr)	Most adv. position	Most ret. position	Tot. ret.	Time span
West side glaciers									
Weyprechtbreen	47	2001–02	-48	2000–01	-1 ± 23	2008	2018	-18	2000-20
Kjerulfbreen	55	2001–02	-39	2002–03	-2 ± 20	2002	2020	-42	2000-20
Svend Foynbreen	20	2000–01	-11	2010–16	-4 ± 8	2006	2016	-80	2000-18
Gjuvbreen	0	2000–02	-89	2002–03	-12 ± 20	2000	2020	-239	2000-20
Charcotbreen	1	2002–03	-22	2016–20	-16 ± 5	2003	2020	-289	2002-20
Hamarbreen	-2	2000–15	-7	2015–20	-3 ± 2	2000	2020	-65	2000-20
Jorisbreen	-4	2003–13	-18	2013–20	-10 ± 7	2002	2020	-178	2002-20
Kerckhoffbreen	23	2016–18	-29	2004–16	-19 ± 16	2001	2016	-364	2001-20
East side glaciers									
Prins Haralds Bre	30	2000–01	-17	2016–18	-4 ± 12	2001	2020	-78	2000-20
Frielebreen	18	2011–12	-83	2018–20	-15 ± 26	2001	2020	-304	2000-20
Dufferinbreen	2	2004–16	-25	2000–04	-5 ± 10	2000	2004	-93	2000-20
Fotherbybreen	-3	2002–16	-17	2016–18	-4 ± 5	2002	2018	-70	2000-18
Griegbreen	1	2011–18	-10	2004–11	-5 ± 6	2004	2011	-64	2004-18
Petersenbreen	-4	2000–03	-20	2016–18	-15 ± 5	2000	2018	-281	2000-18
Sørbreen	36	2016–18	-82	2001–02	-27 ± 44	2001	2016	-459	2001-18
Willebreen	11	2003–04	-45	2016–20	-8 ± 20	2016	2020	-136	2003-20

The absolute value of maximum retreat rates was on average five times larger than maximum advance rate for the same glacier. Gjuvbreen had the maximum single yearly value retreat rate (-89 m/yr, 2002-03; Table 4.3). The marine-terminating glacier Kjerulfbreen had the maximum single value yearly advance rate (55 m/yr, 2001-02), and Weyprechtbreen had the smallest magnitude average retreat (-1 m/yr). The minimum total retreat was also Weyprechtbreen, which is the last marine-terminating glacier on the island. Marine-terminating glaciers generally had larger magnitudes of advances and retreats than land-terminating glaciers, although maximum advance rates for Sørbreen and Kerckhoffbreen do fit in amongst these. Kerckhoffbreen and Sørbreen also changed in very similar ways, both experiencing quick retreats

to 2016, a slight advance to 2018, the fastest average retreat on the island, and the largest total retreat. As they are not very similar in area, slope, or length, this could indicate that it is south-facing glaciers that are the most susceptible to current warming temperatures.

Kerckhoffbreen, Svend Foynbreen, Sørbreen, and possibly Griegbreen advanced between 2016 and 2018. Griegbreen's result is inferred from the 2018 position being further advanced than in 2011, since its 2016 position could not be measured. These four glaciers are separated from each other by at least one other glacier, and thus are not clustered in a specific region of the island. Additionally, Svend Foynbreen was a marine-terminating glacier in 2000, thus it is not only glaciers that were land-terminating for the whole period which experienced the advance (although Svend Foynbreen was land-terminating during said advance).

Weyprechtbreen and Kjerulfbreen had both maximum retreat and maximum advance rates between 2001–2003. Gjuvbreen is the only glacier with a reliable measurement in the year after its last marine-terminating measurement. The retreat within this year is the highest magnitude rate experienced by any glacier on the island, and it is possible that more marine-terminating glaciers experienced a larger retreat over the year that they transition from marine- to land-terminating. Weyprechtbreen is the only glacier that still calves into the ocean; the last year Gjuvbreen, Svend Foynbreen, Frielebreen, Kjerulfbreen, and Prins Haralds Bre had a marine-terminating measurement was: 2002, 2010, 2013, 2016, and 2018, respectively.

The east-side land-terminating glaciers had more variability in their relative lengths than the west side (Figures 4.10–4.11). However, the range of advance and retreat rates for marine-terminating glaciers was similar between the two sides: east side glaciers had a range of -83 to 36 m/yr while west side glaciers had a range of -89 to 55 m/yr. For both sides of the island, the southernmost glacier had the largest retreat (Sørbreen for the east side and Kerckhoffbreen for the

west side). Unrelated to their rates, these southern-most glaciers were both used as the representative land-terminating glaciers for their respective sides. Prins Haralds Bre and Frielebreen had very similar retreat and advance patterns, and their basins are next to each other (Figure 4.10). Willebreen, Dufferinbreen, and Sørbreen advanced over 2004–2011. These glaciers are spaced out along the west side of the island, with three glaciers separating them each from the other, and thus are not clustered in a specific region of the island.

Dufferinbreen and Frielebreen are the two glaciers closest to the location of the last known volcanic eruption (see Section 2.4.4). The magnitudes of the total retreat, maximum retreat rate, and average retreat rate for Dufferinbreen are in the middle range but are the highest for the glaciers on the north end of the east side. However, Frielebreen has the highest maximum retreat rate and the second highest average retreat rate and total retreat on the east side. During this time it did retreat from marine-terminating to land-terminating during this period, which might explain the magnitude of the retreat rate and total retreat.

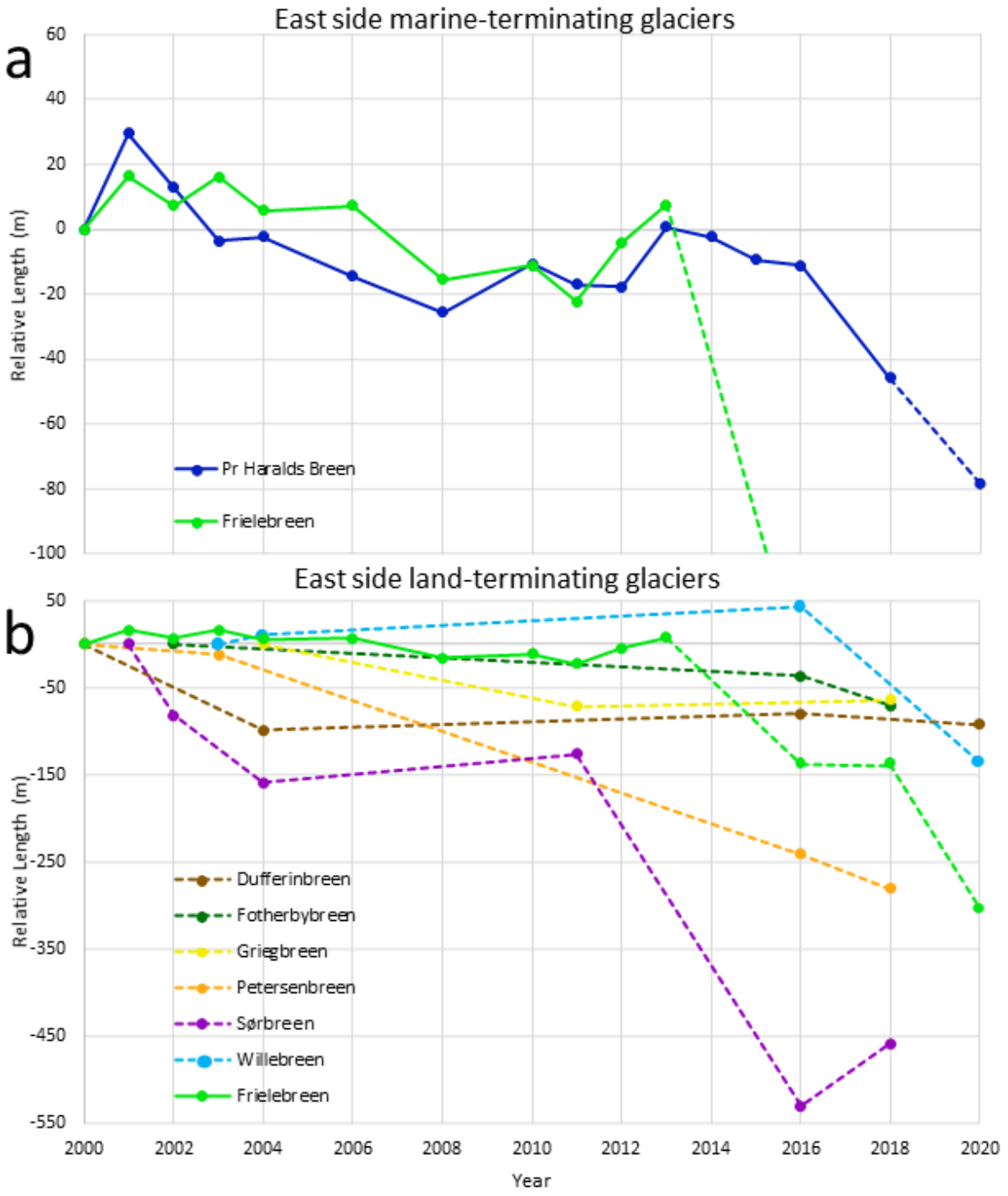

Figure 4.10: East side relative length glacier fluctuations separated into a) marine- and b) land-terminating. Lines are same colors as in Figure 4.9. For periods when glaciers are marine-terminating, lines are solid, while land-terminating glacier lines are dashed. Lines connecting the last marine-terminating measurement to the first land-terminating measurement are dashed. Prins Haralds Bre is included with the marine-terminating glaciers and not the land, as it has only 2 land-terminating measurements.

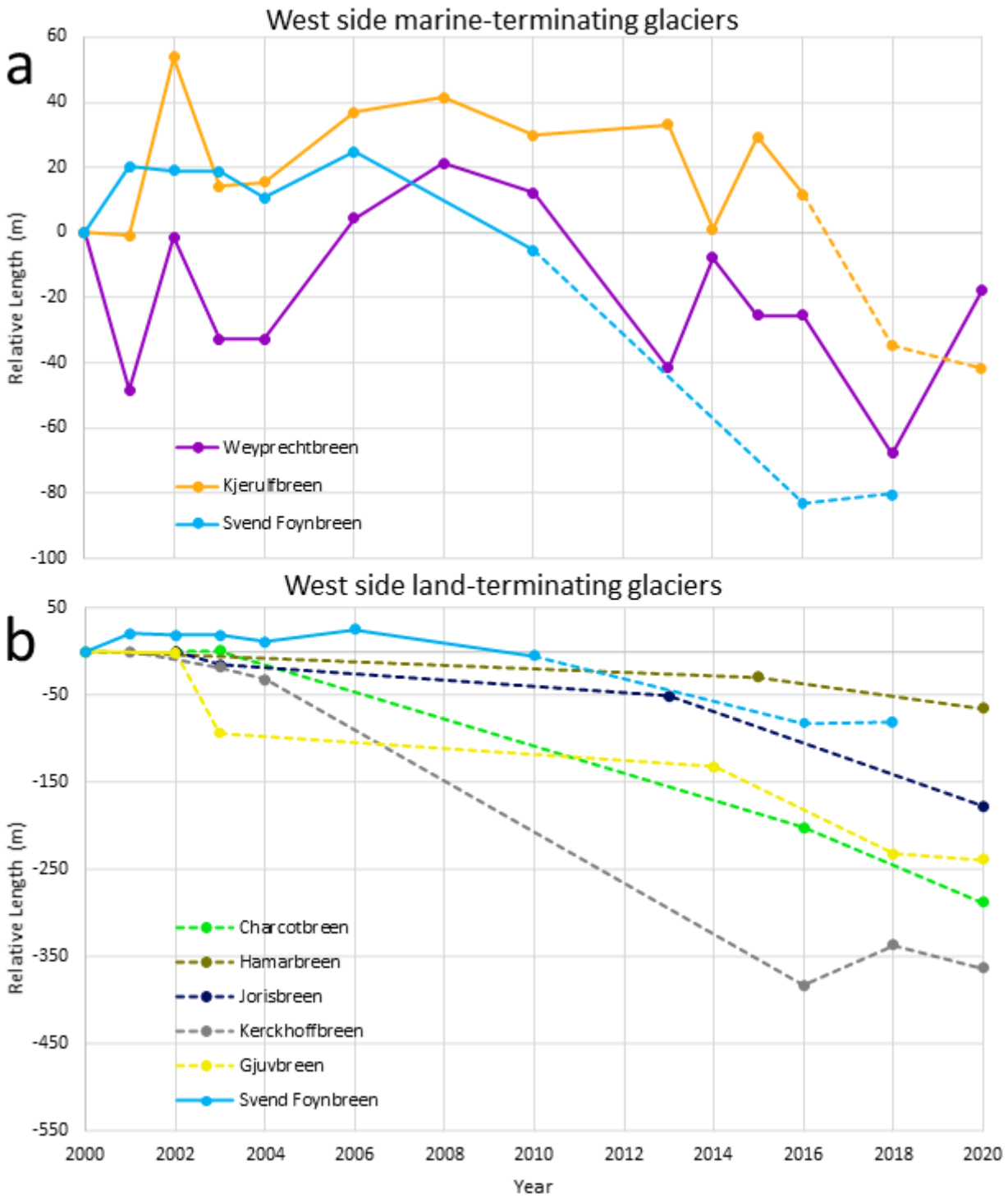

Figure 4.11: West side relative length glacier fluctuations separated into a) marine- and b) land-terminating. Lines are same colors as in Figure 4.9. For periods when glaciers are marine-terminating, lines are solid, while land-terminating glacier lines are dashed. Lines connecting the last marine-terminating measurement to the first land-terminating measurement are dashed. Gjuvbreen is included with the land-terminating glaciers and not the marine, as it has only 2 marine-terminating measurements.

On the west side of the island, the larger marine-terminating glaciers Kjerulfbreen and Weyprechtbreen showed similar trends (Figure 4.11), except for 2013–2014. Both glaciers tended to create a local horizontal protrusion, for Weyprechtbreen along the north side of its calving front and for Kjerulfbreen along the south side, which would break off and reform. Nearly yearly observations indicate that the time frame of protrusion growth and breakoff was between 2-9 years, however, seasonal trends could be important and were not captured in this study. Until Svend Foynbreen became land-terminating in 2010, it had a trend similar to but more moderate than Weyprechtbreen and Kjerulfbreen's. Since then, it retreated similarly to other land-terminating glaciers on the west side. The four representative glaciers are named on Fig 4.12, along with all measurements created in this thesis. For all glacier fluctuations measurements as they will appear in the WGMS FoG database, See Appendix B.

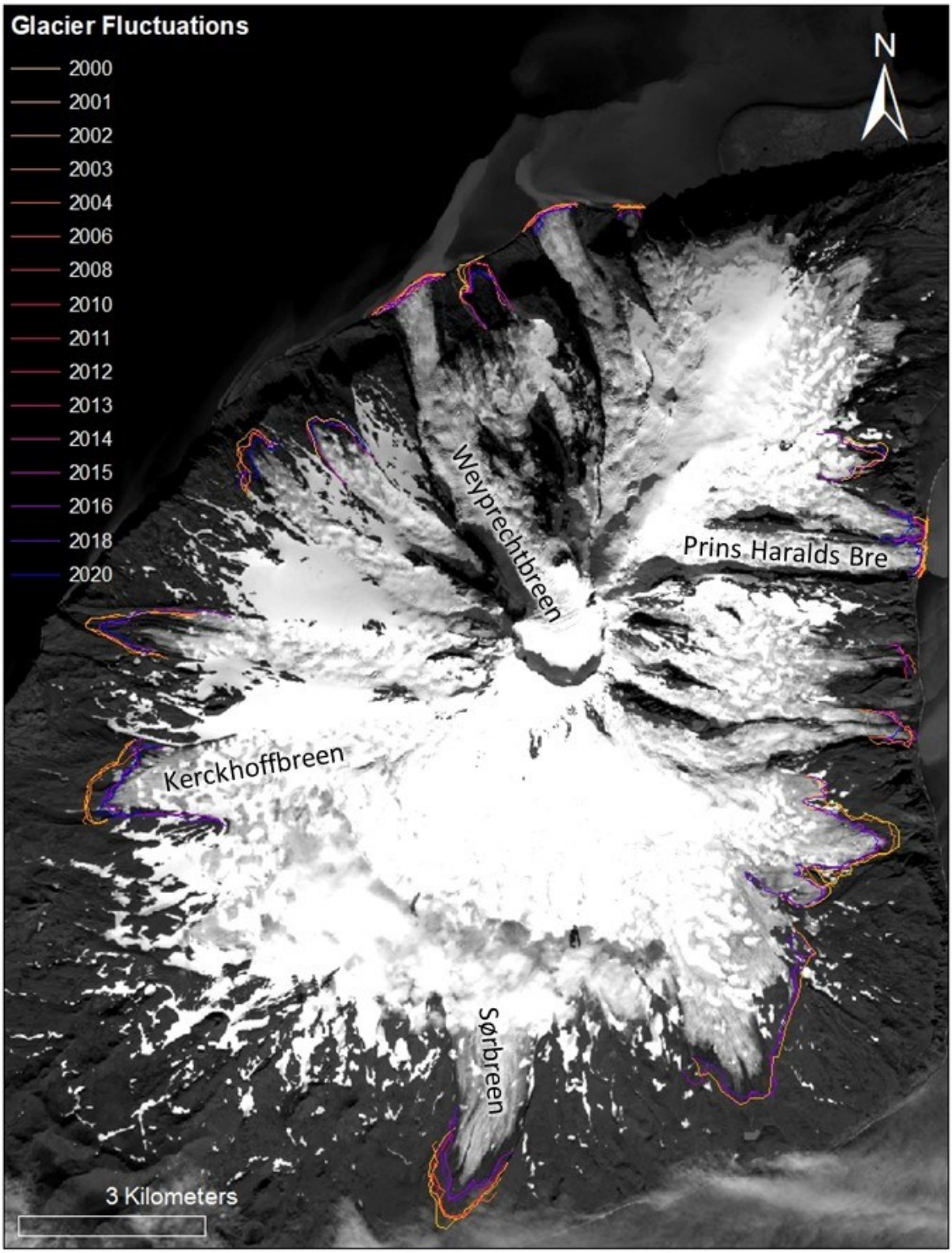

Figure 4.12: All digitized lines for all glaciers considered in this study, with the four representative glaciers named. Background image is Landsat 8 Band 8 of 19 August 2016.

There were only 16 glaciers with frontal measurements for this thesis, and only eight each for the east side and west side of Jan Mayen. Therefore, this is too small a population to derive statistically significant differences between the two sides of the island and between the differing terminus states. However, the glaciers of Jan Mayen were still separated into east- or west-side and marine- or land-terminating, then the average retreat rate, the maximum retreat rate, and the maximum advance rate were calculated for exploration. There was no significant difference between east-side glaciers and west-side glaciers, or between marine-terminating and land-terminating glaciers (Table 4.4). However, for the duration during which the marine-terminating glaciers were marine-terminating, their retreat rate had to be more or less balanced by their advance rate. Hence, even though the average retreat rates of the two terminus states are within the other's standard deviation, it is likely that the marine-terminating glaciers did in general retreat slower than the land-terminating glaciers. Additionally, on the east side of the island, the land-terminating glaciers experienced higher magnitude maximum advance and retreat rates, while on the west side it was the marine-terminating glaciers that experienced the higher magnitude maximum retreat rate.

Table 4.4: Average, maximum, and minimum retreat/advance rates for different bins of the glaciers on Jan Mayen. Glaciers which experienced the maximum or minimum retreat/advance pattern are named to the right of their respective value. Only values between matching terminus states (i.e., marine- or land-) are considered for their respective bins.

Bin	Avg. ret. rate (m/yr) ± st. dev.	Max adv. rate (m/yr)	Glacier	Max ret. rate (m/yr)	Glacier
Marine	-1 ± 17	55	Kjerulfbreen	-48	Weyprechtbreen
Land	-11 ± 19	36	Sørbreen	-83	Frielebreen
E - all	-10 ± 22	36	Sørbreen	-83	Frielebreen
W - all	-8 ± 16	55	Kjerulfbreen	-89	Gjuvbreen
E - Marine	-1 ± 11	30	Prins Haralds Bre	-17	Prins Haralds Bre
W - Marine	0 ± 20	55	Kjerulfbreen	-48	Weyprechtbreen
E - Land	-12 ± 24	36	Sørbreen	-83	Frielebreen
W - Land	-11 ± 11	23	Kerckhoffbreen	-29	Kerckhoffbreen

4.4. Glacier Area Loss and Frontal Ablation

Over the period of 2000-2020, Jan Mayen Island lost a total glacier area of 2.15 km^2 or 1.9% of the island's ice area (Table 4.5). This area loss is a minimum estimate, as it can be assumed that the four glaciers which were not considered in this study also retreated during this period. According to the RGI, the former total glacier area not including ice patches was 118.8 km^2 (RGI Consortium, 2017). While the RGI outlines were not used as the basis for fronts digitized in this thesis, it can be concluded that the previous glacier area was close to 119 km^2, and it is now closer to 117 km^2, or changed from covering 31.2% to 30.7% of the total area of the island.

Table 4.5: Frontal ablation low and high estimates and ice area lost for each glacier considered in this study for the entire time period (2000–2020). Included for context is glacier area (from RGI; Pfeffer et al., 2014) and the percentage of that area that was lost.

Glacier No.	Glacier name	Ice area loss (km^2)	Glacier area (km^2)	Ice area loss (%)	FA (km^3)
8	Weyprechtbreen	-0.024	8.2	0.3	0.1038 ± 0.021
10	Kjerulfbreen	-0.075	5.3	1.4	0.0448 ± 0.008
15	Prins Haralds Bre	-0.051	3.4	1.5	0.0354 ± 0.007
14	Frielebreen	-0.100	2.6	3.9	0.0073 ± 0.001
11	Svend Foynbreen	-0.031	2.5	1.3	0.0058 ± 0.001
9	Gjuvbreen	-0.147	2.7	5.4	0.0011 ± 0.0002
4	Charcotbreen	-0.122	5.4	2.3	
13	Dufferinbreen	-0.047	1.6	3.0	
19	Fotherbybreen	-0.137	9.0	1.5	
16	Griegbreen	-0.023	4.5	0.5	
7	Hamarbreen	-0.034	2.3	1.5	
6	Jorisbreen	-0.139	4.0	3.4	
3	Kerckhoffbreen	-0.377	9.1	4.2	
18	Petersenbreen	-0.421	5.5	7.7	
1	Sørbreen	-0.370	15.4	2.4	
17	Willebreen	-0.053	4.9	1.1	
	Sum:	**-2.151 ± 0.008**	**118.8**	**1.8**	**0.198 ± 0.037**

Petersenbreen, Kerckhoffbreen, and Sørbreen, together, were responsible for 54% of Jan Mayen's total glacier loss (Table 4.5). Sørbreen and Kerckhoffbreen are two of the largest glaciers on the island, and also lost a larger percentage of their area than most other glaciers. These two glaciers, additionally, had the largest average and overall retreat for the glaciers on the island (Table 4.3). Petersenbreen lost the most ice area by percentage (7.7%), and it is neither one of the island's largest or smallest glaciers. Weyprechtbreen and Griegbreen experienced the lowest ice area loss, both in absolute and relative terms.

Data from the ITS_LIVE project using Sentinel-2 imagery that were provided by Dr. Mark Fahnestock (pers. comm., Feb 2019) revealed that Weyprechtbreen and Kjerulfbreen were the fastest moving glaciers on the island, with flow speeds on the order of 1 m/day in their steep upper regions and 0.25 m/day closer to the terminus (Fig 4.13). These data also indicated that most of the marine-terminating glaciers experienced much higher flow speeds than Sørbreen, which is the only glacier with previous velocity measurements (Lamb et al., 1962). The ground-based stake velocity measurement taken in 1961 at Sørbreen measured a maximum of 0.3 m/day at 900 m elevation, while at the glacier terminus speeds of only ~0.05 m/day were observed, a value consistent with velocities from ITS_LIVE. Values of the frontal ablation in Table 4.5 are the average of the high and low estimate, with their difference as the error, while Table 4.6 presents the frontal ablation separated into high and low estimates of both terminus change and ice discharge, as shown in EQ 3.3. The total frontal ablation between 2000-2020 from the entire island of Jan Mayen is 0.18-0.22 km^3, with Weyprechtbreen contributing 52% to this total (Table 4.5). When not considering Weyprechtbreen, glaciers on the west side still contributed more to frontal ablation than glaciers on the east side.

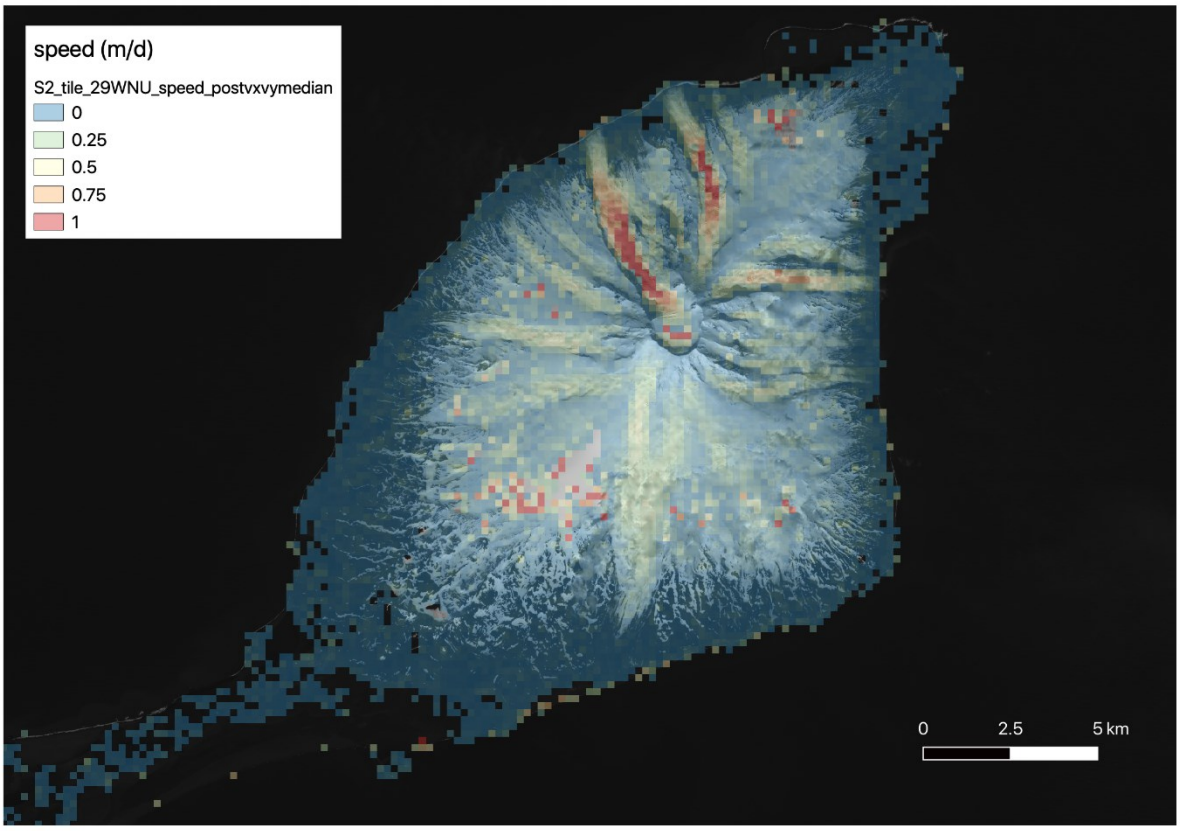

Figure 4.13: Velocity map of Jan Mayen from ITS_LIVE methods (Gardner et al., 2019) with Sentinel-2 images provided by Dr. Mark Fahnestock (pers. comm, Feb 2019).

Table 4.6: Values used to calculate the frontal ablation (FA) for 2000-2020. Low estimate assumes a maximum glacier thickness of 80 m, high estimate assumes 100 m.

Glacier name	Years calving 2000-2020	Term. change LOW (km^3)	Term. change HIGH (km^3)	Ice discharge LOW (km^3)	Ice discharge HIGH (km^3)	2000-2020 FA LOW	2000-2020 FA HIGH
Weyprechtbreen	21	-0.0009	-0.0010	0.0927	0.1130	0.0935	0.1140
Kjerulfbreen	17	0.0004	0.0005	0.0411	0.0494	0.0406	0.0489
Prins Haralds Bre	19	-0.0010	-0.0012	0.0311	0.0374	0.0322	0.0386
Frielebreen	14	0.0000	0.0001	0.0069	0.0079	0.0068	0.0079
Svend Foynbreen	11	-0.0001	-0.0001	0.0053	0.0061	0.0054	0.0062
Gjuvbreen	3	0.0000	0.0000	0.0010	0.0012	0.0010	0.0012

4.5. Glacier Response Time

The response time for Sørbreen was calculated from Eq 3.4 using 3 thickness scenarios estimated from Fig 6 in Anda et al. (1985) and 3 mass balance measurements at the toe (Orheim, 1976; Hulth et al., 2010). Thickness estimates are 30 m, 50 m, and 80 m. These are lower than estimates used for marine-terminating glaciers, however, Sørbreen is both land-terminating and retreated from its maximum extent, which was estimated to have a maximum thickness of 80 m from Fig 6 of Anda et al. (1985). Net mass balance estimates values used were -2 m w.e. from the 1972/73 hydrologic year, -4.25 m w.e. from 1973/1974 (Orheim, 1976), and -6 m w.e. from 2007/08 (Hulth et al., 2010). The results are values that range from 5 to 40 years, with an average of 16. This is in line with a predicted response time of 10–20 years for Jan Mayen glaciers from other studies (Fitch et al., 1962; Anda et al., 1985; Hagen et al., 1993) and with the response time based on the length and slope classes used by Hoelzle et al. (2003). Zemp et al. (2015) observed that glaciers with shorter response times experience intermittent readvances, which matches the behavior of Jan Mayen glaciers. As response times are not generally accurate to within a single year, for the purpose of correlating glacier fluctuations to their potential climate and oceanic drivers (see e.g. Carr et al. (2014) for this practice), a response time of 15 years was used. However, due to the scarcity of mass balance data, the response time was calculated from observations on a land-terminating glacier only, and the marine-terminating glaciers on Jan Mayen may not have the same responses (e.g. Robel et al., 2018).

4.6. Olonkinbyen Weather Station and Climate Reanalysis Results and Trends

Weather measurements at the WMO station at Olonkinbyen are nearly continuous since 1921. During the Second World War there was a brief time period (1 September 1940 to 30 April 1941) when measurements were not taken, and, therefore, these annual averages are not used in

this thesis. As both years had measurements for the entirety of June-August, the summer temperature averages were continuous. However, the station was moved three times between 1921 and 1962 (Fig 3.1) and it has been argued that the precipitation measurements cannot be considered continuous and homogeneous (Steffenson, 1982). Precipitation data prior to 1962 are shown in Figure 4.14 for completeness and to exhibit possible systematic differences in precipitation between different sides of the island, but these data were not considered for further analyses. Additionally, SST measurements were not always taken every day. See Appendix C for the number of SST measurement days per year, and details on why certain measurements were not used in this thesis.

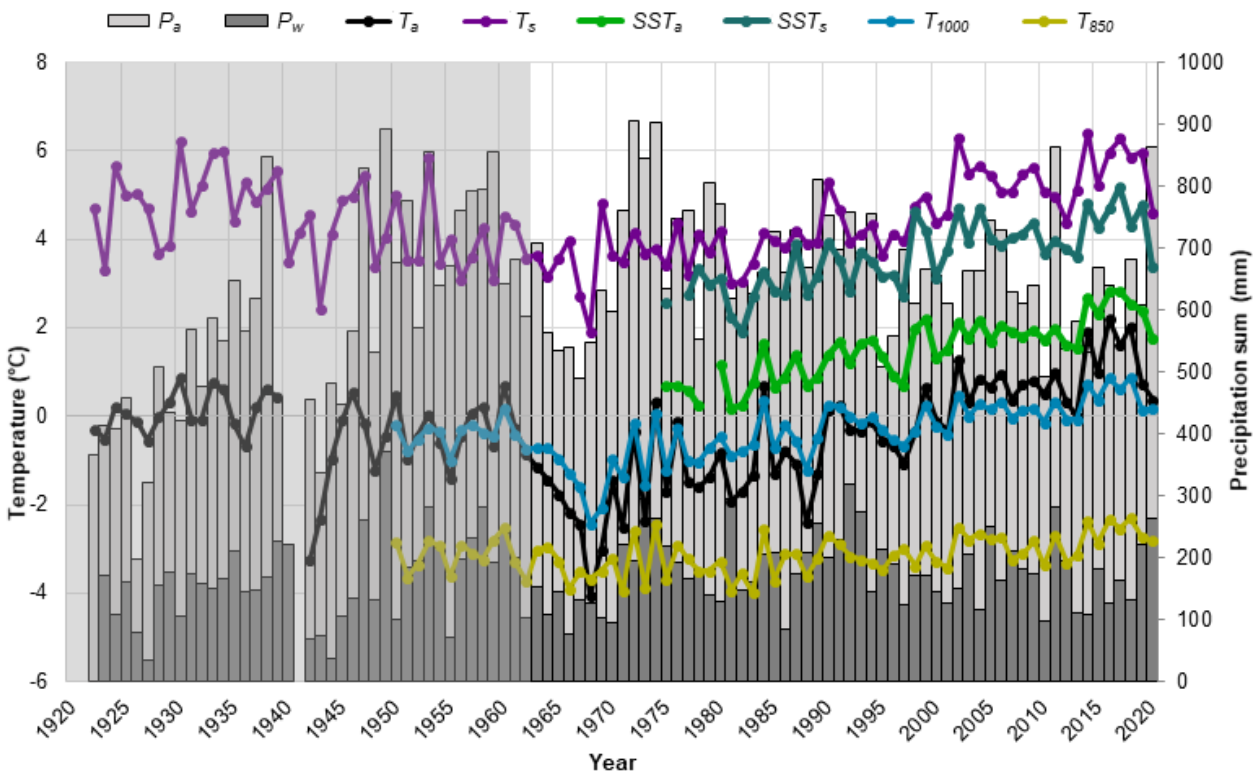

Figure 4.14: Air temperature, precipitation, and SST from the weather station on Olonkinbyen and air temperature from climate reanalysis. Grey shaded area indicates time when weather station was not at its current location. Air temperature can be considered continuous, but precipitation cannot.

Table 4.7 shows the maximum and minimum values for each weather and climate reanalysis parameter, and the year in which that value occurred (for precipitation only years 1962 and later were considered). All temperature-related data (SST, T, PDD, PDDN) and RH_{850} had their maximum values occur post-2013, while P_a, RH_{1000}, and C_{1000} had maximums in the late 1960s to early 1970s and P_w and C_{850} between these time periods. Most minimum values occurred before 1970, with SST_a and SST_s, T_{850}, RH_{1000}, and C_{850} experiencing minimums in the late-1970s to early-1980s and $PDDN_{850}$ and C_{1000} in the mid-2010s. All temperature-related data taken at Olonkinbyen or at the 1000 hPa climate reanalysis level had a minimum in 1968 except for SST.

Table 4.7: Maximum and minimum values and associated years for all climatic and oceanic parameters.

Parameter	Maximum value	Year	Minimum value	Year
P_a (mm)	904.1	1972	197.1	1967
P_w (mm)	371.6	1992	34.7	1966
SST_a (°C)	2.8	2017	0.2	1981
SST_s (°C)	5.2	2017	1.9	1982
T_a (°C)	2.2	2016	-4.1	1968
T_s (°C)	6.4	2014	1.9	1968
T_{1000} (°C)	0.9	2018	-2.4	1968
T_{850} (°C)	-2.3	2018	-4.0	1983
PDD_O (°C)	1144.9	2016	292.9	1968
PDD_{1000} (°C)	517.7	2016	134.6	1968
PDD_{850} (°C)	192.8	2017	54.8	1962
$PDDN_O$	266.0	2018	122.0	1968
$PDDN_{1000}$	288.0	2018	167.0	1968
$PDDN_{850}$	134.0	2017	66.0	2012
RH_{1000} (%)	89.6	1969	79.9	1983
RH_{850} (%)	76.5	2018	67.4	1968
C_{1000}	0.2	1968	0	2015
C_{850}	0.3	2007	0.2	1977

The ranges in most temperature parameters were small, which is to be expected for a small island (Table 4.7). However, there was a large range in PDD and PDDN; as high as 852 (PDD_O) and as low as 144 ($PDDN_O$). This exemplifies the large difference that can occur when using temperature averages versus PDD to calculate melt energy, as PDD is a nonlinear function of temperature (Eq 3.1). PDDN, PDD, and annual average temperature for the weather station and both climate reanalysis levels peaked between 2016–2018 and had their lowest values in 1960s-1980s. This shows good agreement between climate reanalysis at the ground level and weather station data which indicates the validity of using data at the 850 hPa level.

Figure 4.15 shows the climate data trends in conjunction with sea ice and volcanic eruption occurrences, and Figure 4.16 shows the same for winter and annual precipitation. Jan Mayen was within the sea ice exported through the Fram Strait 15 times since 1967, with the most recent occurrence in 1997 (*March through August Ice Edge Positions in the Nordic Seas, 1750-2002 version 1*: https://nsidc.org/data/G02169/versions/1). SST_a and SST_s were generally lower in years when Jan Mayen was within the sea ice, indicating a likely relationship between ocean temperature and sea ice extent. All PDD and PDDN were also frequently lower in these years, which could indicate a connection between atmospheric and oceanic heat conditions. Although RH is always high, as Jan Mayen is surrounded by ocean and the climate reanalysis grid cell also likely includes much of the ocean, RH_{1000} is frequently at a local maximum during sea ice years. There was no obvious pattern between annual average cloud cover at either level or annual average RH_{850} and sea ice, however, which makes sense as the 850 hPa level (~1500 m a.s.l.) should be less influenced by oceanic conditions.

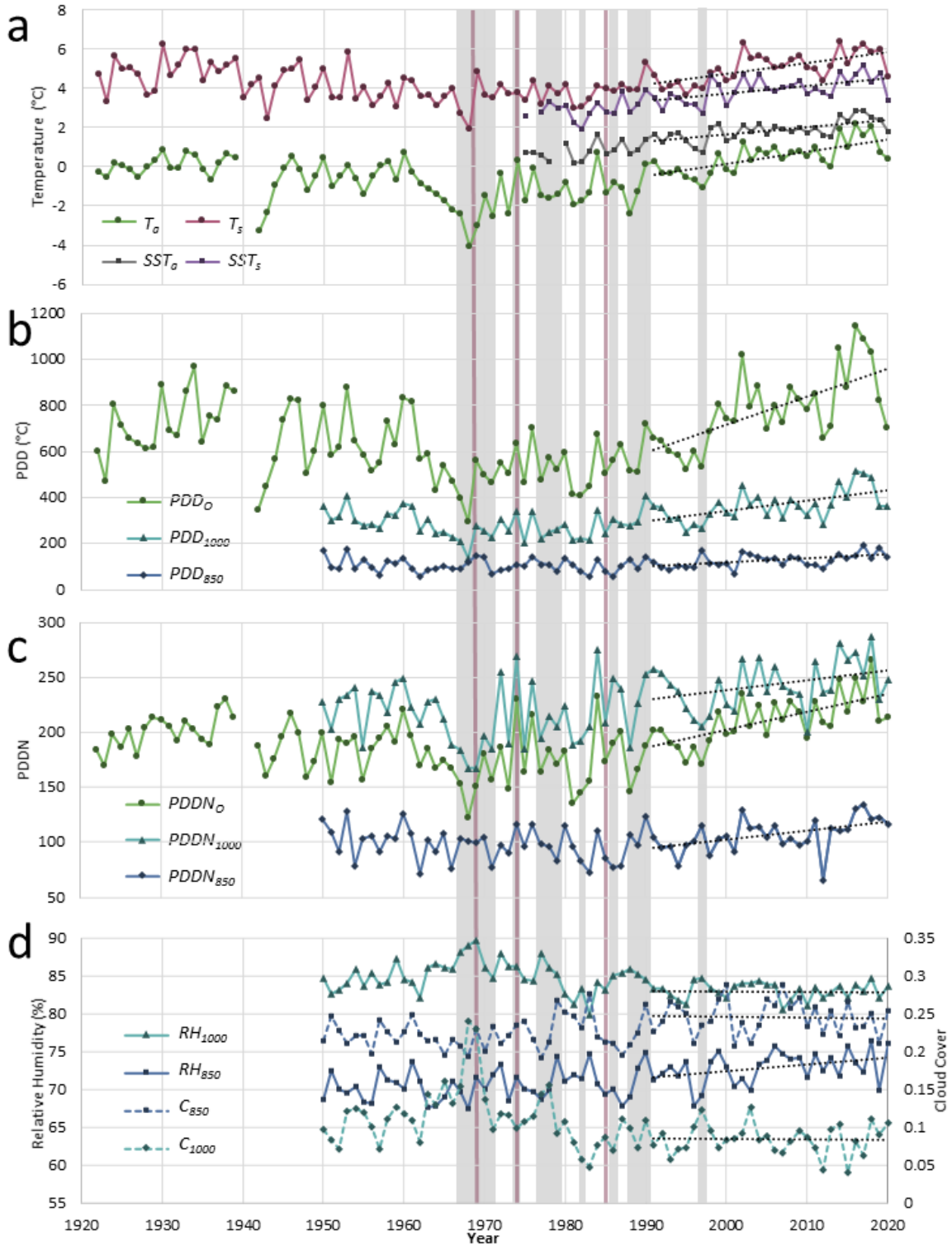

Figure 4.15: Annual average, summer average, or sum of all parameters barring precipitation (next page) with trendline for 1991–2020 (black dotted line). Gray bars indicate years that Jan Mayen was within the Fram Strait sea ice, pink lines indicate Beerenberg volcanic eruption years. a) Annual average and summer (JJA) temperature average for air temperature and SST as taken at the weather station on Olonkinbyen; b) PDD for weather station and both climate reanalysis levels; c) PDDN for weather station and both climate reanalysis levels; d) relative humidity and fractional cloud cover annual average for both climate reanalysis levels.

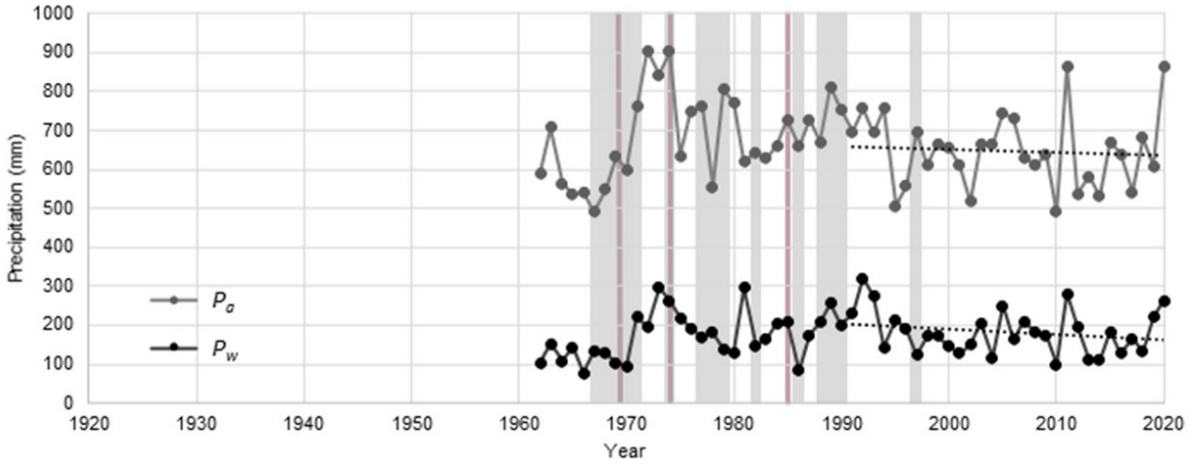

Figure 4.16: Precipitation sums as observed at the weather station on Olonkinbyen. Only data taken from the weather station at its current position (1962+) are included. The trendline for years 1991–2020 (black dotted line) is shown. Gray bars indicate years Jan Mayen was within the Fram Strait sea ice, pink lines indicate eruption years.

Neither annual nor winter precipitation changed significantly over the past 70 years, and although sea ice presence corresponds with reduced precipitation in other Arctic regions (Park et al., 2013; Kopec et al., 2016; Marcovecchio et al., 2021), it does not seem to be coincident with P_a or P_w at Jan Mayen (Figure 4.16). Eruption years do not have a noticeable difference in any climate parameters (Fig 4.15), which is to be expected as Holocene eruptions on Jan Mayen have been relatively small (not exceeding 0.1 km^2: Global Volcanism Program, 2013).

Since climate reanalysis data include ground measurements in its models (Hersbach et al., 2019; Bell et al., 2020), conditions at the 1000 hPa level should be similar to observations at Olonkinbyen. This appears to be true for temperature and PDDN, but not for PDD (Fig 4.15a–c). PDD_{1000} and PDD_{850} were calculated from 3-hour averages, creating a daily average where negative 3-hourly values were not considered in the calculation (following Braithwaite, 1984), whereas PDD_O was calculated from daily averages. Using 3-hour averages should result in a higher PDD, as temperatures that briefly peak above freezing are counted towards the PDD, where these could in the case of weather station data be incorporated into a negative daily average that would then be discarded for PDD sums. Conversely, PDD_O was higher. This could

be because T_a has a broader temperature range (-4.1 to 2.2 °C) than T_{1000} (-2.4 to 0.9 °C; see Table 4.7). As T_a experiences higher temperatures than T_{1000}, this may contribute to a higher PDD.

Climate reanalysis data indicated that RH is higher at the ground level than at 850 hPa, while cloud cover is lower. RH being higher at sea level is intuitive for an oceanic setting, as it is in the atmospheric level directly above the evaporating ocean (hence also the frequent sea fog conditions on Jan Mayen (Anda et al., 1985; Skreslet et al., 2004; Hulth et al., 2010)). As can be seen in Fig 4.15d and Table 4.7, changes in relative humidity are extremely small (~10%). Uncertainty of physical measurements for RH is 3-5% (WMO, 2006), therefore conclusions involving RH will be limited. C_{1000} was more variable than C_{850}, which is also consistent with a small island (Eastman et al., 2011). The higher level was generally cloudier than the surface level, implying that cloud cover is more common than fog, which is in line with Arctic oceanic areas (Eastman and Warren, 2010; Eastman et al., 2011). The cloud cover parameter for ERA5 is the average of a grid box of 1° latitude by 1° longitude for a single level, thus, the average cloud cover reanalysis data for Jan Mayen might be affected by ocean conditions (https://apps.ecmwf.int/codes/grib/param-db?id=248). Furthermore, studies have shown that cloud cover in climate reanalysis can vary widely (Liu and Key, 2016), and neither level studied in this thesis shows much change, therefore conclusions involving cloud cover will also be limited.

Table 4.8 shows the slope of the linear trendline equation as "trend" (any slope values < 0.01 were considered zero), its R^2 value, and the mean average value for all parameters separated into periods 1961–1990 and 1991–2020 (except SST, for which measurements begin in 1975), as well as quantification of changes in said statistics between the two periods. For precipitation,

only values taken from 1962 onwards were used. The change between the two periods was also investigated, and any change < 0.01 is considered "no change". The trends steepen between the two periods for most parameters, with only precipitation and SST_s shallowing, and SST_a, T_{1000}, C_{1000}, and C_{850} showing little change between the two time periods. Mean average values of the two time periods increase for most parameters (though the increase for RH_{1000} is within its uncertainty), with only P_a, RH_{1000}, and C_{1000} decreasing.

*Table 4.8: Trends, R^2, and mean average of all parameters between most current climate (1991–2020) and previous 30–year period (1961–1990). Trend change refers to the change in slope between 1961-90 and 1991-2020, with any changes < 0.01 assigned "0", similarly for mean average value change. Values that increase are in red, values that decrease are in blue. *SST measurements start in 1975.*

Parameter	1961–1990 Trend	1961–1990 R^2	1961–1990 Mean avg.	1991–2020 Trend	1991–2020 R^2	1991–2020 Mean avg.	Trend change	Mean avg. value change
P_a	4.51	0.1	685.6 mm	-0.62	0	646.9 mm	**-5.13**	**-38.7**
P_w	2.61	0.1	174.6 mm	-1.34	0	181.7 mm	**-3.95**	**7.1**
SST_a	0.04	0.2	0.8 °C	0.04	0.4	1.9 °C	0	**1.1**
SST_s	0.05	0.2	2.9 °C	0.04	0.3	3.9 °C	**-0.01**	**1**
T_a	0.03	0.1	-1.4 °C	0.06	0.5	0.5 °C	**0.03**	**1.9**
T_s	0.02	0.1	3.7 °C	0.06	0.4	5.0 °C	**0.04**	**1.3**
T_{1000}	0.03	0.2	-0.8 °C	0.03	0.3	0.1 °C	0	**0.9**
T_{850}	0.01	0	-3.3 °C	0.02	0.3	-2.9 °C	**0.01**	**0.4**
PDD_O	1.08	0	533.7 °C	12.07	0.4	781.2 °C	**10.99**	**247.5**
PDD_{1000}	1.41	0	266.9 °C	4.39	0.3	365.5 °C	**2.98**	**98.6**
PDD_{850}	0.44	0	100.9 °C	1.69	0.2	126.6 °C	**1.25**	**25.7**
$PDDN_O$	0.29	0	173.6	1.62	0.4	211.3	**1.33**	**37.7**
$PDDN_{1000}$	0.91	0.1	213.5	0.91	0.1	243.5	0	**30**
$PDDN_{850}$	0.04	0	96.1	0.81	0.2	106.6	**0.77**	**10.5**
RH_{1000}	-0.09	0.1	85.30%	0	0	83.00%	**0.09**	**-2.3**
RH_{850}	0.06	0.1	70.70%	0.09	0.1	72.90%	**0.03**	**2.2**
C_{1000}	0	0.3	0.1	0	0	0.1	0	0
C_{850}	0	0.1	0.2	0	0	0.2	0	0

The trends of SST_s and P_w between the two time periods both shallowed, while their mean average values increased. This is due to the steeper trend of the earlier period placing the beginning of the later period at a higher starting point, thus even as the trend shallowed it did not decrease the mean average below the mean average value of the earlier period. This is especially visible in the P_w trend (Fig 4.16), where precipitation in the early 1960s was especially low, creating a positive trend for 1961-90. RH_{1000} shows the inverse behavior, with steepening trends but decreasing mean average values. However, changes in annual average RH at both levels are very small, therefore they do not necessarily indicate a specific trend.

SST trends remained the same (near zero; < 0.1) in both time periods, while both SST_a and SST_s mean averages increased by ~1 °C .Other studies indicate that SST increases on the order of 0.2-0.4 °C/decade is more typical in the polar regions, but increases of 0.8 °C/decade are not uncommon (Carvalho and Wang, 2020). Both P_a and P_w trends generally decreased in the recent period. Trends in cloud cover for both levels remained close to zero for both periods; however, the amplitude of year-to-year variability lessened for the more recent period. Trends for RH increased for both levels, even while the trend for P_a decreased.

Annual average temperature, PDD, and PDDN increased for the Olonkinbyen data and level 850 hPa, but at the 1000 hPa level there is not a significant increase in temperature. Trends for annual temperature, PDD and NPDD were noticeably higher for measurements taken at the Olonkinbyen station than either climate reanalysis level. Parameters at level 850 hPa experience the smallest increase of the three. The 1961-1990 mean average for T_a in this thesis was the same as reported by Det Norkse Meteorologiske Institutt (DNMI; Førland et al., 1997). However, the DNMI reports a mean average precipitation of 687 mm, whereas in this thesis it was calculated as 686 mm.

4.7. Correlations Between Glacier Fluctuations and Climatic and Oceanic Drivers

The strength and significance of the linear relationship between each of the 18 climatic and oceanic parameters (hereafter, "parameters"), the relative length change of the four representative glaciers (Weyprechtbreen, Prins Haralds Bre, Sørbreen, and Kerckhoffbreen), and the all-glacier trend were calculated. The all-glacier trend is the best-fit quadratic equation of the relative glacier length changes of all 16 glaciers versus time (Carr et al., 2014). The response time was 15 years, and therefore the Pearson's *r* and associated p-values in Table 4.9 are for the relationship between glacier changes in 2000–2020 and parameter measurements in 1985–2005 (c.f. Carr et al., 2014).

Table 4.9: Pearson's r correlation coefficient for pairwise correlations between all parameters. Bold numbers have a p-value < 0.05, and bold, italicized, blue numbers have a p-value < 0.01. Significant and highly significant correlations are highlighted according to strength: Black cells indicate very strong correlations, dark grey strong, and light grey moderate.

	P_a	P_w	SST_a	SST_s	T_a	T_s	T_{1000}	T_{850}	PDD_O	PDD_{1000}	PDD_{850}	$PDDN_O$	$PDDN_{1000}$	$PDDN_{850}$	RH_{1000}	RH_{850}	C_{1000}	C_{850}	Weyprechtbreen	Prins Haralds Bre	Kerckhoffbreen	Sørbreen
P_a	--																					
P_w	***0.61***	--																				
SST_a	-0.15	-0.19	--																			
SST_s	-0.26	-0.19	***0.91***	--																		
T_a	0.04	0.13	***0.93***	***0.84***	--																	
T_s	-0.1	-0.06	***0.88***	***0.93***	***0.75***	--																
T_{1000}	0.1	0.14	***0.89***	***0.78***	***0.97***	***0.73***	--															
T_{850}	0.18	0.06	***0.76***	***0.73***	***0.79***	***0.63***	***0.79***	--														
PDD_O	0.01	0.03	***0.9***	***0.89***	***0.88***	***0.88***	***0.81***	***0.73***	--													
PDD_{1000}	0.07	0.04	***0.87***	***0.82***	***0.89***	***0.87***	***0.86***	***0.8***	***0.96***	--												
PDD_{850}	-0.07	-0.06	***0.53***	***0.6***	***0.45***	***0.66***	***0.37***	***0.57***	***0.61***	***0.6***	--											
$PDDN_O$	0.04	0.05	***0.85***	***0.81***	***0.89***	***0.72***	***0.89***	***0.82***	***0.84***	***0.87***	***0.43***	--										
$PDDN_{1000}$	0.21	0.17	***0.75***	***0.67***	***0.86***	***0.6***	***0.91***	***0.86***	***0.72***	***0.8***	**0.29**	***0.89***	--									
$PDDN_{850}$	0.1	0.09	***0.5***	***0.52***	***0.52***	***0.56***	***0.46***	***0.67***	***0.62***	***0.66***	***0.8***	***0.49***	***0.43***	--								
RH_{1000}	0.17	-0.15	-0.24	-0.12	***-0.48***	***-0.36***	***-0.51***	0.06	***-0.33***	**-0.27**	-0.01	**-0.29**	**-0.24**	0.03	--							
RH_{850}	0.15	0.15	***0.51***	**0.34**	***0.51***	***0.44***	***0.55***	0.23	***0.42***	***0.45***	0.03	***0.44***	***0.44***	0.11	***-0.47***	--						
C_{1000}	-0.08	-0.23	-0.26	-0.07	***-0.54***	**-0.28**	***-0.61***	-0.1	**-0.3**	***-0.33***	0.17	***-0.36***	***-0.43***	0.1	***0.79***	***-0.49***	--					
C_{850}	0.12	0.17	0.26	0.1	***0.37***	***0.32***	***0.4***	0.03	**0.27**	**0.28**	0.01	**0.25**	**0.25**	0.06	***-0.62***	***0.81***	***-0.51***	--				
Weyprechtbreen	-0.03	0.43	0.07	-0.04	0.04	-0.34	0.08	-0.18	-0.28	-0.32	-0.27	-0.01	0.19	-0.12	-0.47	0.2	-0.53	0.31	--			
Prins Haralds Bre	0.15	-0.45	-0.26	-0.19	-0.37	-0.48	-0.21	-0.29	-0.33	-0.27	**-0.53**	-0.1	0.08	***-0.76***	0.3	-0.05	-0.32	-0.19	0.01	--		
Kerckhoffbreen	0.28	-0.11	***-0.95***	***-0.96***	**-0.81**	**-0.88**	-0.59	-0.46	***-0.93***	-0.73	-0.28	-0.76	-0.2	-0.38	***0.93***	-0.26	-0.48	-0.35	-0.11	0.72	--	
Sørbreen	0.25	-0.1	-0.76	-0.67	-0.74	-0.79	-0.39	0.06	**-0.84**	-0.72	-0.34	-0.46	0.37	-0.58	**0.86**	-0.22	-0.36	-0.06	0.29	0.74	**0.98**	--
All-glacier trend	0.26	0.25	***-0.56***	***-0.59***	***-0.65***	***-0.74***	**-0.44**	**-0.5**	***-0.7***	**-0.45**	-0.4	***-0.58***	-0.24	-0.42	0.06	-0.21	-0.18	-0.19	0.38	**0.52**	***0.93***	**0.91**

Most parameters were significantly, strongly, and directly correlated to each other, mostly because they are derived from each other (most from temperature) or are subsets of each other (P_a and P_w), but some may indicate an interrelated network of forcings of glacier change (Table 4.9). P_a and P_w were significantly, strongly, and directly correlated to each other, but were not correlated with any other weather parameter. The significant, direct linear relationship between T_a and T_{1000} for both positive and negative temperatures was very strong (Fig 4.17), suggesting that the weather station observations and the ERA5 level 1000 hPa data are both reliable metrics for surface temperature, and indicating the validity of the model and thus the data for the 850 hPa level. It is not surprising that these were correlated, as weather data are used as input in ERA models (Hersbach et al., 2019; Bell et al., 2020). Air temperature, PDD, and PDDN at the weather station and the surface level climate reanalysis were all strongly or very strongly, significantly and directly correlated to each other. However, in general, the surface-level 1000 hPa climate reanalysis measurements were lower in both temperature and rate of increase in temperature when compared to data from the Olonkinbyen weather station (Fig 4.15), which should be considered in any synthesis of the climate reanalysis correlations.

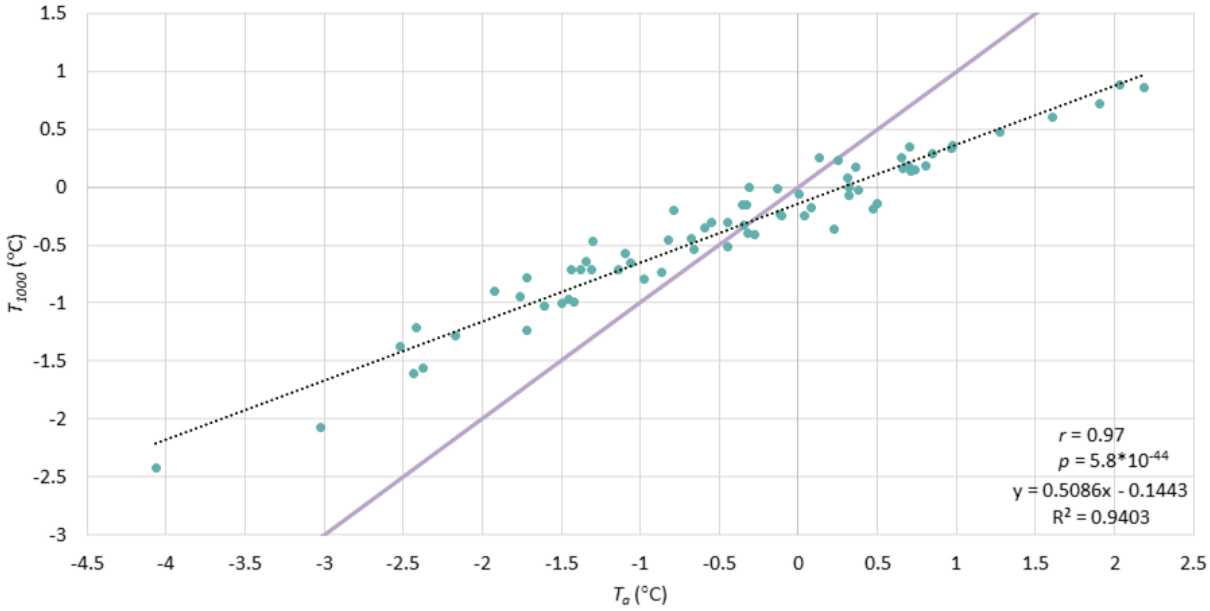

Figure 4.17: Relationship between T_{1000} (ground level climate reanalysis annual average temperature) and T_a (Olonkinbyen weather station observations of annual average temperature) between 1950 and 2020. Note the difference in range of measurements. Solid purple line is a 1:1 line.

T_a was strongly or very strongly, highly significantly, and directly correlated to nearly every other weather parameter. Exceptions were T_a's relationship with conditions at the 850 level, which were generally only of moderate strength, and the inverse relationship with C_{1000} and RH_{1000}, which were moderate and highly significant. Nearly all parameters were either calculated from T_a (PDD and PDDN), are supposed to match it (T_{1000} and thus PDD_{1000} and $PDDN_{1000}$) or are likely interrelated in synoptic process (SST). The relationships between weather parameters should be significant but not necessarily strong, as these parameters are not all necessarily casually related to each other. C_{1000} and RH_{1000} were highly significantly, moderately, and inversely correlated with their corresponding parameter at the 850 level (C_{850} and RH_{850}). This indicates that the humidity and cloud conditions above and below the general fog/temperature inversion top (~1000 m a.s.l.) had opposite trends. Cloud occurring at both climate reanalysis levels are considered "low-level" clouds, and there is little differentiation within cloud levels, therefore it is difficult to say if this inverse relationship has been observed at other locations

(WMO, 1995; Eastman et al., 2011). C_{1000} was highly significantly and inversely correlated to PDD_{1000} and $PDDN_{1000}$, but weak or moderate in strength. Therefore sunny days are not necessarily warmer days, or sunny days are more frequent in winter when temperatures rarely rise above 0 °C. Past studies indicate that summers on Jan Mayen are cloudier than winters (Orheim, 1993; Hulth et al., 2010). C_{850} was not significantly correlated with PDD_{850} or $PDDN_{850}$.

Considering the small number of data points in correlations between glacier trends and any other variables (maximum 21), only strong and very strong relationships between parameters and glacier trends (the four representative glaciers and the all-glacier trend) will be considered and used to draw conclusions from. Moderate strength correlations are suggestive of a relationship that could be further investigated and are therefore these numbers are included in Table 4.10, but the relationship is not conclusive as it is calculated in this thesis.

The two land-terminating representative glaciers, Sørbreen and Kerckhoffbreen, significantly or highly significantly, very strongly correlated with PDD_O and RH_{1000}, and additionally Kerckhoffbreen was significantly or highly significantly, very strongly, and inversely correlated with SST_a, SST_s, T_a, and T_s. The east-side marine-terminating glacier Prins Haralds Bre was highly significantly, strongly, and inversely correlated with $PDDN_{850}$, with which no other glacier trend was correlated. There was no significant or highly significant and strong or very strong correlation between a parameter and only the all-glacier trend; all correlations with the all-glacier trend additionally correlated with at least one representative glacier. The two land-terminating glaciers were significantly or highly significantly, very strongly, and directly correlated with the all-glacier trend, while Prins Haralds Bre was only significantly and moderately correlated with it and Weyprechtbreen was not significantly correlated at all.

Seven parameters were either significantly or highly significantly and strongly or very strongly correlated with at least one of the glacier trends, and six of these were directly correlated: all sea surface and air temperature parameters, PDD_O, PDD_{1000}, and $PDDN_O$; only RH_{1000} was inversely correlated (Table 4.10). Five of these parameters were significantly or highly significantly and strongly or very strongly correlated with two of the glacier trends: T_a, T_s, and RH_{1000}. PDD_O was significantly or highly significantly, strongly or very strongly, and inversely correlated with three of the glacier trends.

Table 4.10: Summary of relationship direction, significance, and strength for all parameters that correlated with at least one of the glacier trends. All strong and very strong relationships are in bold.

Parameter	Correlated Glacier	Relationship Direction	Significance	Strength
PDD_{1000}	All-Glacier	Inverse	Significant	Moderate
PDD_{850}	Prins Haralds Bre	Inverse	Significant	Moderate
$PDDN_{850}$	**Prins Haralds Bre**	**Inverse**	**Highly Significant**	**Strong**
PDD_O	All-Glacier	Inverse	Highly Significant	Moderate
T_{1000}	All-Glacier	Inverse	Significant	Moderate
T_{850}	All-Glacier	Inverse	Significant	Moderate
T_a	**Kerckhoffbreen**	**Inverse**	**Significant**	**Very Strong**
	All-Glacier	**Inverse**	**Highly Significant**	**Strong**
T_s	**Kerckhoffbreen**	**Inverse**	**Significant**	**Very Strong**
	All-Glacier	**Inverse**	**Highly Significant**	**Strong**
SST_a	**Kerckhoffbreen**	**Inverse**	**Highly Significant**	**Very Strong**
	All-Glacier	Inverse	Highly Significant	Moderate
SST_s	**Kerckhoffbreen**	**Inverse**	**Highly Significant**	**Very Strong**
	All-Glacier	Inverse	Highly Significant	Moderate
RH_{1000}	**Kerckhoffbreen**	**Direct**	**Highly Significant**	**Very Strong**
	Sørbreen	**Direct**	**Significant**	**Very Strong**
PDD_O	**Kerckhoffbreen**	**Inverse**	**Highly Significant**	**Very Strong**
	Sørbreen	**Inverse**	**Significant**	**Very Strong**
	All-Glacier	**Inverse**	**Highly Significant**	**Strong**

The following pages contain figures (Figs 4.18-4.21) for all significant and highly significant linear relationships between parameters and glacier trends listed in Table 4.10, except for the significant ($p < 0.05$) relationships between parameters and the all-glacier trend that were not also highly significant ($p < 0.01$). Kerckhoffbreen and Sørbreen were significantly, very

strongly, and directly correlated to each other, and three representative glaciers were also significantly or highly significantly, moderately or very strongly, and directly correlated with the all-glacier trend. Although it is easy to see from Figure 4.9 that Sørbreen and Kerckhoffbreen had similar retreat and advance patterns, there were only four years in which both glaciers had a measurement, and, unless they share ice divides, glaciers retreating simultaneously are not due to dynamic correlation (one causing the other to retreat), but rather implies that they are reacting to similar forcings. Similarly, the all-glacier trend is the average rate of change for all glaciers on the island, and therefore will look similar to most of the individual glacier relative length changes. Thus, these plots are not included.

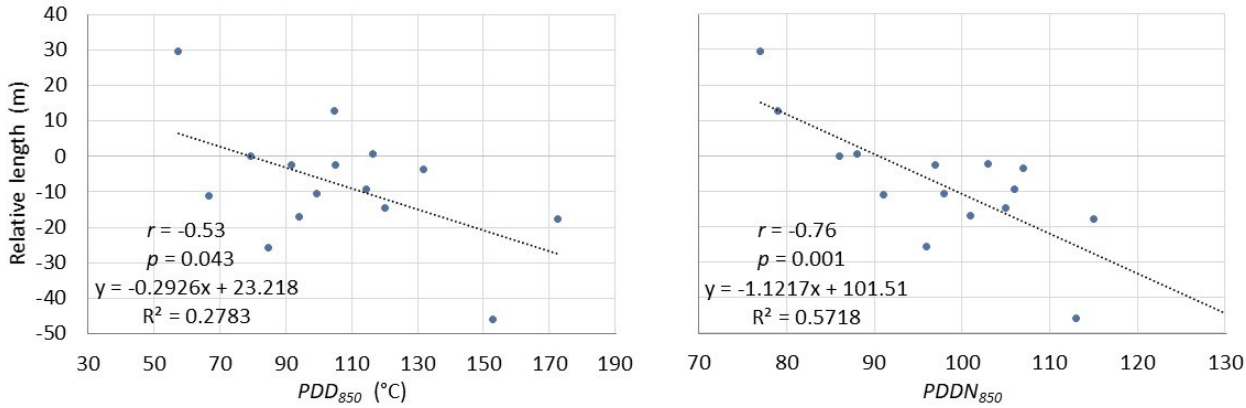

Figure 4.18: Scatterplots for all relationships between Prins Haralds Bre glacier fluctuations and parameters with a p value < 0.05.

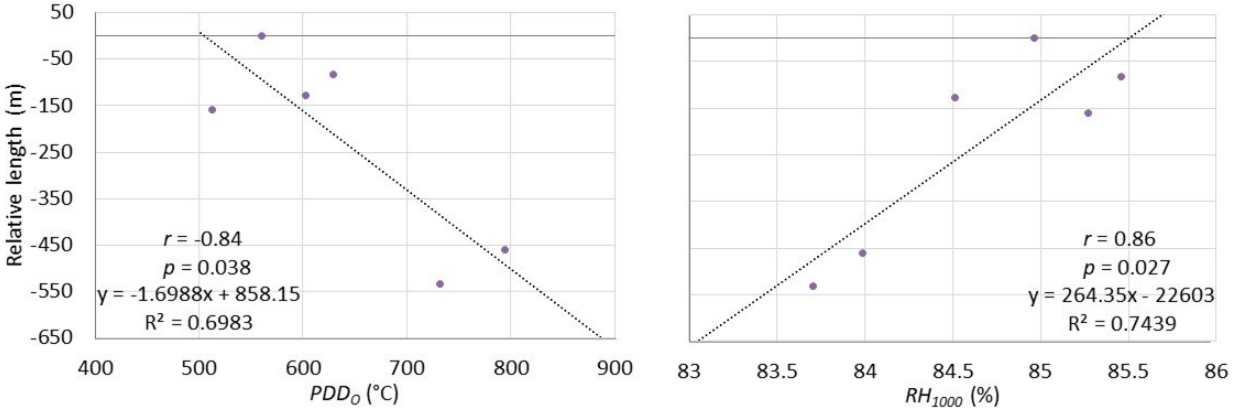

Figure 4.19: Scatterplots for all relationships between Sørbreen glacier fluctuations and parameters with a p-value < 0.05.

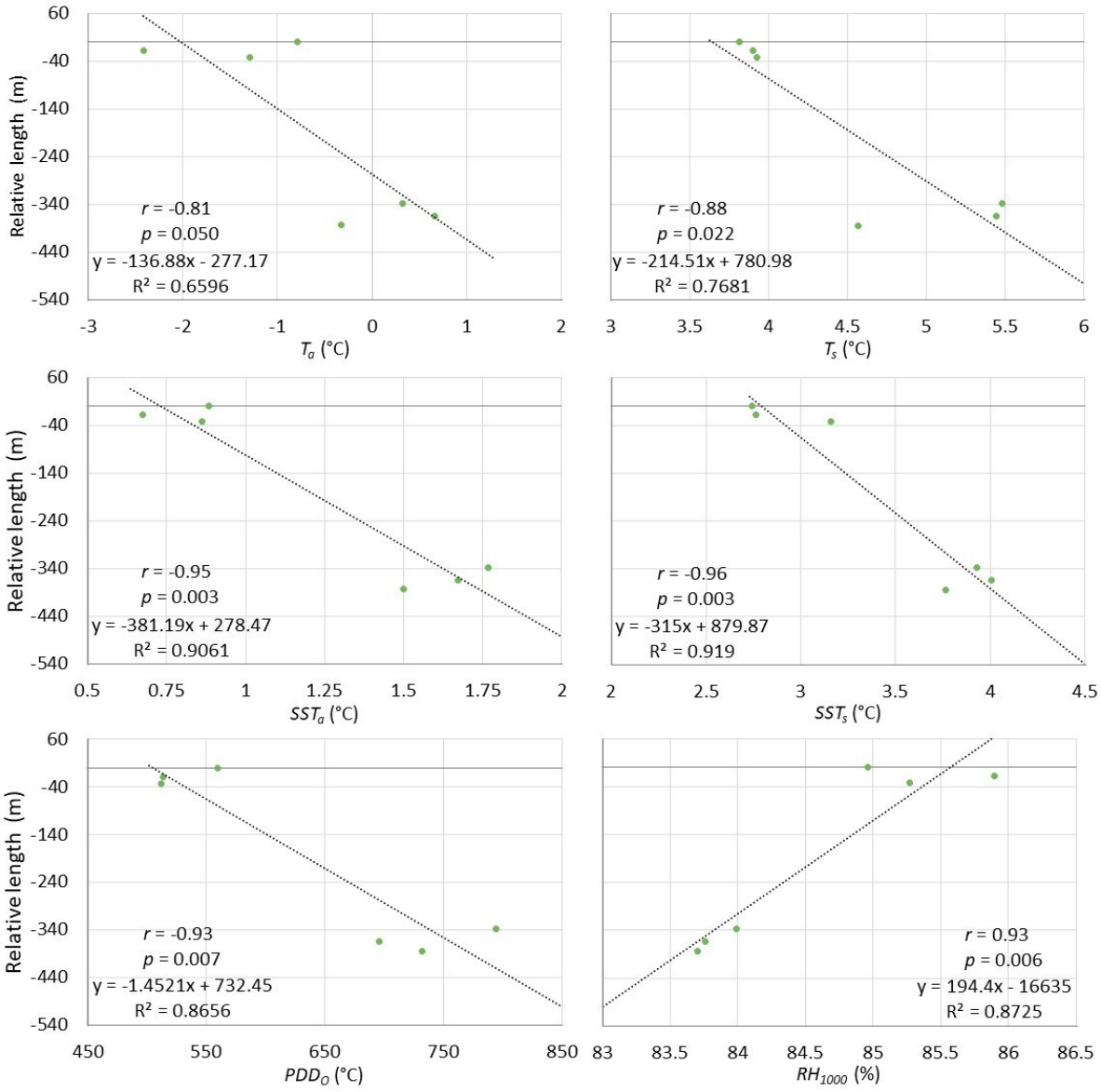

Figure 4.20: Scatterplots for all relationships between Kerckhoffbreen glacier fluctuations and parameters with a p-value < 0.05.

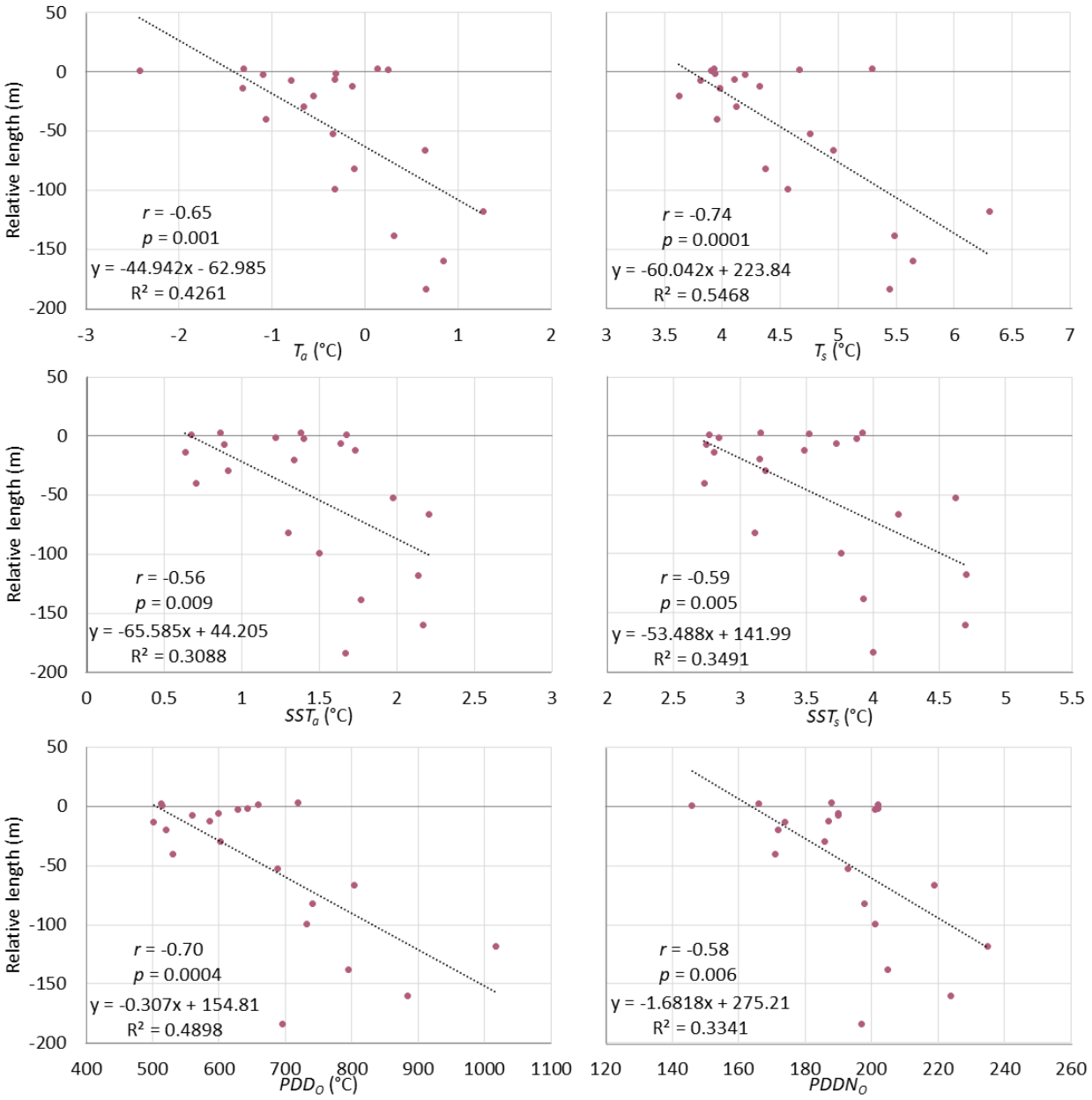

Figure 4.21: Scatterplots for all relationships between the all-glacier trend and parameters with a p-value < 0.01. The all-glacier trend additionally was significantly (but not highly significantly) correlated with T_{1000}, T_{850}, and PDD_{1000}, which are not shown.

The representative land-terminating glaciers had only six data points, which limits the depth to which conclusions can be drawn from the measured correlations. Weyprechtbreen, the last remaining marine-terminating glacier on Jan Mayen in 2020, was not significantly correlated with any parameters used in this study. The all-glacier trend was significantly or highly significantly and inversely correlated to nine of the 18 parameters, although only three of these

relationships were strong (T_a, T_s, PDD_O). Only the highly significant correlations are shown in Figure 4.21, but moderate strength relationships are included for completeness. Some relationships might not be linear (see Section 5.2.3 for more details). In the scatterplots for Kerckhoffbreen and significantly correlated parameters, it becomes apparent that there are two clusters of data points, which might obscure nonlinear correlations.

Hereafter, the parameters that are significantly or highly significantly and strongly or very strongly correlated with >1 glacier trend (T_a, T_s, PDD_O) will be referred to as "the driving parameters". As can be seen in Figs 4.19-4.20, the range in RH_{1000} values which correlated to glacier trends is small, within the physical measurement uncertainty (WMO, 2006). Considering this and the limited number of data points, these results are not indicative of a true correlation. Thus, even though RH_{1000} is significantly or highly significantly and very strongly correlated with both Sørbreen and Kerckhoffbreen, it is not included as a driving parameter.

5. CHAPTER 5: DISCUSSION

5.1. Limitations of the Data Used in this Thesis

Results from this thesis were affected by the quality and frequency of satellite imagery, lack of ground velocity and thickness measurements, inaccuracy of RGI glacier outlines, sparse measurements for the time frame, and constraints of the climate reanalysis products and their spatial scale. The highest resolution satellite imagery was 15 m, and the Jan Mayen glacier fronts are 150-1900 m wide, thus had 10-130 pixels per glacier front. The Jan Mayen glacier fronts are also debris-covered, adding to the need for higher resolution imagery. Glacier front lines are best drawn in the ablation season, which is when cloud cover at Jan Mayen is at its peak (Orheim, 1993). This prevented the use of images that were taken at the same time every year, or of only one image to draw lines for all the glaciers within a year. The effect is that the glacier retreat rates may not be truly annual changes. However, the long-term trends over the period 2000-2020 (e.g. Fig 4.9) are larger than the interannual variability, except for Weyprechtbreen and Kjerulfbreen.

Frontal ablation had to be estimated using broad scenarios as ITS_LIVE velocity measurements were composites from 2015 onwards, while yearly frontal measurements start in 2000, and there were no directly measured thicknesses for the glaciers. Thicknesses used in this thesis were derived from figures (Figure 6 in Anda et al., 1985) and written observations from previous studies (Mohn and Wille, 1882; Jennings, 1948). This affects the individual and overall frontal ablation estimates, as does the assumption that the glaciers were perfectly parabolic (Van Wychen et al., 2014, 2016), and that the smaller glaciers were of the same thickness range as the larger glaciers. It is also assumed that all glaciers have the same response time, as calculated from

data on Sørbreen as the average of three thickness estimates and three mass balance measurements.

By projecting the RGI glacier outlines over satellite scenes, it was noticed that the outlines do not perfectly match with observed glacier basins, resulting in these outlines being deemed unusable as the upstream end of the flux box, and instead a line at an arbitrary distance upstream from the front was used for the box method. The result of this is that the area changes cannot be directly applied to the existing RGI data (which are both obsolete in the ablation zones due to the glacier retreat since the 1980s and are incorrect in the accumulation zone as observed from bedrock ridges separating the individual drainage basins). While DEMs were available for use in this study, difficulties in processing and time constraints prevented processing from being completed in time, thus there are no volume change data and no thinning data. Furthermore, previous DEM differencing by Rolstad Denby and Hulth (2011) proved nearly impossible due to frequent cloud and fog cover. Glacier changes are not always fully revealed by just area change; a study in 1990 found two small glaciers with quick response times both lost 45% of their volume, but for one this was displayed through retreat and for the other through thinning only (Grudd, 1990).

Relationships between glacier frontal positions and climate parameters may not be linear (Cuffey and Paterson, 2010). For example, kinematic adjustment (thinning) of the glaciers, the transition of glaciers from marine- to land-terminating, or the mass-balance elevation feedback (see Section 5.3). Table 5.1 shows correlations for which the R^2 improved when shifting the trendline equation from linear to exponential (x^2) or logarithmic. Relationships between Kerckhoffbreen and correlated parameters were not included, as the pattern of Kerckhoffbreen's retreat and advance created two clusters of data, distorting possible nonlinear relationships. The

only R^2 to increase by > 0.1 is that between Sørbreen and RH_{1000}, implying that the effects of fog on shading might be the strongest of the climatic and oceanic parameters for Sørbreen. However, as mentioned in Section 4.7, the range of values in the correlation between Sørbreen and RH_{1000} is within the uncertainty of the physical measurement of RH (WMO, 2006). Therefore, as only one R^2 increases with a nonlinear relationship, this justifies only investigating linear relationships in this thesis.

Table 5.1: Each significantly correlated parameter for which R^2 increased when shifting the trendline from linear to exponential or logarithmic, and the corresponding R^2.

Glacier	Parameter (strength of linear relationship)	R^2 Linear	R^2 Exponential (x^2)
Prins Haralds Bre	PDD_{850} (moderate)	0.27	0.29 (logarithmic)
	$PDDN_{850}$ (strong)	0.57	0.60 (logarithmic)
Sørbreen	PDD_O (very strong)	0.70	0.76
	RH_{1000} (very strong)	0.74	0.91
All-glacier trend	T_a (strong)	0.43	0.50
	PDD_O (strong)	0.33	0.36
	SST_a (moderate)	0.31	0.33
	SST_s (moderate)	0.35	0.36

The maximum number of frontal measurements for a glacier in this study was 14. Therefore, changing even one data point can skew the results. For example, if the last measurement for Prins Haralds Bre, the measurement when it became a land-terminating glacier, was included for calculating the correlations, the parameters the glacier change correlated to becomes T_a, T_s, P_w, and $PDDN_{850}$ instead of PDD_{850} and $PDDN_{850}$. For this specific instance, the discussion would only change slightly to include precipitation. However, the addition or ommission of a single data point could substantially affect correlation outcomes. Therefore, while each parameter that is significantly correlated with a glacier trend is discussed in the context of

the glacier with which it correlates, for overall interpretation, only parameters that correlated with more than one glacier trend were considered a major driver for glacial changes on Jan Mayen.

Temperature and temperature- derived parameters from climate reanalysis noticeably underestimate values as observed at the Jan Mayen weather station at Olonkinbyen (Fig 4.15). Climate reanalysis data are the average for a 1° x 1° grid, which at this latitude amounts to 3818 km^2. Therefore, Jan Mayen covers only ~10% of this grid. Thus, the ocean exerts a significant influence on all climate reanalysis parameters. Cloud cover measurements in climate reanalysis have been known to be particularly erratic and dissimilar from ground and satellite observations, and are noted to have worse performance over land than over the ocean (Liu and Key, 2016). ERA5 slightly overestimated cloud cover when compared to satellite estimates (Liu and Key, 2016). Annual cycles are the most accurate, however, and for this thesis the seasonal cloud cover was not considered.

5.2. Jan Mayen Glacier Trends in Oceanic and Climatic Context

5.2.1. Glacier Trends

As mentioned in Section 2.4.3, the University of London studies in 1959 and 1961 (Fitch et al., 1962; Kinsman and Sheard, 1963) found Sørbreen advanced 100 m between 1949 and 1959, and an additional 124 m during the following 2 years. They also observed that several other glaciers had advanced since 1949 (Orheim, 1993). These studies show that Sørbreen's advance and retreat pattern exhibits an oscillating pattern, and the frontal position can change by 100 m within a period of ten years or two. Sørbreen's average retreat rate of -27 m/yr is within that of previous observations, but it is an order of magnitude faster than the retreat rates of most other glaciers on Jan Mayen.

For Jan Mayen glaciers, half of the maximum advance rates were in the first quarter of 2000-2020 time period, and 13 of the 16 glaciers had their furthest advanced position in this same time period. Almost half of the maximum retreat rates were in the last quarter of the time period, and 14 of the 16 glaciers had their furthest retreated position in this same time period. This indicates that the glaciers are not only retreating but accelerating in their retreat over the period 2000-2020.

At Jan Mayen, the shallow slope of the submarine bathymetry directly around the island (Fig 2.7) and lack of fjords prevents marine-terminating glaciers from floating or advancing, but rather they terminate very near the coastline (Fig 5.1; Kodaira et al., 2000). The ocean water will only interact with the base of the glacier (and some small percentage of the front), which leads to undercutting of the glacier and destabilizing icebergs (Luckman et al., 2015; Vallot et al., 2018; Ma and Bassis, 2019). The forces keeping these glaciers terminating near the coastline are likely ocean waves. Without fjords, these glaciers are more vulnerable the full force of storms, which could create waves that are powerful enough to destabilize the formation of a glacier tongue without fjord walls to adhere to. If the marine-terminating glaciers at Jan Mayen had glacier tongues, the magnitude of the retreat rates might be higher than what was observed in this thesis. Land and marine-terminating glaciers are subject to different forcings (Cuffey and Paterson, 2010; Benn and Åström, 2018), which can be seen in how the significant correlations differ between the two (Table 4.9).

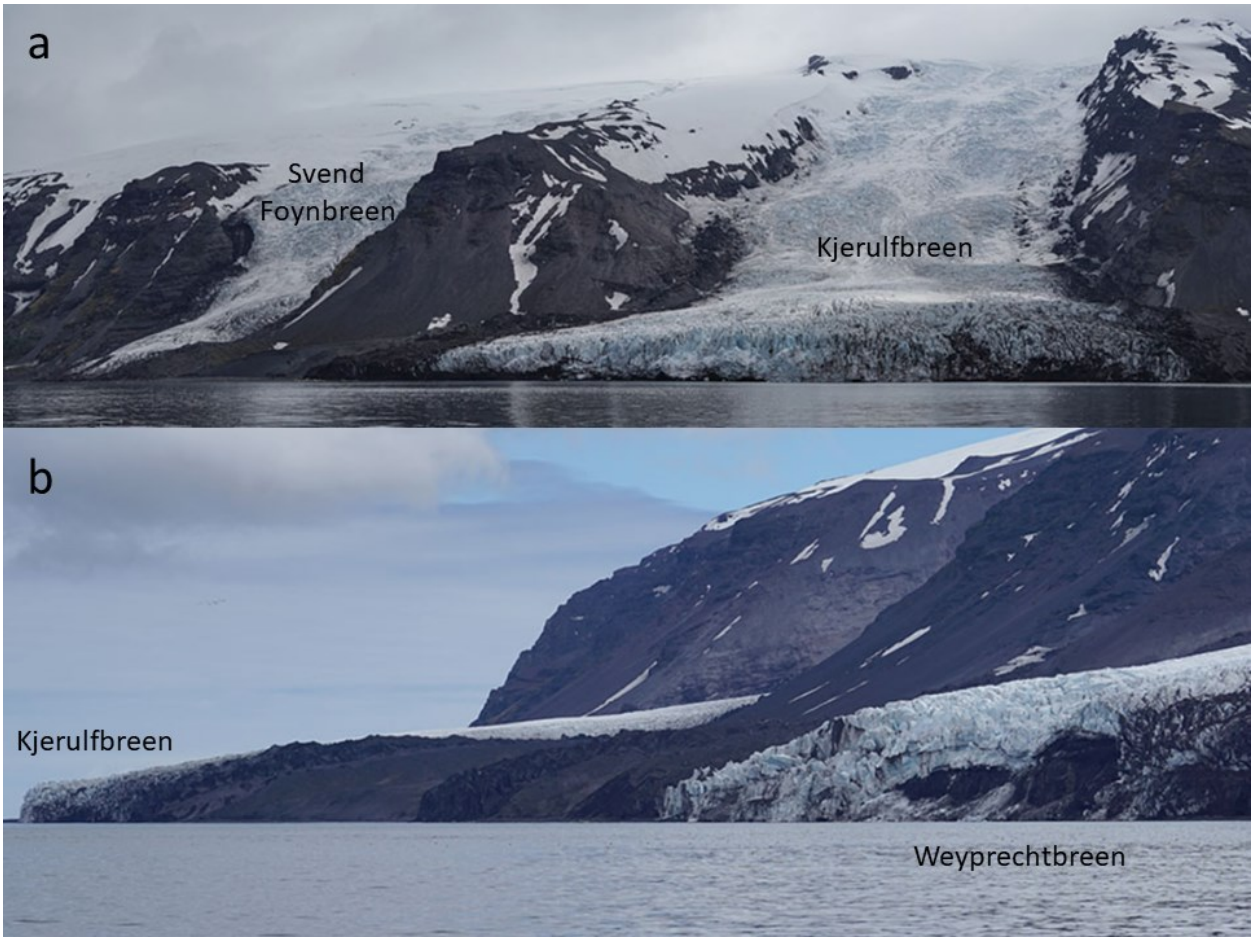

Figure 5.1: a) Svend Foynbreen and Kjerulfbreen, and b) Kjerulfbreen and Weyprechtbreen as seen from the ocean in June 2016 (http://www.mrietze.com/web16/JanMayen16.htm). At this time, Weyprechtbreen and Kjerulfbreen are still considered "marine-terminating" but Svend Foynbreen is not.

The glaciers on the east side of the island did not retreat significantly differently than those on the west side, even when separated into marine- and land-terminating. This indicates that differences in weather and climate across the two sides of the island do not lead to resolvable differences in retreat rate. The previous theory that the west-side glaciers receive more precipitation, based on the years the station was located further west is thus still arguable (Anda et al., 1985; Orheim, 1993). There are further factors to consider: it is possible the west side could be generally colder, as this side faces the direction weather normally approaches Jan Mayen (i.e. northwesterly systems), and it is on the "cold" side of the ocean current. The SST difference between the two sides is on the order of 1-2 °C, see Fig 2.8; (Carr et al., 2017; Lysså et

al., 2021), therefore it is small but not negligible. However, none of these differences noticeably affected glacier retreat and advance trends.

According to observations in previous studies, Jan Mayen glaciers experienced an oscillating retreat and advance pattern since at least 1850 (Anda et al., 1985). This thesis confirms that this pattern continues into the present. In recent years, Kjerulfbreen and Weyprechtbreen, the two largest marine-terminating glaciers which are both located on the west side of the island, experienced the highest magnitude in advance and retreat of the marine-terminating glaciers, and Kjerulfbreen experienced the largest advance of all the glaciers in 2001-2002, and they are also the fastest moving glaciers on the island. These glaciers have also been noted in the past as being the most active (Mohn and Wille, 1882; Orheim, 1993; Hulth et al., 2010).

Aerial photographs from 1949 show Sørbreen was then at its furthest recorded retreat, which was 1200 m from the shore (Orheim, 1993). As of 2018, the minimum distance between the glacier front and the shore was 1100 m and has therefore not yet retreated to its 1949 position. Observations of past retreat rates at Sørbreen measured rates of 10-50 m/yr (Kinsman and Sheard, 1963; Orheim, 1993). For 2000-2020, Sørbreen experienced retreat rates +36 to -82 m/yr, on average -27 m/yr, which are within or not dissimilar to previously observed bounds. Therefore, there is nothing unusual or alarming about its current retreat pattern; unlike most Arctic glaciers, Sørbreen appears relatively sheltered from the effects of the changing climate (IPCC, 2021).

5.2.2. Climatic and Oceanic Parameter Trends

Between 1961-1990 and 1991-2020, T_a increased while RH_{1000} and P_a decreased (Table 4.8). According to the Clausius–Clapeyron relation, warmer air can hold more moisture without

releasing it as rain. This implies that with rising temperatures and decreasing precipitation, absolute humidity would rise. However, relative humidity is a measure of the amount to which the air is saturated, therefore that RH_{1000} was significantly, moderately, and inversely correlated with T_{1000} indicates that the capacity in the air associated with temperature increase surpassed the increase in water particles held in the air. Jan Mayen's total precipitation is relatively small for a coastal location, but not for one in the Arctic (Walsh, 2008), and relative humidity is always high (Table 4.8). Jan Mayen has only the one mountain, so the orographic lift creating rain is relatively weak.

The relationships between RH_{1000} and SST_a, and RH_{1000} and SST_s, were not significant, and weak and very weak, respectively, indicating that even though warming ocean temperatures would evaporate more water, this did not have a great effect at this location. RH_{850} was highly significantly, only moderately, and directly correlated with SST_a, and significantly, weakly, and directly correlated with SST_s. As discussed later in this section, RH and cloud cover conditions at the higher 850 hPa level and conditions at the ground level 1000 hPa were frequently opposing.

Temperatures and derived weather parameters at the 850 hPa level were increasing slower than those at sea level, but the 850 hPa level parameters represent conditions in the accumulation zone, above the theorized ELA. Mild warming at these higher elevations can drive the weather towards a longer rain season and more precipitation in the form of rain. Average winter temperatures at Jan Mayen for 1991-2020 was -2.9 °C, a substantial increase from the previous 1961-1990 average of -5.7 °C. As this is very near 0 °C, it is likely that precipitation as rain is sometimes present in winter. Rain percolates into snow and ice and warms the glacier through release of latent heat when it freezes (Hock, 2005), and can create ice layers that affect snow density, distribution, and ablation season drainage (Sobota et al., 2020). Average winter

temperatures at Jan Mayen at higher elevations (level 850 hPa climate reanalysis) was -10.3 °C in 1991-2020, a noticeable but smaller increase from the 1961-1990 average of -11.5 °C when compared to the ground level change.

Atmospheric circulation patterns influence worldwide temperature and precipitation trends, and the area around Jan Mayen is influenced by the NAO (Kirkbride, 2002; Berdahl et al., 2018; IPCC, 2019a). Previous studies have found that both Greenland and Iceland glacier changes correlate with changes in attributes of the NAO (Kirkbride, 2002; Berdahl et al., 2018). The NAO was on average slightly negative for 1960-1990, and slightly positive for 1990-2020 (Fig 5.2). While this is not a perfect proxy for the effect of this atmospheric oscillation, this first estimation implies that the NAO should have overall slightly cooled and decreased precipitation over Jan Mayen 1960-1990, and warmed and increased precipitation 1990-2020. Results from this thesis do indicate that temperatures increase, however, P_a decreased noticeably (P_w increased slightly) between the two time periods (Table 4.8).

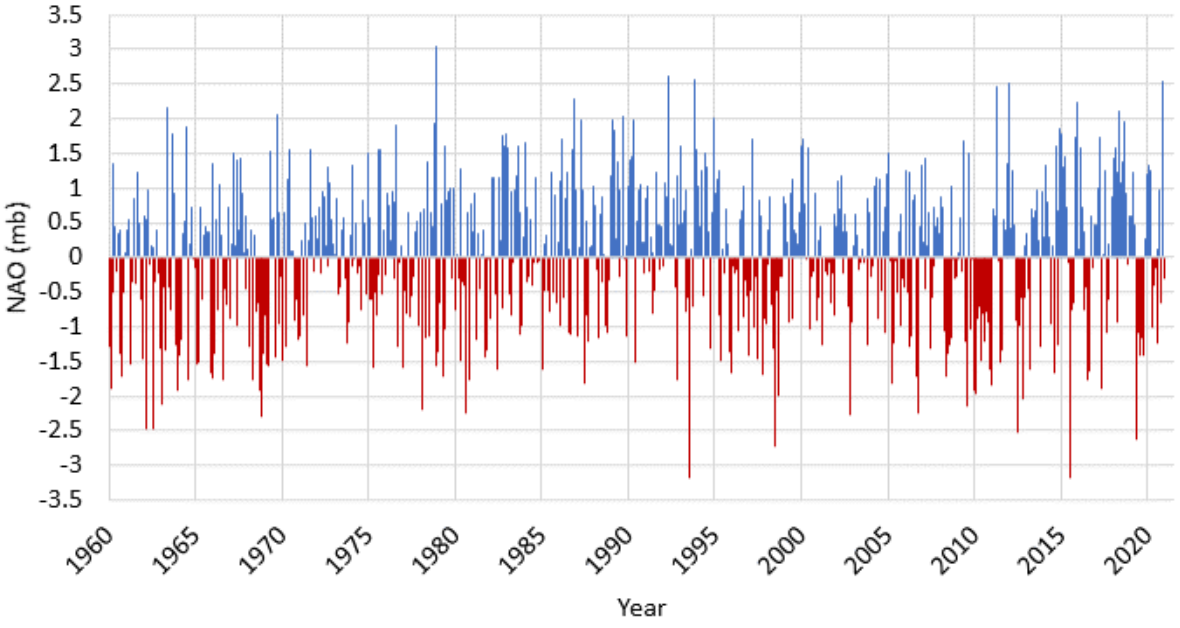

Figure 5.2: Monthly NAO index during the time of relevance for this study (1960-2020). Data from https://www.ncdc.noaa.gov/teleconnections/.

5.2.3. Correlation Between Glacier Trends and Oceanic and Climatic Parameters

Several climatic and oceanic parameters correlated with glacier trends, but there was no one main factor, demonstrating the complexity of climate-glacier interactions even in simple locations like the island of Jan Mayen. PDD_O was significantly or highly significantly, strongly or very strongly, and inversely correlated with three of the glacier trends: Kerckhoffbreen, Sørbreen, and the all-glacier trend. Two parameters were significantly or highly significantly, strongly or very strongly, and inversely correlated with at least two of the glacier trends (T_a, T_s). SST_a and SST_s were highly significantly, only moderately, and inversely correlated with the all-glacier trend but were highly significantly, very strongly, and inversely correlated with Kerckhoffbreen. RH_{1000} was the only of these parameters to be directly correlated, and additionally correlated only with land-terminating glacier trends (Sørbreen and Kerckhoffbreen). However, the range of RH_{1000} values correlated to glacier frontal changes is within the uncertainty of physical measurements (Figs. 4.19 and 4.20; WMO, 2006) and thus is too small to draw conclusions from. Therefore, the dominant factors driving glacier changes on Jan Mayen is the parameter derived from air temperature, PDD_O.

In Section 3.5, it was mentioned that Braithwaite (1984) claimed that PDD is a better indicator of glacial changes than summer average temperature. Anda et al. (1985) theorized that T_s would be the most important driver for glacier ablation on Jan Mayen, even with the frequent inversions. Results from this thesis show that both parameters were significantly or highly significantly correlated with > 1 glacier trend. PDD_O was significantly or highly significantly correlated with more glacier trends than T_s and had a higher Pearson r for Kerckhoffbreen (PDD_O: -0.93; T_s: -0.88), but a lower Pearson r for the all-glacier trend (PDD_O: -0.70; T_s: -0.74). Therefore, T_s might be important for some individual glaciers, but PDD_O is a better indicator of

the general glacier change trend. PDD_O contains more information about melting energy within the full year than T_a or T_s (Braithwaite, 1995; Hock and Holmgren, 2005). Therefore, ablation happening outside the months of June, July and August are integral to explaining glacier changes on Jan Mayen. Average winter temperatures on Jan Mayen were not far from 0, being -5.7 °C for 1961-1990 and -2.9 °C for 1991-2020 according to measurements at the Olonkinbyen weather station, therefore, it is likely some ablation is occurring during this season.

Qualitative analysis of glacier response to volcanic activity suggests that volcanic activity may not play a major role in glacier changes on Jan Mayen over the period 2000-2020. First, the glaciers over the fissures which most recently erupted (Frielebreen and Dufferinbreen) did not retreat substantially quicker than other glaciers nearby, and secondly there was no recorded volcanic activity during this time period (Global Volcanism Program, 2013b). This is not unusual; previous studies in the Chilean Andes found that climatic factors are frequently the dominant driving force for changes in glaciers on volcanoes, except for when the volcano is actively erupting (Rivera et al., 2012; Rivera and Bown, 2013). Another study in Latin America found a statistically insignificant higher ice area loss rate for glaciers on volcanoes with eruptions, when compared to volcanoes that did not erupt (Reinthaler et al., 2019). In addition to GHF changes from volcanic eruption, tephra deposition can affect glacier mass balance (Benn and Evans, 2010). The termini of the land-terminating glaciers on Jan Mayen are mostly debris-covered. As mentioned in Section 2.1.2, tephra deposition's effect on glacier mass balance is nonlinear, and with a thin layer (~1 cm) increasing ablation and a thick layer (~3 cm) decreasing ablation. As the land-terminating glaciers, which are the more debris covered, retreated faster on the island of Jan Mayen, this implies that there could be only a thin layer of tephra, which can be expected with Beerenberg's relatively small eruptions.

The all-glacier trend was highly significantly and very strongly correlated with the land-terminating glaciers but was only significantly and moderately correlated with Prins Haralds Bre and was not significantly correlated with Weyprechtbreen (Table 4.9). Additionally, no parameter that significantly correlated to the marine-terminating glaciers was significantly correlated to other glacier trends. This indicates that marine-terminating glaciers are subject to different forcings and behave significantly differently from land-terminating glaciers. One difference between the marine-terminating and land-terminating glaciers discovered in this thesis was the difference of slope (Table 2.2). Glaciers on the east and west sides of Jan Mayen have a similar average slope (< 0.1° difference), but marine-terminating glaciers are as a group 4° steeper than land-terminating glaciers, with average slopes of 21.0° and 17.2°, respectively. Therefore, this might be the mechanism for those differences, and rather it is because they are steeper that they are marine-terminating and subjected to different forcings, rather than because they are marine-terminating they are subjected to different forcings. Two of the steepest glaciers on the island were land-terminating for 2000-2020 (Griegbreen and Willebreen, Table 2.2) but were marine-terminating in most historical maps (Figs 4.3-4.8). These glaciers might be controlled by similar parameters as controls on Prins Haralds Bre, as they are also on the east side.

Prins Haralds Bre was significantly correlated to parameters at the 850 level, (although only the relationship with $PDDN_{850}$ was strong with r = -0.76), indicating the importance of changes occurring in the accumulation zone, and implies that Prins Haralds Bre is particularly susceptive to warming above the common ground fog (~1000 m a.s.l.; Hulth et al., 2010) and ELA (~600-950 m a.s.l.; Anda et al., 1985). This could indicate that the area of melt that is constant with elevation as seen in past mass balance studies (Fig 2.12) is not as strong on Prins Haralds Bre, which would supports previous studies' theories that the fog and temperature

inversion would be most important for south and east glaciers (Prins Haralds Bre is north and east; Anda et al., 1985; Orheim, 1993; Skreslet, 2004). Why Prins Haralds Bre was correlated to PDDN, instead of PDD or air temperature, could be explained by cloud cover trends. C_{850} was generally higher than C_{1000}, meaning there are not as many sunny days at the higher elevations, therefore the number of warm days is more important than the day's average temperature.

The correlation analysis revealed two unexpected results: Weyprechtbreen's frontal changes were not significantly correlated to any climatic or oceanic parameters used in this study, and SST were correlated with glacier changes for a land-terminating glacier. Weyprechtbreen drains the central basin of the Beerenberg volcano, and thus is likely drawing from a larger accumulation basin than any of the other glaciers on the island. Weyprechtbreen is mentioned in almost every past survey as being by far the most active glacier on Jan Mayen (Mohn and Wille, 1882; Jennings, 1948; Anda et al., 1985; Hulth et al., 2010). This implies that Weyprechtbreen has the capacity to advance further, but is restricted from advancing due to calving, shallow bathymetry, and lack of a fjord. The marine-terminating glaciers at Jan Mayen are pinned to the coastline by submarine melt, ocean waves, and calving, making them less sensitive to changes in climate as they cannot advance. Thus, tracking frontal changes does not capture the glacier's actual response to climatic and oceanic drivers. In Jan Mayen's last glaciation, ice covered most of the edge of the continental shelf (Fig 2.7a; Lysså et al., 2021), so in theory Weyprechtbreen could advance further over the shallow bathymetry. However, all past glacier studies indicate that the glaciers on Jan Mayen retreated in patterns that were more or less cohesive, and the marine-terminating glaciers never terminated far from the coast (Anda et al., 1985; Orheim, 1993; Lysså et al., 2021). There are very few studies on glaciers that do not calve into the ocean from a fjord (i.e. open ocean calving). While there are other locations with open-ocean calving glaciers, as far

as the thesis author knows, the only other information available on open ocean calving is for Basin 3 of Nordaustlandet in Svalbard, which is a surge-type outlet glacier that drains an ice cap, and is 1250 km^2 (Robinson and Dowdeswell, 2011). Therefore, it is difficult to compare results. Several of the smallest glaciers peripheral to the Greenland ice sheet especially those draining from islands, multiple other locations across the Arctic such as Devon Island and Ellesmere, and many Subantarctic islands such as Heard Island have open ocean configuration for iceberg calving (e.g. Jiskoot et al., 2012; RGI Consortium, 2017), but research on this specific topic has not been conducted.

Kerckhoffbreen's highly significant inverse correlation to SST_a and SST_s is likely explained by Jan Mayen's temperature inversion. It has been previously theorized that this inversion is caused by air from the ocean displacing warmer air, cooling the lower elevations of the glacier and suppressing melt (Anda et al., 1985; Skreslet et al., 2004). Kerckhoffbreen's relative length changes were inversely correlated with both SST_a and SST_s, and Jan Mayen's inversions were theorized to cool the base of the glaciers and prevent melting, which implies that a warmer ocean would result in fewer or less intense inversions. As a warming ocean would result in a smaller contrast between temperatures of the land and the sea, which also indicates fewer or less intense inversions, this theory holds. Previous studies have also indicated that the inversions are more frequent in the summer (Trondsen, 2008), although the Pearson r's between Kerckhoffbreen and SST_s and SST_a are similar, and both were highly significant (-0.96 and -0.95, respectively). A warmer ocean could also result in more fog, which would change the radiation regime over the glaciers (Gultepe et al., 2007).

If the physical process explanation is true for Kerckhoffbreen, then Sørbreen should be correlated with SST_a and SST_s changes as well, especially as it is on the same side of the island as

where SST measurements were taken, and previous studies indicate that the inversions are most important for the south and east Jan Mayen glaciers (Anda et al., 1985; Orheim, 1993; Skreslet et al., 2004). Studies of changes in ocean temperature indicate that the ocean north of Jan Mayen island was colder than the south, which could explain why Sørbreen is not significantly correlated with SST (Fig 5.3; Carr et al., 2017). Carr et al. (2017) reported that at Jan Mayen's latitudinal position, the shallow ocean was generally cooler over the period 2000-2010 than in 1995-99. This belies the SST measurements from the Olonkinbyen station, which show a slight increase in temperatures between 1995-99 (mean SST of 1.4°C) and 2000-2010 (mean SST of 1.8°C). The discrepancy between Sørbreen and Kerckhoffbreen's correlation with SST cannot be explained by the elevation of the glacier termini: both are within the area of melt that is constant with elevation as seen in Sørbreen mass balance studies (Fig 2.12; Orheim, 1993; Hulth et al., 2010), although Sørbreen's terminus is currently at a much lower elevation (~150 m a.s.l.) than Kerckhoffbreen's (~500 m a.s.l.). Response time could be relevant, but response time used for these correlations were calculated from observations at Sørbreen, implying that Sørbreen's correlations with the 18 oceanic and climatic parameters are more likely to be accurate than Kerckhoffbreen's correlations.

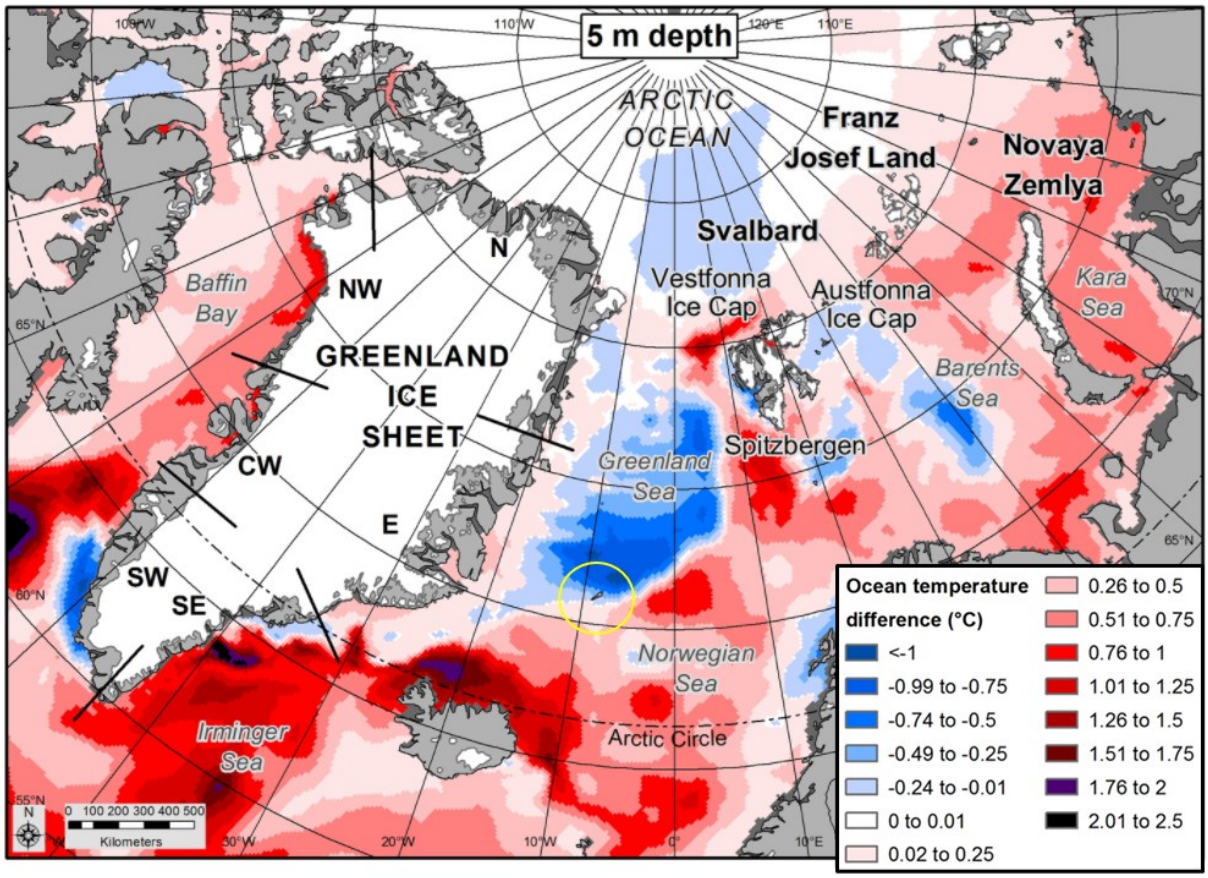

Figure 5.3: Temperature anomaly of the top 5 m of the North Atlantic Ocean for 2000-2010 compared to 1995-99. Jan Mayen is circled in yellow. Modified from Carr et al. (2017).

The sea ice extent around Jan Mayen has been minimal since at least since 1997, so that there is always an oceanic moisture source from the open North Atlantic (Koenig et al., 2014). While RH_{1000} was significantly or highly significantly, very strongly, and directly correlated with the two representative land-terminating glacier trends, neither P_a nor P_w was significantly correlated with any glacier trends. Rain warms glaciers, thus, if there had been a significant amount of rain on snow events, P_w and some glacier trend would have been inversely correlated. It is possible precipitation is not the main accumulation source, and glacier mass is gained by rime ice in fog conditions (Mortimer and Sharp, 2017). The Jan Mayen glaciers are in general retreating, thus, it is also possible that the ablation processes far exceed accumulation processes, to the point of obscuring the effect of the accumulation processes. This implies that Jan Mayen

glaciers may be more sensitive to changes in ablation processes than changes in accumulation processes, and thus summer conditions are more important for determining glacier change. It is ambiguous if coastal glaciers in general are more sensitive to temperature or precipitation, as precipitation is comparatively higher but also varies more (Cuffey and Paterson, 2010).

The value of RH_{1000} can indicate fog (RH > ~85%, Gultepe et al., 2007), and as the relationships were direct this would indicate that more frequent fog occurrence results in lowering the retreat rate and thus fog may in general be a cooling driver, corroborating the shape of the mass balance curve at lower elevations (Fog 2.12; Orheim, 1976; Hulth et al., 2010). Although fog is often theorized to suppress melt (Jiskoot et al., 2012), energy balance studies at McCall Glacier, Arctic Alaska, found that thin fog can increase net shortwave radiation, while thicker fog overall reduces temperature and shortwave radiation to a glacier's surface. In these studies the reduction in shortwave radiation and temperatures was more noticeable at lower elevations while the increase in net shortwave radiation was more noticeable at higher elevations (Jiskoot et al., 2016). Average fractional cloud cover from the climate reanalysis at Jan Mayen was generally low, with the median value for 1991-2020 being 0.05 (or 5%) at the ground level and 0.25 (or 25%) at the higher elevation; maximums were barely above 50% (0.52 at the 1000 hPa level, 0.55 at the 850 hPa level). However, Jan Mayen takes up ~10% of the climate reanalysis pixel, while the remainder is ocean. Therefore, little can be inferred about detailed cloud properties or exact timing of clouds over Jan Mayen Island.

The relationships between T_{1000} and PDD_{1000}, and between T_{850} and PDD_{850} were highly significant, very strong and moderate, respectively, and direct; and the relationships between T_{1000} and T_{850}, and between PDD_{1000} and PDD_{850}, were highly significant, strong, and direct. RH_{1000} and RH_{850} were highly significantly, moderately, and inversely correlated, and the same

relationship holds between C_{1000} and C_{850}. Therefore, even if radiation conditions in the accumulation and ablation zones at an annual scale were frequently disparate, temperatures were not. As mentioned in Section 4.7, "low-level" clouds occur below ~2000 m, which includes both levels of the climate reanalysis, and there is little differentiation within cloud levels, therefore it is uncertain if this relationship is unusual (WMO, 1995; Eastman et al., 2011). The inverse relationship suggests that frequently when fog exists at the ground level, there were few or no clouds above. Fog and temperature inversions frequently occur together and require calm conditions to persist (Oke, 1987): such stable atmospheric conditions may have no clouds above the fog. It has also been noted that low-level clouds have an inverse relationship with SST in the North Atlantic on a seasonal scale (Eastman et al., 2011). This seasonal relationship is not captured in the annual averages used in this thesis for Jan Mayen, however. Thus, that there was no significant relationship between cloud cover and SST observed in this thesis is not conclusive. Additionally, Jan Mayen covers only 10% of the climate reanalysis grid cell, therefore, surface observations at a seasonal scale should be investigated to come to any definite conclusions about relationships between cloud cover and SST.

To determine what the future holds for Jan Mayen glacier changes, Table 5.2 shows the trend and mean average value of the three driving parameters for the time periods over which the glacier fronts outlined in this study were responding to and the subsequent time period (up to present). The continued warming indicated by the columns with "change" suggests a likely continued retreat of the glaciers, as the mean average value for all parameters that were inversely correlated with glacier frontal positions have increased. However, the retreat might be slower than -9 m/yr, as the trends have all shallowed.

Table 5.2: The correlation direction, trend, and mean average parameter value for the 15-year period (glacier response time) before glacier front line measurements and for the most recent time period, and change direction between the two time periods for the driving parameters.

Parameter	Correlation Direction	Parameter trend	1985-2005 mean avg. (°C)	Parameter trend	2006-2020 mean avg. (°C)	Parameter trend change	Mean average change (°C)
T_a	Inverse	0.098	-0.3	0.051	1.0	-0.047	1.3
T_s	Inverse	0.079	4.5	0.043	5.4	-0.036	0.9
PDD_O	Inverse	15.2	663.5	11.6	862.5	-3.639	199.0

5.3. Jan Mayen Glacier Changes in Geographic Context

On average, Jan Mayen glaciers are longer and steeper than glaciers in the nearby regions (Figs 4.1-4.2). However, each region has glaciers that are comparable in length and slope to those on Jan Mayen. The slope of glaciers affects the driving stress, flow speed, and response time of glaciers (Eq 3.4), and plays a role in the mass balance-elevation feedback (Johannesson et al., 1989; Cuffey and Paterson, 2010). The mass-balance elevation feedback refers to a phenomenon where on steep glaciers, because they have a comparatively small area within a given elevation contour interval, small migrations in the elevation of the ELA will have only a minor effect on the overall mass balance of the glacier (Johannesson et al., 1989; Cuffey and Paterson, 2010). This is also related to the thickening and thinning of glaciers, which moves mass to areas of a glacier above or below the ELA. Additionally, a steeper glacier will have a higher driving stress and a higher flow speed but a shorter response time (Fig 4.13; Johannesson et al., 1989; Benn and Evans, 2010).

On Jan Mayen, land-terminating did not retreat in a way that was significantly different from marine-terminating glaciers. This is dissimilar to trends in Greenland, where marine-terminating glaciers tended to have faster retreat rates (Bjørk et al., 2012). However, in Greenland, it has been observed that glaciers in deeper fjords have a more accelerated retreat than

those in shallow waters, possibly due to ocean waters warming more than the shallow ocean (Wood et al., 2021). Jan Mayen glaciers rest in shallow waters, which might explain their slower retreat.

Jan Mayen glaciers are retreating generally slower than glaciers in the surrounding North Atlantic regions, at a rate that is half that of Greenland, the slowest of these surrounding regions (Table 5.3). The difference in rates could be due to glacier attributes or climatic factors. The response time for the glaciers in the other regions could be different, which would affect the time frame and thus the level of change they are responding to. Smaller glaciers are more numerous and more likely to have shorter response times, while larger glaciers tend to dominate by the amount of loss they experience but are more likely to have a longer response time. Additionally, Jan Mayen glacier retreat rates are being compared to all glaciers in other regions, not just ones of similar area, length, and slope. As seen in Fig 4.1, the other regions had a higher number of small glaciers, which experience relatively faster retreat due to their lack of thermal inertia (Cuffey and Paterson, 2010). The relatively higher steepness of the Jan Mayen glaciers could also account for this seemingly weak response to climate change, by the mass-balance elevation feedback. However, glacier retreat rates for Greenland, Iceland, Svalbard, and Norway were not based on a complete inventory of all glaciers, and it is possible the observations are dominated by larger glaciers, rendering this explanation debatable. The marine-terminating glaciers are retreating faster than land-terminating glaciers in Greenland (Bjørk et al., 2012), thus, it is possible that the generally faster retreat rates of marine-terminating glaciers are inflating the average retreat rates of other regions, and if only land-terminating glaciers were compared to those of Jan Mayen's glaciers, the rates would be more similar (this would not greatly affect Iceland's average retreat rate, which has only one marine-terminating glacier).

*Table 5.3: Repeated here is Table 2.1, with *Jan Mayen results from this thesis added.*

Region	No. of glaciers (marine-term.)	Glaciated area (km^2)	Glaciated area (% land cover)	Sea level equivalence (mm)	Frontal Ablation 2010-2020 (km^3/yr)	Lit. ret. rate 2000+ (m/yr)	FoG ret rate 2000+ (m/yr) (No. of glaciers)
Greenland	17500 (534)	130071	0.6	53	4.0 ± 1.5	-19	-18 (86)
Svalbard	1567 (157)	33959	55	24	12.4 ± 13.5	-40	-64 (8)
Iceland	568 (1)	11060	11	11	0.08 ± 0.12		-37 (24)
Scandinavia	3417 (0)	2949	0.4	0.6	0	-20	-20 (66)
Jan Mayen	20 (6)	119	31		0.20 ± 0.037	-9*	-9*

As mentioned in Section 5.2.1, Jan Mayen glaciers are accelerating in their retreat over the period 2000-2020. According to literature, this is in accord with Greenland and Norway: for Greenland the average retreat rate for glaciers not attached to the ice sheet increased from -9 m/yr in the period 1990-2000 to -20 m/yr for 2000-2010 (Bjørk et al., 2012), and for Norway the average glacier retreat rates increased from -5.5 m/yr in the period 1990-2000 to -20 m/yr for 2000-2018 (Winsvold et al., 2014; Andreassen et al., 2020). Studies on Svalbard saw retreats rates double between 1990-2000 and 2000-2010 (from -16 m/yr to -32 m/yr), and this trend of increasing retreat has likely continued into the present (Carr et al., 2017). From WGMS data that was used for additional glacier retreat numbers, Greenland, Scandinavia, and Svalbard did not have a large increase between 2000-2010 and 2010-2020, but on Iceland the average glacier retreat rate increased from -34 m/yr to -42 m/yr (WGMS, 2021). Differences were likely due to data from some studies not being present in the WGMS FoG database.

Beyond glacier attributes, differences could be due to differences in climate and sea ice trends between the regions. To investigate this, changes in the driving forces for glacier changes in the areas nearby need to be compared to Jan Mayen's driving parameters. Dominant factors affecting glacier retreat and advance differs for the four regions around Jan Mayen. For southeast Greenland it is SST (Murray et al., 2010; Straneo et al., 2010), for Scandinavia and Svalbard it is

conditions during the accumulation season (Nesje et al., 2008), and for Iceland it is possible summer conditions are more important (Sigurđsson et al., 2007; Chandler et al., 2016), although glacier changes have been correlated to NAO as well (Kirkbride, 2002; Jensen et al., 2016), and Iceland is generally sensitive to small changes in climate due to the maritime climate (Chandler et al., 2016). For changes on Jan Mayen, the point between these four regions, summer conditions are important, as well as annual average air temperature and PDD. Annual average temperature and annual precipitation sum for Greenland, Svalbard, Iceland, and Scandinavia have all increased in 1991-2020 compared to their 1961-1990 values, except for precipitation yearly sum in Svalbard (Table 5.4). Increases in mean annual average temperatures at Jan Mayen was nearly twice that of most of the other regions (except for Greenland, which was higher). As T_a was inversely and strongly or very strongly correlated with glacier changes, Jan Mayen glaciers should be retreating faster than other regions. Jan Mayen also experienced the most significant decrease in precipitation, but precipitation did not significantly correlate with glacier changes. Greenland experienced the highest increase in temperature, but also had the slowest rate of retreat of glaciers for the areas surrounding Jan Mayen (Table 5.3).

Table 5.4: Mean annual average temperature and yearly precipitation sum for Greenland, Svalbard, Iceland, Scandinavia (Norway and Sweden), and Jan Mayen for 1961-1990 and 1991-2020, and how they have changed. Data except for Jan Mayen from https://climateknowledgeportal.worldbank.org/download-data.

Country/Region	T_a 1961-90 (°C)	T_a 1991-2020 (°C)	P_a 1961-90 (mm)	P_a 1991-2020 (mm)	T_a change	P_a change
Iceland	1.41	2.32	1029.27	1141.44	0.9	112.2
Svalbard	-8.86	-6.7	526.94	525.58	2.2	-1.4
Norway	1.09	2.11	1082.9	1152.66	1.0	69.8
Sweden	1.88	2.99	626.95	663.81	1.1	36.9
Greenland	-16.8	-15.84	595.14	623.34	1.0	28.2
Jan Mayen	-1.4	0.5	685.6	646.9	1.9	-38.7

Table 5.4 indicates that Jan Mayen has experienced a more extreme annual average air temperature increase between 1961-1990 and 1991-2020. Additionally, the trend in Table 5.2 indicates that over the period 1985-2005 (the time period the glacier fluctuations drawn in this thesis are responses to), Jan Mayen experienced a 2.0 °C change. However, SST is an important consideration as well (Wood et al., 2021). As seen in Fig 5.3, around all these regions the mean annual SST mostly increased. The ocean north of Iceland and south of Svalbard experienced the largest temperature anomaly, however, SST has not been noted as the major driving factor for these glaciers. Jan Mayen has a persistent temperature inversion and fog that affects most of the glaciers' termini by reducing melt in the ablation zones and is and especially important for the south-facing glaciers (Orheim, 1976; Anda et al., 1985; Hulth et al., 2010), which might explain why SST increases do not match with glacier changes. Southeast Greenland experienced a relatively high increase in SST, and the glaciers in southeast Greenland are sensitive to changes in SST; despite this, Greenland had a lower overall retreat rate than the other regions. According to the values of mean average annual temperature and SST changes, Greenland and Jan Mayen should be experiencing a faster retreat than the other areas. As they are not, this indicates there are other important drivers that are not being considered. As Jan Mayen glaciers have a short response time, they could be used as an early warning for changes to glaciers in the regions nearby. However, the mechanism which causes Jan Mayen glaciers to retreat slower than the average of the other regions while experiencing a larger increase in inversely correlated controls on glacier change must be explained first.

As mentioned in Section 5.2.1, Sørbreen was not at its most retreated observed position in 2018, and has been known to reach retreat rates similar to those presented in this thesis (~30 m/yr 1930-1950; Kinsman and Sheard, 1963). In Iceland, two glaciers (Skálafellsjökull; Chandler et

al., 2016, and Lambatungnajökull; Bradwell, 2004) retreated quicker over this same period (~19330-1950), and similar to Sørbreen, had a brief period of readvance in the 1960s, then an approximately stable front position from the early 1970s to the early 2000s. Freya glacier in northeast Greenland is similar to Jan Mayen glaciers as it is 6.7 km long, and retreated 170 m between 1985-2008 or ~ 7 m/yr, which is near the island's average of -9±7 m/yr (WGMS, 2021). Therefore, glaciers on Jan Mayen do show some similar patterns in glacier retreat as glaciers in nearby regions.

5.3.1. Frontal Ablation in Context

The high estimate for Jan Mayen's frontal ablation was 0.217 km^3 over a 21-year period. The Pan-Arctic study that used results from this thesis (Kochtitzky et al., in prep) found that most individual marine-terminating glaciers have a frontal ablation < 0.04 km^3/yr. However, Jan Mayen glaciers had a frontal ablation of 0.009 km^3/yr for all glaciers together.

Most Pan-Arctic regions have a small number of larger glaciers that disproportionately contribute to frontal ablation, whereas Jan Mayen glaciers are all similar in area. To put this into perspective, the Columbia Glacier (1000 km^2), which is the largest glacier contributor to ice loss in the Western Chugach mountains, which is one of the largest region contributors to sea level rise from Alaska, had a flux of 4 km^3/yr for 1954-2006 (McNabb and Hock, 2014). Smaller glaciers in the Wester Chugach Mountains had an average ice flux closer to 0.2 km^3/yr. In Svalbard, 28% of the glaciers account for 90% of the regional total frontal ablation, which was 0.7 km^3/yr (Kochtitzky et al., in prep). For Greenland glaciers not attached to the ice sheet, which have a similar total marine-terminating glacier area to Svalbard, the total frontal ablation was only 0.3 km^3/yr.

The relationship between size of glaciers and calving is complex and could be a complete thesis on its own (Benn and Åström, 2018), but it is clear that the 2000-2020 Jan Mayen frontal ablation contribution was small, even negligible, in comparison to other areas. While Jan Mayen is in an interesting location between two important ocean currents, the North Atlantic Current and the East Greenland Current, it does not have the power to influence these currents (AMAP, 2017; Lysså et al., 2021). Rather, icebergs which detach from the glaciers on Jan Mayen are more likely the greatest threat, and even these are likely the size of growlers or bergy bits, which melt quickly (Savage et al., 2001). As in the past, the current "marine-terminating" glaciers of Jan Mayen terminate very near or at the shoreline (Fig 5.1) and are fully grounded (do not displace any water with their mass). Therefore, for future years it can be assumed that all ablation from Jan Mayen glaciers contributes to sea level rise.

5.4. Results in a Broader Geographical Context

The high temporal frequency of observations of the Jan Mayen glaciers in this thesis provides the glaciological community with data on glaciers that surround a single isolated mountain. This reveals that glacier changes are erratic even in simple cases, and glacier changes can differ even when glaciers are located directly next to each other and subjected to similar forcings and weather patterns. This has previously been observed in areas around Jan Mayen, such as Greenland, where it was the calving mechanism that was cited as being the cause for large differences in climate response (Warren and Glasser, 1992). Despite the similarities in their retreat and advance pattern, by total retreat and average retreat rate Frielebreen and Prins Haralds Bre had the largest difference in retreat rates for glaciers with adjoining basins on Jan Mayen, and yet these glaciers were close enough to have been considered a single glacier with a continuous calving front in the past.

Of the 16 glaciers that had measurements in this thesis, Sørbreen is the largest glacier by area (Table 4.5) and has the third shallowest slope. Across the globe, steep glaciers generally retreated less over 1900-2000 than glaciers with a gentler slope (Leclercq et al., 2014), as steeper glaciers are less sensitive to climate change (Oerlemans, 2001). Additionally, Kerckhoffbreen, which had the second largest retreat of the 16 glaciers measured in this thesis (Table 4.3), is the second largest glacier by area (Table 4.5) and has the second shallowest slope. Fotherbybreen, which has the shallowest slope and third largest area, however, did not experience a particularly large retreat. Therefore, the glaciers on Jan Mayen in general depict similar responses to climate change when considering glacier attributes, with some exceptions.

There is a remote, glacierized, volcanic island much like Jan Mayen in the Southern Ocean: Heard Island. Located at 53.1° S, 73.5° E, the island is 367 km^2 and ~70% of this is covered by glaciers. Unfortunately, the glaciers of Heard island are not included in the RGI 6.0 (RGI Consortium, 2017), and so information on their exact dimensions is limited. However, many glaciers on this island are of comparable length and slope to Jan Mayen glaciers, with 19 reaching heights above 2000 m a.s.l. and lengths in excess of 7 km (Thost and Truffer, 2008). These cover the stratovolcano Big Ben, which has been more active than Beerenberg with 13 eruptions since 1881 (Global Volcanism Program, 2013a). Additionally, temperature inversions and low-level clouds are common on Heard Island (Thost and Truffer, 2008). The Heard Island glaciers experienced very little change 1874-1929 (while 4-6 marine-terminating glaciers on Jan Mayen retreated onto land; Table 4.1), then rapid oscillating changes 1963-1971, then glacier retreat after 1983 that continued into the early 2000s (Thost and Truffer, 2008). The Stephenson Glacier (~8 km long) on Heard Island retreated by 200 m between 2003-04, much faster than Sørbreen, while the Brown glacier (4.8 km long) on Heard Island had an average retreat rate of -

21 m/yr for 2000-2003, similar to Sørbreen's rate (Thost and Truffer, 2008). It is theorized that air temperature is most important for explaining glacier retreat on Heard Island (Ruddell and Allison, 1998) and neither precipitation nor GHF could have been a major driver, as they both would have had to change by an unreasonable margin (Thost and Truffer, 2008). These same influences (or lack thereof) were demonstrated on Jan Mayen, where most glacier changes were explained through a parameter derived from air temperature. While the glaciers on Heard Island are similar to Jan Mayen glaciers in size, slope, and climate, they are retreating much faster (Kiernan and McConnell, 2002; Thost and Truffer, 2008).

Approximately 25% of glaciers on volcanoes are located in the Arctic (Edwards et al., 2020), and most detailed studies of glaciers on volcanoes are individual case studies (Gudmundsson et al., 1997; Hannesdóttir et al., 2015b; Möller et al., 2016). Studies at a continental scale in Latin America found that while glacier area loss trends for glaciers on volcanoes are predominantly explained by climatic factors, these glaciers still tend to change in ways different from nonvolcanic glaciers nearby which are subject to the same climatic conditions (Rivera et al., 2012). Rivera et al. (2012) observed that glaciers on volcanoes occasionally advanced, while the nearby nonvolcanic glaciers only retreated, and theorized tephra deposition cooling the glaciers as a possible mechanism responsible for this difference. Another hypothesis for differences in the responses of glaciers on volcanoes to other glaciers nearby is the higher slope of glaciers on volcanoes and the related mass-balance elevation feedback (Rivera and Bown, 2013).

This thesis delineated glacier outlines 2000-2020, the changes of which were likely still dynamic responses to climate over the period 1985-2005: the period just after the most recent volcanic activity. Glacier response to high GHF related to a volcanic eruption is likely far more

immediate, rather than being visible 15 years after an eruption (Smellie and Edwards, 2016; Jóhannesson et al., 2020). However, the measured GHF around JM is ~100 mW/m^2, which is high enough to contribute to some basal ablation (Dahl-Jensen et al., 2003; van der Veen et al., 2007). For context, at a location in Greenland covered in ~3.5 km of ice (therefore the ice at the base is already near the pressure-melting point), 120 mW/m^2 corresponds to ~0.77 cm/yr of melt (Dahl-Jensen et al., 2003). There was no observable difference in the retreat patterns between the glaciers near the most likely sources of GHF on the island and glaciers adjacent to them. The earlier eruptions deposited tephra on the Jan Mayen glaciers, which is visible in satellite imagery. As the Jan Mayen glaciers are retreating slower than glaciers in areas nearby despite having a higher temperature increase for 1990-2020, this indicates that the tephra could be a cooling factor. However, the land-terminating glaciers (which were in general more debris-covered) retreated faster than the marine-terminating glaciers on the island itself, and so the tephra deposition might be a warming driver. Regardless of the magnitude of the volcanic effects on the Jan Mayen glaciers, these glaciers behaved similarly to glaciers on volcanoes in other areas: they retreated slower than other glaciers not on volcanoes nearby, but seem to be responding to climatic factors (Rivera et al., 2012).

6. CHAPTER 6: SUMMARY AND CONCLUSIONS

The study of individual glaciers is important to further understanding of their response to climate change, and the timing and amount of melt they will contribute to sea level rise (IPCC, 2021). Arctic glaciers are changing more quickly than ice sheets, and thus should be studied now (Vaughan et al., 2013; Edwards et al., 2021). Glacier changes can be quantified by measuring mass balance, volume change or by delineating glacier area and measuring changes in length. Glacier shape and mass balance can be affected by processes in four areas: frontal, surficial, basal, and englacial. Surficial processes are in general the dominant factor influencing glacier change for land-terminating glaciers, while frontal processes are dominant for marine-terminating glaciers. For glaciers overlying volcanic regions, basal melt cannot be neglected (van der Veen et al., 2007; Jóhannesson et al., 2020). This study is unique in its scale, in that most studies are either a case study of a single glacier or of a larger geographic region.

Jan Mayen is a small glacierized volcanic island in the middle of the North Atlantic ocean, located between a warm and a cool ocean current, and is situated centrally between four important highly glaciated regions: Greenland, Svalbard, Iceland, and Scandinavia (Lysså et al., 2021). Based on data from the RGI (Pfeffer et al., 2014; RGI Consortium, 2017), Jan Mayen's 20 glaciers are on average longer and steeper than glaciers in the surrounding regions. However, these nearby regions have far more glaciers, and each has more than 20 glaciers in the same length and steepness range as Jan Mayen. This island has several unique geologic and climatic properties: it is an isolated mountain that is an active volcano, and temperature inversions and fog are almost ubiquitous. No systematic records of glacier changes exist after 1975 and the only attempt to map volume changes of Jan Mayen glaciers was through DEM differing of surface elevation data from 1949, 1975 and 2008, over which time the glacier volume did not change

significantly (Hagen et al., 1993; Rolstad Denby and Hulth, 2011). This DEM study suffered from significant data gaps and did not have full coverage of the ablation region of the glaciers (Rolstad Denby and Hulth, 2011). The main objective of this thesis was to present the changes in frontal positions for 16 of the 20 glaciers on Jan Mayen Island for 2000-2020, changes in 18 climatic and oceanic parameters for as long as their records allowed, climate trends for 1961-1990 and 1991-2020, and correlations between the glacier relative length changes and the 18 oceanic and climatic factors. This information will be added to two international databases.

In this thesis, historical maps from 1861-1975 were used to qualitatively determine Jan Mayen glacier terminus characteristics and satellite imagery from Landsat and ASTER were used to outline a total of 113 glacier frontal measurements (near-annual for marine-terminating and every 5-10 years for land-terminating glaciers) of 16 of the 20 glaciers over the period 2000 – 2020 and calculate their annual changes in area and length using the box method. In the 19th century, Jan Mayen had more marine-terminating glaciers than land-terminating, and these dominated both the east and northwest side of the island. Five of these glaciers retreated onto land between the late-19th century and mid-20th century. In general, the glaciers have continued to retreat into the 21st century, with a further five glaciers retreating onto land between 2000-2020. The total ice area lost between 2000 and 2020 was 2.15 km^2. The ice flux from the marine-terminating glaciers on Jan Mayen for 2000-2020 was 0.20 km^3, which is insignificant in comparison to regions nearby.

Glacier changes were correlated to 18 observed, modelled, and derived climatic and oceanic parameters. Of these, annual average and summer average air temperature and positive degree days as measured at the meteorological station on Olonkinbyen had the greatest overall affect. As climate trends in these parameters continue to increase into current times, and these

climate trends were inversely correlated with the glacier frontal fluctuations, Jan Mayen glaciers will continue to retreat. One glacier was not significantly correlated with any parameter; this glacier is the only marine-terminating glacier remaining on the island as of 2020, and the inability of the marine-terminating glaciers on Jan Mayen to advance past the coastline might account for the lack of correlating parameters. The glaciers on Jan Mayen Island are changing at a slower rate than in the nearby regions, despite the relatively larger increase in air temperature at Jan Mayen.

6.1. Future Studies

There are many futures studies which could stem from this thesis and from the observed scarcity of measurements on the island of Jan Mayen (e.g. Skreslet et al., 2004). Some example queries are: Why are the Jan Mayen glaciers retreating slower than nearby regions, even though the temperature is increasing faster? Can the answer to this be applied to other glaciers? What is the relationship between temperature inversions/fog and glacier changes at Jan Mayen, and can this be applied to other maritime glaciers? What creates the most substantial difference in forcings on marine-terminating glaciers not in a fjord compared to those in a fjord? How strong of a buttressing effect does local landfast ice have on marine-terminating glaciers, compared to pack ice? Data that are missing for the island of Jan Mayen and that are more common for other regions, and essential for glaciological work, include glacier thickness measurements and in situ ice velocity measurements. The RGI glacier outlines should be updated, as it currently includes small perennial snow patches that are not glaciers and should be removed from the database. An updated DEM study since Rolstad Denby and Hulth (2011) should be conducted, with complete DEMS from the year 2008 onwards.

To continue studies on Sørbreen specifically, Anda et al.'s (1985) frontal position history could be digitized, so that trends in Sørbreen's retreat and advance could be quantified as far back

as 1850. There are also likely more historical maps than this study found, and some of the accounts that were not in English could be translated (Vogt, 1863; Bóbrik von Boldva, 1886), which might reveal further insight, possibly into thickness or activity of the glaciers (Mohn and Wille, 1882; Jennings, 1948). Additionally, Hulth et al. (2010) conducted energy and mass balance measurements of Sørbreen between 2007-2011, and while the results from the 2007/2008 hydrologic year have been published (Hulth et al., 2010) the final three years have never been processed. Analyzing these additional years will give insight into the inversions and fog of Jan Mayen and their effect on glaciers.

There is still much work which could be done in investigating Jan Mayen glacier changes' relationship to climatic and oceanic factors. Any moderate correlations found between glacier trends and parameters could be further investigated (Table 4.10). Additionally, temperature inversions, fog, and sea ice concentration could be important. The first two were not considered in this thesis, while the third was looked at only qualitatively. As the NSIDC sea ice concentration used in this thesis is at a 25 x 25 km grid cell, this is too low a resolution to truly capture conditions around Jan Mayen. Diving into the sea ice concentration data at a higher resolution or examining satellite imagery from the winter would reveal conditions on the local sea ice that surrounds Jan Mayen in the winters, distinct from the ice exported through the Fram Strait into the Greenland Sea (Fig 6.1). Jan Mayen often is surrounded by such landfast sea ice (Fig 6.1b), which could be strong enough to slightly restrict calving rates, or broken pieces of the larger sea ice from the north (Fig 6.1a). The images in Fig 6.1 are only 48 days apart, and either sea ice condition could create noticeably different atmospheric conditions that affect the glacier, such as changes in humidity and inversion characteristics.

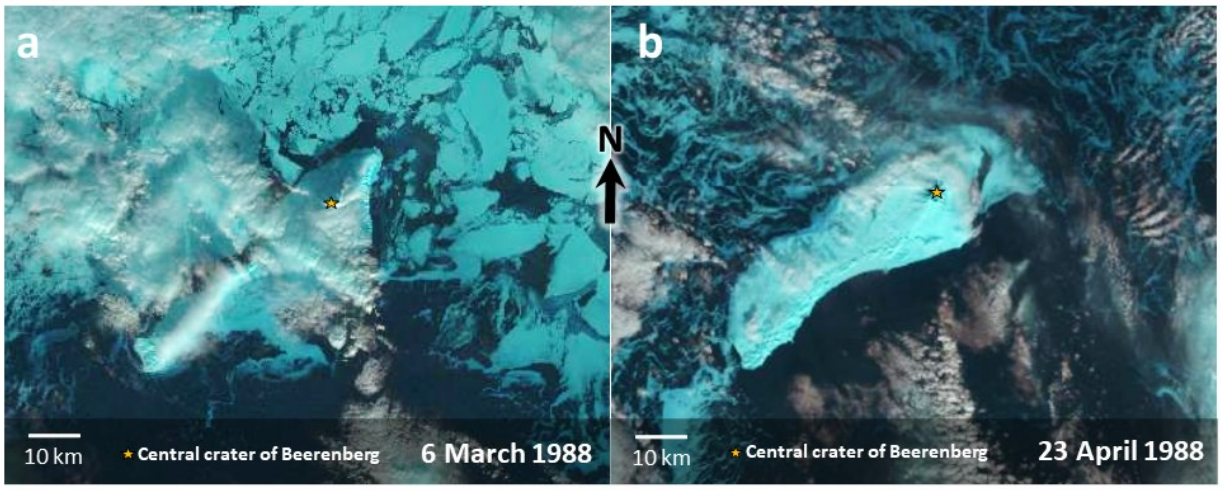

Figure 6.1: Examples of different sea ice conditions around the island of Jan Mayen. In March 1988, Jan Mayen was considered within the sea ice exported through the Fram Strait (March through August Ice Edge Positions in the Nordic Seas, 1750-2002 version; https://nsidc.org/data/G02169/versions/1). Both images are from Landsat 5.

Inversion characteristics could be investigated with radiosonde data available through the Integrated Global Radiosonde Archive (IGRA: Durre et al., 2006). Conducting surface mass balance studies on additional glaciers, ideally in the four quadrants (NW, NE, SW, SE) would substantially aid in verifying if the original theory that fog and inversions are most important for the south and east glaciers is correct (Anda et al., 1985), and perhaps explain the mechanism behind the similarity of Kerckhoffbreen and Sørbreen's retreat pattern. This would require additional field measurements that have not been attempted and considering the difficulties inherent with traveling to the Jan Mayen glaciers, could possibly only be extended to a few glaciers beyond Sørbreen. However, it would more clearly reveal patterns in driving forces between marine- and land-terminating glaciers, as well as spatial patterns, such as determining if glaciers in an east/west grouping behave more similarly than those in a north/south grouping. If additional field work can be completed on the highly crevassed glaciers, glacier thickness estimates and stake velocity measurements would allow for the individual calculation of response times for all glaciers, and thus individual correlation to climatic and oceanic factors.

To further investigate how Jan Mayen glaciers fit within the broader regions, a study could compare the trends in Jan Mayen glaciers changes to trends in specific glaciers of other regions of similar area and length, instead of comparing only regional averages. The WGMS FoG database (WGMS, 2021) would be a starting point for this, although it is not a complete record of every glacier that has been observed in these regions. From the RGI, glaciers that are similar in size and slope to the Jan Mayen glaciers could be determined, and these could then be searched for within the WGMS database or other regional studies, making the comparison between glaciers more applicable. If comparing these more similar glaciers does not make the trends converge, further climatic and oceanic factors that differ between the regions can be investigated. Jan Mayen glacier changes could be compared to locations with known inversions, or polar glaciers on volcanoes in the southern hemisphere (e.g. Heard island: Thost and Truffer, 2008) or outside of the Arctic (Edwards et al., 2020). For the latter, glacier frontal fluctuations would have to be delineated in years immediately before and after the most recent eruption (1985).

Further investigations into the importance of the volcano Beerenberg, its eruptions, and related changes in GHF on Jan Mayen glacier changes could be conducted. Heat flow databases include thousands of geophysical measurements, with several in the vicinity of Jan Mayen (Fig 2.13; Pollack et al., 1993; Davies, 2013; Lucazeau, 2019). Based on the time of the measurements and their proximity to the glaciers, these could be included into a melt model to account for ablation from basal heating (see end of Section 2.1; Thost and Truffer, 2008; Jóhannesson et al., 2020), and simplify the extraction of accurate climatic and oceanic response of the glaciers. The effect of tephra on the Jan Mayen glaciers could also be studied by examining satellite imagery before and after eruptions. As satellite imagery from Landsat theoretically goes back to 1972, the 1985 and perhaps the 1973 eruptions could be studied. Patterns in tephra

changes on the glaciers could be studied by mapping the clean ice in reference to the glacier fronts (Kirkbride and Dugmore, 2003; Reinthaler et al., 2019), and ideally field work could be conducted to determine thickness of the tephra currently covering glacier fronts (Dragosics et al., 2016; Möller et al., 2016).

The single isolated mountain of Jan Mayen presents an excellent opportunity for numerical energy balance - mass balance modelling, which can estimate the timing and amount of melt from glaciers, and thus is vital for those studying climate and alpine systems, sea level rise, and ecosystems downstream of glaciers. The glaciers are similar in size and slope and cover all aspects. The influence of fog, temperature inversions, localized sea ice, GHF, and other volcanic effects could be incorporated into a numerical mass balance model that can account for these second order controls on ablation, and then be applied to other relevant glaciers in polar regions.

7. REFERENCES

Aars, J., Marques, T.A., Lone, K., Andersen, M., Wiig, Ø., Bardalen Fløystad, I.M., Hagen, S.B., and Buckland, S.T. (2017) The number and distribution of polar bears in the western Barents Sea. *Polar Research*, *36*, doi:10.1080/17518369.2017.1374125.

Acharya, A., and Kayastha, R.B. (2018) Mass and energy balance estimation of Yala Glacier (2011-2017), Langtang Valley, Nepal. *Water*, *11*(6), doi:10.3390/w11010006.

AMAP (2017) Snow, Water, Ice and Permafrost in the Arctic (SWIPA) 2017:, https://www.amap.no/documents/doc/snow-water-ice-and-permafrost-in-the-arctic-swipa-2017/1610.

AMS (2012) American Meteorological Society Glossary of Meteorology: "turbulent flux.", https://glossary.ametsoc.org/wiki/Turbulent_flux (accessed May 2021).

Amundson, J.M., Fahnestock, M.A., Truffer, M., Brown, J., Lüthi, M.P., and Motyka, R.J. (2010) Ice mélange dynamics and implications for terminus stability, Jakobshavn Isbrae, Greenland. *Journal of Geophysical Research: Earth Surface*, *115*(F01005), doi:10.1029/2009JF001405.

Anda, E., Orheim, O., and Mangerud, J. (1985) Late Holocene glacier variations and climate at Jan Mayen. *Polar Research*, *3*(2), 129–140, doi:10.1111/j.1751-8369.1985.tb00501.x.

Andreassen, L.M., Elvehøy, H., Kjøllmoen, B., and Belart, J.M.C. (2020) Glacier change in Norway since the 1960s - An overview of mass balance, area, length and surface elevation changes. *Journal of Glaciology*, *66*(256), 313–328, doi:10.1017/jog.2020.10.

Andreassen, L.M., Kääb, A., Paul, F., and J.E.Hausberg (2008) Landsat- derived glacier inventory for Jotunheimen, Norway, and deduced glacier changes since the 1930s. *The Cryosphere*, *2*(3), 131–145, doi:10.5194/tcd-2-299-2008.

Aster, R.C., and Winberry, J.P. (2017) Glacial seismology. *Reports on Progress in Physics*, *80*(12), 126801, doi:10.1088/1361-6633/aa8473.

Barr, W. (2008) The Expeditions of the First International Polar Year 1882-83: Arctic Institute of North America, doi:10.1007/978-3-642-12402-0_3.

Bartholomaus, T.C., Larsen, C.F., and O'Neel, S. (2013) Does calving matter? Evidence for significant submarine melt. *Earth and Planetary Science Letters*, *380*, 21–30, doi:10.1016/j.epsl.2013.08.014.

Bartholomaus, T.C., Larsen, C.F., O'Neel, S., and West, M.E. (2012) Calving seismicity from iceberg-sea surface interactions. *Journal of Geophysical Research: Earth Surface*, *117*(4), 1–16, doi:10.1029/2012JF002513.

Bell, B. et al. (2020) ERA5 monthly averaged data on pressure levels from 1950 to 1978 (preliminary version). *Copernicus Climate Change Service (C3S) Climate Data Store (CDS)*, https://cds.climate.copernicus-climate.eu/cdsapp#!/dataset/reanalysis-era5-pressure-levels-monthly-means-preliminary-back-extension?tab=overview.

Benn, D.I., and Åström, J.A. (2018) Calving glaciers and ice shelves. *Advances in Physics: X*, *3*(1), 1049–1076, doi:10.1080/23746149.2018.1513819.

Benn, D.I., and Evans, D.J. (2010) Glaciers and Glaciation: New York, NY, USA, Routledge, 816 p.

Benn, D.I., Warren, C.R., and Mottram, R.H. (2007) Calving processes and the dynamics of calving glaciers. *Earth-Science Reviews*, *82*(3–4), 143–179, doi:10.1016/j.earscirev.2007.02.002.

Berdahl, M., Rennermalm, A., Hammann, A., Mioduszweski, J., Hameed, S., Tedesco, M., Stroeve, J., Mote, T., Koyama, T., and McConnell, J.R. (2018) Southeast Greenland winter precipitation strongly linked to the Icelandic Low position. *Journal of Climate*, *31*(11), 4483–4500, doi:10.1175/JCLI-D-17-0622.1.

Bintanja, R., Van Oldenborgh, G.J., Drijfhout, S.S., Wouters, B., and Katsman, C.A. (2013) Important role for ocean warming and increased ice-shelf melt in Antarctic sea-ice expansion. *Nature Geoscience*, *6*, 376–379, doi:10.1038/ngeo1767.

Bjørk, A.A., Kjær, K.H., Korsgaard, N.J., Khan, S.A., Kjeldsen, K.K., Andresen, C.S., Box, J.E., Larsen, N.K., and Funder, S. (2012) An aerial view of 80 years of climate-related glacier fluctuations in southeast Greenland. *Nature Geoscience*, *5*(6), 427–432, doi:10.1038/ngeo1481.

Björnsson, H. (2011) Understanding jökulhlaups: From tale to theory. *Journal of Glaciology*, *56*(200), 1002–1010, doi:doi:10.3189/002214311796406086.

Bóbrik von Boldva, A.A. (1886) Aufnahme und Beschreibung der Insel Jan.Mayen und Beobachtungen über Gletscherbeweflng, *in* Die Osterreichische Polarstation Jan Mayen, v. 1, pt. 2, Kaiserlichen Akademie der Wissenschaften.

Bradwell, T. (2004) Annual moraines and summer temperatures at Lambatungnajökull, Iceland. *Arctic, Antarctic, and Alpine Research*, *36*, 502–508, doi:10.1657/1523-0430(2004)036[0502:AMASTA]2.0.CO;2.

Braithwaite, R.J. (1984) Calculation of degree-days for glacier-climate research. *Zeitschrift fur Gletscherkunde und Glazialgeologie*, *20*, 1–8.

Braithwaite, R.J. (1995) Positive degree-day factors for ablation on the Greenland ice sheet studied by energy-balance modelling. *Journal of Glaciology*, *41*(137), 153–160, doi:10.1017/S0022143000017846.

Carr, J.R., Stokes, C.R., and Vieli, A. (2014) Recent retreat of major outlet glaciers on Novaya Zemlya, Russian Arctic, influenced by fjord geometry and sea-ice conditions. *Journal of Glaciology*, *60*(219), 155–170, doi:10.3189/2014JoG13J122.

Carr, J.R., Stokes, C.R., and Vieli, A. (2017) Threefold increase in marine-terminating outlet glacier retreat rates across the Atlantic Arctic: 1992–2010. *Annals of Glaciology*, *58*(74), 72–91, doi:10.1017/aog.2017.3.

Carvalho, K.S., and Wang, S. (2020) Sea surface temperature variability in the Arctic Ocean and its marginal seas in a changing climate: Patterns and mechanisms. *Global and Planetary Change*, *193*, 103265, doi:10.1016/J.GLOPLACHA.2020.103265.

Chandler, B.M.P., Evans, D.J.A., and Roberts, D.H. (2016) Recent retreat at a temperate Icelandic glacier in the context of the last ~80 years of climate change in the North Atlantic region. *Arktos*, *2*(24), doi:10.1007/s41063-016-0024-1.

Cogley, J.G. et al. (2011) Glossary of Glacier Mass Balance and Related Terms, *in* IHP-VII Technical Documents in Hydrology, Paris, UNESCO-IHP, v. 86, p. 124.

Cuffey, K., and Paterson, W.S.B. (2010) The Physics of Glaciers: Elsevier, 704 p.

Dadic, R., Mullen, P.C., Schneebeli, M., Brandt, R.E., and Warren, S.G. (2013) Effects of bubbles, cracks, and volcanic tephra on the spectral albedo of bare ice near the Transantarctic Mountains: Implications for sea glaciers on Snowball Earth. *Journal of Geophysical Research: Earth Surface*, *118*(3), 1658–1676, doi:10.1002/jgrf.20098.

Dahl-Jensen, D., Gundestrup, N., Gogineni, S.P., and Miller, H. (2003) Basal melt at NorthGRIP modeled from borehole, ice-core and radio-echo sounder observations. *Annals of Glaciology*, *37*, 207–212, doi:10.3189/172756403781815492.

Davies, J.H. (2013) Global map of solid Earth surface heat flow. *Geochemistry, Geophysics, Geosystems*, *14*(10), 4608–4622, doi:10.1002/ggge.20271.

Davis, J.C. (2002) Statistics and Data Analysis in Geology: Kansas Geological Survey; The University of Kansas, 638 p.

Davis, P.T., Menounos, B., and Osborn, G. (2009) Holocene and latest Pleistocene alpine glacier fluctuations: a global perspective. *Quaternary Science Reviews*, *28*(21–22), 2021–2033, doi:10.1016/j.quascirev.2009.05.020.

Dragosics, M., Meinander, O., Jónsdóttír, T., Dürig, T., De Leeuw, G., Pálsson, F., Dagsson-Waldhauserová, P., and Thorsteinsson, T. (2016) Insulation effects of Icelandic dust and volcanic ash on snow and ice. *Arabian Journal of Geosciences*, *9*(2), 1–10, doi:10.1007/s12517-015-2224-6.

Durre, I., Vose, R.S., and Wuertz, D.B. (2006) Overview of the Integrated Global Radiosonde Archive. *Journal of Climate*, *19*, 53–68, doi:10.1175/JCLI3594.1.

Eastman, R., and Warren, S.G. (2010) Arctic cloud changes from surface and satellite observations. *Journal of Climate*, *23*, 4233–4242.

Eastman, R., Warren, S.G., and Hahn, C.J. (2011) Variations in Cloud Cover and Cloud Types over the Ocean from Surface Observations, 1954-2008. *Journal of Climate*, *24*, 5914–5934.

Edwards, T.L. et al. (2021) Projected land ice contributions to twenty-first-century sea level rise. *Nature*, *593*, 74–82, doi:10.1038/s41586-021-03302-y.

Edwards, B.R., Kochtitzky, W., and Battersby, S. (2020) Global mapping of future glaciovolcanism. *Global and Planetary Change*, *195*(March), 103356, doi:10.1016/j.gloplacha.2020.103356.

Fahnestock, M.A., Abdalati, W., Joughin, I., Brozena, J., and Gogineni, P. (2001) High geothermal heat flow, basal melt, and the origin of rapid ice flow in central Greenland. *Science*, *294*(5550), 2338–2342, doi:10.1126/science.1065370.

Farinotti, D., Huss, M., Fürst, J.J., Landmann, J., Machguth, H., Maussionn, F., and Pandit, A. (2019) A consensus estimate for the ice thickness distribution of all glaciers on Earth. *Nature Geoscience*, *12*(3), 168–173, doi:10.1038/s41561-019-0300-3.

Fitch, F.J., Kinsman, D.J.J., Sheard, J.W., and Thomas, D. (1962) Glacier readvance on Jan Mayen, *in* IUGG/IASH, Symposium of Obergurgl: International Association of Scientific Hydrology Publication, no. 58, p. 201–211.

Førland, E.J., Hanssen-Bauer, I., and Nordli, P.Ø. (1997) Climate statistics & longterm series of temperature and precipitation at Svalbard and Jan Mayen, *in* DNMI Klima Report No. 21/97 Klima, Det Norske Meteorologiske Institutt.

Fürst, J.J., Durand, G., Gillet-Chaulet, F., Tavard, L., Rankl, M., Braun, M., and Gagliardini, O. (2016) The safety band of Antarctic ice shelves. *Nature Climate Change*, *6*(5), 479–482, doi:10.1038/nclimate2912.

Gajek, W., Trojanowski, J., and Malinowski, M. (2017) Automating long-term glacier dynamics monitoring using single-station seismological observations and fuzzy logic classification: A case study from Spitsbergen. *Journal of Glaciology*, *63*(240), 581–592, doi:10.1017/jog.2017.25.

Gardner, A.S., Fahnestock, M.A., and Scambos, T.A. (2019) ITS_LIVE Regional Glacier and Ice Sheet Surface Velocities. *Data archived at National Snow and Ice Data Center*, doi:10.5067/6II6VW8LLWJ7.

Gardner, A.S., Moholdt, G., Scambos, T., Fahnstock, M., Ligtenberg, S., Broeke, M. van den, and Nilsson, J. (2018) Increased West Antarctic and unchanged East Antarctic ice discharge over the last 7 years. *The Cryosphere*, *12*(2), 521–547, doi:10.5194/tc-12-521-2018.

Gilson, G.F., Jiskoot, H., Cassano, J.J., Gultepe, I., and James, T.D. (2018) The Thermodynamic Structure of Arctic Coastal Fog Occurring during the Melt Season. *Boundary-Layer Meteorology*, *168*, 443–467, doi:10.1007/s10546-018-0357-3.

Global Volcanism Program (2013a) Heard (234010) (E. Venzke, Ed.): Smithsonian Institution, doi:10.5479/si.GVP.VOTW4-2013.

Global Volcanism Program (2013b) Jan Mayen (376010) (E. Venzke, Ed.): Smithsonian Institution, doi:10.5479/si.GVP.VOTW4-2013.

Greve, R. (2005) Relation of measured basal temperatures and the spatial distribution of the geothermal heat flux for the Greenland ice sheet. *Annals of Glaciology*, *42*, 424–432, doi:10.3189/172756405781812510.

Gudmundsson, M.T., Sigmundsson, F., and Björnsson, H. (1997) Ice–volcano interaction of the 1996 Gjálp subglacial eruption, Vatnajökull, Iceland. *Nature*, *389*(October), 954–957, doi:10.1038/40122.

Gultepe, I. et al. (2007) Fog Research: A Review of Past Achievements and Future Perspectives. *Pure and Applied Geophysics*, *164*(6–7), 1121–1159, doi:10.1007/s00024-007-0211-x.

Hagen, J.O., Liestøl, O., Roland, E., and Jørgensen, T. (1993) Glacier atlas of Svalbard and Jan Mayen: 169 p., https://brage.bibsys.no/xmlui/handle/11250/173065.

Hannesdóttir, H., Björnsson, H., Pálsson, F., Aalgeirsdóttir, G., and Gumundsson, S. (2015a) Variations of southeast Vatnajökull ice cap (Iceland) 1650-1900 and reconstruction of the glacier surface geometry at the Little Ice Age maximum. *Geografiska Annaler, Series A: Physical Geography*, *97*(2), 237–264, doi:10.1111/geoa.12064.

Hannesdóttir, H., Björnsson, H., Pálsson, F., Adalgeirsdõttir, G., and Gudmundsson, S. (2015b) Changes in the southeast Vatnajokull ice cap, Iceland, between ~1890 and 2010c. *The Cryosphere*, *9*, 565–585, doi:10.5194/tc-9-565-2015.

Hersbach, H. et al. (2019) ERA5 monthly averaged data on pressure levels from 1979 to present. *Copernicus Climate Change Service (C3S) Climate Data Store (CDS)*, doi:10.24381/cds.6860a573.

Hidore, J.J., Oliver, J.E., Snow, M., and Snow, R. (2010) Climatology: An Atmospheric Science: Pearson Education, Inc, 385 p.

Hill, E.A., Rachel Carr, J., Stokes, C.R., and Hilmar Gudmundsson, G. (2018) Dynamic changes in outlet glaciers in northern Greenland from 1948 to 2015. *The Cryosphere*, *12*(10), 3243–3263, doi:10.5194/tc-12-3243-2018.

Hock, R. (2005) Glacier melt: a review of processes and their modelling. *Progress in Physical Geography*, *29*(3), 362–391.

Hock, R., and Holmgren, B. (2005) A distributed surface energy-balance model for complex topography and its application to Storglaciären, Sweden. *Journal of Glaciology*, *51*(172), 25–36, doi:10.3189/172756505781829566.

Hock, R., and Holmgren, B. (1996) Some Aspects of Energy Balance and Ablation of Storglaciären , Northern Sweden. *Geografiska Annaler*, *78*(2/3), 121–131.

Hoelzle, M., Haeberli, W., Dischl, M., and Peschke, W. (2003) Secular glacier mass balances derived from cumulative glacier length changes. *Global and Planetary Change*, *36*, 295–306, doi:10.1016/S0921-8181(02)00223-0.

Hooke, R.L. (2005) Principles of Glacier Mechanics: New York, USA, Cambridge University Press, 429 p., doi:10.2307/1552137.

Howat, I.M., Box, J.E., Ahn, Y., Herrington, A., and McFadden, E.M. (2010) Seasonal variability in the dynamics of marine-terminating outlet glaciers in Greenland. *Journal of Glaciology*, *56*(198), 601–613, doi:10.3189/002214310793146232.

Huintjes, E., Li, H., Sauter, T., Li, Z., and Schneider, C. (2010) Degree-day modelling of the surface mass balance of Urumqi Glacier No. 1, Tian Shan, China. *The Cryosphere Discussions*, *4*, 207–232, doi:10.5194/tcd-4-207-2010.

Hulth, J., Rolstad Denby, C., and Hock, R. (2013) Estimating glacier snow accumulation from backward calculation of melt and snowline tracking. *Annals of Glaciology*, *54*(62), 1–7, doi:10.3189/2013AoG62A083.

Hulth, J., Rolstad, C., Trondsen, K., and Rødby, R.W. (2010) Surface mass and energy balance of Sorbreen, Jan Mayen, 2008. *Annals of Glaciology*, *51*(55), 110–119, doi:doi:10.3189/172756410791392754.

Hurrell, J.W., Kushnir, Y., Ottersen, G., and Visbeck, M. (Eds.) (2003) The North Atlantic Oscillation: Climate Significance and Environmental Impact, *in* Geophysical Monograph Series, American Geophysical Union, v. 134, doi:10.1029/GM134.

International Trade Administration (2019) Iceland - Market Overview. *Export.gov*,.

IPCC (2021) Climate Change 2021: The Physical Science Basis, *in* Masson-Delmotte, V. et al. eds., Contribution of Working Group I to the Sixth Assessment Report of the Intergovernmental Panel on Climate Change, Cambridge University Press.

IPCC (2019a) Polar regions, *in* IPCC Special Report on the Ocean and Cryosphere in a Changing Climate, p. 203–320, doi:10.1016/S1366-7017(01)00066-6.

IPCC (2019b) Summary for policymakers (N. M. W. [H.-O. Pörtner, D.C. Roberts, V. Masson-Delmotte, P. Zhai, M. Tignor, E. Poloczanska, K. Mintenbeck, A. Alegría, M. Nicolai, A. Okem, J. Petzold, B. Rama, Ed.): 3–22 p., doi:10.1017/CBO9781139177245.003.

Jennings, J.N. (1948) Glacier retreat in Jan Mayen. *Journal of Glaciology*, *1*(4), 167–181, doi:10.3189/S0022143000008029.

Jensen, T.S., Box, J.E., and Hvidberg, C.S. (2016) A sensitivity study of annual area change for Greenland ice sheet marine terminating outlet glaciers: 1999-2013. *Journal of Glaciology*, *62*(231), 72–81, doi:10.1017/jog.2016.12.

Jiskoot, H. (2011) Glacier Surging, *in* Singh, V.P., Singh, P., and Haritashya, U.K. eds., Encyclopedia of Snow, Ice and Glaciers, Dordrecht, Springer Netherlands, p. 415–428, doi:10.1007/978-90-481-2642-2_559.

Jiskoot, H., Boyle, P., and Murray, T. (1998) The incidence of glacier surging in Svalbard: evidence from multivariate statistics. *Computers and Geosciences*, *24*(4), 387–399, doi:10.1016/S0098-3004(98)00033-8.

Jiskoot, H., Fox, T.A., and Nolan, M. (2016) The Effects of Fog on the Surface Energy Balance of McCall Glacier, Alaska: Combining Time-Lapse Photography with Weather Station Data. *American Geophysical Union, Fall Meeting 2016*,(abstract #C41E-0716), https://ui.adsabs.harvard.edu/abs/2016AGUFM.C41E0716J/abstract.

Jiskoot, H., Juhlin, D., St Pierre, H., and Citterio, M. (2012) Tidewater glacier fluctuations in central East Greenland coastal and fjord regions (1980s-2005). *Annals of Glaciology*, *53*(60), 35–44, doi:10.3189/2012AoG60A030.

Jóhannesson, T., Pálmason, B., Hjartarson, Á., Jarosch, A.H., Magnússon, E., Belart, J.M.C., and Gudmundsson, M.T. (2020) Non-surface mass balance of glaciers in Iceland. *Journal of Glaciology*, *65*(258), 685–697, doi:10.1017/jog.2020.37.

Johannesson, T., Raymond, C., and Waddington, E. (1989) Time-scale for adjustment of glaciers to changes in mass balance. *Journal of Glaciology*, *35*(121), 355–369, doi:10.1017/S002214300000928X.

Joughin, I., Alley, R.B., and Holland, D.M. (2012) Ice-Sheet Response to Oceanic Forcing. *Science*, *338*, 1172–6, doi:10.1126/science.1226481.

Joughin, I., Shean, D., Smith, B., and Floricioiu, D. (2020) A Decade of Variability on Jakobshavn Isbrae: Ocean Temperatures Pace Speed Through Influence on Mélange Rigidity. *The Cryosphere*, *14*, 211–227, doi:10.5194/tc-2019-197.

Khromova, T., Nosenko, G., Kutuzov, S., Muraviev, A., and Chernova, L. (2014) Glacier area changes in Northern Eurasia. *IOP Science: Enviromental Research Letters*, *9*(1).

Kiernan, K., and McConnell, A. (2002) Glacier retreat and melt-lake expansion at Stephenson Glacier, Heard Island World Heritage Area. *Polar Record*, *38*(207), 297–308, doi:10.1017/S0032247400017988.

Kinsman, D.J.J., and Sheard, J.W. (1963) The glaciers of Jan Mayen. *Journal of Glaciology*, *4*(34), 439–448, doi:10.1017/S0022143000027854.

Kirkbride, M.P. (2002) Icelandic climate and glacier fluctuations through the termination of the "Little Ice Age." *Polar Geography*, *26*(2), 116–133, doi:10.1080/789610134.

Kirkbride, M.P., and Dugmore, A.J. (2003) Glaciological response to distal tephra fallout from the 1947 eruption of Hekla, south Iceland. *Journal of Glaciology*, *49*(166), 420–428, doi:10.3189/172756503781830575.

Klok, E.J., and Oerlemans, J. (2004) Climate reconstructions derived from global glacier length records. *Arctic, Antarctic, and Alpine Research*, *36*(4), 575–583, doi:10.1657/1523-0430(2004)036[0575:CRDFGG]2.0.CO;2.

Kneib-Walter, A., Lüthi, M.P., Moreau, L., and Vieli, A. (2021) Drivers of Recurring Seasonal Cycle of Glacier Calving Styles and Patterns. *Frontiers in Earth Science*, *9*(667717), doi:10.3389/feart.2021.667717.

Kochtitzky, W. et al. Constraining frontal ablation, the significant unquantified mass loss mechanism for Northern Hemisphere marine-terminating glaciers, 2000-2020 (in prep). *Nature Geoscience*,.

Kochtitzky, W., Winski, D., McConnell, E., Kreutz, K., Campbell, S., Enderlin, E.M., Copland, L., Williamson, S., Main, B., and Jiskoot, H. (2020) Climate and surging of Donjek Glacier, Yukon, Canada. *Arctic, Antarctic, and Alpine Research*, *52*(1), 264–280, doi:10.1080/15230430.2020.1744397.

Kodaira, S., Mjelde, R., Gunnarsson, K., Shiobara, H., and Shimamura, H. (2000) Structure of the Jan Mayen microcontinent and implications for its evolution. *Geophysics Journal International*, *132*(2), 383–400, doi:10.1046/j.1365-246X.1998.00444.x.

Koenig, S.J., DeConto, R.M., and Pollard, D. (2014) Impact of reduced Arctic sea ice on Greenland ice sheet variability in a warmer than present climate. *Geophysical Research Letters*, *41*(11), 3933–3942.

Kopec, B.G., Feng, X., Michel, F.A., Posmentier, E.S., and Farquhar, G.D. (2016) Influence of sea ice on Arctic precipitation. *113*(1), 46–51, doi:10.1073/pnas.1504633113.

Lamb, H.H., Probert-Jones, J.R., and Sheard, J.W. (1962) A new advance of the Jan Mayen glaciers and a remarkable increase of precipitation. *Journal of Glaciology*, *4*(33), 355–365, doi:10.1017/S0022143000027684.

Leclercq, P.W. (2012) Glacier fluctuations, global temperature and sea-level change: Universiteit Utrecht, https://dspace.library.uu.nl/bitstream/handle/1874/221008/leclercq.pdf.

Leclercq, P.W., Oerlemans, J., Basagic, H.J., Bushueva, I., Cook, A.J., and Le Bris, R. (2014) A data set of worldwide glacier length fluctuations. *The Cryosphere*, *8*, 659–672, doi:10.5194/tc-8-659-2014.

Lefauconnier, B., and Hagen, J.O. (1991) Surging and calving glaciers in eastern Svalbard. *Meddelelser - Norsk Polarinstitutt*, *116*.

Leigh, J., Stokes, C.R., Carr, J.R., Evans, I., Andreassen, L.M., and Evans, D. (2019) Identifying and mapping very small (<0.5 km^2) mountain glaciers on coarse to high-resolution imagery. *Journal of Glaciology*, *65*(254).

Litt, M., Shea, J., Wagnon, P., Steiner, J., Koch, I., Stigter, E., and Immerzeel, W. (2019) Glacier ablation and temperature indexed melt models in the Nepalese Himalaya. *Scientific Reports*, *9*(5264), doi:10.1038/s41598-019-41657-5.

Liu, Y., and Key, J.R. (2016) Assessment of Arctic Cloud Cover Anomalies in Atmospheric Reanalysis Products Using Satellite Data. *Journal of Climate*, *29*(17), 6065–6083, doi:10.1175/JCLI-D-15-0861.1.

Lloyd, J., Moros, M., Perner, K., Telford, R.J., Kuijpers, A., Jansen, E., and McCarthy, D. (2011) A 100 yr record of ocean temperature control on the stability of Jakobshavn Isbrae, West Greenland. *Geology*, *39*(9), 867–870, doi:10.1130/G32076.1.

Locarnini, R.A., Mishonov, A. V., Antonov, J.I., Boyer, T.P., and Garcia, H.E. (2006) World Ocean Atlas 2005, Volume 1: Temperature (S. Levitus, Ed.): Washington D.C., U.S. Government Printing Office, 182 p.

Lucazeau, F. (2019) Analysis and Mapping of an Updated Terrestrial Heat Flow Data Set. *Geochemistry, Geophysics, Geosystems*, *20*(8), 4001–4024, doi:10.1029/2019GC008389.

Luckman, A., Benn, D.I., Cottier, F., Bevan, S., Nilsen, F., and Inall, M. (2015) Calving rates at tidewater glaciers vary strongly with ocean temperature. *Nature Communications*, *6*, 1–7, doi:10.1038/ncomms9566.

Lysså, A., Larsen, E.A., Anjar, J., Akçar, N., Ganerød, M., Hiksdal, A., Van Der Lelij, R., and Vockenhuber, C. (2021) The last glaciation of the Arctic volcanic island Jan Mayen. *Boreas*, *50*, 6–28, doi:10.1111/bor.12482.

Ma, Y., and Bassis, J.N. (2019) The Effect of Submarine Melting on Calving From Marine Terminating Glaciers. *Journal of Geophysical Research: Earth Surface*,(2014), 334–346, doi:10.1029/2018JF004820.

Magnússon, E., Björnsson, H., Dall, J., and Pálsson, F. (2005) Volume changes of Vatnajökull ice cap, Iceland, due to surface mass balance, ice flow, and subglacial melting at geothermal areas. *Geophysical Research Letters*, *32*(5), doi:10.1029/2004GL021615.

Marcovecchio, A., Behrangi, A., Dong, X., Xi, B., and Huang, Y. (2021) Precipitation influence on and response to early and late Arctic sea ice melt onset during melt season. *International Journal of Climatology*, doi:10.1002/JOC.7233.

McNabb, R.W., and Hock, R. (2014) Alaska tidewater glacier terminus positions , 1948 – 2012. *Journal of Geophysical Research : Earth Surface*, *119*, 153–167, doi:10.1002/2013JF002915.Tidewater.

Mernild, S.H., and Liston, G.E. (2010) The Influence of air temperature inversions on snowmelt and glacier mass balance simulations, Ammassalik Island, Southeast Greenland. *Journal of Applied Meteorology and Climatology*, *49*(1), 47–67, doi:10.1175/2009JAMC2065.1.

Mohn, H., and Wille, C. (1882) Den Norske Nordhavs-expedition 1876-1888. , 36.

Möller, R., Möller, M., Kukla, P.A., and Schneider, C. (2016) Impact of supraglacial deposits of tephra from Grímsvötn volcano, Iceland, on glacier ablation. *Journal of Glaciology*, *62*(235), 933–943, doi:10.1017/jog.2016.82.

Moon, T., and Joughin, I. (2008) Changes in ice front position on Greenland's outlet glaciers from 1992 to 2007. *Journal of Geophysical Research: Earth Surface*, *113*(2), 1–10, doi:10.1029/2007JF000927.

Mortimer, C.A., and Sharp, M. (2017) Characterization of Canadian High Arctic glacier surface albedo from MODIS C6 data, 2001-2016. *The Cryosphere Discussions*, *2003*, 1–34, doi:10.5194/tc-2017-160.

Murray, T. et al. (2010) Ocean regulation hypothesis for glacier dynamics in southeast Greenland and implications for ice sheet mass changes. *Journal of Geophysical Research: Earth Surface*, *115*(F03026), doi:10.1029/2009JF001522.

Nesje, A., Bakke, J., Dahl, S.O., Lie, Ø., and Matthews, J.A. (2008) Norwegian mountain glaciers in the past, present and future. *Global and Planetary Change*, *60*, 10–27, doi:10.1016/j.gloplacha.2006.08.004.

Nield, J.M., Chiverrell, R.C., Darby, S.E., Leyland, J., Vircavs, L.H., and Jacobs, B. (2013) Complex spatial feedbacks of tephra redistribution, ice melt and surface roughness modulate ablation on tephra covered glaciers. *Earth Surface Processes and Landforms*, *38*, 95–102, doi:10.1002/esp.3352.

NOAA (2021) Bathymetric Data Viewer. *National Oceanic and Atmospheric Administration*, https://maps.ngdc.noaa.gov/viewers/bathymetry/.

NOAA (2020) North Atlantic Oscillation. *National Oceanic and Atmospheric Administration*, https://www.ncdc.noaa.gov/teleconnections/nao/.

Norwegian Polar Institute (2014) Kartdata Jan Mayen 1:100 000 (J100 Kardata)., doi:10.21334/npolar.2014.f16ab884.

NSIDC (2020a) Facts About Glaciers. *National Snow and Ice Data Center*, https://nsidc.org/cryosphere/glaciers/quickfacts.html.

NSIDC (2020b) National Snow and Ice Data Center: "All About Arctic Climatology and Meteorology.", https://nsidc.org/cryosphere/arctic-meteorology/arctic.html (accessed August 2021).

Nuth, C., Kohler, J., König, M., Von Deschwanden, A., Hagen, J.O., Kääb, A., Moholdt, G., and Pettersson, R. (2013) Decadal changes from a multi-temporal glacier inventory of Svalbard. *The Cryosphere*, *7*, 1603–1621, doi:10.5194/tc-7-1603-2013.

O'Neel, S., Larsen, C.F., Rupert, N., and Hansen, R. (2010) Iceberg calving as a primary source of regional-scale glacier-generated seismicity in the St. Elias Mountains, Alaska. *Journal of Geophysical Research: Earth Surface*, *115*(4), 1–12, doi:10.1029/2009JF001598.

O'Neel, S., Marshall, H.P., McNamara, D.E., and Pfeffer, W.T. (2007) Seismic detection and analysis of icequakes at Columbia Glacier, Alaska. *Journal of Geophysical Research: Earth Surface*, *112*(3), 1–14, doi:10.1029/2006JF000595.

Ødegård, R.S., Hamran, S.-E., Bø, P.H., Etzelmuller, B., Vatne, G., and Sollid, J.L. (1992) Thermal regime of a valley glacier, Erikbreen, northern Spitsbergen. *Polar Research*, *11*(2), 69–79, doi:10.1111/j.1751-8369.1992.tb00413.x.

Oerlemans, J. (2001) Glaciers and Climate Change: Rotterdam, A. A. Balkema Publishers, xii + 148 p.

Oerlemans, J. (1994) Quantifying Global Warming from the Retreat of Glaciers. *Science*, *264*(5156), 243–245.

Oerlemans, J. (2010) The microclimate of valley glaciers. *Journal of Glaciology*, *57*(206), 173–1174, doi:10.3189/002214311798843313.

Oerlemans, J., and Klok, E.J. (2002) Energy Balance of a Glacier Surface: Analysis of Automatic Weather Station Data from the Morteratschgletscher, Switzerland. *Arctic, Antarctic, and Alpine Research*, *34*(4), 477–485, doi:10.2307/1552206.

Ohmura, A. (2001) Physical basis for the temperature-based melt-index method. *Journal of Applied Meteorology*, *40*(4), 753–761, doi:10.1175/1520-0450(2001)040<0753:PBFTTB>2.0.CO;2.

Oke, T.R. (1987) Boundary Layer Climates: London, Methuen & Co. Ltd.

Olesen, O. et al. (2010) New aeromagnetic and gravity compilations from Norway and adjacent areas : Methods and applications Petroleum Geology Conference series New aeromagnetic and gravity compilations from Norway and adjacent areas : *Petroleum Geology Conference series*, *7*, 559–586, doi:10.1144/0070559.

Orheim, O. (1976) Bremålinger på Jan Mayen. *Norsk Polarinstitutt Årbok*,, 249–252.

Orheim, O. (1993) Glaciers of Jan Mayen, Norway, *in* Williams, R.S.J. and Ferrigno, J. eds., Satellite Image Atlas of Glaciers of the World: USGS Professional Paper 1386-E, Denver, CO, USA, US Geological Survey, p. E153–E164.

Østerhus, S., and Gammelsrød, T. (1999) The abyss of the nordic seas is warming. *Journal of Climate*, *12*(11), 3297–3304, doi:10.1175/1520-0442(1999)012<3297:TAOTNS>2.0.CO;2.

Park, H., Walsh, J.E., Kim, Y., Nakai, T., and Ohata, T. (2013) The role of declining Arctic sea ice in recent decreasing terrestrial Arctic snow depths. *Polar Science*, *7*(2), 174–187, doi:10.1016/J.POLAR.2012.10.002.

Paul, F. et al. (2013) On the accuracy of glacier outlines derived from remote-sensing data. *Annals of Glaciology*, *54*(63), 171–182, doi:10.3189/2013AoG63A296.

Paul, F., Kääb, A., Maisch, M., Kellenberger, T., and Haeberli, W. (2004) Rapid disintegration of Alpine glaciers observed with satellite data. *Geophysical Research Letters*, *31*(L21402), doi:10.1029/2004GL020816.

Pellicciotti, F., Brock, B., Strasser, U., Burlando, P., Funk, M., and Corripio, J. (2005) An enhanced temperature-index glacier melt model including the shortwave radiation balance: Development and testing for Haut Glacier d'Arolla, Switzerland. *Journal of Glaciology*, *51*(175), 573–587, doi:10.3189/172756505781829124.

Pfeffer, W.T. et al. (2014) The Randolph Glacier inventory: A globally complete inventory of glaciers. *Journal of Glaciology*, *60*(221), 537–552, doi:10.3189/2014JoG13J176.

Pfirman, S.L., and Solheim, A. (1989) Subglacial meltwater discharge in the open-marine tidewater glacier environment: Observations from Nordaustlandet, Svalbard Archipelago. *Marine Geology*, *86*, 265–281, doi:10.1016/0025-3227(89)90089-3.

Podolskiy, E.A., and Walter, F. (2016) Cryoseismology. *Reviews of Geophysics*, *54*(4), 708–758, doi:10.1002/2016RG000526.

Pollack, H.N., Hurter, S.J., and Johnson, R. (1993) Heat flow from the earth′s interior: analysis of the global data set. *Reviews of Geophysics*, *31*(3), 267–280, doi:10.1029/93RG01249.

Pritchard, H.D., and Vaughan, D.G. (2007) Widespread acceleration of tidewater glaciers on the Antarctic Peninsula. *Journal of Geophysical Research*, *112*(F03S29), doi:10.1029/2006JF000597.

Qamar, A. (1988) Calving icebergs: a source of low-frequency seismic signals from Columbia Glacier, Alaska. *Journal of Geophysical Research: Solid Earth*, *93*(B6), 6615–6623.

Raper, V., Bamber, J.L., and Krabill, W. (2005) Interpretation of the anomalous growth of Austfonna, Svalbard, a large Arctic ice cap. *Annals of Glaciology*, *42*, 373–379, doi:10.3189/172756405781812790.

Rastner, P., Bolch, T., Mölg, N., Machguth, H., Bris, R. Le, and Paul, F. (2012) The first complete inventory of the local glaciers and ice caps on Greenland. *The Cryosphere*, *6*, 1483–1495, doi:10.5194/tc-6-1483-2012.

Reeh, N., Thomsen, H.H., Higgins, A.K., and Weidick, A. (2001) Sea ice and the stability of north and northeast Greenland floating glaciers. *Annals of Glaciology*, *33*, 474–480, doi:10.3189/172756401781818554.

Reinthaler, J., Paul, F., Granados, H.D., Rivera, A., and Huggel, C. (2019) Area changes of glaciers on active volcanoes in Latin America between 1986 and 2015 observed from multi-temporal satellite imagery. *Journal of Glaciology*, *65*(252), 542–556, doi:10.1017/jog.2019.30.

RGI Consortium (2017) Randolph Glacier Inventory - a Datset of Global Glacier Outlines: Vesion 6.0. *GLIMS Technical Report*,.

Rivera, A., and Bown, F. (2013) Recent glacier variations on active ice capped volcanoes in the Southern Volcanic Zone (37°-46°s), Chilean Andes. *Journal of South American Earth Sciences*, *45*, 345–356, doi:10.1016/j.jsames.2013.02.004.

Rivera, A., Bown, F., Carrión, D., and Zenteno, P. (2012) Glacier responses to recent volcanic activity in Southern Chile. *Environmental Research Letters*, *7*, doi:10.1088/1748-9326/7/1/014036.

Robel, A.A. (2017) Thinning sea ice weakens buttressing force of iceberg mélange and promotes calving. *Nature Communications*, *8*, 14596, doi:10.1038/ncomms14596.

Robel, A.A., Roe, G.H., and Haseloff, M. (2018) Response of marine-terminating glaciers to forcing: time scales, sensitivities, instabilities, and stochastic dynamics. *Journal of Geophysical Research: Earth Surface*, *123*(9), 2205–2227.

Robinson, P., and Dowdeswell, J.A. (2011) Submarine landforms and the behavior of a surging ice cap since the last glacial maximum: The open-marine setting of eastern Austfonna, Svalbard. *Marine Geology*, *286*(1–4), 82–94, doi:10.1016/j.margeo.2011.06.004.

Rolstad Denby, C., and Hulth, J. (2011) Assessment of differentiated surface elevation data from 1949, 1975 and 2008 for estimates of ice-volume changes at Jan Mayen. *Journal of Glaciology*, *57*(205), 976–980, doi:10.3189/002214311798043663.

Rosqvist, N. (2019) Southern peak of Kebnekaise, lowest height ever measured. *Stockholm University: Deparmtent of Physical Geography*, https://www.natgeo.su.se/english/research/resarch-news/southern-peak-of-kebnekaise-lowest-height-ever-measured-1.452263.

Ruddell, A., and Allison, I. (1998) The sensitivity of glaciers at Heard Island to climate change, and their recent response, *in* Selkirk, P. ed., Heard Island Wilderness Reserve: Reports on Natural Science and Cultural Heritage Research, Kingston, Tasmania, Australian Antarctic Division, p. 32.

Rye, C.J., Arnold, N.S., Willis, I.C., and Kohler, J. (2010) Modeling the surface mass balance of a high Arctic glacier using the ERA - 40 reanalysis. *Journal of Geophysical Research*, *115*(F02014), doi:10.1029/2009JF001364.

Rysgaard, S., Bendtsen, J., Mortensen, J., and Sejr, M.K. (2018) High geothermal heat flux in close proximity to the Northeast Greenland Ice Stream. *Scientific Reports*, *8*(1), 1344, doi:10.1038/s41598-018-19244-x.

Savage, S.B., Crocker, G.B., Sayed, M., and Carrieres, T. (2001) Bergy bit and growler melt deterioration. *Journal of Geophysical Research: Oceans*, *106*(C6), 11493–11504, doi:10.1029/2000jc000270.

Sevestre, H., Benn, D.I., Hulton, N.R.J., and Bælum, K. (2015) Thermal structure of Svalbard glaciers and implications for thermal switch models of glacier surging. *Journal of Geophysical Research F: Earth Surface*, *120*(10), 2220–2236, doi:10.1002/2015JF003517.

Shahgedanova, M., Nosenko, G., Bushueva, I., and Ivanov, M. (2017) Changes in area and geodetic mass balance of small glaciers, Polar Urals, Russia, 1950-2008. *Journal of Glaciology*, *58*(211), 953–964, doi:10.3189/2012JoG11J233.

Sigurđsson, O., Jónsson, T., and Jóhannesson, T. (2007) Relation between glacier-termini variations and summer temperature in Iceland since 1930. *Annals of Glaciology*, *46*, 170–176, doi:10.3189/172756407782871611.

Singh, V.P., Singh, P., and Haritashya, U.K. (Eds.) (2011) Encyclopedia of snow, ice, and glaciers: Springer, 1254 p., doi:10.1007/978-90-481-2642-2.

Skreslet, S. et al. (2004) Proceedings of the NATO Advanced Research Workshop on Jan Mayen Island in Scientific Focus, *in* Skreslet, S. ed., NATO Science Series IV: Earth and Environmental Sciences, Oslo, Norway, Kluwer Academic Publishers, v. 45, p. 363, doi:10.1007/978-1-4020-2957-8.

Smellie, J.L., and Edwards, B.R. (2016) Glaciovolcanism on Earth and Mars: Products, Processes, and Palaeoenvironmental Significance: Cambridge University Press, 484 p.

Smith, B. et al. (2020) Pervasive ice sheet mass loss reflects competing ocean and atmosphere processes. *Science*, *368*(6496), 1239–1242, doi:10.1126/science.aaz5845.

Sobota, I., Weckwerth, P., and Grajewski, T. (2020) Rain-On-Snow (ROS) events and their relations to snowpack and ice layer changes on small glaciers in Svalbard, the high Arctic. *Journal of Hydrology*, *590*(125279), doi:10.1016/J.JHYDROL.2020.125279.

Squire, V.A. (2020) Ocean Wave Interactions with Sea Ice: A Reappraisal. *Annual Review of Fluid Mechanics*, *52:37-60*, doi:10.1146/annurev-fluid-010719-060301.

Statistics Iceland (2020) Population. *Hagstofa Íslands*, https://statice.is/.

Statistics Norway (2020) Population. *Statistisk sentralbyrå*, https://www.ssb.no/en (accessed May 2021).

Statistics Sweden (2020) Population. *SCB*, https://www.scb.se/en.

Stearns, L.A. (2011) Dynamics and mass balance of four large East Antarctic outlet glaciers. *Annals of Glaciology*, *52*(59), 116–126, doi:10.3189/172756411799096187.

Steffenson, E. (1982) The climate at Norwegian arctic stations. *Klima*, *5*, 3–44.

Steiner, J.F., Litt, M., Stigter, E.E., Shea, J., Bierkens, M.F.P., and Immerzeel, W.W. (2018) The Importance of Turbulent Fluxes in the Surface Energy Balance of a Debris-Covered Glacier in the Himalayas. *Frontiers in Earth Science*, *6*(144), doi:10.3389/feart.2018.00144.

Stocker, T.F., Qin, D., Plattner, G.-K., Tignor, M., Allen, S.K., Boschung, J., Nauels, A., Xia, Y., Bex, V., and Midgley, P.M. (2015) Summary for Policymakers. In: Climate Change 2013: The Physical Science Basis. Contribution of Working Group I to the Fifth Assessment Report of the Intergovernmental Panel on Climate Change. *CEUR Workshop Proceedings*, *1542*, 33–36, doi:10.1017/CBO9781107415324.004.

Straneo, F., Hamilton, G.S., Sutherland, D.A., Stearns, L.A., Davidson, F., Hammill, M.O., Stenson, G.B., and Rosing-Asvid, A. (2010) Rapid circulation of warm subtropical waters in a major glacial fjord in east Greenland. *Nature Geoscience*, *3*, 182–186.

Thost, D.E., and Truffer, M. (2008) Glacier recession on Heard Island, southern Indian Ocean. *Arctic, Antarctic, and Alpine Research*, *40*(1), 199–214, doi:10.1657/1523-0430(06-084)[THOST]2.0.CO;2.

Trondsen, K. (2008) Estimating the mass balance of Sørbreen glacier from 1973–2008 using degree-day models: Norwegian University of Life Sciences.

Tsai, V.C., Rice, J.R., and Fahnestock, M.A. (2008) Possible mechanisms for glacial earthquakes. *Journal of Geophysical Research: Earth Surface*, *113*(3), 1–17, doi:10.1029/2007JF000944.

USGS (2017) What are the band designations for the Landsat satellites? *United States Geological Survey: Mapping, Remote Sensing, and Geospatial Data*, https://www.usgs.gov/faqs/what-are-band-designations-landsat-satellites?qt-news_science_products=0#qt-news_science_products.

Vallot, D., Åström, J., Zwinger, T., Pettersson, R., Everett, A., Benn, D.I., Luckman, A., van Pelt, W.J.J., Nick, F., and Kohler, J. (2018) Effects of undercutting and sliding on calving: A global approach applied to Kronebreen, Svalbard. *Cryosphere*, *12*(2), 609–625, doi:10.5194/tc-12-609-2018.

van der Veen, C.J., Leftwich, T., von Frese, R., Csatho, B.M., and Li, J. (2007) Subglacial topography and geothermal heat flux: Potential interactions with drainage of the Greenland ice sheet. *Geophysical Research Letters*, *34*(L12501), 1–5, doi:10.1029/2007GL030046.

Van Tricht, K., Lhermitte, S., Lenaerts, J.T.M., Gorodetskaya, I. V., L'Ecuyer, T.S., Noël, B., van den Broeke, M.R., Turner, D.D., and van Lipzig, N.P.M. (2016) Clouds enhance Greenland ice sheet meltwater runoff. *Nature Communications*, *7*(10266), doi:10.1038/ncomms10266.

Van Wychen, W., Burgess, D.O., Gray, L., Copland, L., Sharp, M., Dowdeswell, J.A., and Benham, T.J. (2014) Glacier velocities and dynamic ice discharge from the Queen Elizabeth Islands, Nunavut, Canada. *Geophysical Research Letters*, *41*(2), 484–490, doi:10.1002/2013GL058558.

Van Wychen, W., Davis, J., Burgess, D.O., Copland, L., Gray, L., Sharp, M., and Mortimer, C. (2016) Characterizing interannual variability of glacier dynamics and dynamic discharge (1999–2015) for the ice masses of Ellesmere and Axel Heiberg Islands, Nunavut, Canada. *Journal of Geophysical Research: Earth Surface*, *121*(1), 39–63, doi:10.1002/2015JF003708.

Vaughan, D.G. et al. (2013) Observations: Cryosphere, *in* Climate Change 2013 the Physical Science Basis: Working Group I Contribution to the Fifth Assessment Report of the Intergovernmental Panel on Climate Change, p. 317–382, doi:10.1017/CBO9781107415324.012.

Vavrus, S., Holland, M.M., and Bailey, D.A. (2011) Changes in Arctic clouds during intervals of rapid sea ice loss. *Climate Dynamics*, *36*(7), 1475–1489, doi:10.1007/s00382-010-0816-0.

Vieli, A., and Nick, F.M. (2011) Understanding and Modelling Rapid Dynamic Changes of Tidewater Outlet Glaciers: Issues and Implications. *Surveys in Geophysics*, *32*(4–5), 437–458, doi:10.1007/s10712-011-9132-4.

Vogt, K.C. (1863) Zweites Buch - Jan Mayen, *in* Nord-fahrt, entlang der Norwegischen küste, nach dem Nordkap, den Inseln Jan Mayen und Island, auf dem Schooner Joachim Hinrich, Frankfurt am Main, p. 429.

Wake, L.M., and Marshall, S.J. (2015) Assessment of current methods of positive degree-day calculation using in situ observations from glaciated regions. *Journal of Glaciology*, *61*(226), 329–344, doi:10.3189/2015JoG14J116.

Walsh, J.E. (2008) Climate of the Arctic Marine Environment. *Ecological Applications*, *18*(2), S3–S22, https://www.jstor.org/stable/40062154 (accessed October 2021).

Walter, F., Amundson, J.M., O'Neel, S., Truffer, M., Fahnestock, M.A., and Fricker, H.A. (2012) Analysis of low-frequency seismic signals generated during a multiple-iceberg calving event at Jakobshavn Isbr, Greenland. *Journal of Geophysical Research: Earth Surface*, *117*(1), 1–11, doi:10.1029/2011JF002132.

Warren, C.R., and Glasser, N.F. (1992) Contrasting response of south Greenland glaciers to recent climatic change. *Arctic & Alpine Research*, *24*(2), 124–132, doi:10.2307/1551532.

Wasserstein, R.L., and Lazar, N.A. (2016) The ASA Statement on p-Values: Context, Process, and Purpose. *The American Statistician*, *70*(2), 129–133, doi:10.1080/00031305.2016.1154108.

Wessel, P., and Smith, W.H.F. (1996) A global, self-consistent, hierarchical, high-resolution shoreline database. *Journal of Geophysical Research*, *101*(B4), 8741–8743, doi:10.1029/96JB00104.

WGMS (2021) Fluctuations of Glaciers (FoG) Database: Zurich, Switzerland, World Glacier Monitoring Service, doi:10.5904/wgms-fog-2021-05.

WGMS (2020) Global Glacier Change Bulletin No. 3 (M. Zemp, I. Gärtner-Roer, S. U. Nussbaumer, J. Bannwart, P. Rastner, F. Paul, & M. Hoelzle, Eds.): Zurich, Switzerland, ISC(WDS)/IUGG(IACS)/UNEP/UNESCO/WMO, doi:10.5904/wgms-fog-2019-12.

White, A., and Copland, L. (2019) Loss of floating glacier tongues from the Yelverton Bay region, Ellesmere Island, Canada. *Journal of Glaciology*, *65*(251), 376–394, doi:10.1017/jog.2019.15.

Winsvold, S.H., Andreassen, L.M., and Kienholz, C. (2014) Glacier area and length changes in Norway from repeat inventories. *The Cryosphere*, *8*, 1885–1903, doi:10.5194/tc-8-1885-2014.

WMO (2006) Guide to Meteorological Instruments and Methods of Observation (R. Artz et al., Eds.): Geneva, Switzerland, The World Meteorological Organization.

WMO (1995) Volum I.1: part AA - Alphanumeric Codes, *in* World Meteorological Organization: Manual on Codes, Geneva, p. 503.

Wood, M. et al. (2021) Ocean forcing drives glacier retreat in Greenland. *Science Advances*, *7*(1), doi:10.1126/sciadv.aba7282.

Yde, J.C., and Paasche, Ø. (2010) Reconstructing Climate Change: Not All Glaciers Suitable. *EOS, Transactions, American Geophysical Union*, *91*(21), doi:10.1029/2010EO210001.

Zemp, M. et al. (2015) Historically unprecedented global glacier decline in the early 21st century. *Journal of Glaciology*, *61*(228), 745–762, doi:10.3189/2015jog15j017.

Appendix A: Creating Consistent Glacier Outlines

For consistency, each glacier had specific features deemed "glacial" or "nonglacial" after preliminary examination of every best satellite image for the glacier. This was intended to remove from consideration snow patches, shading, or other features that might change between years, obfuscating ice area changes. Glacial features were then included in every outline, and nonglacial features were not included. Restarting glacier outlines with 2018-2020 Landsat images after completing the 2000-2016 period in the year prior did reveal some corrections that had to be made to outlines previously drawn: this included Willebreen no longer being considered as "calving" for the entire period 2000-2020.

In general, a conservative approach was used in outlining glacier margins (Fig 7.1), and only what is highly likely glacier ice is outlined, with any questionable landmarks not included. Land-terminating glaciers are also generally debris covered on Jan Mayen, in which case it becomes difficult to determine exact glacier fronts, and outlining only the clean ice, which will change differently from the actual glacier and thus obfuscate glacier retreat and advance trends, was avoided. For these, either high resolution satellite scenes browsed through the Google Earth timeline, Sentinel scenes (https://www.sentinel-hub.com/explore/) or infrared bands of the Landsat images were used. Satellite scenes from Google Earth and Sentinel are much higher resolution and vertical differences can more easily be noted – the glacier front is likely a rather sudden increase in elevation of the topography. Infrared images help decipher which areas are colder and thus more likely part of the glacier.

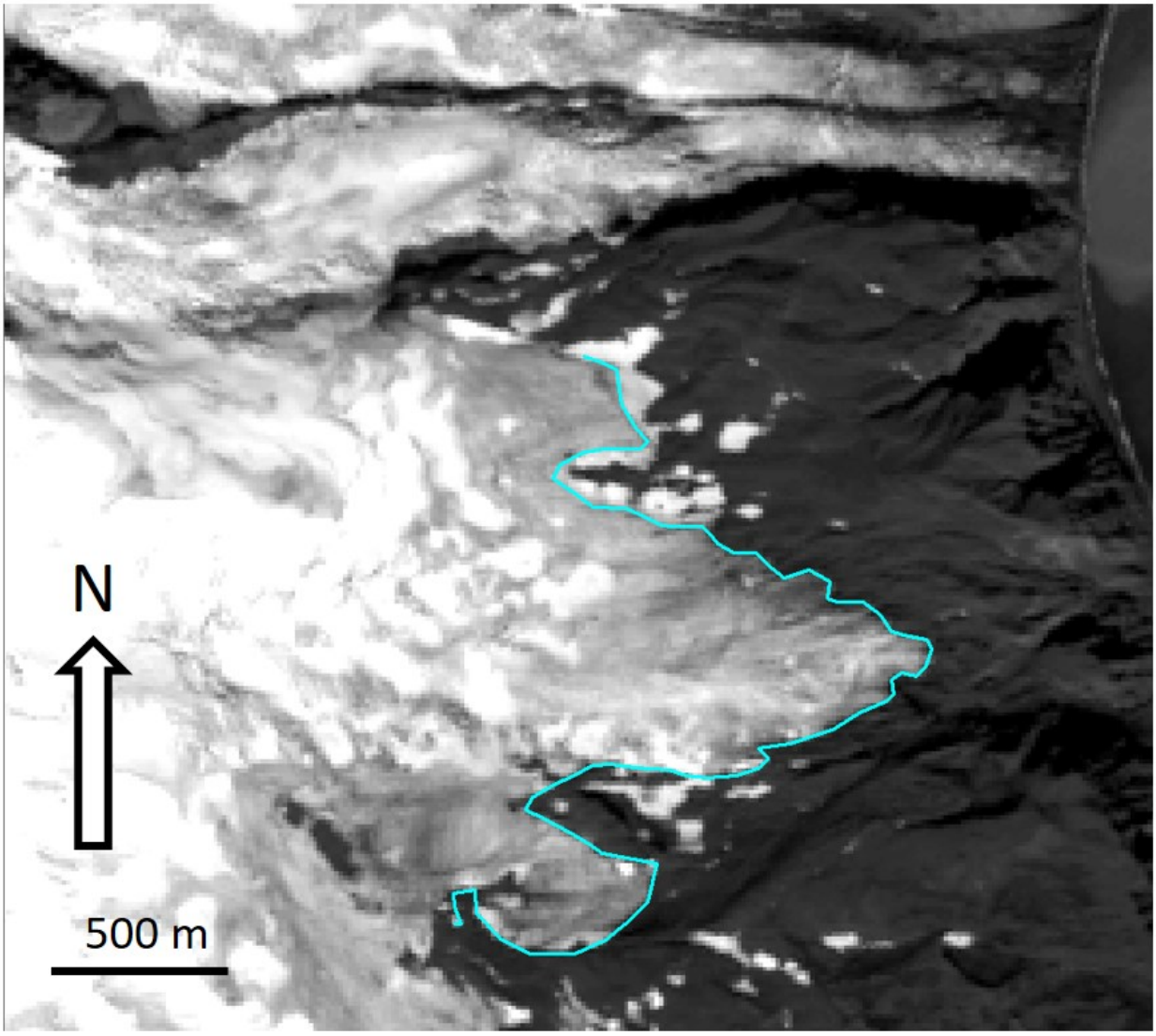

Figure 7.1: Petersenbreen, on the East side of the island. The rippling pattern downstream of the glacier could be debris on top of glacier ice, or an area of glacial runoff, therefore it is not included in the glacier outline. Medium grey cells are assumed glacier ice, white is assumed snow. Background is Landsat 8 image Band 8 from 19 Aug 2016.

Appendix B: Full Glacier Fluctuations as Will Appear in WGMS FoG Database

Glacier length changes are presented here in a format similar to the WGMS Fluctuations of Glaciers (FoG) database (https://wgms.ch/data_databaseversions/), which stores the year of the measurement and the change in length or area since the previous measurement. Headers are as defined by the WGMS FoG terms (WGMS, 2021).

POLITICAL_UNIT	NAME	WGMS_ID	Year	FRONT_VARIATION	FRONT_VAR_UNC	QUALITATIVE_VARIATION	SURVEY_DATE	SURVEY_PLATFORM_METHOD	REFERENCE_DATE	PUB_IN_FOG	INVESTIGATOR	SPONS_AGENCY	REFERENCE	REMARKS
SJ	Charcotbreen		2003	1	23		20030628	sP	20020904		Jade Cooley	Uleth: University of Lethbridge, 4401 University Dr W, Lethbridge, AB T1K 3M4, Canada. NSERC to Hester Jiskoot	Cooley, J. (2021)	ASTER
SJ	Charcotbreen		2016	-203	23		20160819	sP	20030628		Jade Cooley	Uleth: University of Lethbridge, 4401 University Dr W, Lethbridge, AB T1K 3M4, Canada. NSERC to Hester Jiskoot	Cooley, J. (2021)	Landsat 8 panchromatic
SJ	Charcotbreen		2020	-86	23		20200828	sP	20160819		Jade Cooley	Uleth: University of Lethbridge, 4401 University Dr W, Lethbridge, AB T1K 3M4, Canada. NSERC to Hester Jiskoot	Cooley, J. (2021)	Landsat 8 panchromatic
SJ	Dufferinbreen		2004	-98	23		20040810	sP	20000930		Jade Cooley	Uleth: University of Lethbridge, 4401 University Dr W, Lethbridge, AB T1K 3M4, Canada. NSERC to Hester Jiskoot	Cooley, J. (2021)	Landsat 7 panchromatic
SJ	Dufferinbreen		2016	19	23		20160819	sP	20040810		Jade Cooley	Uleth: University of Lethbridge, 4401 University Dr W, Lethbridge, AB T1K 3M4, Canada. NSERC to Hester Jiskoot	Cooley, J. (2021)	Landsat 8 panchromatic
SJ	Dufferinbreen		2020	-13	23		20200828	sP	20160819		Jade Cooley	Uleth: University of Lethbridge, 4401 University Dr W, Lethbridge, AB T1K 3M4, Canada. NSERC to Hester Jiskoot	Cooley, J. (2021)	Landsat 8 panchromatic
SJ	Fotherbybreen		2016	-36	23		20160819	sP	20020906		Jade Cooley	Uleth: University of Lethbridge, 4401 University Dr W, Lethbridge, AB T1K 3M4, Canada. NSERC to Hester Jiskoot	Cooley, J. (2021)	Landsat 8 panchromatic
SJ	Fotherbybreen		2018	-34	23		20180910	sP	20160819		Jade Cooley	Uleth: University of Lethbridge, 4401 University Dr W, Lethbridge, AB T1K 3M4, Canada. NSERC to Hester Jiskoot	Cooley, J. (2021)	Landsat 8 panchromatic
SJ	Frielebreen		2001	16	23		20010717	sP	20000721		Jade Cooley	Uleth: University of Lethbridge, 4401 University Dr W, Lethbridge, AB T1K 3M4, Canada. NSERC to Hester Jiskoot	Cooley, J. (2021)	Landsat 7 panchromatic
SJ	Frielebreen		2002	-9	23		20020913	sP	20010717		Jade Cooley	Uleth: University of Lethbridge, 4401 University Dr W, Lethbridge, AB T1K 3M4, Canada. NSERC to Hester Jiskoot	Cooley, J. (2021)	Landsat 7 panchromatic
SJ	Frielebreen		2003	9	23		20030925	sP	20020913		Jade Cooley	Uleth: University of Lethbridge, 4401 University Dr W, Lethbridge, AB T1K 3M4, Canada. NSERC to Hester Jiskoot	Cooley, J. (2021)	Landsat 7 panchromatic
SJ	Frielebreen		2004	-10	23		20040810	sP	20030925		Jade Cooley	Uleth: University of Lethbridge, 4401 University Dr W, Lethbridge, AB T1K 3M4, Canada. NSERC to Hester Jiskoot	Cooley, J. (2021)	Landsat 7 panchromatic
SJ	Frielebreen		2006	2	23		20060816	sP	20040810		Jade Cooley	Uleth: University of Lethbridge, 4401 University Dr W, Lethbridge, AB T1K 3M4, Canada. NSERC to Hester Jiskoot	Cooley, J. (2021)	Landsat 7 panchromatic
SJ	Frielebreen		2008	-23	23		20080913	sP	20060816		Jade Cooley	Uleth: University of Lethbridge, 4401 University Dr W, Lethbridge, AB T1K 3M4, Canada. NSERC to Hester Jiskoot	Cooley, J. (2021)	Landsat 7 panchromatic

SJ	Frielebreen		2010	4	23		20100903	sP	20080913		Jade Cooley	Uleth: University of Lethbridge, 4401 University Dr W, Lethbridge, AB T1K 3M4, Canada. NSERC to Hester Jiskoot	Cooley, J. (2021)	Landsat 7 panchromatic
SJ	Frielebreen		2011	-11	23		20110620	sP	20100903		Jade Cooley	Uleth: University of Lethbridge, 4401 University Dr W, Lethbridge, AB T1K 3M4, Canada. NSERC to Hester Jiskoot	Cooley, J. (2021)	ASTER
SJ	Frielebreen		2012	18	23		20120715	sP	20110620		Jade Cooley	Uleth: University of Lethbridge, 4401 University Dr W, Lethbridge, AB T1K 3M4, Canada. NSERC to Hester Jiskoot	Cooley, J. (2021)	Landsat 7 panchromatic
SJ	Frielebreen		2013	12	23		20130726	sP	20120715		Jade Cooley	Uleth: University of Lethbridge, 4401 University Dr W, Lethbridge, AB T1K 3M4, Canada. NSERC to Hester Jiskoot	Cooley, J. (2021)	Landsat 8 panchromatic
SJ	Frielebreen		2016	-56	23		20160819	sP	20130726		Jade Cooley	Uleth: University of Lethbridge, 4401 University Dr W, Lethbridge, AB T1K 3M4, Canada. NSERC to Hester Jiskoot	Cooley, J. (2021)	Landsat 8 panchromatic
SJ	Frielebreen		2018	0	23		20180604	sP	20160819		Jade Cooley	Uleth: University of Lethbridge, 4401 University Dr W, Lethbridge, AB T1K 3M4, Canada. NSERC to Hester Jiskoot	Cooley, J. (2021)	Landsat 8 panchromatic
SJ	Frielebreen		2020	-166	23		20200828	sP	20180604		Jade Cooley	Uleth: University of Lethbridge, 4401 University Dr W, Lethbridge, AB T1K 3M4, Canada. NSERC to Hester Jiskoot	Cooley, J. (2021)	Landsat 8 panchromatic
SJ	Gjuvbreen		2002	-1	23		20020913	sP	20000721		Jade Cooley	Uleth: University of Lethbridge, 4401 University Dr W, Lethbridge, AB T1K 3M4, Canada. NSERC to Hester Jiskoot	Cooley, J. (2021)	Landsat 7 panchromatic
SJ	Gjuvbreen		2003	-89	23		20030716	sP	20020913		Jade Cooley	Uleth: University of Lethbridge, 4401 University Dr W, Lethbridge, AB T1K 3M4, Canada. NSERC to Hester Jiskoot	Cooley, J. (2021)	ASTER
SJ	Gjuvbreen		2014	-39	23		20140625	sP	20030716		Jade Cooley	Uleth: University of Lethbridge, 4401 University Dr W, Lethbridge, AB T1K 3M4, Canada. NSERC to Hester Jiskoot	Cooley, J. (2021)	Landsat 8 panchromatic
SJ	Gjuvbreen		2018	-100	23		20180708	sP	20140625		Jade Cooley	Uleth: University of Lethbridge, 4401 University Dr W, Lethbridge, AB T1K 3M4, Canada. NSERC to Hester Jiskoot	Cooley, J. (2021)	Landsat 8 panchromatic
SJ	Gjuvbreen		2020	-6	23		20200828	sP	20180708		Jade Cooley	Uleth: University of Lethbridge, 4401 University Dr W, Lethbridge, AB T1K 3M4, Canada. NSERC to Hester Jiskoot	Cooley, J. (2021)	Landsat 8 panchromatic
SJ	Griegbreen		2011	-71	23		20110620	sP	20040810		Jade Cooley	Uleth: University of Lethbridge, 4401 University Dr W, Lethbridge, AB T1K 3M4, Canada. NSERC to Hester Jiskoot	Cooley, J. (2021)	ASTER
SJ	Griegbreen		2018	7	23		20180604	sP	20110620		Jade Cooley	Uleth: University of Lethbridge, 4401 University Dr W, Lethbridge, AB T1K 3M4, Canada. NSERC to Hester Jiskoot	Cooley, J. (2021)	Landsat 8 panchromatic
SJ	Hamarbreen		2015	-30	23		20150831	sP	20000721		Jade Cooley	Uleth: University of Lethbridge, 4401 University Dr W, Lethbridge, AB T1K 3M4, Canada. NSERC to Hester Jiskoot	Cooley, J. (2021)	Landsat 8 panchromatic
SJ	Hamarbreen		2020	-36	23		20200828	sP	20150831		Jade Cooley	Uleth: University of Lethbridge, 4401 University Dr W, Lethbridge, AB T1K 3M4, Canada. NSERC to Hester Jiskoot	Cooley, J. (2021)	Landsat 8 panchromatic

SJ	Jorisbreen		2003	-16	23		20030716	sP	20020904		Jade Cooley	Uleth: University of Lethbridge, 4401 University Dr W, Lethbridge, AB T1K 3M4, Canada. NSERC to Hester Jiskoot	Cooley, J. (2021)	ASTER
SJ	Jorisbreen		2013	-36	23		20130726	sP	20030716		Jade Cooley	Uleth: University of Lethbridge, 4401 University Dr W, Lethbridge, AB T1K 3M4, Canada. NSERC to Hester Jiskoot	Cooley, J. (2021)	Landsat 8 panchromatic
SJ	Jorisbreen		2020	-127	23		20200828	sP	20130726		Jade Cooley	Uleth: University of Lethbridge, 4401 University Dr W, Lethbridge, AB T1K 3M4, Canada. NSERC to Hester Jiskoot	Cooley, J. (2021)	Landsat 8 panchromatic
SJ	Kerckhoffbreen		2003	-19	23		20030628	sP	20010802		Jade Cooley	Uleth: University of Lethbridge, 4401 University Dr W, Lethbridge, AB T1K 3M4, Canada. NSERC to Hester Jiskoot	Cooley, J. (2021)	ASTER
SJ	Kerckhoffbreen		2004	-14	23		20040810	sP	20030628		Jade Cooley	Uleth: University of Lethbridge, 4401 University Dr W, Lethbridge, AB T1K 3M4, Canada. NSERC to Hester Jiskoot	Cooley, J. (2021)	Landsat 7 panchromatic
SJ	Kerckhoffbreen		2016	-351	23		20160819	sP	20040810		Jade Cooley	Uleth: University of Lethbridge, 4401 University Dr W, Lethbridge, AB T1K 3M4, Canada. NSERC to Hester Jiskoot	Cooley, J. (2021)	Landsat 8 panchromatic
SJ	Kerckhoffbreen		2018	46	23		20180910	sP	20160819		Jade Cooley	Uleth: University of Lethbridge, 4401 University Dr W, Lethbridge, AB T1K 3M4, Canada. NSERC to Hester Jiskoot	Cooley, J. (2021)	Landsat 8 panchromatic
SJ	Kerckhoffbreen		2020	-26	23		20200828	sP	20180910		Jade Cooley	Uleth: University of Lethbridge, 4401 University Dr W, Lethbridge, AB T1K 3M4, Canada. NSERC to Hester Jiskoot	Cooley, J. (2021)	Landsat 8 panchromatic
SJ	Kjerulfbreen		2001	-1	23		20010624	sP	20000721		Jade Cooley	Uleth: University of Lethbridge, 4401 University Dr W, Lethbridge, AB T1K 3M4, Canada. NSERC to Hester Jiskoot	Cooley, J. (2021)	ASTER
SJ	Kjerulfbreen		2002	55	23		20020904	sP	20010624		Jade Cooley	Uleth: University of Lethbridge, 4401 University Dr W, Lethbridge, AB T1K 3M4, Canada. NSERC to Hester Jiskoot	Cooley, J. (2021)	Landsat 7 panchromatic
SJ	Kjerulfbreen		2003	-39	23		20030716	sP	20020904		Jade Cooley	Uleth: University of Lethbridge, 4401 University Dr W, Lethbridge, AB T1K 3M4, Canada. NSERC to Hester Jiskoot	Cooley, J. (2021)	ASTER
SJ	Kjerulfbreen		2004	1	23		20040810	sP	20030716		Jade Cooley	Uleth: University of Lethbridge, 4401 University Dr W, Lethbridge, AB T1K 3M4, Canada. NSERC to Hester Jiskoot	Cooley, J. (2021)	Landsat 7 panchromatic
SJ	Kjerulfbreen		2006	21	35		20060721	sP	20040810		Jade Cooley	Uleth: University of Lethbridge, 4401 University Dr W, Lethbridge, AB T1K 3M4, Canada. NSERC to Hester Jiskoot	Cooley, J. (2021)	Landsat 5 TM
SJ	Kjerulfbreen		2008	4	35		20080913	sP	20060721		Jade Cooley	Uleth: University of Lethbridge, 4401 University Dr W, Lethbridge, AB T1K 3M4, Canada. NSERC to Hester Jiskoot	Cooley, J. (2021)	Landsat 7 panchromatic
SJ	Kjerulfbreen		2010	-12	23		20100903	sP	20080913		Jade Cooley	Uleth: University of Lethbridge, 4401 University Dr W, Lethbridge, AB T1K 3M4, Canada. NSERC to Hester Jiskoot	Cooley, J. (2021)	Landsat 7 panchromatic
SJ	Kjerulfbreen		2013	3	23		20130802	sP	20100903		Jade Cooley	Uleth: University of Lethbridge, 4401 University Dr W, Lethbridge, AB T1K 3M4, Canada. NSERC to Hester Jiskoot	Cooley, J. (2021)	Landsat 8 panchromatic

SJ	Kjerulfbreen		2014	-32	23		20140625	sP	20130802		Jade Cooley	Uleth: University of Lethbridge, 4401 University Dr W, Lethbridge, AB T1K 3M4, Canada. NSERC to Hester Jiskoot	Cooley, J. (2021)	Landsat 8 panchromatic
SJ	Kjerulfbreen		2015	28	23		20150831	sP	20140625		Jade Cooley	Uleth: University of Lethbridge, 4401 University Dr W, Lethbridge, AB T1K 3M4, Canada. NSERC to Hester Jiskoot	Cooley, J. (2021)	Landsat 8 panchromatic
SJ	Kjerulfbreen		2016	-18	23		20160819	sP	20150831		Jade Cooley	Uleth: University of Lethbridge, 4401 University Dr W, Lethbridge, AB T1K 3M4, Canada. NSERC to Hester Jiskoot	Cooley, J. (2021)	Landsat 8 panchromatic
SJ	Kjerulfbreen		2018	-47	23		20180604	sP	20160819		Jade Cooley	Uleth: University of Lethbridge, 4401 University Dr W, Lethbridge, AB T1K 3M4, Canada. NSERC to Hester Jiskoot	Cooley, J. (2021)	Landsat 8 panchromatic
SJ	Kjerulfbreen		2020	-7	23		20200828	sP	20180604		Jade Cooley	Uleth: University of Lethbridge, 4401 University Dr W, Lethbridge, AB T1K 3M4, Canada. NSERC to Hester Jiskoot	Cooley, J. (2021)	Landsat 8 panchromatic
SJ	Petersenbreen		2003	-12	23		20030716	sP	20000930		Jade Cooley	Uleth: University of Lethbridge, 4401 University Dr W, Lethbridge, AB T1K 3M4, Canada. NSERC to Hester Jiskoot	Cooley, J. (2021)	ASTER
SJ	Petersenbreen		2016	-229	23		20160819	sP	20030716		Jade Cooley	Uleth: University of Lethbridge, 4401 University Dr W, Lethbridge, AB T1K 3M4, Canada. NSERC to Hester Jiskoot	Cooley, J. (2021)	Landsat 8 panchromatic
SJ	Petersenbreen		2018	-40	23		20180910	sP	20160819		Jade Cooley	Uleth: University of Lethbridge, 4401 University Dr W, Lethbridge, AB T1K 3M4, Canada. NSERC to Hester Jiskoot	Cooley, J. (2021)	Landsat 8 panchromatic
SJ	Prins Haralds Bre		2001	30	23		20010624	sP	20000930		Jade Cooley	Uleth: University of Lethbridge, 4401 University Dr W, Lethbridge, AB T1K 3M4, Canada. NSERC to Hester Jiskoot	Cooley, J. (2021)	ASTER
SJ	Prins Haralds Bre		2002	-17	23		20020913	sP	20010624		Jade Cooley	Uleth: University of Lethbridge, 4401 University Dr W, Lethbridge, AB T1K 3M4, Canada. NSERC to Hester Jiskoot	Cooley, J. (2021)	Landsat 7 panchromatic
SJ	Prins Haralds Bre		2003	-16	23		20030716	sP	20020913		Jade Cooley	Uleth: University of Lethbridge, 4401 University Dr W, Lethbridge, AB T1K 3M4, Canada. NSERC to Hester Jiskoot	Cooley, J. (2021)	ASTER
SJ	Prins Haralds Bre		2004	1	23		20040810	sP	20030716		Jade Cooley	Uleth: University of Lethbridge, 4401 University Dr W, Lethbridge, AB T1K 3M4, Canada. NSERC to Hester Jiskoot	Cooley, J. (2021)	Landsat 7 panchromatic
SJ	Prins Haralds Bre		2006	-12	23		20060816	sP	20040810		Jade Cooley	Uleth: University of Lethbridge, 4401 University Dr W, Lethbridge, AB T1K 3M4, Canada. NSERC to Hester Jiskoot	Cooley, J. (2021)	Landsat 7 panchromatic
SJ	Prins Haralds Bre		2008	-11	23		20080913	sP	20060816		Jade Cooley	Uleth: University of Lethbridge, 4401 University Dr W, Lethbridge, AB T1K 3M4, Canada. NSERC to Hester Jiskoot	Cooley, J. (2021)	Landsat 7 panchromatic
SJ	Prins Haralds Bre		2010	15	23		20100903	sP	20080913		Jade Cooley	Uleth: University of Lethbridge, 4401 University Dr W, Lethbridge, AB T1K 3M4, Canada. NSERC to Hester Jiskoot	Cooley, J. (2021)	Landsat 7 panchromatic
SJ	Prins Haralds Bre		2011	-6	23		20110620	sP	20100903		Jade Cooley	Uleth: University of Lethbridge, 4401 University Dr W, Lethbridge, AB T1K 3M4, Canada. NSERC to Hester Jiskoot	Cooley, J. (2021)	ASTER

SJ	Prins Haralds Bre		2012	-1	23		20120715	sP	20110620		Jade Cooley	Uleth: University of Lethbridge, 4401 University Dr W, Lethbridge, AB T1K 3M4, Canada. NSERC to Hester Jiskoot	Cooley, J. (2021)	Landsat 7 panchromatic
SJ	Prins Haralds Bre		2013	18	23		20130726	sP	20120715		Jade Cooley	Uleth: University of Lethbridge, 4401 University Dr W, Lethbridge, AB T1K 3M4, Canada. NSERC to Hester Jiskoot	Cooley, J. (2021)	Landsat 8 panchromatic
SJ	Prins Haralds Bre		2014	-3	23		20140625	sP	20130726		Jade Cooley	Uleth: University of Lethbridge, 4401 University Dr W, Lethbridge, AB T1K 3M4, Canada. NSERC to Hester Jiskoot	Cooley, J. (2021)	Landsat 8 panchromatic
SJ	Prins Haralds Bre		2015	-7	23		20150605	sP	20140625		Jade Cooley	Uleth: University of Lethbridge, 4401 University Dr W, Lethbridge, AB T1K 3M4, Canada. NSERC to Hester Jiskoot	Cooley, J. (2021)	Landsat 8 panchromatic
SJ	Prins Haralds Bre		2016	-2	23		20160819	sP	20150605		Jade Cooley	Uleth: University of Lethbridge, 4401 University Dr W, Lethbridge, AB T1K 3M4, Canada. NSERC to Hester Jiskoot	Cooley, J. (2021)	Landsat 8 panchromatic
SJ	Prins Haralds Bre		2018	-35	23		20180604	sP	20160819		Jade Cooley	Uleth: University of Lethbridge, 4401 University Dr W, Lethbridge, AB T1K 3M4, Canada. NSERC to Hester Jiskoot	Cooley, J. (2021)	Landsat 8 panchromatic
SJ	Prins Haralds Bre		2020	-18	23		20200828	sP	20180604		Jade Cooley	Uleth: University of Lethbridge, 4401 University Dr W, Lethbridge, AB T1K 3M4, Canada. NSERC to Hester Jiskoot	Cooley, J. (2021)	Landsat 8 panchromatic
SJ	Sørbreen	3763	2002	-82	23		20020913	sP	20010622		Jade Cooley	Uleth: University of Lethbridge, 4401 University Dr W, Lethbridge, AB T1K 3M4, Canada. NSERC to Hester Jiskoot	Cooley, J. (2021)	Landsat 7 panchromatic
SJ	Sørbreen	3763	2004	-78	23		20040810	sP	20020913		Jade Cooley	Uleth: University of Lethbridge, 4401 University Dr W, Lethbridge, AB T1K 3M4, Canada. NSERC to Hester Jiskoot	Cooley, J. (2021)	Landsat 7 panchromatic
SJ	Sørbreen	3763	2011	33	23		20110620	sP	20040810		Jade Cooley	Uleth: University of Lethbridge, 4401 University Dr W, Lethbridge, AB T1K 3M4, Canada. NSERC to Hester Jiskoot	Cooley, J. (2021)	ASTER
SJ	Sørbreen	3763	2016	-405	23		20160819	sP	20110620		Jade Cooley	Uleth: University of Lethbridge, 4401 University Dr W, Lethbridge, AB T1K 3M4, Canada. NSERC to Hester Jiskoot	Cooley, J. (2021)	Landsat 8 panchromatic
SJ	Sørbreen	3763	2018	72	23		20180629	sP	20160819		Jade Cooley	Uleth: University of Lethbridge, 4401 University Dr W, Lethbridge, AB T1K 3M4, Canada. NSERC to Hester Jiskoot	Cooley, J. (2021)	Landsat 8 panchromatic
SJ	Svend Foynbreen		2001	20	23		20010622	sP	20000721		Jade Cooley	Uleth: University of Lethbridge, 4401 University Dr W, Lethbridge, AB T1K 3M4, Canada. NSERC to Hester Jiskoot	Cooley, J. (2021)	Landsat 7 panchromatic
SJ	Svend Foynbreen		2002	-1	23		20020904	sP	20010622		Jade Cooley	Uleth: University of Lethbridge, 4401 University Dr W, Lethbridge, AB T1K 3M4, Canada. NSERC to Hester Jiskoot	Cooley, J. (2021)	Landsat 7 panchromatic
SJ	Svend Foynbreen		2003	0	23		20030716	sP	20020904		Jade Cooley	Uleth: University of Lethbridge, 4401 University Dr W, Lethbridge, AB T1K 3M4, Canada. NSERC to Hester Jiskoot	Cooley, J. (2021)	ASTER
SJ	Svend Foynbreen		2004	-8	23		20040810	sP	20030716		Jade Cooley	Uleth: University of Lethbridge, 4401 University Dr W, Lethbridge, AB T1K 3M4, Canada. NSERC to Hester Jiskoot	Cooley, J. (2021)	Landsat 7 panchromatic

SJ	Svend Foynbreen		2006	14	35		20060721	sP	20040810		Jade Cooley	Uleth: University of Lethbridge, 4401 University Dr W, Lethbridge, AB T1K 3M4, Canada. NSERC to Hester Jiskoot	Cooley, J. (2021)	Landsat 5 TM
SJ	Svend Foynbreen		2010	-30	35		20100903	sP	20060721		Jade Cooley	Uleth: University of Lethbridge, 4401 University Dr W, Lethbridge, AB T1K 3M4, Canada. NSERC to Hester Jiskoot	Cooley, J. (2021)	Landsat 7 panchromatic
SJ	Svend Foynbreen		2016	-63	23		20160819	sP	20100903		Jade Cooley	Uleth: University of Lethbridge, 4401 University Dr W, Lethbridge, AB T1K 3M4, Canada. NSERC to Hester Jiskoot	Cooley, J. (2021)	Landsat 8 panchromatic
SJ	Svend Foynbreen		2018	3	23		20180604	sP	20160819		Jade Cooley	Uleth: University of Lethbridge, 4401 University Dr W, Lethbridge, AB T1K 3M4, Canada. NSERC to Hester Jiskoot	Cooley, J. (2021)	Landsat 8 panchromatic
SJ	Weyprechtbreen		2001	-48	23		20010624	sP	20000721		Jade Cooley	Uleth: University of Lethbridge, 4401 University Dr W, Lethbridge, AB T1K 3M4, Canada. NSERC to Hester Jiskoot	Cooley, J. (2021)	ASTER
SJ	Weyprechtbreen		2002	47	23		20020913	sP	20010624		Jade Cooley	Uleth: University of Lethbridge, 4401 University Dr W, Lethbridge, AB T1K 3M4, Canada. NSERC to Hester Jiskoot	Cooley, J. (2021)	Landsat 7 panchromatic
SJ	Weyprechtbreen		2003	-31	23		20030716	sP	20020913		Jade Cooley	Uleth: University of Lethbridge, 4401 University Dr W, Lethbridge, AB T1K 3M4, Canada. NSERC to Hester Jiskoot	Cooley, J. (2021)	ASTER
SJ	Weyprechtbreen		2004	0	23		20040810	sP	20030716		Jade Cooley	Uleth: University of Lethbridge, 4401 University Dr W, Lethbridge, AB T1K 3M4, Canada. NSERC to Hester Jiskoot	Cooley, J. (2021)	Landsat 7 panchromatic
SJ	Weyprechtbreen		2006	37	35		20060721	sP	20040810		Jade Cooley	Uleth: University of Lethbridge, 4401 University Dr W, Lethbridge, AB T1K 3M4, Canada. NSERC to Hester Jiskoot	Cooley, J. (2021)	Landsat 5 TM
SJ	Weyprechtbreen		2008	17	35		20080913	sP	20060721		Jade Cooley	Uleth: University of Lethbridge, 4401 University Dr W, Lethbridge, AB T1K 3M4, Canada. NSERC to Hester Jiskoot	Cooley, J. (2021)	Landsat 7 panchromatic
SJ	Weyprechtbreen		2010	-9	23		20100903	sP	20080913		Jade Cooley	Uleth: University of Lethbridge, 4401 University Dr W, Lethbridge, AB T1K 3M4, Canada. NSERC to Hester Jiskoot	Cooley, J. (2021)	Landsat 7 panchromatic
SJ	Weyprechtbreen		2013	-54	23		20130606	sP	20100903		Jade Cooley	Uleth: University of Lethbridge, 4401 University Dr W, Lethbridge, AB T1K 3M4, Canada. NSERC to Hester Jiskoot	Cooley, J. (2021)	Landsat 8 panchromatic
SJ	Weyprechtbreen		2014	34	23		20140625	sP	20130606		Jade Cooley	Uleth: University of Lethbridge, 4401 University Dr W, Lethbridge, AB T1K 3M4, Canada. NSERC to Hester Jiskoot	Cooley, J. (2021)	Landsat 8 panchromatic
SJ	Weyprechtbreen		2015	-18	23		20150831	sP	20140625		Jade Cooley	Uleth: University of Lethbridge, 4401 University Dr W, Lethbridge, AB T1K 3M4, Canada. NSERC to Hester Jiskoot	Cooley, J. (2021)	Landsat 8 panchromatic
SJ	Weyprechtbreen		2016	0	23		20160819	sP	20150831		Jade Cooley	Uleth: University of Lethbridge, 4401 University Dr W, Lethbridge, AB T1K 3M4, Canada. NSERC to Hester Jiskoot	Cooley, J. (2021)	Landsat 8 panchromatic
SJ	Weyprechtbreen		2018	-42	23		20180708	sP	20160819		Jade Cooley	Uleth: University of Lethbridge, 4401 University Dr W, Lethbridge, AB T1K 3M4, Canada. NSERC to Hester Jiskoot	Cooley, J. (2021)	Landsat 8 panchromatic

SJ	Weyprechtbreen		2020	50	23		20200828	sP	20180708		Jade Cooley	Uleth: University of Lethbridge, 4401 University Dr W, Lethbridge, AB T1K 3M4, Canada. NSERC to Hester Jiskoot	Cooley, J. (2021)	Landsat 8 panchromatic
SJ	Willebreen		2004	11	23		20040810	sP	20030628		Jade Cooley	Uleth: University of Lethbridge, 4401 University Dr W, Lethbridge, AB T1K 3M4, Canada. NSERC to Hester Jiskoot	Cooley, J. (2021)	Landsat 7 panchromatic
SJ	Willebreen		2016	32	23		20160819	sP	20040810		Jade Cooley	Uleth: University of Lethbridge, 4401 University Dr W, Lethbridge, AB T1K 3M4, Canada. NSERC to Hester Jiskoot	Cooley, J. (2021)	Landsat 8 panchromatic
SJ	Willebreen		2020	-178	23		20200828	sP	20160819		Jade Cooley	Uleth: University of Lethbridge, 4401 University Dr W, Lethbridge, AB T1K 3M4, Canada. NSERC to Hester Jiskoot	Cooley, J. (2021)	Landsat 8 panchromatic

Appendix C: SST Data

To review the validity of the annual and summer SST values, Figure 7.2 presents the number of daily average SST measurements within each year for 1 Jan 1975 to 31 Dec 2020, and Figure 7.13 presents the number of daily average SST measurements within each month for 1 Jan 1976 to 31 Dec 2020 (1975 is not shown as it had 365 measurements). Summer average temperature was not used for 1976, as there were no measurements in the month of August. The annual average for 1976 was used, however, as the month of September was also missing all measurements and thus August and September balance their respective contribution to the annual average without removing too many total measurements. Annual average for 1979 was not used, as two consecutive months in the same season (September and October) were missing all values.

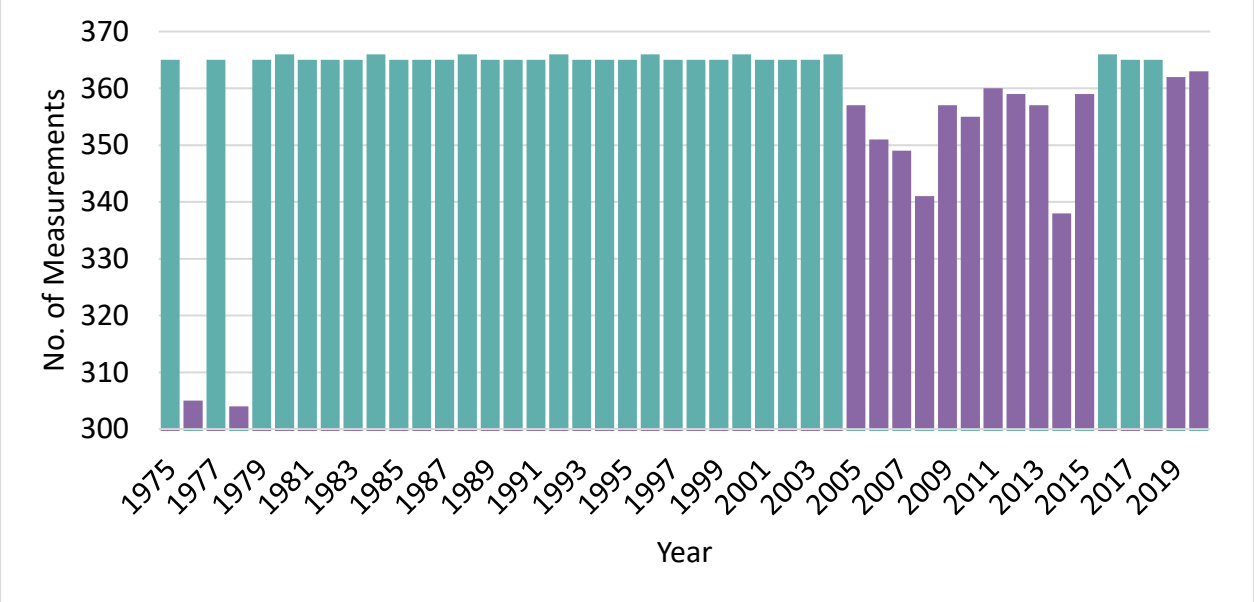

Figure 7.2: Number of daily average SST measurements for each year there were SST measurements taken at Olonkinbyen. Teal bars indicate years with measurements every day, purple bars indicate years with fewer measurements than days. Data from web portal https://seklima.met.no/

Figure 7.3: Number of daily average SST measurements for each month, in the years there were not SST measurements taken every day. Any value not showing on the bar chart was 0. Teal bars indicate months with measurements every day, purple bars indicate months with fewer measurements than days. Data from web portal https://seklima.met.no/